CRANFIELD UNIVERSITY

Payam Zargarzadeh

Structural Integrity of CO_2 Transportation Infrastructures

SCHOOL OF ENGINEERING
Department of Offshore, Process and Energy Engineering

PhD Thesis
Academic Year: 2012 - 2013

Supervisor: Professor Feargal Brennan
Jan 2013

CRANFIELD UNIVERSITY

SCHOOL OF ENGINEERING
Department of Offshore, Process and Energy Engineering

PhD Thesis

Academic Year 2012 - 2013

Payam Zargarzadeh

Structural Integrity of CO_2 Transportation Infrastructures

Supervisor: Professor Feargal Brennan
Jan 2013

This thesis is submitted in partial fulfilment of the requirements for the degree of Doctor of Philosophy

Abstract

Carbon Capture and Storage (CCS) is recognised as having a significant role to play in tackling climate change and reducing carbon dioxide (CO_2) emissions. In CCS schemes, CO_2 is captured from anthropogenic sources, and transported to suitable sites either for EOR (Enhanced Oil Recovery) or storage. The transport of such huge amount of CO_2 causes new challenges. The main concern is in the difference between natural gas and CO_2 transportation pipelines. CO_2 phase behaviour during decompression, existence of different impurities and very high operating pressure are some of the new challenges for pipeline designer and operators.

This PhD study has taken a systematic approach to understand the mechanics involved in the fracture of pipes containing high pressure flue-gas CO_2. The work involved the development of a novel weight function stress intensity factor solution that can be used with complex stress fields induced by residual and/or thermal stresses in addition to applied pressure.

In addition, the thesis reports a substantial experimented test programme which involved low temperature fracture toughness tests linked to a detailed finite element based stress analysis.

Overall, the thesis presents an integrated engineering criticality means to assess the suitability or otherwise of a pipeline system to transport high pressure flue-gas CO_2.

Keywords: CO_2 pipeline-Fracture mechanics-Weight function-Fracture toughness test-FEA-SIF-FAD-ECA-Back Face Strain-

Acknowledgements

This dissertation would not have been possible without the guidance and the help of several individuals who in one way or another contributed and extended their valuable assistance in the preparation and completion of a work of this magnitude during the last three years.

First and foremost, I offer my utmost gratitude to Professor Feargal Brennan for his valuable guidance throughout this research. His patience, motivation, enthusiasm, and immense knowledge helped me to make it all possible.

I would like to express special thanks to Dr. Amir Chahardehi, Atkins London, for his support and advice during the early stages of this research.

I would like to thank Prof. Luca Susmel from Sheffield University, Dr. Athanasios Kolios and Dr. Andrew Shires from Offshore, Process and Energy Engineering and Dr. Steve James from Department of Engineering Photonics at Cranfield University for their constructive comments.

I wish to thank my dear friends and colleagues at Cranfield University: Jafar Alzaili, Mahadi Abd Murad, Wilson Vesga Rivera, Grema Alhaji, Xiaojian Hung, Chet Biliyok, Phil Elks, and Reza Haghpanah, Stanford University for their constructive support, help and friendship which has had an enormous impact on my work.

I would like to thank our expert technicians Mr. Barry Walker, Mr. Derek Brown and Mr. Scott Booden for all their assistance and help.

Finally, thanks to my parents and family for giving support, love and encouragement to me to pursue my studies, especially dear Narges for her care and support of my family.

May God bless them all.

I would like to gratefully acknowledge the financial support of EPSRC - E.ON for this research.

Dedicated to my beloved wife

Laleh and our sweet daughter Raha.

Table of Contents

List of Figures

List of Tables

List of Equations

List of Abbreviations

ACPD	Alternating Current Potential Difference
CAT	Crack Arrest Temperature
CCS	Carbon Capture and Storage
COD	Crack Opening Displacement
CT	Compact Tension
CTOD	Crack Tip Opening Displacement
CVN	Charpy V Notch
DBTT	Ductile to Brittle Transition Temperature
DCB	Dual Cantilever Beam
DIC	Digital Image Correlation
ECA	Engineering Criticality Assessment
EOR	Enhanced Oil Recovery
FAD	Failure Assessment Diagram
FEA	Finite Element Analysis
IEA	The International Energy Agency
LEFM	Linear Elastic Fracture Mechanics
MRS	Multiple Reference State weight function
NDT	Non Destructive Test
OSSL	Opposing Section Surface Load
ppm	Part per million
SECT	Single edge crack under pure tension
SIF	Stress Intensity Factor
WF	Weight Function

Nomenclature

a/W	Crack length to specimen width as defined
K_I	Mode one SIF
K_{II}	Mode two SIF
K_{III}	Mode three SIF
K_{IC} or K_{mat}	Material fracture toughness
K_Q	Provisional fracture toughness
a_0	Notch length + Pre-crack length
B	Specimen thickness
W	Specimen width (see the drawing)
P	Pipe design pressure
S	Specified minimum yield strength
D	Nominal pipe outside diameter
r_p	Plastic zone radius
σ_y	Yield stress
a	Half of crack length
R	Pipe diameter mean radius
t	Pipe thickness
U	Elastic energy
E	Young's modulus
G	Elastic energy release rate
v	Poisson's ratio
δ	CTOD
S_r or L_r	Stress ratio
K_r	Stress intensity ratio
J	J integral
V_p	Plastic component of COD
V_e	Elastic component of COD
e_{xx}	Strain along x direction
e_{yy}	Strain along y direction
e_{zz}	Strain along z direction

Chapter 1. Introduction

Carbon Capture and Storage (CCS) is recognised as having a significant role to play in tackling climate change and reducing carbon dioxide (CO_2) emissions. In CCS schemes, CO_2 is captured from anthropogenic sources, and transported to suitable sites either for EOR (Enhanced Oil Recovery) or storage.

This project is part of a MATTRAN project (Materials for Next Generation CO_2 Pipeline Transport Systems) which is a multi-consortium project sponsored by the Engineering and Physical Sciences Research Council (EPSRC) and E-on. The aim is to provide the tools and information necessary for pipeline engineers to select appropriate materials and operating conditions to control corrosion, stress corrosion cracking and fracture propagation in pipelines and associated equipment carrying supercritical CO_2 from the capture processes likely to be realised in the near and long term future.

Captured CO_2 from different sources and various techniques has different chemical compositions. This has a huge effect on CO_2 phase behaviour. When CO_2 is carried in a supercritical/dense phase (very high pressure), in the case of sudden expansion due to cracks or porosities, the temperature around the crack may fall below -70°C. Different CO_2 chemical compositions can change the CO_2 saturation point and the expansion temperature. If the crack front temperature falls below the ductile to brittle temperature (DBTT) of the pipe material it can caused brittle fracture and consequently unzip the pipe very quickly.

The transport of such huge amount of CO_2 causes new challenges. The main concern is in the difference between natural gas and CO_2 transportation pipelines. CO_2 phase behaviour during decompression, existence of different impurities and very high operating pressure are some of the new challenges for pipeline designer and operators.

1.1 Problem statement

Some of the new challenges that distinguish the CO_2 pipelines from natural gas pipelines are as follow:

- High operating pressure
- Different level of impurities (depends on different capture technologies)
- Constant pressure behaviour during gas decompression
- Very low temperature during decompression

The problem is to better understand the fracture mechanics behaviour of CO_2 pipeline in the case of existence of longitudinal crack in the pipe.

1.2 Aims and objectives

The aim of this research is to have a systematic approach to understand the mechanics involved in the fracture of pipes containing high pressure flue-gas CO_2. For this purpose it needs to reports a substantial experimented test programme which involved low temperature fracture toughness tests linked to a detailed finite element based stress analysis.

1.3 Scope of thesis

The objective of this research is both to develop a novel engineering criticality assessment for CO_2 transportation pipelines and a better understanding of CO_2 pipeline behaviour in case of sudden gas decompression due to the existence of a longitudinal through thickness crack. To achieve this goal, and for a better understanding of the tools and process, Chapter 1 presented a literature review about the process of CCS and CO_2 transportation, and the fracture mechanics of pipelines, with a special focus on longitudinal cracks. Current state-of-the-art regarding the pipeline material fracture toughness and failure assessment diagram is explained.

In Chapter 2 the finite element analysis (FEA) technique, a powerful tool using numerical simulations to calculate the SIF for non standard geometries, is presented. Also stress analyses and SIF predictions for different loading conditions for CT specimens are reported using the FEA model.

In Chapter 3, pipeline material fracture toughness for different temperature conditions is measured by conducting fracture toughness tests on CT specimens. Material fracture toughness is a critical value for the design and assessment of a pipeline.

In Chapter 4, using an analytical model and multiple reference state weight function, a general solution for the calculation of SIF in a pipe with longitudinal through thickness crack is presented. The results are verified against FEA models for a number of different crack lengths and pipe diameters.

Chapter 5 presents an engineering criticality assessment methodology for CO_2 pipelines based on the FAD diagram along with other tools and results developed in previous chapters. Also, the FADs for CO_2 pipes with different through thickness crack length are presented.

Overall, the thesis presents a comprehensive methodology for assessing the fitness-for-service of pipelines transporting CO_2.

Chapter 2. Background and literature review

The new generation of CO_2 pipelines dedicated to the transportation of captured CO_2 as part of the Carbon Capture and Storage (CCS) process, demands a new focus on both safety and design of these pipelines. CCS is recognised as having a significant role to play in tackling climate change and reducing CO_2 emissions. A multi-consortium of seven universities in the UK, sponsored by the Engineering and Physical Sciences Research Council (EPSRC), has been established to provide the tools and information necessary for the next generation of CO_2 pipeline designs. Challenges such as phase behaviour, understanding thermodynamic properties using existing equation of state, solubility of water in supercritical CO_2 stream, corrosion, stress corrosion cracking and fracture propagation in CO_2 pipelines are some of the proposed results of this project. As a part of this project, structural integrity and fracture behaviour of the pipeline material is the objective of this research (MATTRAN 2011).

2.1 Carbon Capture and Storage, and CO_2 Transportation

Greenhouse gas emissions, and consequent global warming, has become one of the most important issues in the current decade. Man-made CO_2 emanating from large industries such as oil refineries, cement factories and especially power plants, should be captured before its released to atmosphere and transport to a safe site. From 1973 to 2008 CO_2 emissions have almost doubled worldwide. Future of the industries in the energy sector should lean towards low-carbon production. The International Energy Agency (IEA)'s Energy Technology Perspective Blue Maps for 2030 and 2050 are required to meet an atmospheric CO_2 stabilization target of 45 ppm (IEA 2011).

In particular coal-fired power generation has a huge contribution towards CO_2 emissions. For instance, a 1 GW coal-fired power plant emits about 8 million tonnes of CO_2 per annum, which means that this number will be 400 million tonnes of CO_2 in its 50-year life. Coal-fired power plants construction is

growing rapidly in developing countries, especially China and India. China plans to build about 50 GW of new coal-fired capacity in future (IEA 2008) (Figure 2-1,Figure 2-2). The International Energy Agency predicts a possible growth in the use of coal over next 20 years by 70%. Currently in the UK 37% of electricity is generated from coal (WBCSD 2005).

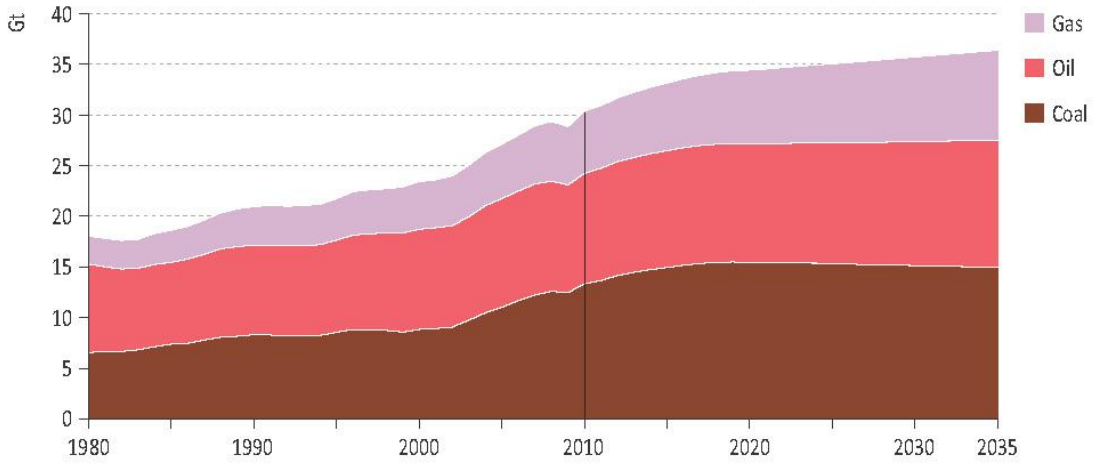

Figure 2-1 World energy-related CO_2 emissions by fuel
(IEA 2011)

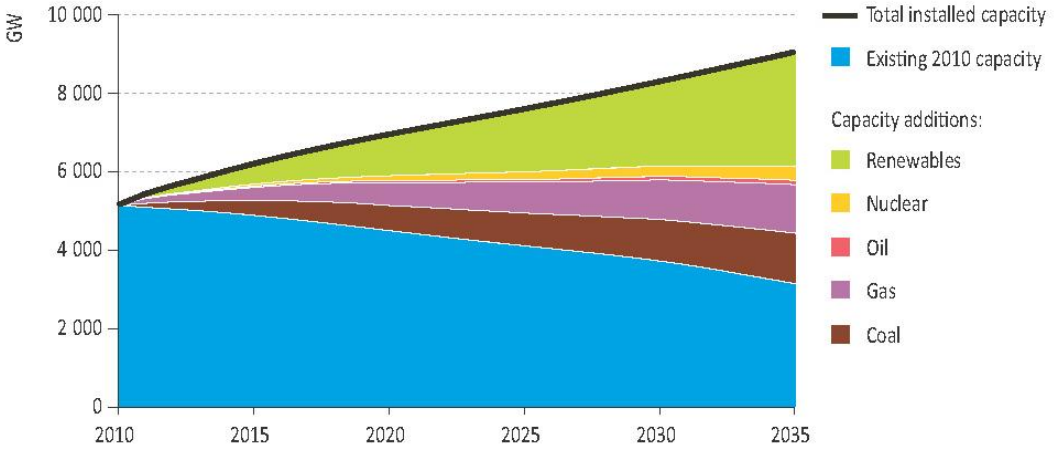

Figure 2-2 Worldwide installed power generation capacity and under construction
(IEA 2011)

Approximately 80-90% of CO_2 emitted by coal-fired power plants could be captured by engineering methods; in the main these are known as pre-combustion, oxyfuel and post-combustion methods. These capturing techniques are the starting point for a process called: Carbon Capture and Storage (CCS).

CCS is the process of capturing industrial CO_2 emissions, transporting and storing them several thousand feet below the Earth in porous rock, such as sandstone, or to be used for recovering depleted oil wells as Enhanced Oil Recovery (EOR) (Figure 2-3). In the UK, available storage sites are depleted oil and gas reservoirs in the North Sea. In more general terms, carbon storage via natural biological processes is named Carbon sequestration. Scientists believe that CCS is a safe and cost effective way of reducing the amount of CO_2 sent out into the atmosphere. It offers a low-carbon way to ensure the security of electricity supply using fossil fuels. Until 2030, CCS will play an important role in reducing CO_2 emissions from the developing world.

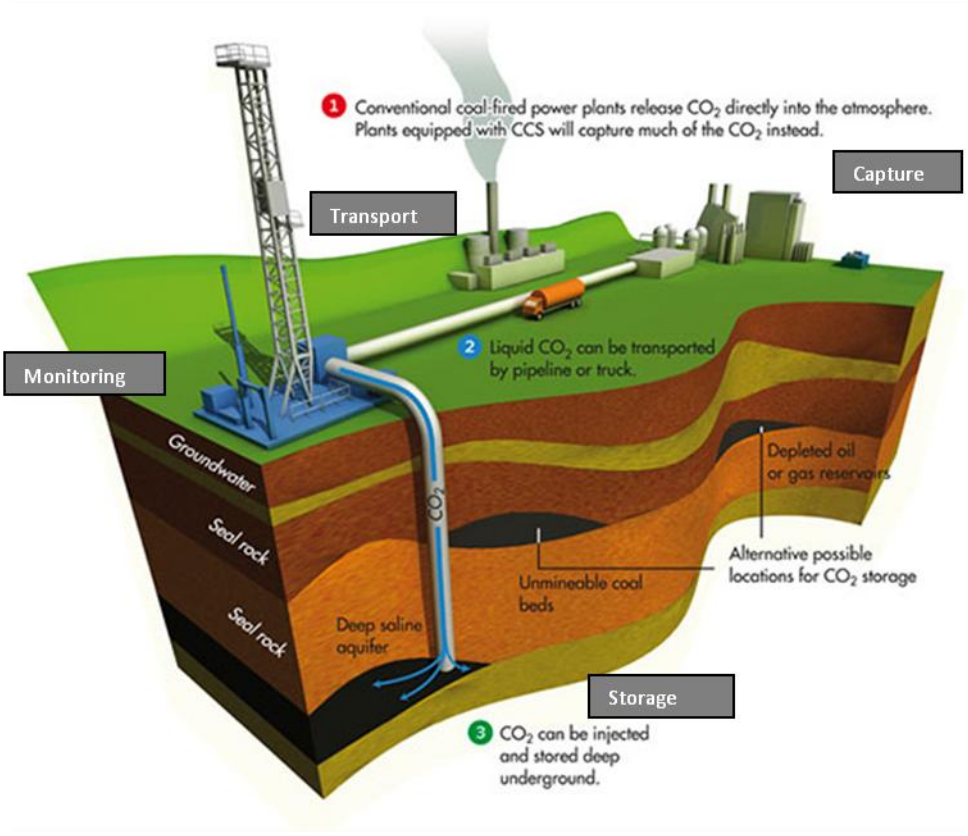

Figure 2-3 CCS process overview, CO_2 SINK study, Germany (CO2SINK 2008)

The “Pathways to 2050” report, prepared by The World Business Council for Sustainable Development (WBCSD) shows that by 2050 about 1,000 large coal-fired power plants could be in operation utilising CCS technology (UKNG 2010). Existing UK coal-fired power plants are aging and the construction of new stations is vital. In April 2009 the Department of Energy and Climate Change (DECC) announced a new concept: CCR, which stands for Carbon Capture Ready. It means that all new combustion power plants producing 300 MWe or above will have to be designed in such way as to be ready to retrofit CCS technology. It not only covers any possible space and engineering facilities in power stations, but should also carry out technical assessments in order to have plausible transport routes and feasible geological storage. The timing of CCS deployment is also critical. A study using the Shell World Energy Model (Haigh 2008) shows that each year delaying the widespread deployment of CCS beyond 2020 would translate into a 1-ppm increase in the long term atmospheric stabilization levels of CO_2.

Focusing on the CCS as a valid emissions reduction technology is a priority under the Clean Development Mechanism (CDM) of the Kyoto Protocol (Kyoto 1998). To prevent any delay in the execution of CCS projects in the UK and to complete the CCS chain, transportation of captured CO_2 should be taken into account. When dealing with large-scale CCS projects, the most effective, economic and safe solution for CO_2 transportation would be pipelines. In the USA and Canada millions of tonnes of CO_2 are already transported by pipelines. Most of these existing pipelines are routed through low population areas and they convey pure CO_2 from gasification plants for Enhanced Oil Recovery.

The next generation of CO_2 pipelines in the UK should be designed to transport captured CO_2 under supercritical or dense phase conditions from CCS plants through the mostly densely populated areas to offshore storage sites. Although transporting CO_2 in a supercritical condition is more efficient, temperatures in an underground pipeline are unlikely to reach the necessary

point to become supercritical (>31°C); pure CO_2 critical point is identified by 74 bar and 31°C for its pressure and temperature respectively.

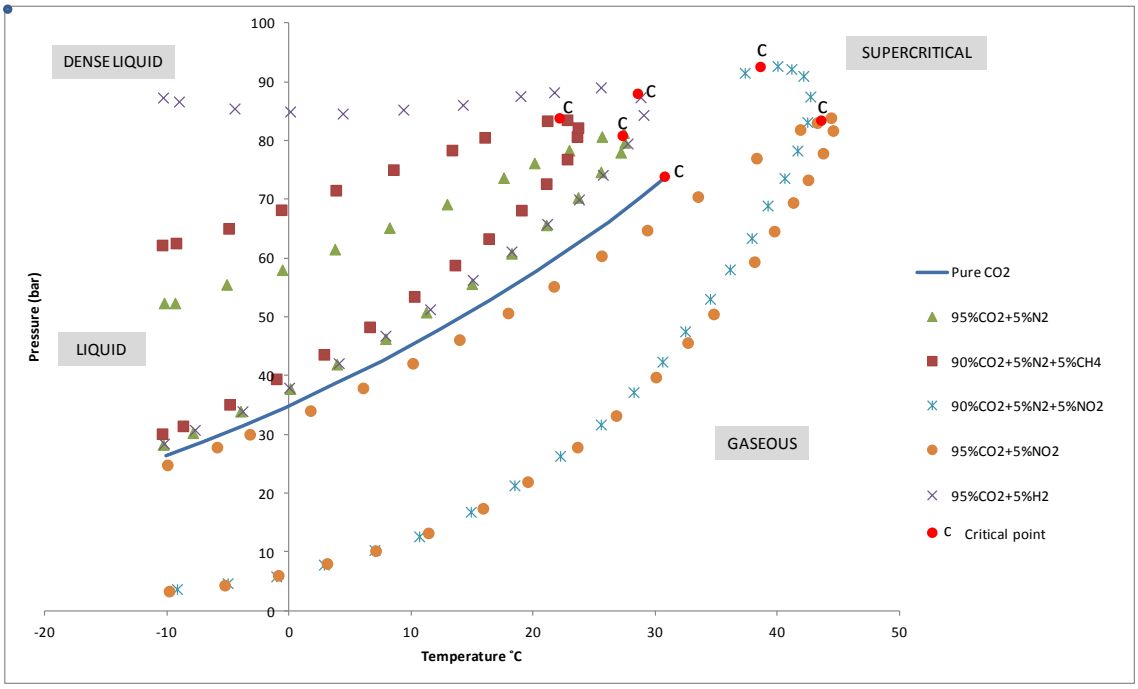

Figure 2-4 Effect of impurities on CO_2 phase diagram (P.N. Seevam 2009; Seevam, Race et al. 2009)

For operators it is important to maintain a single-phase flow in CO_2 pipelines by avoiding abrupt pressure drops. Two-phase flow creates problems for compressors and other equipment, increasing the chance of pipeline failure. Working on pressures very close to the critical point is particularly dangerous; a small change in temperature or pressure yields a very large change in CO_2 density, resulting in slug flow[1] in the pipeline.

To address the knowledge gaps in dealing with next generation of CO_2 pipelines, the Health and Safety Executive (HSE) is working with industry to indentify the behaviour of high pressure CO_2. Compared to high pressure natural gas pipelines, the worldwide experience of CO_2 pipelines is relatively low, especially for offshore transportation. There is no standard or specification for CO_2 pipeline and related facilities (DNV is working on a recommended

[1] Simultaneous formation of gas and liquid flow in certain ranges of flow rates that fills pipe cross section.

practice for CO_2 pipelines). the prediction of phase behaviour, thermodynamic properties and suitable equation of state is important in order to model the hydraulic behaviour of the CO_2 pipeline. Also, specifications of the pipeline and associated equipment are crucial to determine under which conditions corrosion, stress corrosion cracking and fracture propagation may occur (Cosham and Eiber 2008).

CO_2 captured from the CCS process may contain impurities such as water vapour, H_2S, N_2, Methane (CH_4), O_2, Argon, Mercury and Hydrocarbons all of which affect the CO_2 phase behaviour critical point (Figure 2-4) (Caraballo, Patino et al. 2011). Unfortunately the hydraulic and mechanical designs of pipelines are very sensitive to the level of impurities. As depicted in Figure 2-4, CO_2 impurities can change the width and shape of the phase envelope of a two phase flow region. Impurities can reduce the supercritical area and even eliminate the liquid region. The composition of captured CO_2 in different CCS methods is not similar. In most cases the post combustion method has a lower degree of impurities. Table 2-1 presents the predicted composition of CO_2 from coal fired and gas fired power plants. The presence of water in a CO_2 pipeline forms highly corrosive carbonic acid that can corrode carbon steel pipes at the rate of 100mm/year. Another important point about water as an impurity, is its solubility in pure CO_2 which is a function of gas pressure and temperature. Purification of captured CO_2 to prevent transporting impurities requires a huge amount of investment in the CCS process (Seevam, Race et al. 2010).

Table 2-1 Predicted composition of CO_2 from power plant capture (IEAGHG 2004)

	Component	Coal Fired % Volume	Gas Fired % Volume
Post Combustion Capture	SO_2	<0.01	<0.01
	NO_x	<0.01	<0.01
	$N_2/Ar/O_2$	0.01	0.01
Pre Combustion Capture (IGCC[2])	H_2S	0.01-0.6	<0.01
	H_2	0.8-2.0	1
	CO	0.03-0.4	0.04
	CH_4	0.01	2
	$N_2/Ar/O_2$	0.03-0.6	1.3
Oxyfuel	SO_2	0.5	<0.01
	NO_x	0.01	<0.01
	$N_2/Ar/O_2$	3.7	4.1

The other important CO_2 behaviour, is maintaining its pressure during depressurisation (Figure 2-5). This high pressure results in having a high driving force on the crack mouth for crack propagation in a leakage scenario (Leis, Eiber et al. 1998; Chahardehi 2011). At high pressure, supercritical CO_2 behaves as a liquid, and has a liquid-like density, but it yields a very large volume of gas when its pressure is lowered. Depending on its impurities, the temperature can be as low as -50°C which is far below a normal pipeline operating temperature.

[2] IGCC: Integrated Gasification Combined Cycle

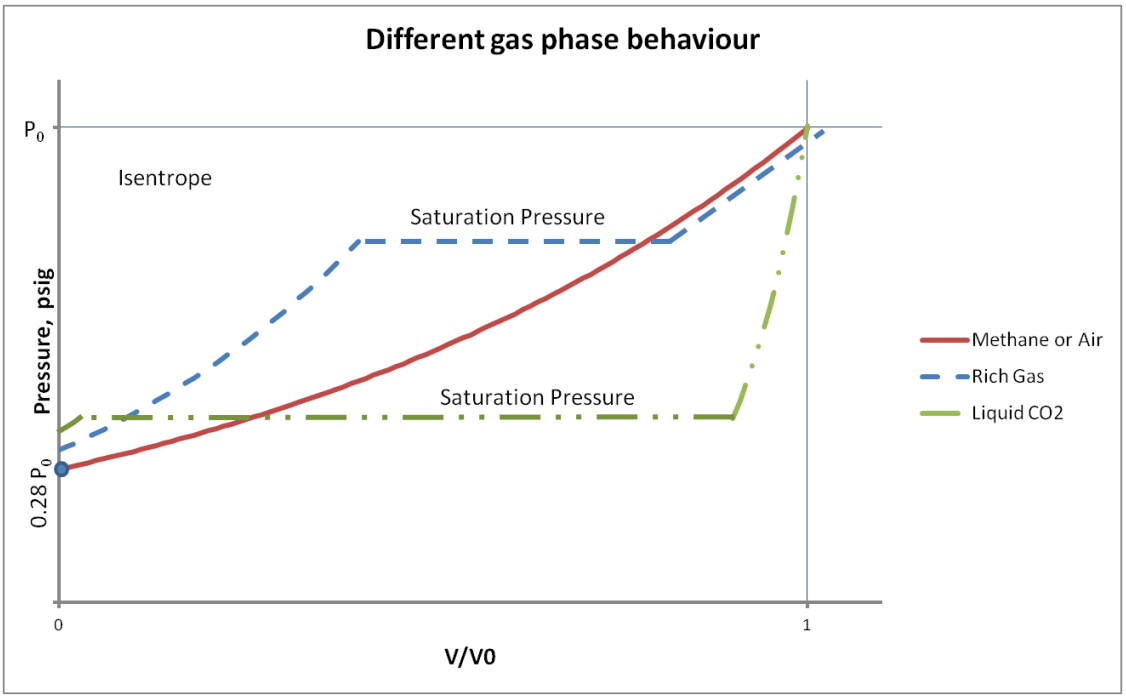

Figure 2-5 Depressurisation behaviour of different gases (Leis, Eiber et al. 1998)

The most important parameters in designing pipelines are the pressure and temperature of the conveying media. Other parameters such as properties of the fluid, the elevation and slope of the terrain, and dynamic effects such as live and dead loads, earthquakes, waves and thermal expansion and contraction, should also be considered. Pressure ranges of existing CO_2 pipelines are from 1250 to 2200 psi, since most natural gas pipelines operate at pressures at or below 1200psi. CO_2 is generally transported at pressure and temperature ranges between1250 psi (86.1 bar) to 2200 psi (151.6 bar) and 12.7°C to 43.3°C (Mohitpour, Golshan et al. 2007). The selection of upper and lower pressure and temperature limits for designing CO_2 pipelines is briefly explained in Table 2-2 (Farris 1983).

Table 2-2 CO_2 pipeline design criteria selection basis

Design Criteria Limits	*Selection basis*
Upper Pressure	ASME –ANSI Flange Rating
Upper Temperature	Compressor Discharge and Pipeline coating
Lower Pressure	Phase behaviour of CO_2
Lower Temperature	Winter ground temperature

The operating pressure calculation and consequent wall thickness of gas transmission pipelines can be obtained from ASME B31.8 (ASMEB31.8 2012):

$$P = (\frac{2St}{D}) \times F \times E \times T \quad (2\text{-}1)$$

Where P is the design pressure (Mpa), S is the specified minimum yield strength (Mpa), t is the nominal wall thickness (mm), D is the nominal outside diameter (mm), F is the design factor, E is the longitudinal joint factor and T is the temperature derating factor. For F, E and T values, different tables are presented in the standard.

For countries such as the UK, that have many coal powered plants, another solution to reduce CO_2 emissions is coal gasification. Figure 2-6 illustrates the process of coal gasification. Instead of burning coal directly and making steam then running a steam turbine (traditional coal powered plants), Syngas can be burned as fuel in a gas turbine that drives an electric generator. Syngas is primarily hydrogen and carbon monoxide and is one of the gasification's products. Coal is burnt with oxygen and after the separation of sulphur and other unwanted products Syngas and hydrogen are generated. In a combined cycle power plant, the efficiency can be doubled when compared with conventional power plants. The other important advantage of implementing this technology is having concentrated CO_2 in the exhaust gases, which makes the capture process much easier and less expensive.

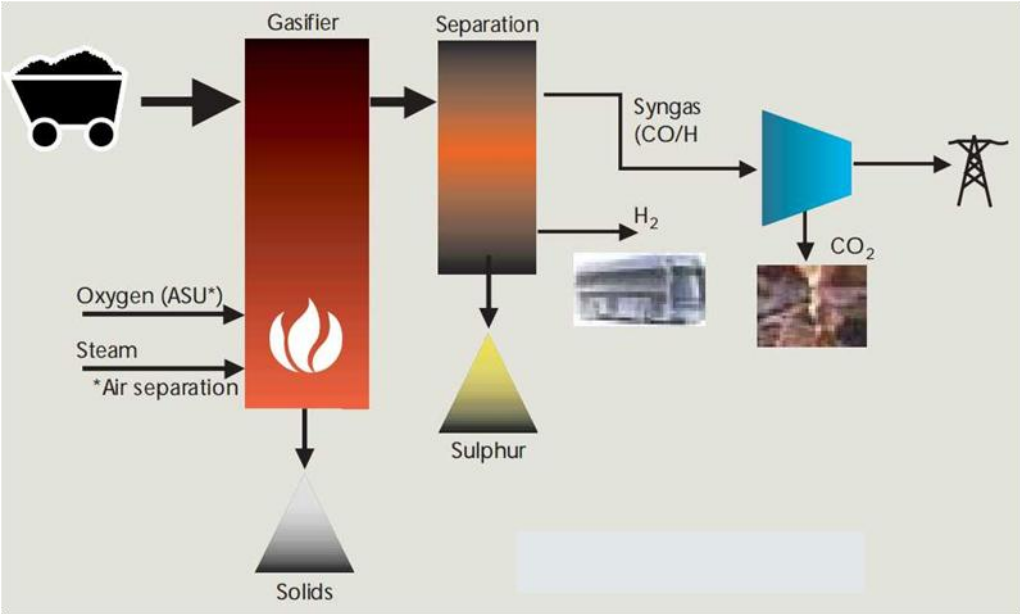

Figure 2-6 Coal gasification

(WBCSD 2005)

2.2 Fracture Mechanics

The study of the propagation of cracks in materials in the field of mechanics has been defined as fracture mechanics. An analytical and numerical solid mechanics tool is used for the calculation of crack driving force. Also materials' resistance to fracture characterisation is the experimental field of this science.

2.3 Stress Intensity Factor

In a homogeneous linear-elastic body, the Stress Intensity Factor (SIF) can be defined as the magnitude of the elastic stress field singularity. The SIF is a function of crack length, applied force and specimen geometry. It describes the crack tip stress field. K_{mat} or material fracture toughness is a material property and the relation of K (SIF) and K_{mat} is similar to σ and σ_y. To make it more clear, if a crack in any structure and under any loading condition is under investigation, after finding the proper SIF (K_I or K_{II} or K_{III} or combination of them) and depending on the loading condition, K_{mat} is a benchmark to understand whether the structure fails due to the existence of the crack or not. Similar to simple engineering problems, if the magnitude of stress in a body reaches the yield stress, the body deforms plastically and cannot return to its elastic region. During analysis of the SIF, the critical K is represented as K_{IC} and should be compared to K_{mat}.

As illustrated in Figure 2-7, analysis of fracture mechanics is described as three pure modes (or a combination of them). In mode one (I) or "opening mode" the displacement of crack surfaces due to normal stresses, are perpendicular to the plane of the crack. In forward shear or mode two (II) or "sliding mode", the displacement of crack surfaces is in the plane of the crack and normal to the crack front line. The "tearing mode" or mode three (III) is caused by anti plane shear and the crack surface displacements are parallel to the crack front line and in the plane of the crack. The SIF represented by capital K. The K subscripts I, II and III stands for different loading conditions.

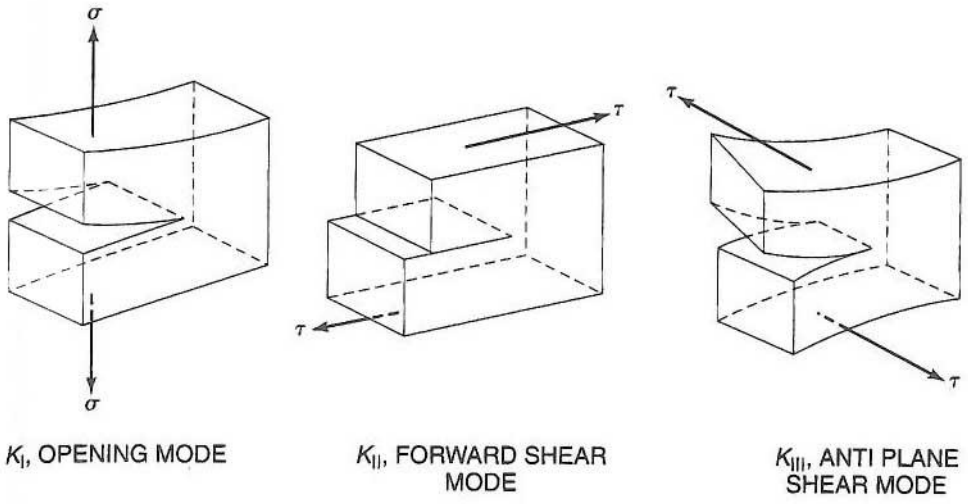

Figure 2-7 The three modes of loading
(Sanford 2003)

In an arbitrary body with a through thickness crack loaded by arbitrary mode I loading (Figure 2-8), the in plane crack tip stresses can be expressed as:

$$\sigma_{ij} = \frac{K_I}{\sqrt{2\pi r}} f_{ij}(\theta) \tag{2-2}$$

Where, σ_{ij} are the stresses on an element in front of the crack at a distance r and at angle θ from the crack front line (tip). $f_{ij}(\theta)$ is known as the geometry function and is related to the geometry of the cracked body. K_I is the mode one SIF. Similar solutions with different geometry functions are obtained for the other modes with SIFs K_{II} and K_{III}.

For many cases $K_I=\sigma\sqrt{\pi a}$, apart from finite size correction factors. For a central crack in an infinite plate under pure tension as depicted in (Figure 2-8), the crack tip stresses can be written as:

$$\sigma_x = \sigma\sqrt{\frac{a}{2r}}\cos\frac{\theta}{2}\left[1-\sin\frac{\theta}{2}\sin\frac{3\theta}{2}\right] \tag{2-3}$$

$$\sigma_y = \sigma\sqrt{\frac{a}{2r}}\cos\frac{\theta}{2}\left[1+\sin\frac{\theta}{2}\sin\frac{3\theta}{2}\right]$$

$$\tau_{xy} = \sigma\sqrt{\frac{a}{2r}}\sin\frac{\theta}{2}\cos\frac{\theta}{2}\cos\frac{3\theta}{2}$$

$\sigma_z = 0$ Plane stress

$\sigma_z = \nu(\sigma_x + \sigma_y)$ Plane strain

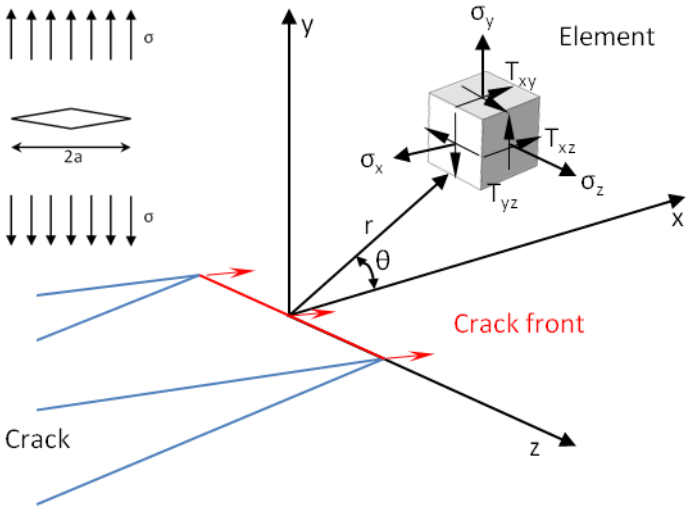

Figure 2-8 Element of arbitrary body in front of crack

Figure 2-9 illustrates the distribution of σ_y as a function of r at θ=0. It is a central crack in an infinite plate under pure tension. According to eq. (2-2) and Figure 2-9, for small r, the stress σ_y approaches infinity. This condition is called

“Singularity at crack tip”. In reality, due to plastic deformation of the crack tip, it cannot occur and the crack tip stresses remain finite. Also for very large r, it shows that the stress σ_y approaches zero, while in reality it should go to σ (pure tension). The reason is that eq. (2-6) is sufficiently accurate for the area in the vicinity of the crack tip whereas further away the other, larger terms will have to be taken into account, as in eq.(2-4).

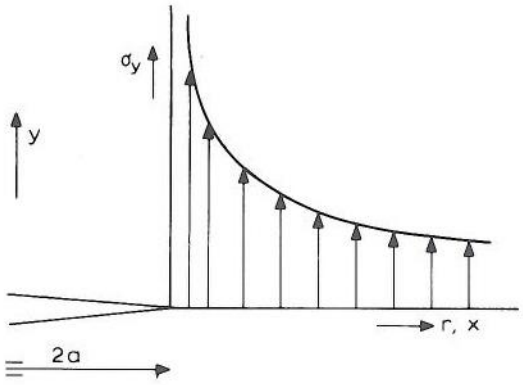

Figure 2-9 Singularity on crack tip
(Sanford 2003)

$$\sigma_{ij} = \frac{K_I}{\sqrt{2\pi r}} + 2^{nd}\,term + 3^{rd}\,term + ... \qquad (2\text{-}4)$$

In a pure elastic crack, stress singularity at the crack tip is dominant. Due to the yield stress of materials especially in metals, for stresses above the σ_y the material deforms plastically. So stress singularity cannot exist. A rough estimation of the crack plastic zone has been calculated as eq.(2-5).

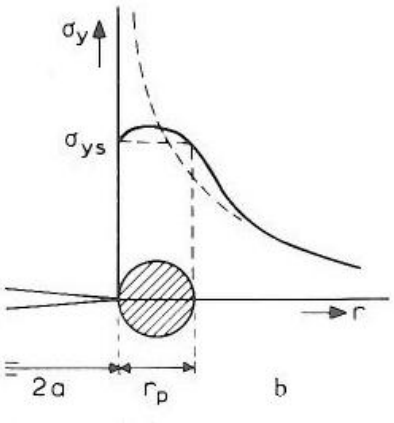

Figure 2-10 Crack tip plastic zone
(Sanford 2003)

$$r_p = \frac{K_I^2}{2\pi\sigma_y^2} = \frac{\sigma^2 a}{2\sigma_y^2} \tag{2-5}$$

Figure 2-10 illustrates an approximate stress distribution at the crack tip with a plastic zone. Irwin argues that the crack tip plasticity causes lower stiffness and larger displacements than in the elastic case (Irwin 1960). Also the occurrence of plasticity lets the crack behave as if it were longer than its physical size.

There are many resources available to find the SIF of a known geometry and loading condition. Handbook of “The stress analysis of cracks” by (Paris, Tada et al. 2000) or “Stress intensity factors” by (Murakami 1987) are well known resources to find solutions for SIF. Most of the research and findings are for known geometries but for real problems, analytical solutions such as finite elements analysis are still the most reliable approaches.

For the case of a longitudinal crack in a pipe under internal pressure, the only available solution has been presented by Folias, erdogan and Tada (Paris, Tada et al. 2000). As illustrated in Figure 2-11, the longitudinal crack length is shown at 2a and the pipe is under an internal pressure loading of p, with the pipe thickness depicted as t.

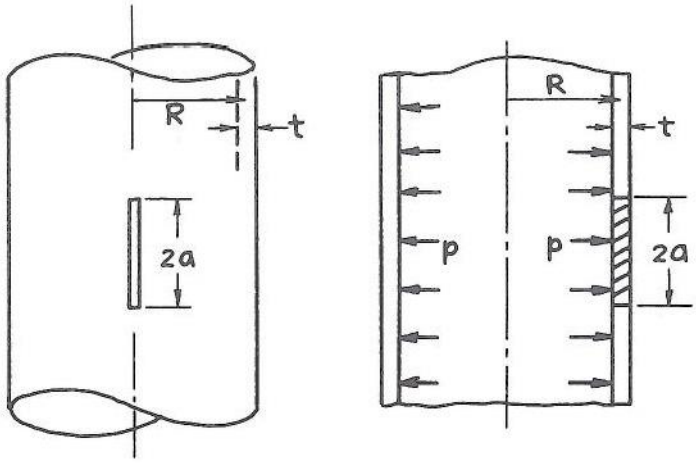

Figure 2-11 Longitudinal crack in a pipe
(Paris, Tada et al. 2000)

The SIF for this scenario is as follows:

$$K_I = \sigma\sqrt{\pi a}.F(\lambda) \tag{2-6}$$

Where σ and F(λ) are:

$$\sigma = P\frac{R}{t} \tag{2-7}$$

And

$$F(\lambda) = (1+1.25\lambda^2)^{0.5} \longrightarrow 0 < \lambda \le 1 \tag{2-8}$$

$$F(\lambda) = 0.6 + 0.9\lambda \longrightarrow 1 \le \lambda \le 5$$

$$\lambda = \frac{a}{\sqrt{Rt}} \tag{2-9}$$

Where σ is the hoop stress due to the internal pressure P, and R defines the mean radius of the pipe.

Harris presented the SIF when crack length tends towards infinity. (Harris 1967) as:

$$a \to \infty, K_I \to \sigma\sqrt{R}\left(\frac{\sqrt{27\pi}}{2}.\frac{R}{t}\right) \tag{2-10}$$

Figure 2-12 illustrates the normalised SIF for different thicknesses in a 24 inch (609.6mm OD) pipe. The pipe is under an internal pressure of 15 MPa and its crack is located longitudinally. The pipe schedule (designated wall thicknesses, STD, XS, X100…) is one of the most important design factors in pipeline design that not only has an influences on pipe hoop stress but also changes its SIF.

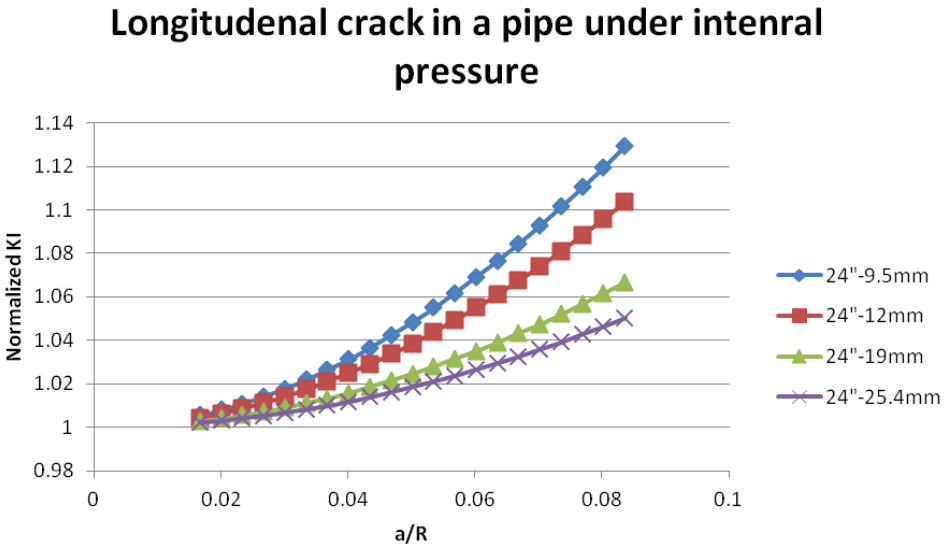

Figure 2-12 Thickness effect on SIF for a longitudinal crack in a pipe under internal pressure

2.4 Energy criterion and J-Integral

Linear elastic fracture mechanics (LEFM) is subject to the behaviour of bodies containing cracks with limited plasticity at their crack tip. It has been argued that this region is very small and the rest of the behaviour is completely elastic (2.3 Stress Intensity Factor). This approach normally cover a wide variety of problems, notably fatigue problems for which the applied loads are generally less than 30% of yield stress. In small scale yielding conditions (no plasticity on crack tip) crack tip conditions can be characterised by a single parameter such as K, J or CTOD which are used as geometry independent fracture criteria. In the presence of excessive plasticity, characterising crack tip conditions by a single parameter does not work as fracture toughness depends on the geometry and size of the test specimen.

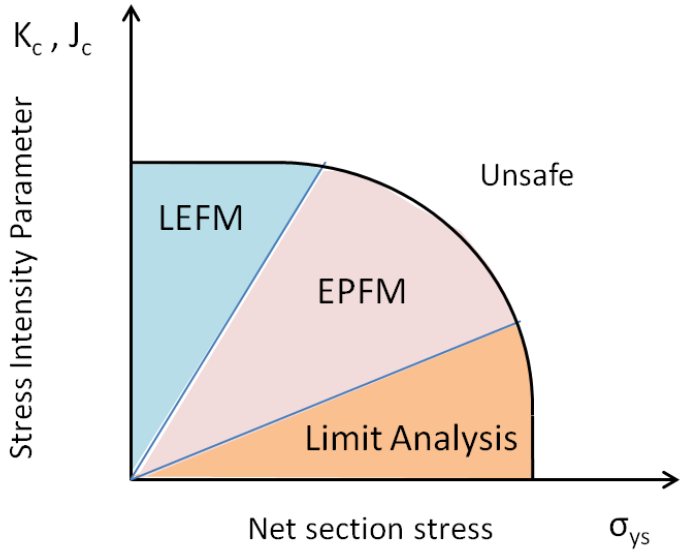

Figure 2-13 Failure Analysis Diagram for a ductile material (Sanford 2003)

As illustrated in Figure 2-13, there is a region between plastic collapse and linear elastic fracture mechanics (LEFM) that has been known as elastic plastic fracture mechanics (EPFM). J-integral is an approach to obtain the stress intensity parameter for this region. Before explaining the J-integral a brief overview of the Griffith energy criterion is essential.

2.4.1 The Griffith criterion (Energy)

Griffith in 1921 stated that crack propagation will occur if the energy released upon crack growth is sufficient to provide all the energy that is required for crack growth. Consider an infinite cracked plate of unit thickness with a central transverse crack of length 2a, both ends of the plate are fixed and the plate is stressed to a stress of σ.

The condition for crack growth is:

$$\frac{dU}{da} = \frac{dW}{da} \tag{2-11}$$

Where U is the elastic energy and W the energy required for crack growth. Based on calculations of the stress field for an elliptical flaw by Inglis (Inglis 1913), Griffith calculated dU/da as:

$$\frac{dU}{da} = \frac{2\pi\sigma^2 a}{E} \tag{2-12}$$

Per unit plate thickness, where E is Young's modulus. As usual, the derivative of elastic energy with respect to crack length is replaced by G:

$$G = \frac{\pi\sigma^2 a}{E} \tag{2-13}$$

G is the elastic energy release rate or the crack driving force, and its dimension is energy per unit plate thickness and per unit crack extension. The crack resistance R, has been defined as dW/da (2-11). So G must be at least equal to R before crack propagation can occur. G_{Ic} can be defined as a critical value, called the critical energy release rate, and can be determined by measuring the critical stress σ_c required to fracture a plate with a crack of size 2a.

$$G_{Ic} = \frac{\pi \sigma_c^2 a}{E} \rightarrow \sigma_c = \sqrt{\frac{E G_{Ic}}{\pi a}} \tag{2-14}$$

It is important to know if sufficient energy for crack propagation can be provided; the crack will not propagate unless stress intensity of the plate at the crack tip has reached its critical value (material fracture toughness). However the energy criterion says:

$$G = \frac{K^2}{E} \tag{2-15}$$

Since the SIF has been defined as $\sigma\sqrt{\pi a}$, in the case of plane strain, this leads to:

$$(1-\nu^2)\frac{K_I^2}{E} = G_I \rightarrow (1-\nu^2)\frac{K_{Ic}^2}{E} = G_{Ic} \tag{2-16}$$

This is the relation between the energy release rate and SIF for plane stress and plane strain condition.

2.4.2 J-Integral

The load displacement diagram for a nonlinear elastic material (but still elastic) has the appearance shown in Figure 2-14. As the energy available for the crack extension can be defined in terms of area in the load displacement diagram, U, the area under the curve is the strain energy. The area above the curve, called the complementary strain energy U*, is related to the potential energy Π.

$$U^* = P\delta - U = -\Pi \tag{2-17}$$

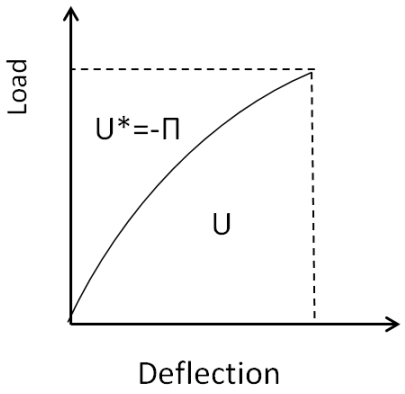

Figure 2-14 Energy components in a non linear elastic material

The potential energy of a two dimensional body of area A and surface tractions of T_i is given by:

$$\Pi = \int_A W dA - \int_\Gamma T_i u_i ds \tag{2-18}$$

Where Γ is the portion of bounding surface and W is the strain energy density defined as:

$$W = \int \sigma_x d\varepsilon_x \text{ and } W = \int \tau_{xy} d\varepsilon_{xy} \tag{2-19}$$

Where the strain energy density is calculated based on deformations resulting from unidirectional normal and shear stresses acting on a differential element of elastic material. Similar to linear elastic cases, an energy release rate for nonlinear elastic bodies can be defined as the area on the load displacement diagram between crack areas A and A+dA, as shown in Figure 2-15. The nonlinear energy release rate J, for constant load and constant displacement has been defined as:

$$J = \left| \frac{\partial \Pi}{\partial A} \right| \tag{2-20}$$

For the special case of a linear elastic body that Pδ=2U, substituting in Eq. (2-17) then U=-Π. From Equations (2-12) and (2-15) :

$$J = \left|\frac{\partial \Pi}{\partial A}\right| = G = \frac{K^2}{E'} \tag{2-21}$$

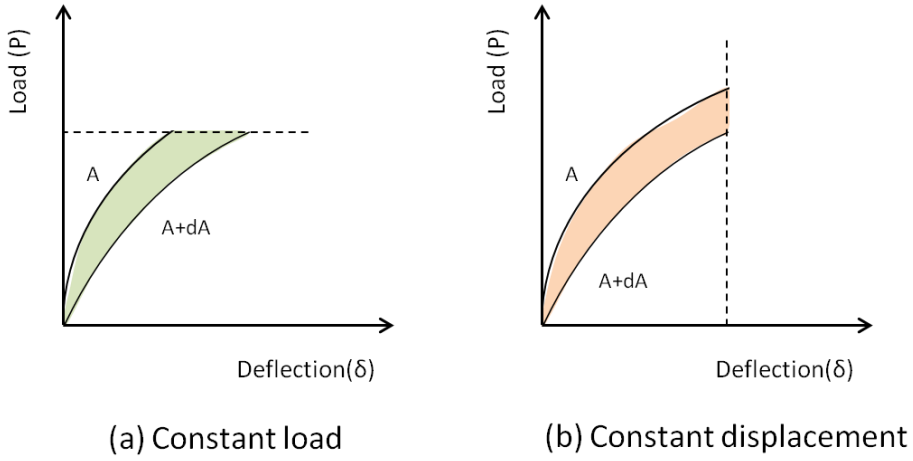

Figure 2-15 Available energy for crack extension in a non linear elastic body under different conditions

Alternatively, by differentiating Eq.(2-18) that is a formal definition of J:

$$J = -\frac{\partial \Pi}{\partial A} = \frac{1}{B}\int_A \frac{dW}{da} dA - \frac{1}{B}\int_\Gamma T_i \frac{du_i}{da} ds \tag{2-22}$$

Also this equation can be written as (Kanninen and Popelar 1985)

$$J = \int_\Gamma (W dy - T_i \frac{du_i}{dx} ds) \tag{2-23}$$

2.5 Plane Stress and Plane Strain

The importance of understanding plane stress and plane strain in fracture mechanics problems is clear. In plane stress the stress normal to plate plane is zero (σ_z=0). Very thin plate (especially in aviation design) loaded only by forces or displacements in the plane of the plate, is a good example of plane stress problems. When the value of strain normal to plate plane is zero it is a plane strain condition (ϵ_z=0). For these two conditions, the modulus of elasticity has been defined as:

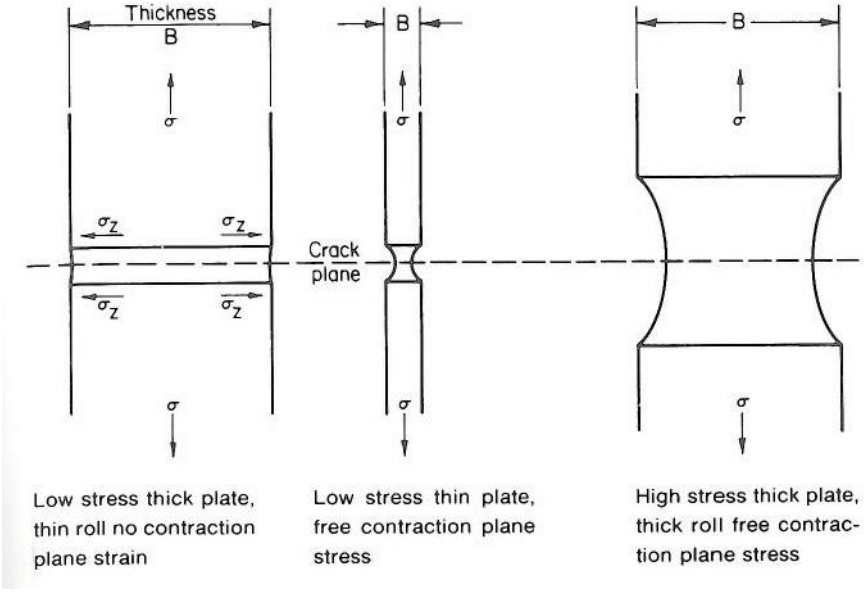

Figure 2-16 Plane strain (left), plane stress (centre & right) (Broek 1986)

$$E' = E \quad for\ plane\ stress\ condition \tag{2-24}$$

$$E' = \frac{E}{1-\vartheta^2} \quad for\ plane\ strain\ condition \tag{2-25}$$

To have a valid fracture toughness test, the specimen has to follow plane strain criteria to have the minimum plastic zone size. From Irwin's model (Irwin

1957), the size of the plastic zone in the plane strain condition can be calculated from equation (2-26) .

$$r_p = \frac{1}{3\pi}\left(\frac{K_{Ic}}{\sigma_{ys}}\right)^2 \qquad (2\text{-}26)$$

For an experimental determination of K_{Ic} of the material, by taking the specimen thickness to be much larger than the plastic zone size, the plane strain condition can be assured. It is recommended that specimen thickness should be 25 times the plastic zone size.

$$B \geq 25 \times \frac{1}{3\pi}\left(\frac{K_{Ic}}{\sigma_{ys}}\right)^2 \qquad (2\text{-}27)$$

And

$$B \geq 2.5\left(\frac{K_{Ic}}{\sigma_{ys}}\right)^2 \qquad (2\text{-}28)$$

It is clear that the thickness of the plate has a strong influence on fracture behaviour. Actually stress intensity factor (K) is independent of the specimen thickness but on the other hand fracture toughness test and measurement (K_{mat}) depends on the specimen thickness.

When a crack is loaded in a thick test specimen, a small applied load into the crack caused opening of the crack and a small plastic zone forms in front of crack tip. Increasing the load will increase the size of the plastic zone. When load increases to its critical value (that means SIF reaches to the plane strain fracture toughness of material) crack starts extending inside the larger plastic zone. It will continue straight in plane strain condition due to effect of surrounding material on crack tip stresses. In plane stress as the minimum stresses are perpendicular to the crack plane crack tends to grow in 45 degrees and shear lips occur.

2.6 Current State-of the-Art

There is no specific standard for CO_2 pipelines' design and operation. In the UK most of the potential storage reservoirs are located in the North Sea, so the design of future CO_2 pipelines has a special focus on offshore pipelines. In gas industries less work has been conducted on fracture propagation in offshore pipelines. For gas pipelines the methods for calculating fracture propagation and fracture arrest conditions are conservative when applied to offshore pipelines. They will be more complicated when designing CO_2 pipelines for offshore use. The interaction of escaping fluid with the ocean water reduces the hoop stress in the pipe wall (Race, Seevam et al. 2007). As mentioned before the challenges on designing CO_2 pipelines are that they have to work in much higher pressure, and CO_2 phase behaviour during decompression and possible level of impurities are different compare to natural gas pipelines (Figure 2-4 and Figure 2-5).

2.6.1 Fracture mechanics in pipelines

Different research efforts have been conducted regarding pipeline fracture analysis which can be categorised as follows: (a) theoretical work to calculate fracture-fatigue quantities parameters such as Stress intensity factor, Crack opening displacement or J-integral, which are representative of external load and flow geometry.; (b) theoretical and experimental work aimed at the development of proper models, criteria or theories for fatigue crack propagation, corrosion fatigue, stress corrosion cracking and fracture in pipeline materials ; (c) experimental work mostly to verify and demonstrate the related theories in pipes, including crack morphology studies; and (d) dynamics of crack propagation in pipelines. Most of the theoretical work, especially on pipelines, has been on the elastic solutions for through cracks in shells and part-through cracks in pipelines. However, in the presence of relatively large-scale plastic deformations, the effect of specimen and crack geometry, elastic-plastic stress-strain behaviour of material, and the nature of the external loads on fracture

initiation and propagation are far too great to permit the treatment of the phenomenon by means of a single parameter (such as K_{IC}, G_{IC} or J_{IC}) (Erdogan 1982).

2.6.2 Existing methods for the evaluation of fracture toughness in pipeline industries

❖ ***Introduction***

Most pipe manufacturers follow the current standards, such as API 5L, ISO 3183 or DNV OS-F101, for their fracture toughness test requirements. On the other hand, customers' lack of knowledge and the ambiguity of CO_2 behaviour do prevent them from asking manufacturers to do more specific tests on requested pipes. The Battelle two curve method, Charpy-V-notch (CVN) impact test and Drop Weight Tear Test (DWTT) are common requirements to control fracture initiation and prevent propagation. For instance the Nippon Steel Corporation (Nippon 2010) apply CVN and DWTT tests during production for each heat or one out of fifty or a hundred pipes. They also use the CTOD test only for qualification, because it is not a suitable test (in terms of cost and time) for frequent use during mass production (Aihara 2010).

In most of the current fracture toughness tests, the specimen is broken by the impact of a heavy weight. The energy needs for this purpose, the so-called propagation energy, could be divided to "initiation energy" and "impact energy". To reduce the error and deviation from actual fracture toughness of material, initiation energy should be minimised. Statically pre-cracked, chevron notch, embrittled notch and back slotted are the recommended solutions for reducing initiation energy to be as low as possible.

The Charpy V-notch test is not suitable for fracture toughness measurement, but it is the most common test requirement in standards and consequently customer requirements. The weakness of the Charpy test appeared with the manufacture of high strength materials. CVN energy only

correlated to full crack burst test results up to materials with X70 grade. However, some correction factors were defined to solve this problem but accuracy of the results in comparison with full burst tests were not acceptable (Hara, Shinohara et al. 2008). This will be more explained in greater detail in this chapter.

Using high strength line pipe steel needs, there to have been extensive studies on cracks in the pipe body even if brittle fractures occur at welds, or running ductile fractures occur in the pipe body. The DWTT is one of the major test methods used to evaluate crack arrest-ability, brittle and running ductile fractures, and the most important one: ductile-brittle transition temperature (Hara, Shinohara et al. 2008).

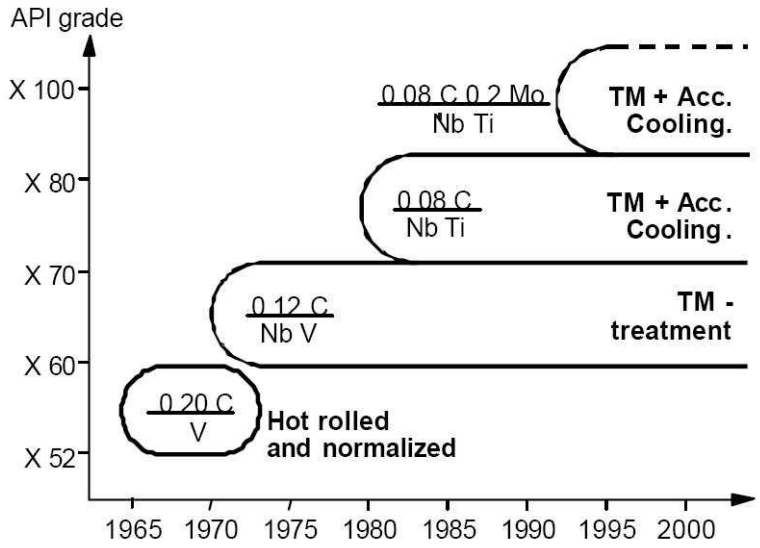

Figure 2-17 Development of high strength steels
(Hillenbrand, Gras et al. 2001)

To transport captured CO_2 within pipelines there are two obvious possibilities. The first is assessment and inspection of existing pipelines to transport captured CO_2 with all possible impurities under high pressure, and the second is to design new pipelines. Due to the high pressure transportation of CO_2 new pipeline material should be selected from grades greater than X80 (Figure 2-17). For such high strength steel pipes, the fracture propagation resistance cannot be specified by relying on Charpy-V energy values only.

❖ *Weakness of existing methods to measure fracture toughness for high grade materials*

Material fracture resistance, so-called fracture toughness, is an important parameter to have in a safe design against ductile fracture propagation. Ductile fracture propagation is a phenomenon that can affect the pipeline over a long distance with serious economic and safety consequences. The Battelle two curve and CVN tests are conventional methods to measure fracture toughness. Charpy's intrinsic limitations to measure fracture propagation resistance for high strength steel pipes in severe conditions such as low temperature, rich gas, high pressure, etc. will be discussed in the following paragraphs (Mannucci, demofonti et al. 2001).

Maxey presented the Battelle two curve which is generally considered to be the most reliable empirical method for ductile fracture prevention (Maxey, Kiefner et al. 1976). The two curves are the Driving Curve which represents gas decompression and the Resistance Curve which depicts dynamic crack propagation resistance. The thermodynamic property of the fluid is the dominant parameter for determining the pressure trend at the crack tip regulated by the decompression process of gas on the flaw.

In the Resistance curve, the crack speed V_f depends on flow stress σ_0 and fracture resistance R, where constant value C for No backfill is 2.75, for Soil backfill is 2.34 and for Sea backfill is 3.79:

$$V_f = C\frac{\sigma_0}{\sqrt{R}}\left(\frac{P}{P_a}-1\right)^{\frac{1}{6}} \qquad (2\text{-}29)$$

P_a is the pressure arrest level. This method requires the determination of fracture velocity variation with pressure. For pressure levels higher than the arrest pressure P_a, the potential of propagation or arrest could be determined by comparing the relative positions of two driving and resistance force curves.

The relation between K_{IC} and CVN per unit area A_C was found to be:

$$K_{IC}^2 = 12\frac{CVN.E}{A_c} \qquad (2\text{-}30)$$

As depicted in Figure 2-18, the predicted CVN energy by the Battelle two curve method versus actual CVN does not correspond to high strength steel pipes. It also could be concluded that equation (2-29)) gives a reliable K_{IC} only for steel pipe grades lower than X80. A correction factor of 1.43, was proposed by CSM (Italy) in order to properly modify the Battelle two curve arrest predictions for X80 (Demofonti, Mannucci et al. 2007).

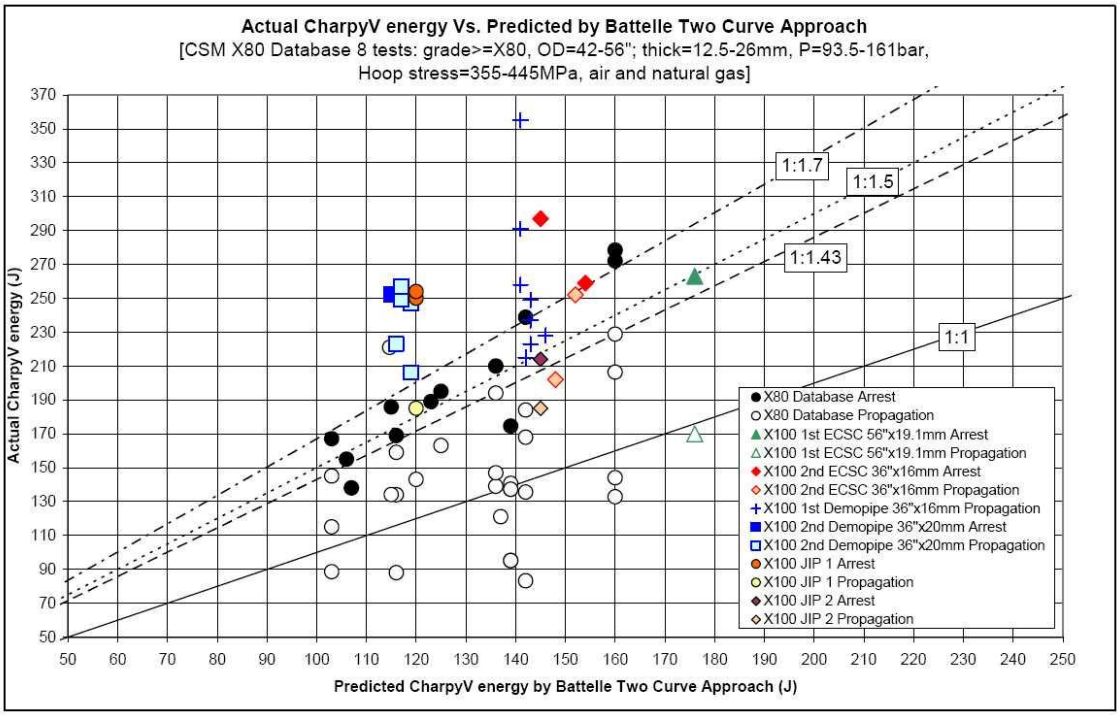

Figure 2-18 CVN energy, Actual vs. Predicted (CSM's database) (Demofonti, Mannucci et al. 2007)

The Maxey approach, through an empirical correlation relates K_{IC} as the plane-stress fracture resistance R of the pipe to CVN energy. As discussed before, this approach did not give the correct results for high strength steel pipe in comparison with full burst test results.

The CVN test has some disadvantages when measuring the fracture toughness of a material. Very small sizes of specimen, specially ligaments, do

not replicate the steady state propagation. The measured total energy to failure from the CVN test consists of two parts: initiation of crack and propagation. Most of this value is used to initiate the crack!

There are alternative solutions for the Charpy parameter: Absorbed energy in the DWTT, Absorbed propagation energy in a DWTT, Absorbed propagation energy in Charpy test, Two parameter approach (Rc and Sc) and Crack Tip Opening Angle (CTOA) all of which will be briefly explained.

In the DWTT specimen, which was the first full thickness specimen test and identified the ductile brittle transition temperature of steel, Wilkowski (Wilkowski 1979) presented an imperial expression to correct the CVN results.

$$(\frac{E}{A})_{DWTT} = 3(\frac{E}{A})_{CharpyV} + 63.04 \quad (2\text{-}31)$$

Where E is total fracture energy (Joule) and A is fracture area (cm^2).

Full pipe thickness and longer ligaments are the power points of the DWTT, but on the other hand the relative role of the initiation and propagation energy is not clear. Its linear correlation with CVN energy deviates from linearity for high grade carbon steels. As depicted in Figure 2-19, this deviation starts from $(E/A)_{CharpyV}$>125 joule/cm^2.

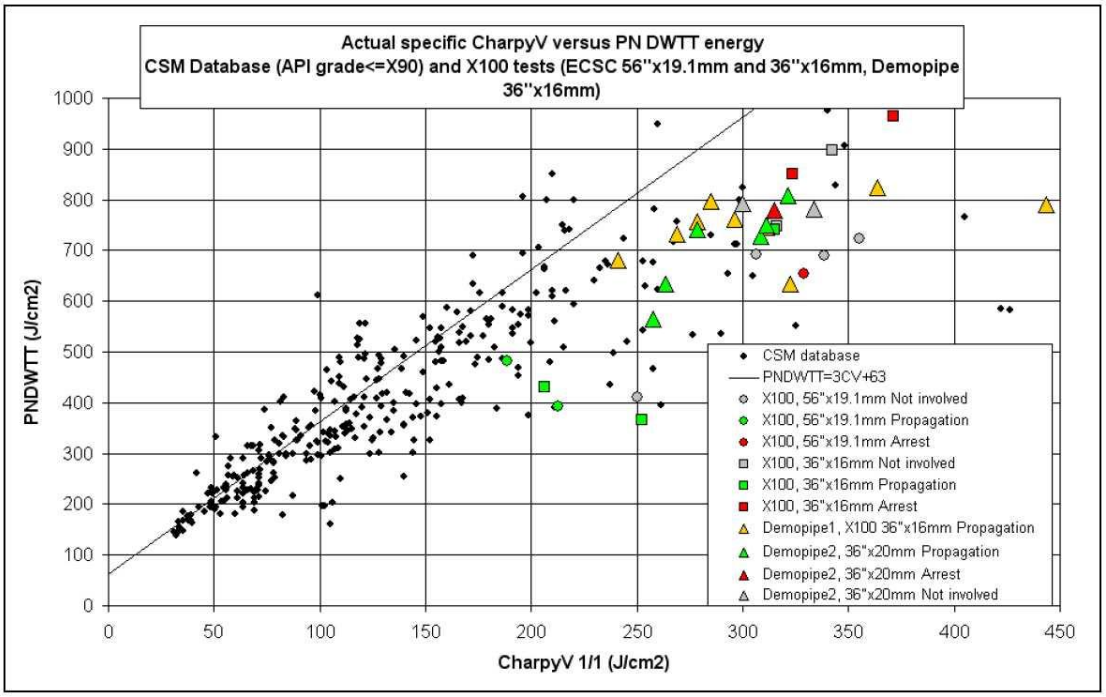

Figure 2-19 CVN and DWTT specify energy correlation (CSM database) (Demofonti, Mannucci et al. 2007)

Many works have been conducted on the notch configuration of DWTT specimens to minimise the fraction of the impact energy caused by crack initiation on the specimen as it does not play any part during the fracture propagation. Some of these techniques are: the DWTT specimen with embrittled notch(Wilkowski, Maxey et al. 1977), the statically precracked DWTT specimen (Wilkowski 1981), the chevron notched DWTT specimen (Maxey and Barnes 1990; Vogt and Junker 1994) and back slotted DWTT specimen(Pussegoda and Malik 1999). The main concept is to minimise the initiation energy so that the total measured impact energy can present an adequate estimate of the propagation energy (Demofonti, Mannucci et al. 2007).

In 1977, Wilkowski presented a prediction method, the so-called “Wilkowski 1977 prediction method” to predict propagation or arrest events in full scale burst tests when using DWTT propagation specific energy instead of Charpy-V energy in the fracture resistance measurement of material (Wilkowski,

Maxey et al. 1977). The equivalent Charpy-V energy from DWTT energy is presented as:

$$(\frac{E}{A})_{Charpy(W1977)} = \frac{175[(\frac{E}{A})_{PN-DWTT}]^{0.358} - 1800}{3} \quad (2\text{-}32)$$

Where the two parameters are, Wilkowski 1977 Charpy-V minimum arrest toughness to be used in conjunction with the Battelle two curve method (ft-lb/in^2) and total pressed notch DWTT energy per unit area (ft-lb/in^2).

In 2000, several full scale burst tests on X70 and lower were performed but Wilkowski 1977 prediction was not able to distinguish between arrest and propagate. So Wilkowski offered a correction factor of 1.3 to his previous formula (Wilkowski, Rudland et al. 2000). Then Wilkowski 2000 DWTT minimum arrest toughness is presented below:

$$(\frac{E}{A})_{PN-DWTT(W2000)} = \frac{1}{1.3}[\frac{3(\frac{E}{A})_{CVN\min} + 1800}{175}]^{\frac{1}{0.385}} \quad (2\text{-}33)$$

Even though Wilkowski 2000 equation is better than Charpy-V based equations but for pipe grades X80 and higher, the results are fairly able to capture the trend of data versus full burst test results.

Later Priest from British Steel (Priest and Holmes 1981) proposed a linear dependent on test specimen ligament length and specific fracture energy for Three Point Bend (3PB) specimens. Priest used two parameter approach to define his equation. R_c and S_c represent the energy necessary for formation of the two new fracture surfaces and denote the average energy expended for plastic deformation of the zones adjacent to the fracture surfaces.

$$\frac{E_t}{A} = R_c + S_c(W - a_0) \quad (2\text{-}34)$$

Where E_t is the total energy absorbed by the test specimen and A is the initial fracture area, W is the specimen width and a_0 is the notch depth. Using

two sets of 3PB specimens with two different ligament lengths broken using a dynamic load, R_c and S_c could be measured and steel toughness evaluated.

Priest also presented the energy per unit area required for a fracture in a pipeline, where the plastic deformation is limited by the pipe diameter and not by the ligament size (Priest and Holmes 1988):

$$\frac{E_t}{A} = 2R_c + ZS_cD \tag{2-35}$$

R_c and S_c are calculated from laboratory tests, D is the pipe diameter and Z is a constant equal to the proportion of the diameter which is plastically deformed adjacent to the crack. Using the CSM database for a 56" diameter pipe, Z is approximately equal to 0.3D. As there is no database for the experimental dimension of the plastic zone associated with the crack in propagating test pipes, Z could not be calculated easily and this is the weakness of this method.

The Charpy-V test instrument, in its early stage of development, was calibrated with relatively low toughness steels. For such steels the fracture process shows little resistance to the initiation of ductile fracture propagation, so the total absorbed energy represents well the fracture propagation resistance of the material. On the other hand, for the high strength steels a large portion of the energy absorbed during impact is spent on the initial deformation phase and the initiation of the crack.

Leis define a correction factor for the total energy absorbed by Standard CVN to be used in conjunction with the Battelle two curve method (Leis, Eiber et al. 1998). They developed equations as follows:

For $CVN_{test} \geq 95$ Joule

$$CVN_{arrest} = CVN_{BMI} + 0.002CVN_{BMI}^{2.04} - 21.18 \tag{2-36}$$

For CVN_{test} < 95 Joule

$$CVN_{arrest} = CVN_{BMI}$$

Where CVN_{test} is the total absorbed energy in a standard Charpy-V test and CVN_{BMI} is the predicted Charpy-V arrest toughness based on the Battelle Two Curve method.

Later, in 2000, Leis et al.(1988) found that because of significant differences in fracture behaviour between modern high toughness steels and low toughness steels, the Charpy-V test failed to correctly predict arrest toughness. The presented equation (2-36) indicates that the rate of correction drops as toughness increases, whilst there are experimental evidences to the contrary (Demofonti, Mannucci et al. 2007).

2.6.3 Compact Tension test (CT)

The compact tension test is one of the most accurate measurement methods to measure the fracture toughness of materials. API 5L refers to ASTME1290 (2002) for measuring the CTOD and the fracture toughness calculation. In this standard three different alternative specimen designs are presented: Square section SE(B), Compact Tension C(T) and Arc-shaped bend A(B) specimens. For the sake of brevity, measurement of CTOD from the C(T) specimen is described in this section (ASTME1290 2002).

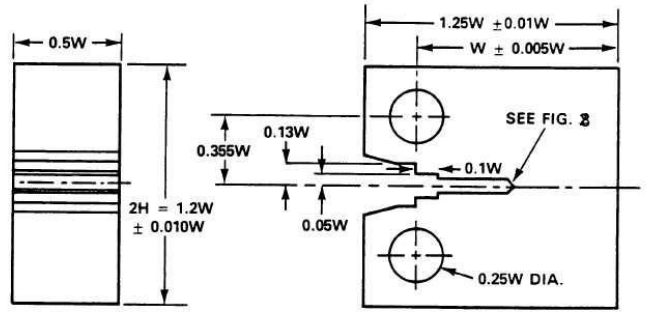

C(T) Specimen for pin of 0.24*W* (+0.000 *W*/−0.005*W*) diameter

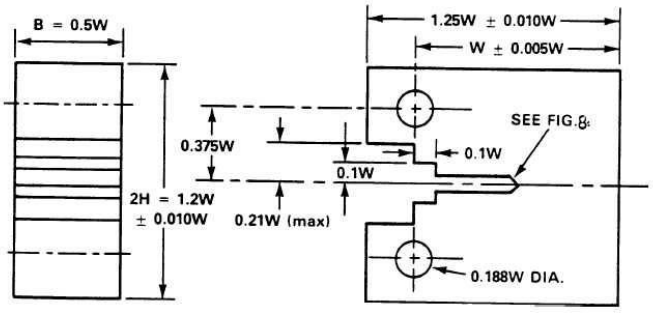

C(T) Specimen for pin of 0.1875*W* (+0.000*W*/−0.001*W*) diameter

Figure 2-20 Alternative CT specimen desgins

(ASTME1290 2002)

The original crack length , a_0 shall be within the range of:

$$0.45W \le a_0 \le 0.70W \qquad (2\text{-}37)$$

The C(T) Specimen shall be pre-cracked in fatigue loading conditions at force values not greater than F_f:

$$F_f = 0.4Bb_0^2\sigma_y/(2W + a_0) \quad (2\text{-}38)$$

Where F_f is the maximum applied force, B is the specimen thickness, b_0 is the original uncracked ligament, σ_y is the effective yield strength, that is $(\sigma_{YS}+\sigma_{TS})/2$, and the values for σ_{YS} and σ_{TS} are determined in accordance with test method E8 (ASTME8 2009). W and a_0 are depicted in Figure 2-20. N, the notch mouth, must not exceed W/16.

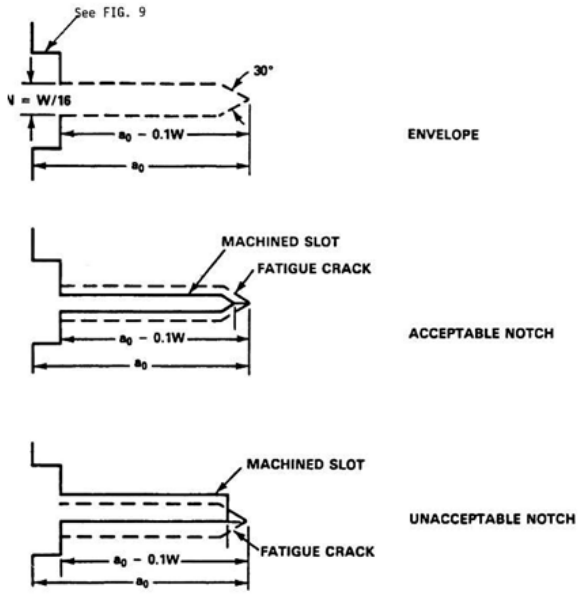

Figure 2-21 Acceptable notch shape

(ASTME1290 2002)

The notch shape should be machined precisely in the centre of two supporting holes (pin holes) and the pre-crack should fall within the depicted envelope (Figure 2-21). The fracture toughness of a material is usually dependent on the crack lane orientation and direction of propagation.

For the SIF dominant in the elastic region of the test we have:

$$K = YP/(B\sqrt{W}) \tag{2-39}$$

Where Y is a function of $\alpha=(a_0/W)$ and is determined as follows:

$$Y = \frac{(2+\alpha)(0.886+4.64\alpha-13.32\alpha^2+14.72\alpha^3-5.6\alpha^4)}{\sqrt{1-\alpha^3}} \tag{2-40}$$

For CTOD, three different δ have been defined as δ_c, δ_p, δ_m. In Figure 2-22 the reading locations of δ are depicted by P and V accordingly. The area under plot of load versus plastic component of clip gauge opening displacement v_p corresponds to v_c, v_u or v_m defined as A_p and will be used in formulae to calculate δ.

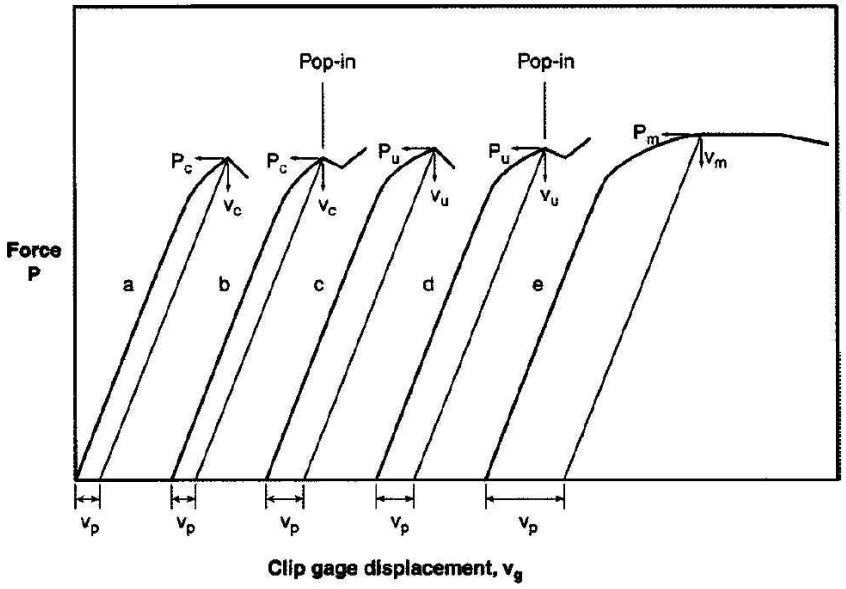

Figure 2-22 Force versus clip gauge displacement

(ASTME1290 2002)

To calculate δ_c, δ_p or δ_m :

$$\delta = (\frac{1}{m\sigma_Y})\{\frac{K^2(1-\nu^2)}{E} + \frac{\eta A_p}{B(W-a_0)(1+\frac{\alpha+z}{0.8a_0+0.2W})}\} \tag{2-41}$$

Where

$$n = 1.724 - \frac{6.098}{R} + \frac{8.326}{R^2} - \frac{3.965}{R^3} \quad (2\text{-}42)$$

And R= σ_{TS}/ σ_{YS}

Interpretation of the results depends on the results' graphic shape and maximum load. In Figure 2-22 typical load-displacement results are illustrated.

If:

$$\frac{f_{\max}}{f_Q} > 1.1 \quad (2\text{-}43)$$

Then critical CTOD and J should be reported. If:

$$\frac{f_{\max}}{f_Q} < 1.1 \quad (2\text{-}44)$$

Then provisional fracture toughness (K_Q) can be presented. If all the requirements to have a valid fracture toughness test have been met, then a valid fracture toughness can be reported. Further explanation about this test and results interpretation can be found in the section on Fracture toughness testChapter 4.

2.6.4 Failure Assessment Diagram (FAD)

During the process of pipe manufacturing for new pipe designs and throughout years of operation, the existence of defects is unavoidable. Levels of acceptance of defects in terms of overall safety are important. Interval inspections and maintenance procedures for pipelines should define a maximum acceptable defect size for pipeline operation conditions. Several methods such as: CTOD, FAD and R6 with different degrees of conservativeness are presented for assessment purposes. There are two known standards on FAD diagram: API 579 “Recommended Practice for Fitness-for-Service” (2000) and British standard BS7910 “Guide to methods for assessing the acceptability of flaws in metallic structure” (2012). An advantage of FAD, is that it takes into the account both failure due to fracture and failure caused by collapse but in a graphical interpretation.

Dowling (Dowling and Townley 1975) and Harrison (Harrison, Loosemore et al. 1976) presented the graphical interpretation of FAD for the first time. As depicted in Figure 2-23, for any structure, if the calculated points are located beyond the curve, the structure is in an unsafe region. The FAD axes are presented as dimensionless parameters known as the Stress Ratio (S_r) and Stress Intensity ratio (K_r). The horizontal axis represents the mechanics of material dealt with stress and loading condition and the vertical axis is the fracture mechanics part of the problem.

The failure assessment curve equation is:

$$K_r = \frac{S_r}{\sqrt{\frac{8}{\pi^2}\ln\sec(\frac{\pi}{2}S_r)}} \tag{2-45}$$

Where

$$S_r = \frac{\sigma}{\sigma_c} \rightarrow and \rightarrow K_r = \frac{K_I}{K_{eff}} \tag{2-46}$$

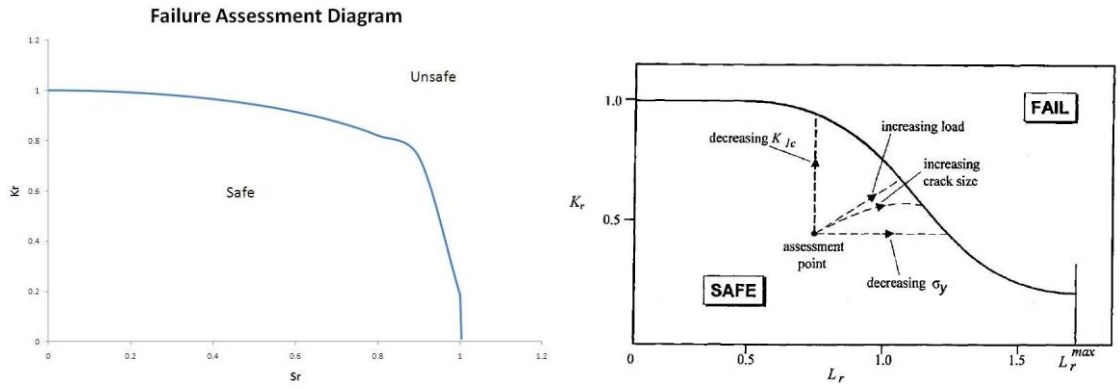

Figure 2-23 First development of FAD (Lidbury and Hirsch 2003; Campbell 2012)

In BS7910, based on the required level of accuracy and the quality of the input data analysis, FAD method is divided into 3 levels. Level 1 as a screening tool is the most simplified one. The assessment of failure due to fracture could be obtained using either the Stress Intensity ratio (K_r) or the CTOD.

$$K_r = \frac{K_I}{K_{mat}}, \sqrt{\delta_r} = \sqrt{\frac{\delta_I}{\delta_{mat}}} \tag{2-47}$$

Where δ_I is the applied CTOD obtained from the CTOD design curve and δ_{mat} is the material toughness measured by the CTOD method. Similarly, K_I is the SIF due to tensile stress and K_{mat} is the material toughness measured through tests. The stress ratio S_r for level 1 is:

$$S_r = \frac{\sigma_{ref}}{\sigma_{flaw}} \tag{2-48}$$

Where σ_{ref} is obtained from appropriate reference solution given in Annex P(2005; BS7910 2012) and: $\sigma_{flaw}=(\sigma_y+ \sigma_{uts})/2$:

For up to 1.2 σ_y (Flow Strength)

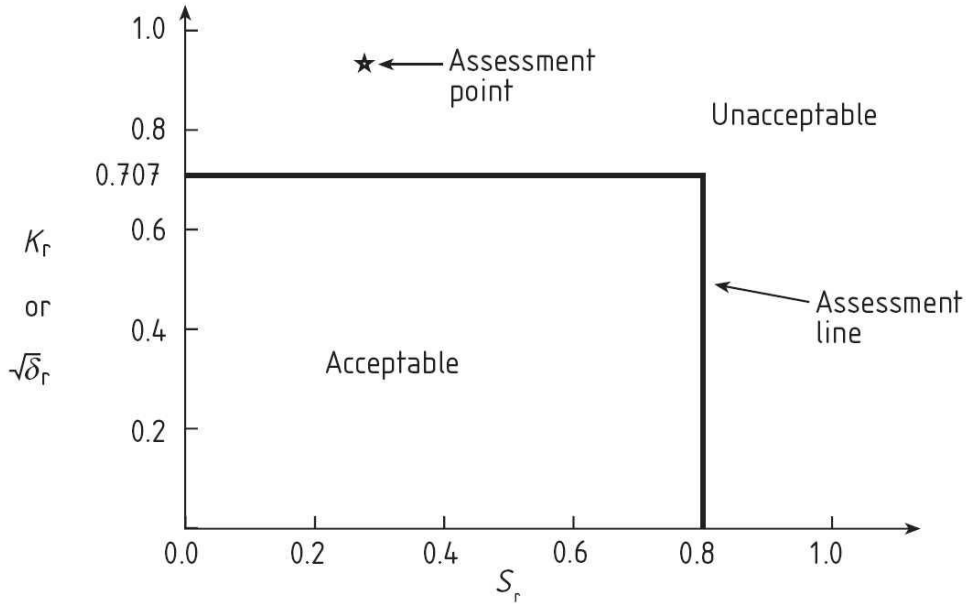

Figure 2-24 FAD level 1 (Simplified assessment)
(Staat 2004; 2005; BS7910 2012)

A safety factor of about 2 is taking into account for level one assessment.

For a more accurate analysis Standards suggest level 2 for investigation of crack acceptability. More detailed information is required regarding the stress distributions surrounding the defect. In this approach the “x” axes values replace from Stress ratio (S_r) with Load ratio (L_r).

$$L_r = \frac{\sigma_{ref}}{\sigma_{yield}} \rightarrow L_{r\max} = \frac{\sigma_Y + \sigma_u}{2\sigma_Y} \tag{2-49}$$

For general application this is the normal assessment route. Level 2 has two methods (2A and 2B) with different assessment lines. Similarly to the other levels, if the assessment point lies under the assessment line bounded by the axes, the flaw is acceptable, if not then the flaw is unacceptable.

For level 2A (generalised FAD) the equations describing the assessment line are as follows. In this level the stress/strain data are not required.

Where :

a) For $L_r \le L_{r\max}$: (Figure 2-25)

$$K_r or \sqrt{\delta} = (1-0.14L_r^2)\{0.3+0.7\exp(-0.65L_r^6)\} \quad (2\text{-}50)$$

And for $L_r > L_{r\max}$ $K_r or \sqrt{\delta}$ =0

The second level of failure assessment in BS 7910 is named FAD Level 2 (Normal assessment). It is the most common method for general application, and has two approaches. In both approaches a cut-off line is defined to prevent plastic collapse that is as follow: (Figure 2-25)

$$L_{r\max} = \frac{\sigma_Y + \sigma_u}{2\sigma_Y} \quad (2\text{-}51)$$

This level (2A) is suitable for HAZs. For materials with a material curve which is not monotonically increasing, level 2B should be used.

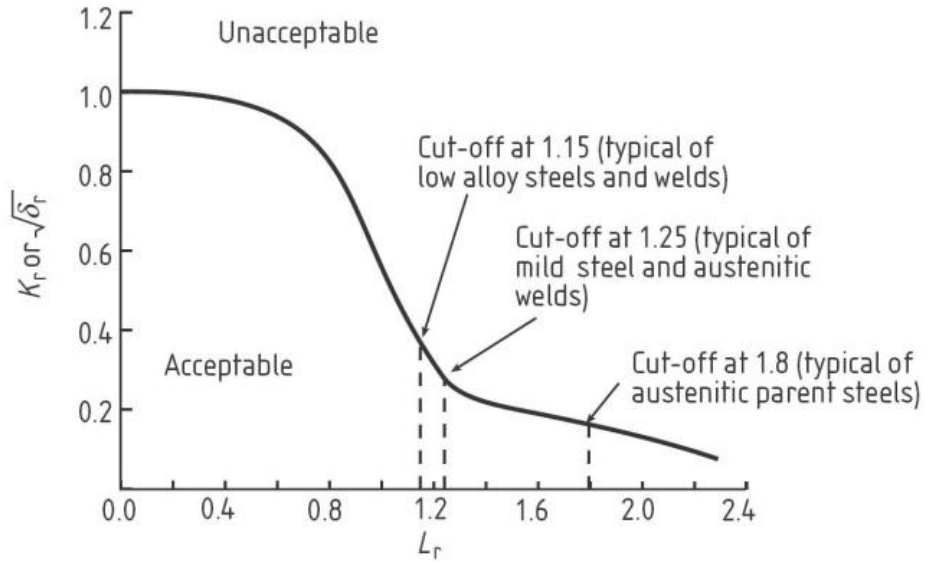

Figure 2-25 Level 2A FAD (Normal assessment) (2005; BS7910 2012)

Level 2B generally gives more accurate results than level 2A but requires more data, such as material specific (stress-strain) curve. The accuracy of stress-strain curve data (σ/σ_Y) especially near the σ_Y point is very important.

The equations describing the assessment line in this level are as follows:

a) For $L_r \leq L_{rmax}$ (Figure 2-26)

$$\sqrt{\delta_r} or K_r = \left(\frac{E\varepsilon_{ref}}{L_r\sigma_Y} + \frac{L_r^3\sigma_Y}{2E\varepsilon_{ref}}\right)^{-0.5} \quad (2\text{-}52)$$

b) For $L_r > L_{rmax}$

$$\sqrt{\delta_r} or K_r = 0 \quad (2\text{-}53)$$

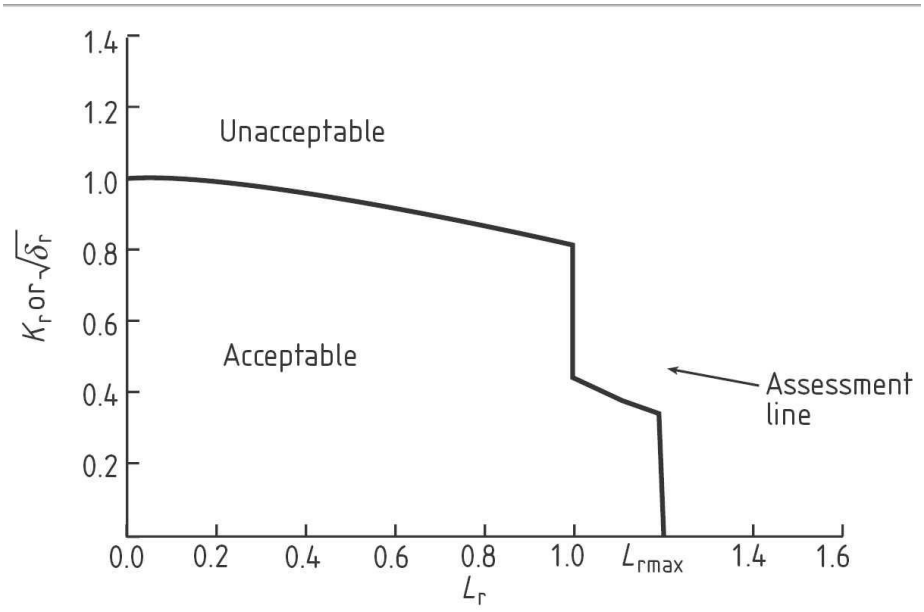

Figure 2-26 Level 2B FAD (Normal assessment)
(BS7910 2012)

The fracture ratio for levels 2 and 3 is different. The value for (Yσ) is the summation of $(Y\sigma)_p$ and $(Y\sigma)_s$ which represent contributions from primary and secondary stresses, respectively. The equations are as follows:

$$K_r = \frac{K_I}{K_{mat}}, K_I = (Y\sigma)\sqrt{\pi a} \tag{2-54}$$

$$(Y\sigma) = (Y\sigma)_p + (Y\sigma)_s \tag{2-55}$$

Where:

$$(Y\sigma)_p = Mf_W[k_{tm}M_{km}M_mP_m + k_{tb}M_{kb}M_b\{P_b + (k_m - 1)P_m\}] \tag{2-56}$$

$$(Y\sigma)_s = M_mQ_m + M_bQ_b \tag{2-57}$$

All expressions mentioned above, are explained in BS 7910, tables M.2a, M.4 and M.6. Also, references are available in BS 7910 Annex D.

For a full analysis of ductile tearing, BS 7910 suggest using FAD level 3 (Instability assessment). Level 3 assessments may apply to austenitic steels and ferritic steels and even for materials exhibiting a brittle failure mechanism. This level is categorised into three levels: 3A, 3B and 3C.

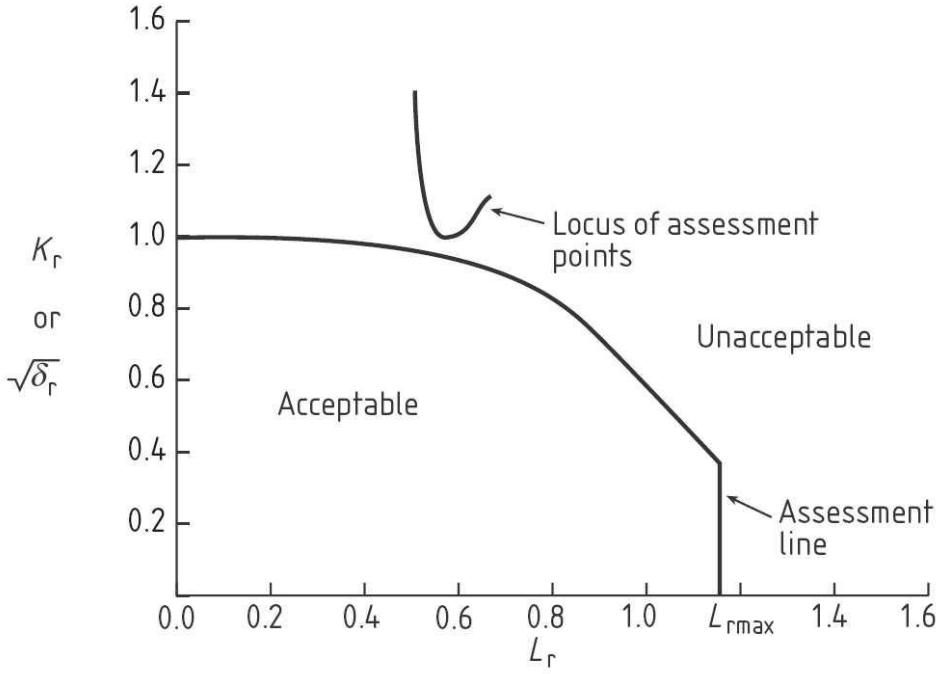

Figure 2-27 Level3 FAD (Instability assessment)
(BS7910 2012)

For a plate with the material of the pipe subjected to an edge crack with the following input data: “a” is the crack depth, “B” is the plate thickness, “w” is the plate width, the values for L_r and K_r can be calculated as follows:

From API PR579 :

$$K_{IC} = 33.2 + 2.806\exp[0.02(T - T_{ref} + 100)] \tag{2-58}$$

Where T is the service temperature and T_{ref} could be obtained from ASME code section VIII division I, and from API PR 579:

$$\sigma_{ref} = \frac{P_b + \sqrt{(P_b^2 + 9P_m^2)}}{3(1-\alpha)} \tag{2-59}$$

Where α=a/w and the primary membrane stress P_m=F/BW, F is the maximum axial load. To calculate K_I:

$$K_I = YP_m\sqrt{\pi a} \tag{2-60}$$

Where geometry factor Y could be obtained from:

$$Y = 1.22 - 0.231\alpha + 10.55\alpha^2 - 21.71\alpha^3 + 30.382\alpha^4 \quad (2\text{-}61)$$

σ_{ys} could be obtained from ASME code section II.D. By calculating L_r and K_r of the pipe and finding the location of the point in the FAD diagrams, acceptability of flaws in terms of safety is achievable. Also maximum safe applied loads could be suggested depending on FAD levels of assessment.

As an example, assume points P and Q in Figure 2-28 belong to an engineering problem under different loading condition. Points P and Q are unacceptable if the problem have to be assessed with level 1 FAD. Point P is acceptable using level 2 and 3 FAD and in case of point Q, it is unacceptable if using level 2 and is acceptable if has been assessed with level 3 FAD.

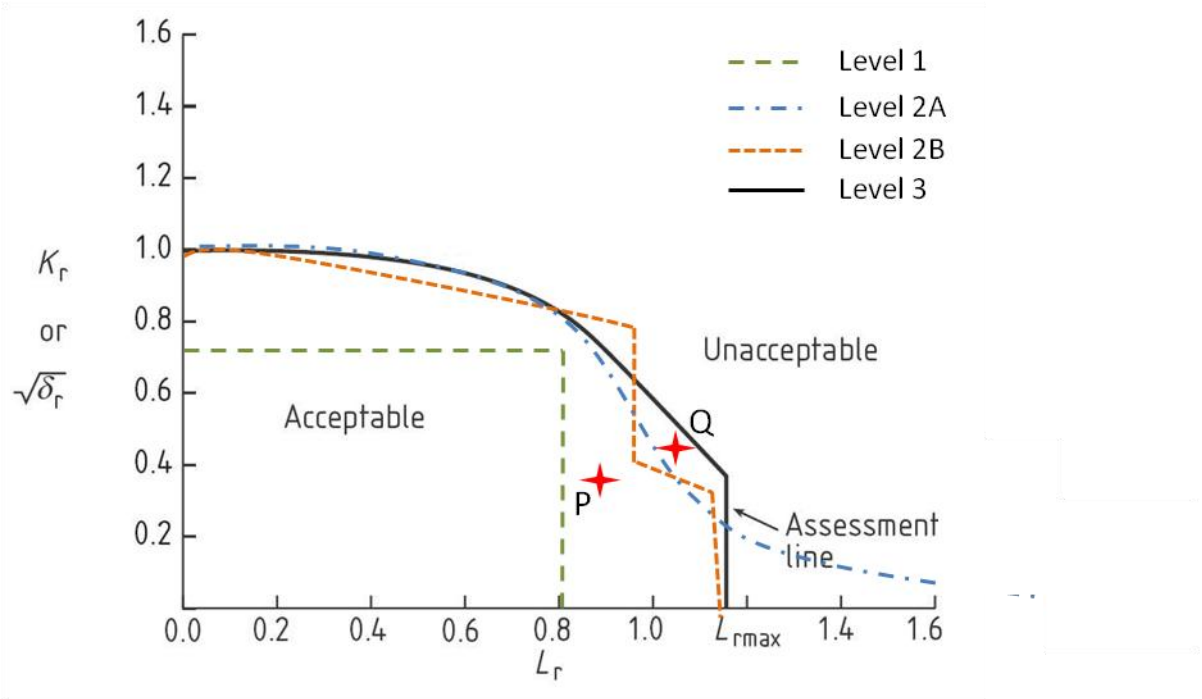

Figure 2-28 an example of safe assessment having all 3 FAD levels

2.6.5 Weight function background

Weight function has been introduced by Bueckner and Rice as a powerful solution for The calculation of SIF (Bueckner 1970; Rice 1972). The SIF has previously (in Chapter 1) been pointed out as depending on the geometry and loading of the crack body. Weight function as a very powerful technique that can be used to generate the SIF for any loading condition when for the same geometry the SIF solution is known for a set of boundary conditions. It has been defined as:

$$K = \int_0^a \sigma(x) m(a,x)\, dx \tag{2-62}$$

Where *m(a,x)* is the weight function along the crack at a distance of x from the crack mouth and subjected to a stress distribution of σ(x).

Bueckner presented another form of weight function that identifies the stress singularity in the elastic region of a cracked body as a function of stress intensity, independent of externally applied loads as follows:

$$m(a,x) = \frac{E'}{2K_r} \frac{\partial u_r(a,x)}{\partial a} \tag{2-63}$$

Where E' is equal to E for plane stress conditions and is equal to E/1-v^2 for plane strain conditions. $\partial u_r(a,x)$ is the reference crack opening displacement field.

It can be observed from Eq.(2-63) that weight function can be determined if the K_r and $u_r(a,x)$ for a given loading condition are known (its unit is 1/√m). It has been proven that weight function can be used for 2D and 3D cracked bodies as well as isotropic and anisotropic materials. Even though there is dissension between scholars about the definition of 2D and 3D crack bodies (Chahardehi and Brennan 2010).

The merit of weight function is that, when it has been derived it can be used to generate the SIF for any other loading condition of the same geometry. Weight function could separate the geometry function of a crack body from its

crack line state of stress. It is a great functionality that can be applied to an infinite number of loading conditions to generate the SIF for the same body (Teh 2002).

Petroski and Achenbach presented an approximation for the reference crack opening displacement (Petroski and Achenbach 1978). They has considered their equation for small cracks and limiting behaviour near the crack tip as follows:

$$u(a,x) = \frac{\sigma_0}{E'\sqrt{2}}\left[4F\left(\frac{a}{t}\right)\sqrt{a(a-x)} + \frac{G\left(\frac{a}{t}\right)(a-x)^{\frac{3}{2}}}{\sqrt{a}}\right] \quad (2\text{-}64)$$

Where

$$F\left(\frac{a}{t}\right) = \frac{K}{\sigma_o\sqrt{\pi a}} \quad (2\text{-}65)$$

And $G\left(\frac{a}{t}\right)$ can be determined from

$$G\left(\frac{a}{t}\right) = \frac{\left(\frac{\sqrt{2}}{\sigma_0}I_1 - 4F\left(\frac{a}{t}\right)a^{\frac{1}{2}}I_2\right)a^{\frac{1}{2}}}{I_3} \quad (2\text{-}66)$$

Where

$$I_1 = \int_0^a [k(a)]^2\,da\,; I_2 = \int_0^a \sigma(x)\,(a-x)^{\frac{1}{2}}dx\,;\; I_3 = \int_0^a \sigma(x)\,(a-x)^{\frac{3}{2}}dx$$

Later Petroski's COD function has been used in conjunction with weight function to calculate the SIF for a 3D semi elliptical crack (Niu and Glinka 1989; Niu and Glinka 1990).

By differentiation of Equation (2-63) the weight function can be obtained as:

$$m(a,x) = \frac{E'}{2K_r}\frac{\partial}{\partial a}\left(\frac{\sigma_0}{E'\sqrt{2}}\left(4F\left(\frac{a}{t}\right)\sqrt{a(a-x)} + \frac{G\left(\frac{a}{t}\right)(a-x)^{\frac{3}{2}}}{\sqrt{a}}\right)\right) \quad (2\text{-}67)$$

as

$$m(a,x) = \frac{1}{\sqrt{2\pi(a-x)}}\left(1 + M_1\left(\frac{a-x}{a}\right) + M_2\left(\frac{a-x}{a}\right)^2\right) \quad (2\text{-}68)$$

Where M1 and M2 are parametric equations for a specific reference system as:

$$M_1 = \frac{4F'\left(\frac{a}{t}\right)a + 2F\left(\frac{a}{t}\right) + \frac{3}{2}G\left(\frac{a}{t}\right)}{2F\left(\frac{a}{t}\right)} \quad (2\text{-}70)$$

and

$$M_2 = \frac{\left(G'\left(\frac{a}{t}\right)a - \frac{1}{2}G\left(\frac{a}{t}\right)\right)}{2F\left(\frac{a}{t}\right)} \quad (2\text{-}71)$$

and

$$F'\left(\frac{a}{t}\right) = \frac{d}{d\left(\frac{a}{t}\right)}\left[F\left(\frac{a}{t}\right)\right] \quad (2\text{-}72)$$

and

$$G'\left(\frac{a}{t}\right) = \frac{d}{d\left(\frac{a}{t}\right)}\left[G\left(\frac{a}{t}\right)\right] \quad (2\text{-}73)$$

Brennan has presented that the mentioned equations are computationally inefficient. Because of the numerical differentiation they could lead to inaccurate weight function and consequently not a perfect SIF (Brennan 1994).

2.6.6 Multiple reference state weight function approach

To improve computational efficiency, Ojdrovic propose the multiple reference state (MRS) weight function method (Ojdrovic and Petroski 1991). Instead of using numerical differentiation of the COD function, MRS employs numerical integration. This method uses more than one reference SIF and associated stress field to calculate a general weight function for a specific body.

Ojdrovic and Petroski suggest that the crack profile derivative can be expressed in the form of a series given by:

$$\frac{\partial u(a,x)}{\partial a} = \frac{4\sigma_0}{H}\sqrt{2}\sum_{j=0}^{m} C_j \left(1-\frac{x}{a}\right)^{\left(j-\frac{1}{2}\right)} \tag{2-74}$$

Where the C0 as the initial constant is:

$$C_0 = \frac{F_1\left(\frac{a}{t}\right)}{2} \tag{2-75}$$

$F_1(a/t)$ can be derived from the general definition of the SIF:

$$K = F\left(\frac{a}{t}\right)\sigma\sqrt{\pi a} \tag{2-76}$$

And $F_1\left(\frac{a}{t}\right) = \frac{K}{\sigma\sqrt{\pi a}}$

C_j are unknown coefficients and for m symmetrical loading states (K_1, K_2, $K_3 \ldots K_m$, $m \geq 1$), the number of terms can be assumed as m+1. If the equation is solved on known K_i:

$$\int_0^a \frac{E'}{2}\sigma_i(x)\frac{\partial u(a,x)}{\partial a}dx = K_i(a)K_1(a) \tag{2-77}$$

Where *i* represents the *ith* reference loading case and $K_1(a)$ is the first reference loading state.

Substituting Equations (2-74) and $K = \int_0^a \sigma(x) m(a,x)\, dx$

$$2\sqrt{2}\sigma_0 \int_0^a \sigma_i(x) \sum_{j=0}^{m} C_j \left(1 - \frac{x}{a}\right)^{\left(j-\frac{1}{2}\right)} dx = K_i(a) K_1(a) \tag{2-78}$$

Defining W_{ij} as:

$$W_{ij} = \int_0^a \sigma_i(x) \left(1 - \frac{x}{a}\right)^{\left(j-\frac{1}{2}\right)} dx \tag{2-79}$$

gives

$$\sum_{j=0}^{m} W_{ij} C_j = K_i(a) \frac{F_1\left(\frac{a}{t}\right)}{2} \sqrt{\frac{\pi a}{2}} \tag{2-80}$$

Knowing C_0 from Equation (2-75):

$$\sum_{j=1}^{m} W_{ij} C_j = \frac{F_1\left(\frac{a}{t}\right)}{2} \left(K_i(a) \sqrt{\frac{\pi a}{2}} - W_{i0} \right) \tag{2-81}$$

Let us name the right hand side of equation (2-81), q, then unknown C_J can be determined by solving a system of m simultaneous linear equations with m unknowns (Ojdrovic and Petroski 1991).

$$\begin{aligned} W_{11} C_1 + W_{12} C_2 &= q_1 \\ W_{21} C_1 + W_{22} C_2 &= \mathrm{q}_2 \end{aligned} \tag{2-82}$$

Gives

$$C_1 = \frac{\mathrm{q}_1 W_{22} - \mathrm{q}_2 W_{12}}{\mathrm{W}_{11} W_{22} - W_{21} W_{12}} \tag{2-83}$$

$$C_2 = \frac{\mathrm{q}_2 W_{11} - \mathrm{q}_1 W_{21}}{\mathrm{W}_{11} W_{22} - W_{21} W_{12}} \tag{2-84}$$

Knowing the coefficients C_j the weight function can be derived as:

$$m(a,x) = \frac{E'}{2K_1(a)} \frac{\partial u_r(a,x)}{\partial a} = 2\sqrt{2} \frac{\sigma_0}{K_1(a)} \sum_{j=0}^{m} C_j \left(1 - \frac{x}{a}\right)^{\left(j-\frac{1}{2}\right)} \tag{2-85}$$

The MRS method and the derived weight function are relatively more accurate and more stable (Brennan 1994). A code based on the MRS weight function approach for the pipe with longitudinal through thickness crack has been written in MATLAB (Appendix D).

For validation of the written code in MATLAB and the MRS method, pure tension and bending loading conditions in an edge crack body have been selected as two well known references. The single edge crack under pure tension reference SIF has been given (Gross 1964; Brown and Srawley 1966)

$$Y_1 = \frac{K_I}{\sigma_0 \sqrt{\pi a}} = 1.122 - 0.231 \left(\frac{a}{b}\right) + 10.550 \left(\frac{a}{b}\right)^2 - 21.710 \left(\frac{a}{b}\right)^3 + 30.382 \left(\frac{a}{b}\right)^4 \tag{2-86}$$

Figure 2-29 depicts the single edge crack under pure tension on the left and the single edge crack under pure bending on the right side.

As the second reference, the single edge crack under pure bending SIF has been given as (Brown and Srawley 1966):

$$Y_2 = \frac{K_I}{\sigma\sqrt{\pi a}} = 1.122 - 1.40\left(\frac{a}{b}\right) + 7.33\left(\frac{a}{b}\right)^2 - 13.08\left(\frac{a}{b}\right)^3 + 14\left(\frac{a}{b}\right)^4 \quad (2\text{-}87)$$

Where

$$\sigma = \frac{6M}{b^2} \quad (2\text{-}88)$$

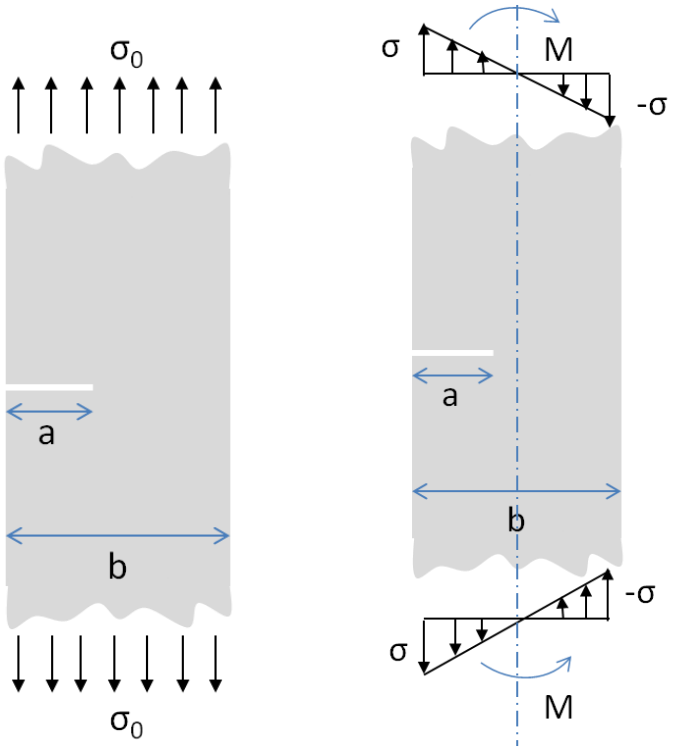

Figure 2-29 The Single edge crack under Left: Pure tension, Right: Pure bending

The accuracy of the reference solution SIF is 0.5% for a/b<=0.6. So the domain for crack length to width ratio has been selected from 0 to 0.6.

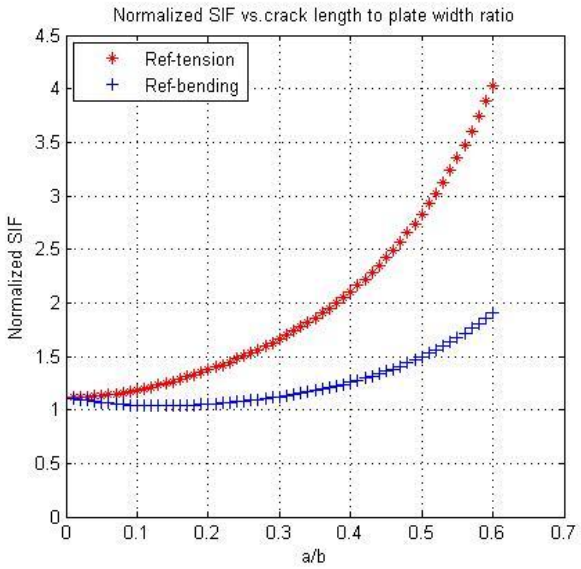

Figure 2-30 The reference solution's normalized SIF

By inserting the state of stress in the weight function equation (Eq. (2-85)) and performing integration over the crack domain the weight function SIF results are as follows:

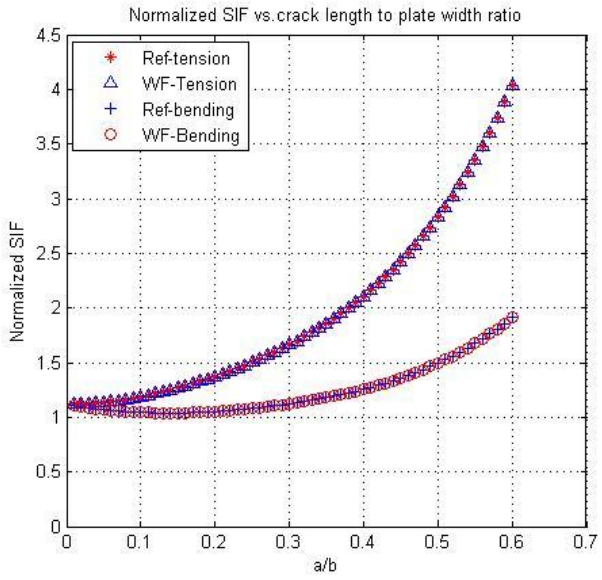

Figure 2-31 Comparison of the reference solution and the MRS WF

The MRS WF and the reference solution have a very good agreement with each other. The correlation coefficient is better than 0.99.

2.7 Summary

In Chapter one, carbon capture and storage process and the importance of CO_2 transportation were discussed. Pipelines, as the most economical and effective way of gas transportation, have to be designed for a long operating life. Captured CO_2 pipelines and associated challenges have to be carefully addressed and guidelines for an effective design prepared for pipeline engineers. Fundamental fracture mechanics approach, SIF, J-Integral and energy method have been reviewed. The only available theoretical solutions for longitudinal through thickness cracks in a pipe were presented. To understand the pipeline fracture mechanics analysis, current state-of-the-art methods have been discussed. Fracture toughness tests using compact tension specimens to calculate fracture toughness of pipeline material have been presented. The failure assessment diagram as a powerful tool to assess the acceptance of an existing crack in a structure/pipe has also been discussed.

Calculation of the SIF and J-integral using the finite element technique will be discussed in chapter two. Also a comprehensive fracture toughness test and its results will be presented in chapter three. In chapter four, a fracture mechanics model for a through thickness crack in a CO_2 pipe will be explained. The last chapter is dedicated to fitness for service and engineering criticality assessments of pipelines.

Chapter 3. Finite Element Analysis

As mentioned in chapter 1, one of the most powerful methods for calculating the SIF is finite element analysis (FEA). Using high performance computing techniques makes this method faster and more reliable. In this chapter a study of the Abaqus SIF calculation potential is presented. Also a series of crack models and their SIFs for well-known geometries are studied and their results compared with available literature.

3.1 Stress Intensity Factor calculation using FEA with Abaqus Software

Abaqus uses the J-Integral method as a fracture mechanics parameter for both nonlinear and linear material responses. For the linear material response, the SIF can be addressed and the automatically calculated from the J. Abaqus, based on the virtual crack domain integral method presented by (Shih, Moran et al. 1986) calculates the J-Integral. As mentioned in the previous section, J is related to the energy release associated with crack growth and is a measure of the intensity of deformation at a notch or crack tip, especially for non linear materials (Abaqus 2009).

In two dimensional problems, J-Integral is defined as:

$$J = \lim_{\Gamma \to 0} \int_{\Gamma} nHq \, d\Gamma \tag{3-1}$$

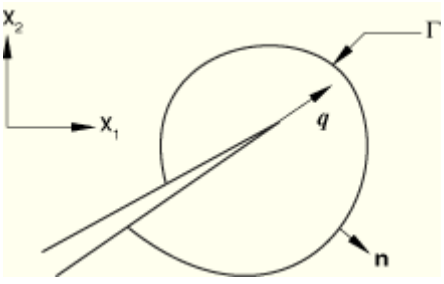

Figure 3-1 Contour integral method for evaluation of the J

Where Γ is a contour beginning and ending on each side of the crack, q is a unit vector in the crack front direction, n is the outward normal to Γ (Figure 3-1) and H is given by:

$$H = WI - \sigma \frac{\partial u}{\partial x} \tag{3-2}$$

Where, W represents the strain energy in an equivalent elastic material. This means that for elastic material behaviour W is the elastic energy and for elastic-viscoplastic or elastic-plastic material behaviour W is plastic dissipation plus the elastic strain energy. σ is the surface traction on the crack surfaces C_+ and C_- .

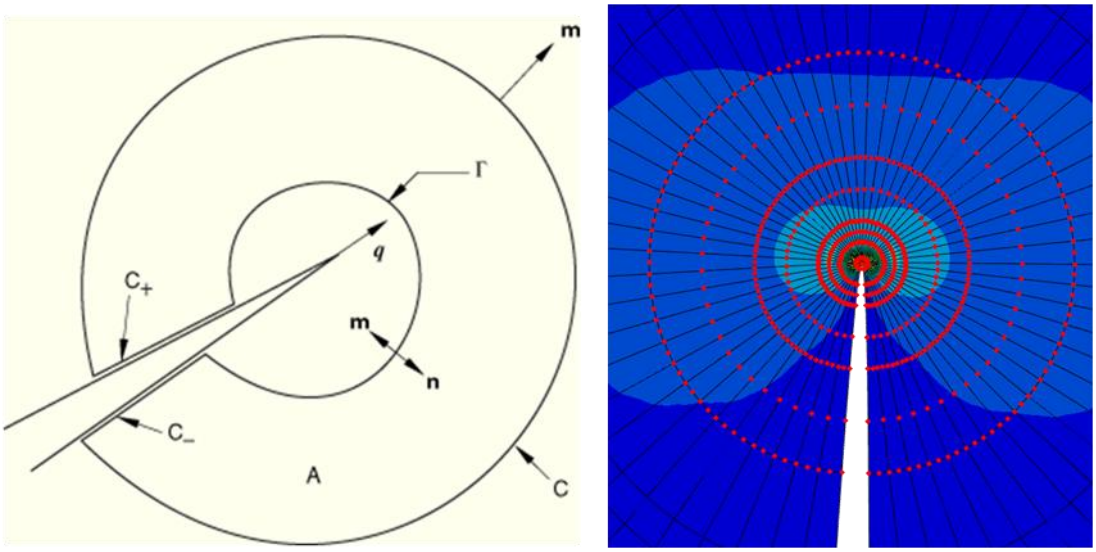

Figure 3-2 Closed contour and crack tip contours

In Figure 3-2 closed contour $C+C_+ +Γ+C_-$ encloses a domain A that includes the crack tip region as Γ→0. Using the divergence theorem, J can be rewritten as:

$$J = -\int_A \left(\frac{\partial}{\partial x}\right).(H.p)d\Gamma - \int_{C_+ + C_-} t.\frac{\partial u}{\partial x}.p d\Gamma \tag{3-3}$$

Where A is the defined domain, and q is the weighting function within the region enclosed by the closed contour and has the value p=q on Γ and p=0 on C. m is the outward normal to the domain enclosed by the closed contour, m=-n on Γ (Figure 3-2).

$$J = -\int_A [H\left(\frac{\partial p}{\partial x}\right) + \left(f\frac{\partial u}{\partial x} - \sigma\frac{\partial \varepsilon^{th}}{\partial x}\right)p]d\Gamma - \int_{C_+ + C_-} t.\frac{\partial u}{\partial x}.pd\Gamma \quad (3\text{-}4)$$

Where f is the body force per unit volume and ε^{th} is the thermal strain.

As has been illustrated in Figure 3-2, to evaluate these integrals, Abaqus defines the domain (A) in terms of rings of elements surrounding the crack tip. During the meshing of the crack front, a very fine mesh around the crack tip should be considered. The number of contours when calculating the integral is important.

The SIF (K) can be related to the energy release rate (J) for a linear elastic material through the following equation:

$$J = \frac{1}{8\pi}K^T.B^{-1}.K \quad (3\text{-}5)$$

Where $K=[K_I,K_{II},K_{III}]^T$ and B is the pre logarithmic energy factor matrix (Barnett and Asaro 1972; Suo 1990; Gao, Abbudi et al. 1992). For homogeneous isotropic materials B is diagonal and the equation simplifies to:

$$J = \frac{1}{E'}(K_I^2 + K_{II}^2) + \frac{1}{2G}K_{III}^2 \quad (3\text{-}6)$$

Where

$$E' = E \quad for\ plane\ stress\ condition \quad (3\text{-}7)$$

$$E' = \frac{E}{1-\vartheta^2} \quad for\ plane\ strain\ condition$$

And G is the shear module. K_I, K_{II} and K_{III} are the SIFs in three different modes of fracture.

For more information about SIF calculation in Abaqus please refer to Abaqus reference manual (Abaqus 2009).

3.2 Verifying finite element modelling base on empirical formulae in the literature

Calculating the SFI for complicated loading and geometry problems is easier with the help of high performance FEA packages Such as Abaqus. But it must be remembered that the modeller should understand the background mechanisms of these types of problem solving. Very simple mistakes in defining the problem or the boundary conditions can obtain incorrect results. The aim of this section is to compare the SIF calculation using FEA with the published empirical formulae in the literature. In simple problems, crack modelling and analysis using FEA techniques could be verified with already available solutions. For this purpose a single edge crack under pure tension has been selected.

3.2.1 Single Edge Crack under pure Tension (SECT)

Srawley presented a well known empirical formula to calculate SIF for SECT (Brown and Srawley 1966). It purports to be an infinite plate under tension with the W and t for its width and thickness (Figure 3-3).

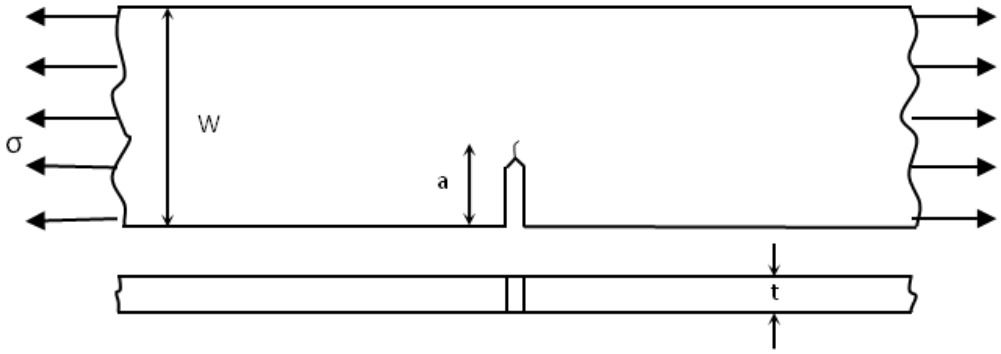

Figure 3-3 Single edge cracked plate tension specimen

The SIF can be calculated from:

$$K_I = \sigma\sqrt{\pi a}\, F_I(\alpha)\ ,\ \ \alpha = a/W \tag{3-8}$$

$$F_I(\alpha) = 1.12 - 0.231\alpha + 10.55\alpha^2 - 21.72\alpha^3 + 30.39\alpha^4 \tag{3-9}$$

With an accuracy of ±0.5% for a/W<=0.6 and a is the notch length plus pre-crack. For such specimens normally pre-crack can be made using three or four point bending fixtures.

$F_I(\alpha)$ is a dimensionless parameter, called the geometry factor or Y.

Considering 1 MPa stress as tension and a plate of 100mm width and 1mm thickness, for different crack lengths the SIF values are as follows:

Table 3-1 SIF values for different crack lengths

α	Y
0.2	1.37
0.3	1.66
0.4	2.10
0.5	2.83
0.6	4.03

The imperial formulae presented by Srawley did not consider the thickness of the specimen. Most previous experiences in calculating SIF belong to aerospace industries that dealt with thin skins used in the aircraft fuselage. For comparison and a better understanding of the thickness effect, both two and three dimensional problems have been modelled and the results compared and these are given in the next section.

3.2.2 Calculating SIF in a SECT specimen using FEA

For step by step learning of how to model a SECT specimen in Abaqus please refer to 7.4Appendix AAppendix A. In this section both 2D and 3D models of SECT have been considered and different issues, such as: effect of the thickness, number of contours on the crack front, number of elements through the thickness, and singularity at the crack tip are discussed.

A crack could be modelled as a sharp or blunted crack. In the former the crack has been started from the edge of the specimen and has its own length. In this case singularity of behaviour could be observed at the crack tip. In the later, using open geometry, as with the notch there is non-singular behaviour at the crack tip and this is useful for finite strain analysis. It is, however, essential to do mesh refinement. To obtain accurate stresses and strains in the vicinity of the crack tip, the finite element mesh must be refined. Due to stress concentrations of the crack tip, there are large gradients of stress and strain on crack tip vicinity. The quadratic-reduced integration plane stress elements (CPE8R) for 2D modelling and quadratic-reduced integration 3D stress elements (C3D20R) for 3D modelling have been used in the meshing techniques. Actually it can be said that the average of the through thickness nodes SIF does not change as much with thickness change; on the other hand thickness has a significant effect on measuring fracture toughness in experimental tests.

In Figure 3-4 SECT models for different conditions have been analysed and the results for 2D and 3D models with different thicknesses depicted.

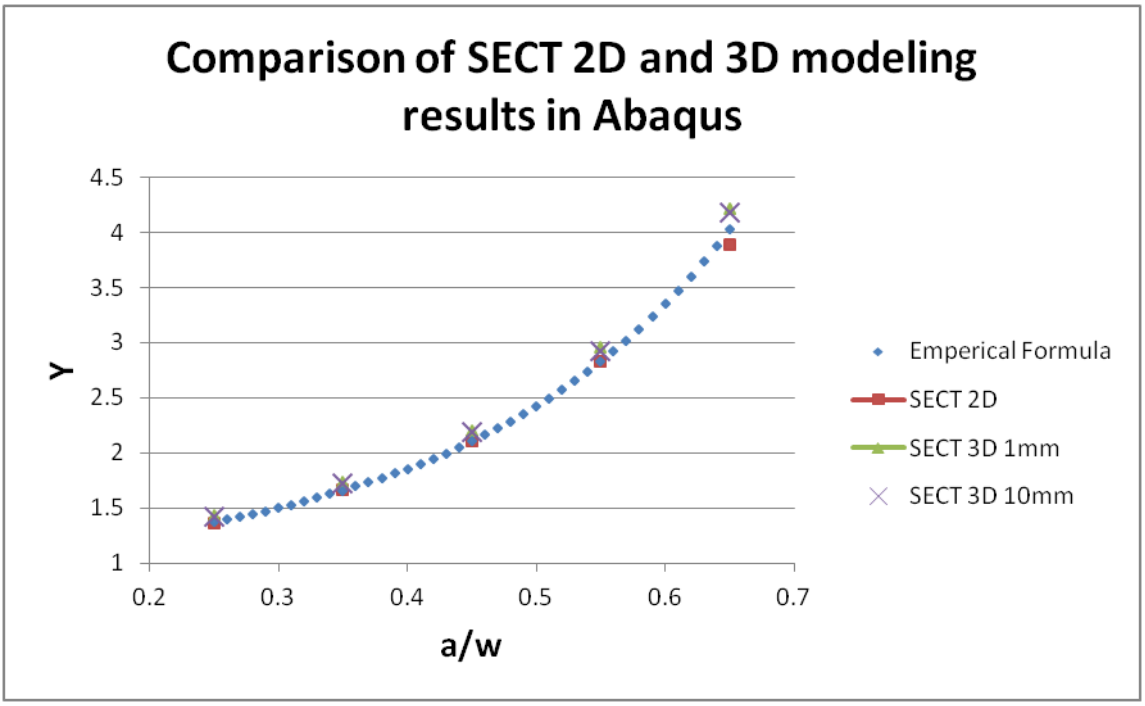

Figure 3-4 2D and 3D SECT results comparison

3.2.2.1 Notch effect on calculating SIF

Modelling sharp cracks in two dimensions in Abaqus included considering crack tip singularity. There are different methods of collapsing nodes in an 8-node isoparametric element. In mode one, fracture only, the crack on a symmetry plane could be defined in the edit crack dialogue box and does not need to define a seam.

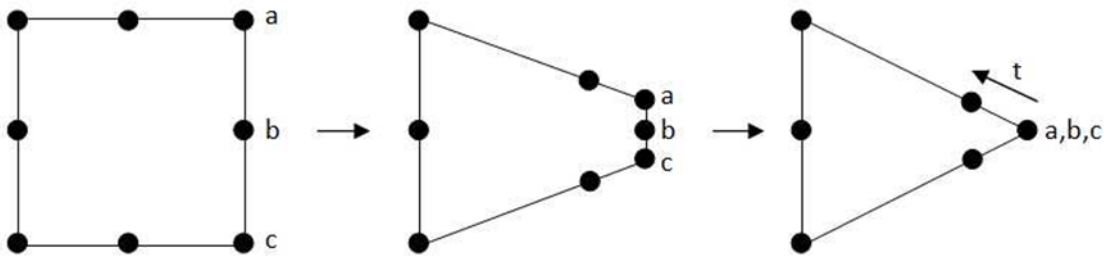

Figure 3-5 Node collapse at the crack tip

One side of the element is near to the crack tip collapse (a,b,c) so all three nodes have the same geometric location at the crack tip. Then the

midside nodes on the sides that are connected to the crack tip will move to the 0.25 point nearest the crack tip. Midside node parameter (t) is defined as 0<t<1, considering the location of the crack tip is at t=0.

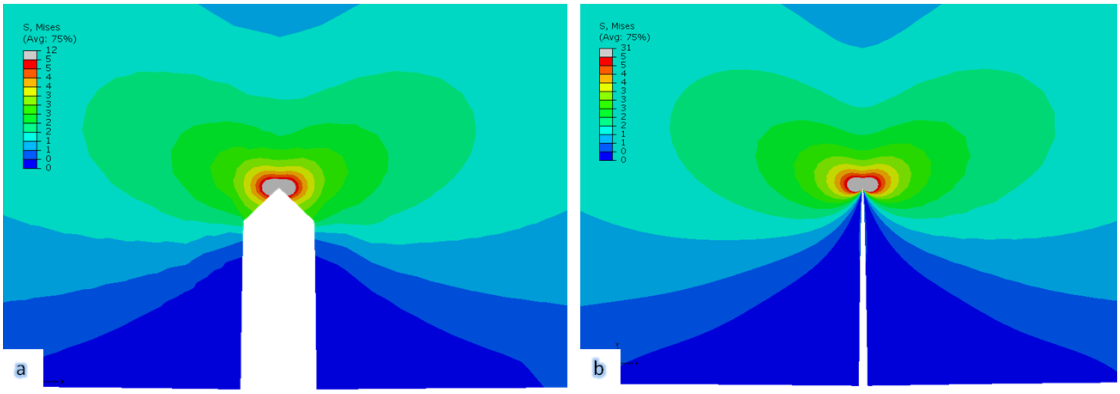

Figure 3-6 The crack tip state of stress-
a: Blunt crack, b: Sharp crack

Due to stress concentration caused by the notch, there is a significant difference in the stress values of the crack tip. The value of stresses in a sharp crack is about 3 to 5 times greater than in a blunt notch. Consequently the value of the SIF is different.

3.2.2.2 Effect of thickness on calculating SIF

The dimensions of the modelled 3D single edge crack under pure tension are 300×100×10 mm. The SIF (KI) has been measured in different layers through the thickness and the results are depicted in Figure 3-9. In 3D modelling Abaqus computes contour integrals at each node along the crack line (Abaqus 2009). The thickness of the specimen has been properly seeded as depicted in Figure 3-8 it has four elements. Including the element midset nodes, there are nine nodes along the thickness.

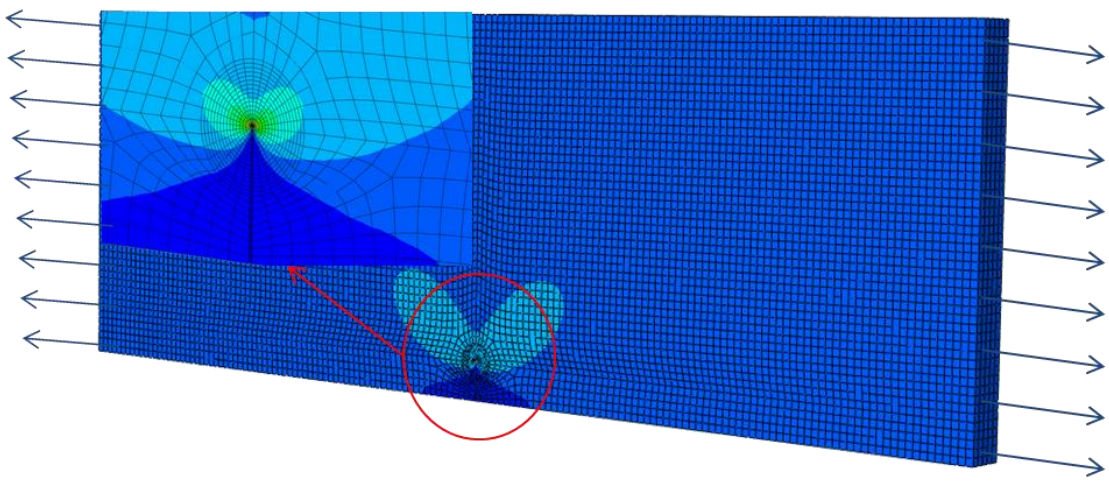

Figure 3-7 Mesh size and density

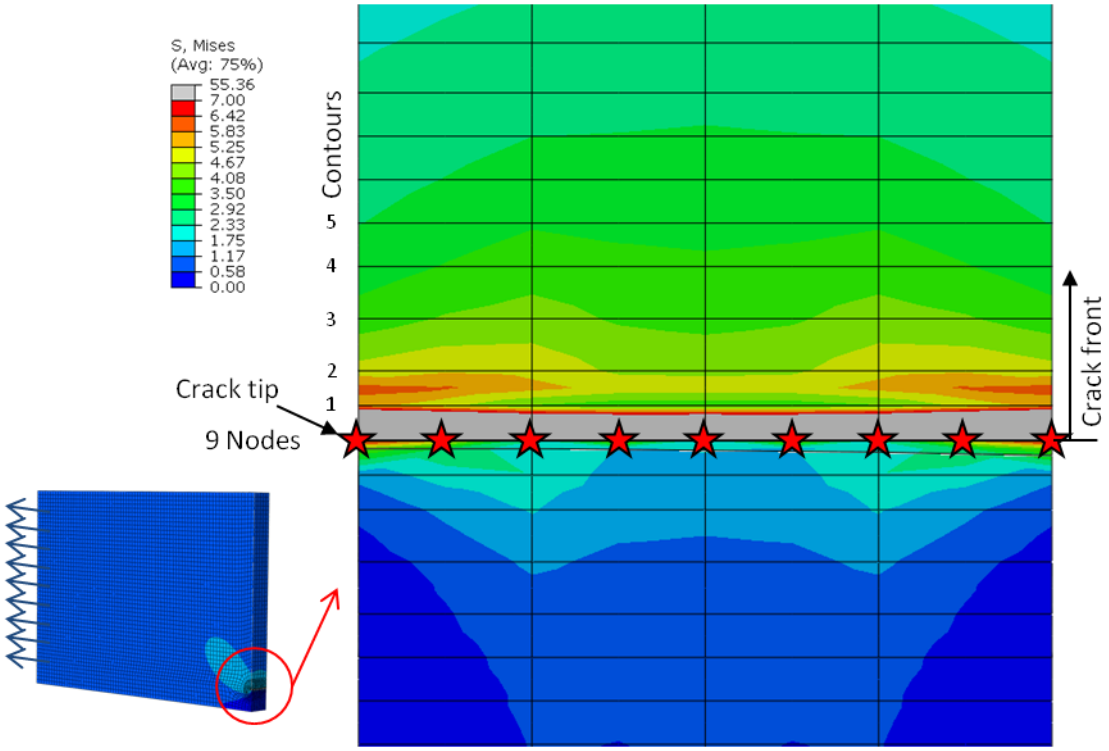

Figure 3-8 Cross section view of the specimen

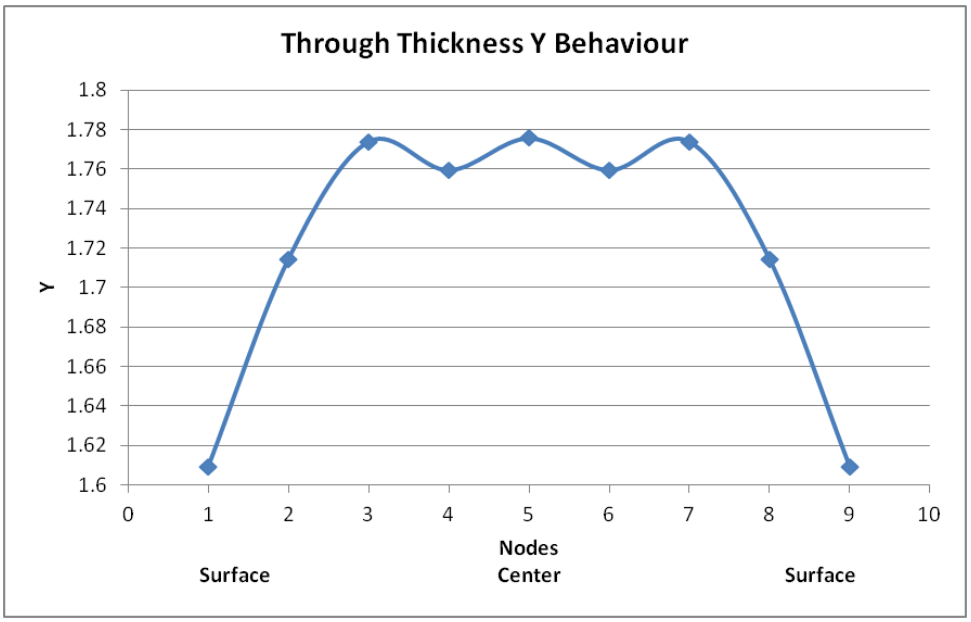

Figure 3-9 Through thickness Y values

In Table 3-2, SIF results for each node and for different contours are presented. These results are based on the problem assumptions of σ=1 MPa.

Table 3-2 Through thickness Normalised K results

		Y								
Nodes		1	2	3	4	5	6	7	8	9
Contours	1	1.6	1.71	1.77	1.76	1.78	1.76	1.77	1.71	1.6
	2	1.6	1.70	1.76	1.75	1.77	1.75	1.76	1.70	1.6
	3	1.6	1.70	1.76	1.75	1.77	1.75	1.76	1.70	1.6
	4	1.6	1.70	1.76	1.75	1.77	1.75	1.76	1.70	1.6
	5	1.6	1.70	1.76	1.75	1.77	1.75	1.76	1.70	1.6
Average		1.6	1.70	1.76	1.75	1.77	1.75	1.76	1.70	1.6

As depicted in Figure 3-9, the SIF values increase when moving from the surface towards the inside of the specimen. On each surface the minimum values of SIF are calculated. Due to symmetry of the geometry, loading and

boundary conditions the calculated SIF values through thickness produced a symmetric graph.

If the number of through thickness nodes increases to 57, the results will show a smoother domed graph which demonstrates the stress triaxiality effect within the specimen.

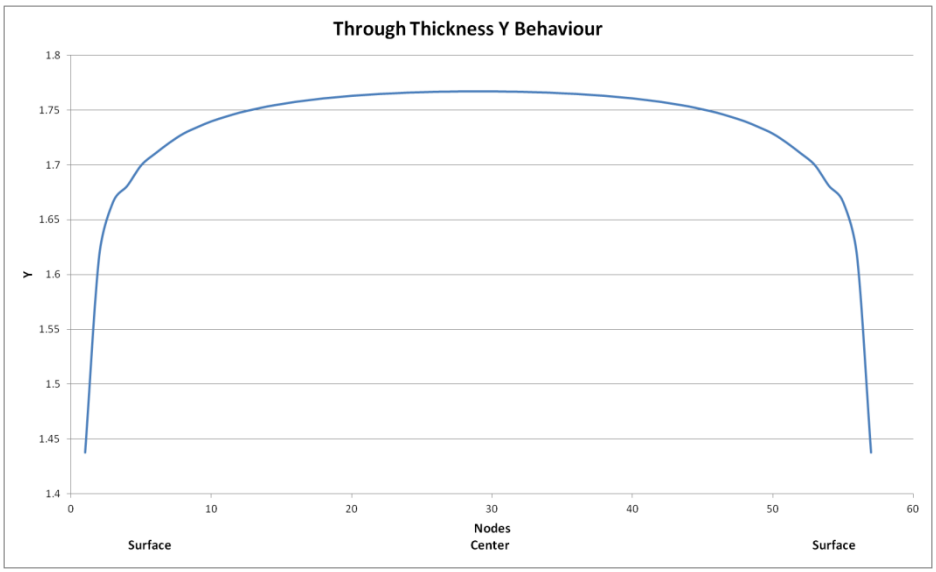

Figure 3-10 Through thickness Y values for 57 nodes

Due to this stress triaxiality effect, during the pre-cracking procedure the cracks always grow faster inside the specimen. Figure 3-11 shows the cross section of a fatigue pre-cracked specimen and the crack growth behaviour is clearly observable.

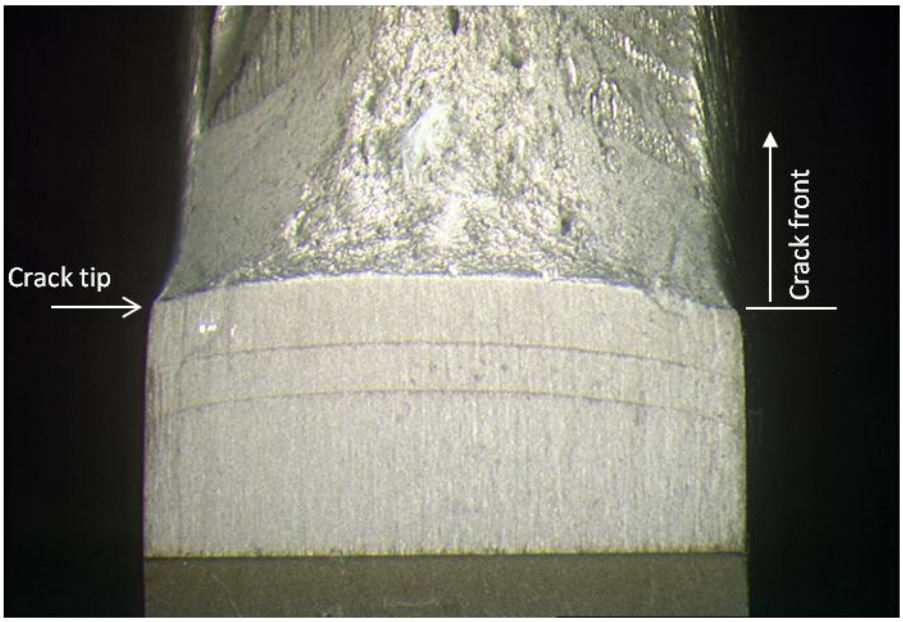

Figure 3-11 The cross section of a fatigued pre-cracked specimen

So, during the pre-cracking procedure, to reach an exact crack length, optical or digital microscope monitoring of the specimen surface can only give an estimation of the real crack length. It has been suggested that for better results, measurement of the crack length could be done by back face strain method or Alternating Current Potential Difference (ACPD) approach.

In Figure 3-12 different scenarios based on the number of contours on the crack front and number of nodes through the thickness, have been illustrated. For example, Y_10_5 is stands for the value of Y in the case of 10 contours and 5 nodes. As can be observed, by increasing the number of nodes through the thickness, the SIF results tend to be closer to empirical formulae.

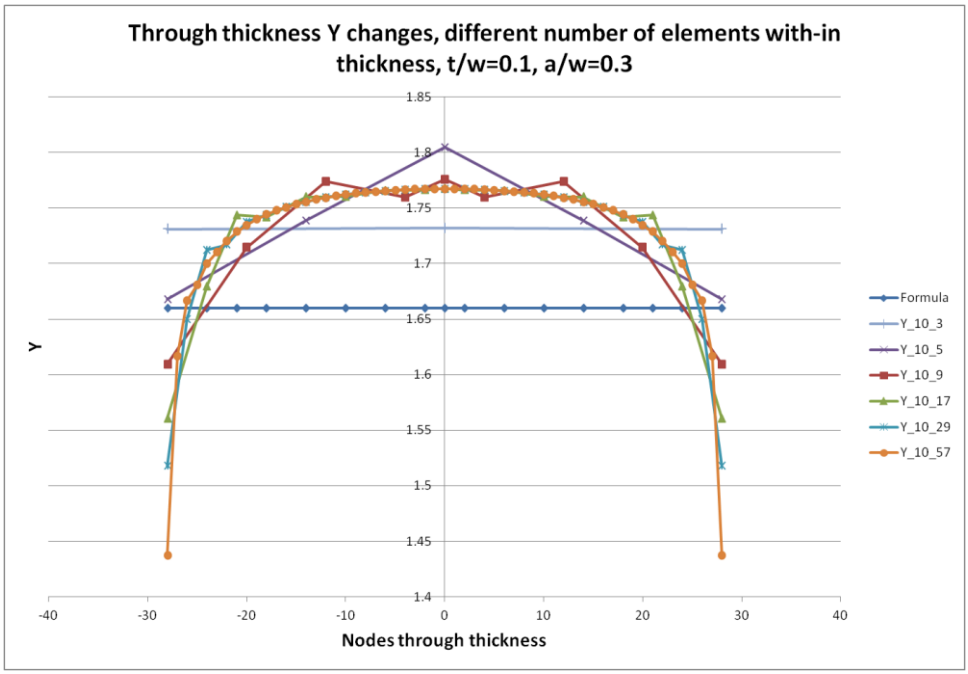

Figure 3-12 Through thickness Y value for different scenarios

Figure 3-13 illustrates the percentage of error when calculating Y in a 3D model, compared to an empirical formulae solution. A minimum number of eight nodes for this specimen can give accurate SIF results. This number for thicker specimens (t/w>0.4) could be larger. Table 3-3 presents the calculated Y values for different number of elements through thickness, where the Y value based on empirical formula was 1.7671.(equations (3-8) and (3-9))

Table 3-3 Y values for different number of elements through thickness

Number of elements through thickness	FEA calculated Y value
2	1.8
4	1.77
8	1.7678
16	1.7672
32	1.7671

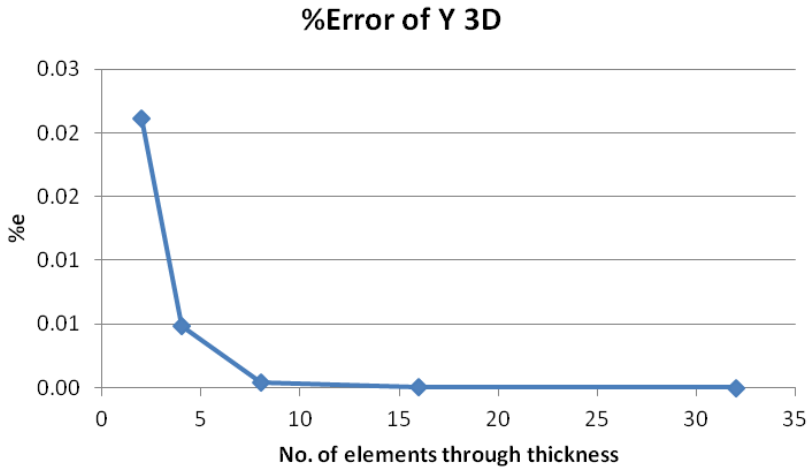

Figure 3-13 Percentage error when calculating Y in a 3D model compared to empirical formulae

Very close to the crack tip (first and second contours), due to crack tip singularity and plastic zone (as discussed in the previous section), the SIF results are not accurate. In this region “small scale yielding” happens and that means the nonlinear zone at the crack tip is small compared with the region in which the elastic crack tip stress fields apply. How small the plastic zone must be, depends on the accuracy desired.

3.3 Stress intensity factor calculation of CT specimen

To estimate the state of stress and calculate the SIF of the CT specimen, a finite element model of the CT specimen has been developed using Abaqus software. As part of this project, a fracture toughness test on pipeline material has been planned and is accomplished and fully described in Chapter 4. A step notched CT specimen with exactly the same dimensions as the experimental test has been modelled and different values of loading, stresses and SIF for a series of a/w were calculated.

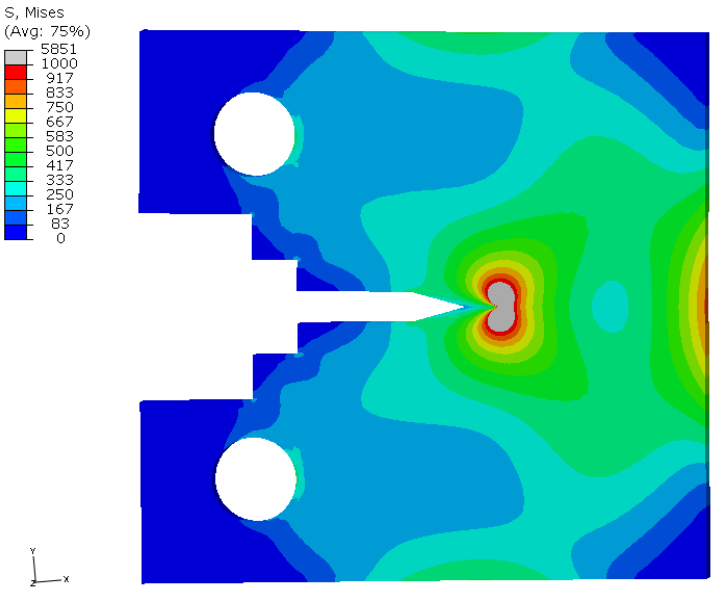

Figure 3-14 Von-Mises stress in step notched CT

The FEA SIF results have been compared with different available references and have good agreement. Figure 3-15 illustrates the FEA results comparison with (BS7448-1 1991; ASTME1290 2002) as references and the formulae are given in Chapter 4. As the reference formula is accurate only for 0.5<a/W<0.6, the results have been presented in this domain.

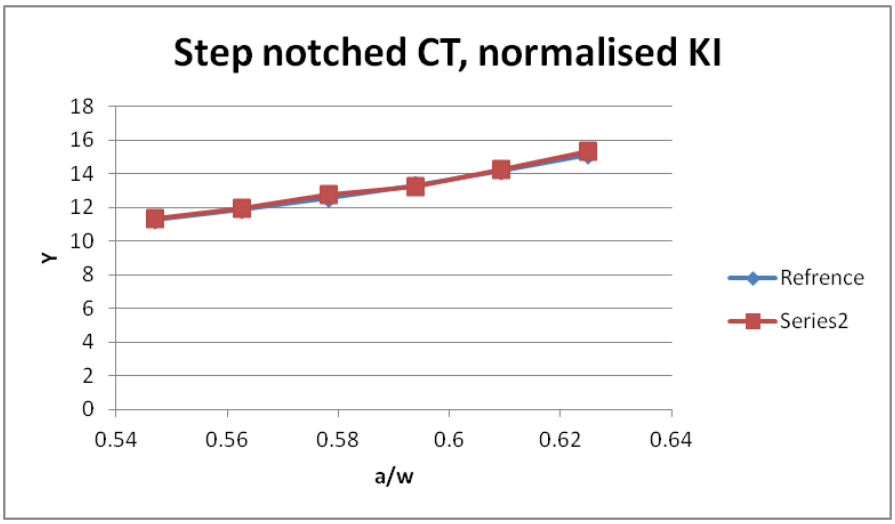

Figure 3-15 Normalised KI results for step notched CT

In Figure 3-16, for six different crack lengths, the state of stress has been depicted. The results presented in Figure 3-15 are based on these different crack lengths modelled in Abaqus. For modelling the CT specimen, nine elements through the thickness and C3D20R as the element type have been used. The crack tip is meshed using collapsed quadratic quadrilateral elements oriented as a ring. To obtain a mesh singularity at the crack tip, second-order elements have been used. For modelling the pin loads, the upper and lower surfaces of the pin holes have been considered under tension and compression force loads and the load point (in the center of the hole) can freely rotate around the z axes (normal to the CT surface). The crack tip meshes are very important for the accuracy of the SIF results. Very fine mesh should be applied on the crack tip and in the symmetrical specimen; half of the specimen can be modelled and the results will be accurate.

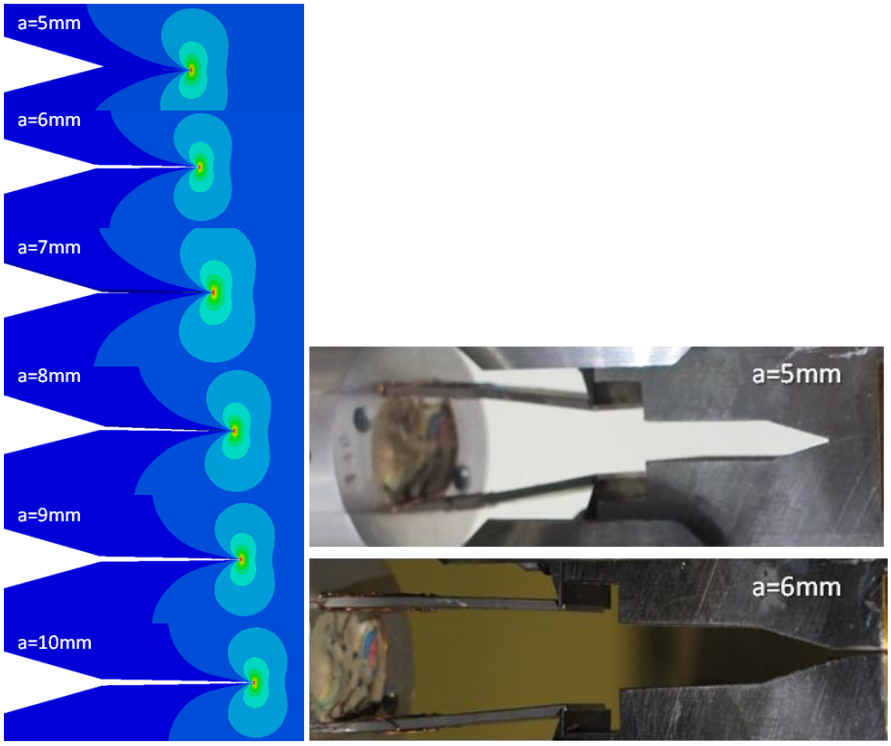

Figure 3-16 Calculation of SIF for different crack lengths

With the linear behaviour of KI versus applied load, by understanding the fracture toughness of the material, fracture propagation can be predicted. Following the outcomes of Chapter 4 at room temperature for API X100 material, the fracture toughness is about 140 MPam^0.5 which needs about a 40KN load to start propagation. These results agree very well with FEA outcomes with similar boundary conditions.

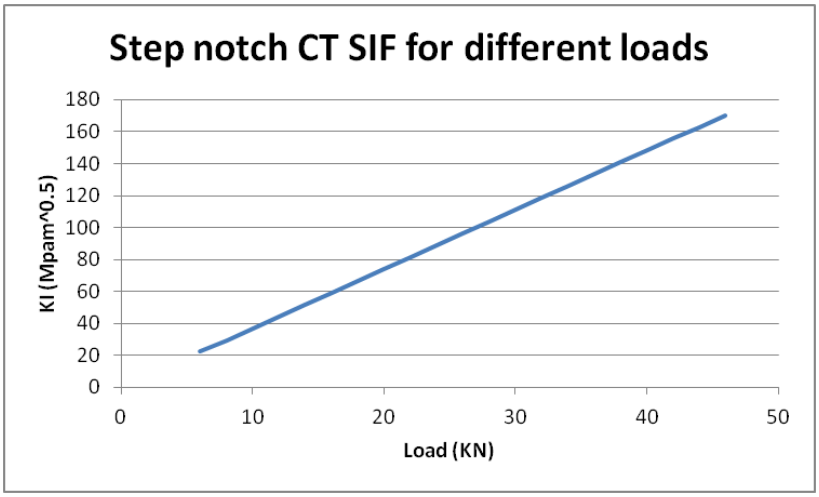

Figure 3-17 KI values for different loads in a step notch CT

3.4 Study of the thickness effect using FEA

“Lack of constraint” is a term in fracture mechanics that has been used in plane stress conditions; also, on the lateral faces of a thick test specimen it happens. As depicted in Figure 3-18 and Figure 3-19 it has significant effects on fracture behaviour. It can be understood that for thick specimens, cracks tend to grow from the centre point with the highest KI value.

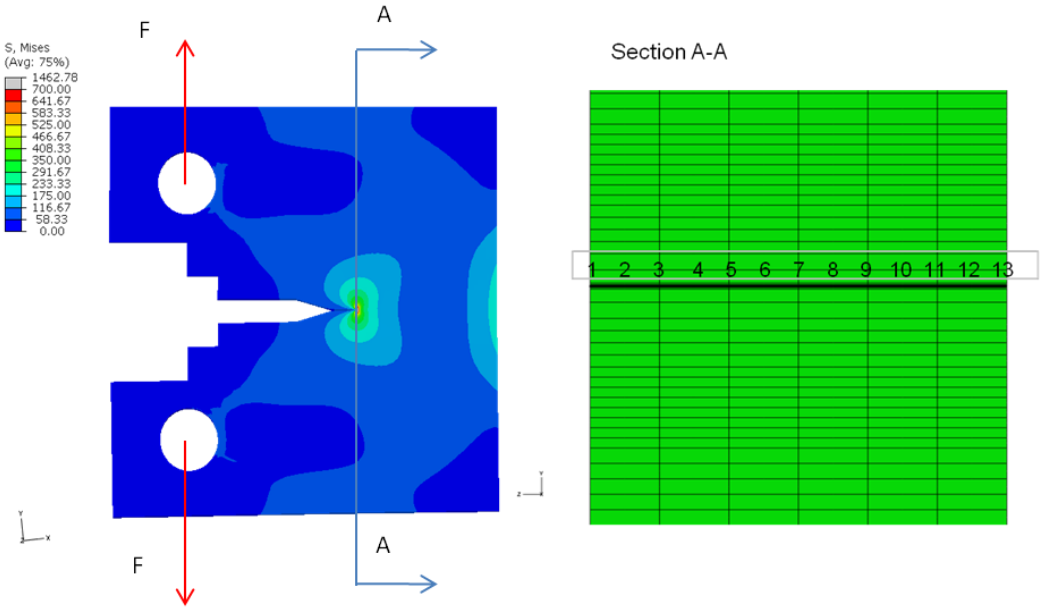

Figure 3-18 CT under tension cross section

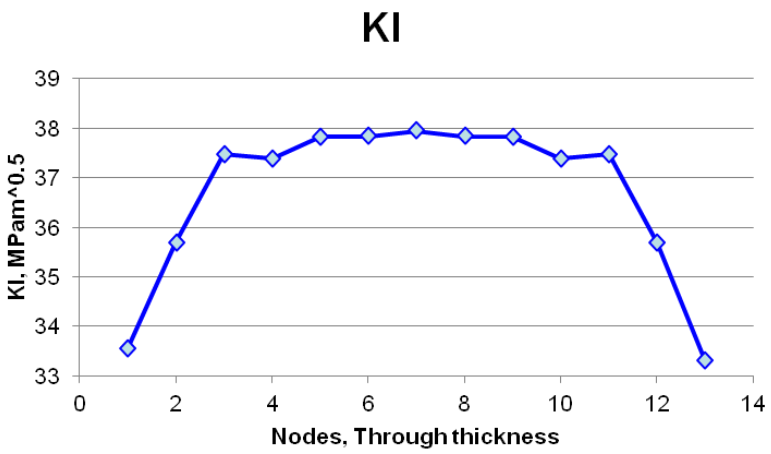

Figure 3-19 CT through thickness KI values

3.5 Constant K specimen analysis

The constant K (mode I SIF) specimens are specially designed (geometry point of view) to have constant K during crack growth steps. The idea of having a constant K specimen and conducting different tests in different temperatures will give a good prediction of the effect of temperature on material fracture toughness. For creep and fatigue crack growth rate tests, measuring the effect of different environments and temperatures on the behaviour of K_I, having constant K, is essential. When there are different microstructures being tested in an aggressive environment, it is not possible to isolate the influence of either the environment or microstructure under increasing K conditions. Also it could be taken into the account that keeping K constant during an experiment lets us observe the effects of different temperatures in a particular environment in a single test.

There are several constant K specimens in the literature. Using numerical simulation with Abaqus, most of them modelled a SIF within the specified range calculated. Due to lack of space inside the cooling chamber, a new optimum constant K specimen was designed and modelled in Abaqus. The new specimen depicted very good constant K results. Figure 3-22 shows a part of full library of constant K specimen finite element modelling which have been studied.

3.5.1 Crack Arrest Temperature Experimental Design

Identifying the Crack Arrest Temperature (CAT) of CO_2 pipelines is one of the concerns of any pipeline operator. Many studies are ongoing to find the temperature drop in CO_2 pipelines in case of sudden decompression due to a growing crack or defect. As explained before, different phase behaviours of CO_2 in comparison to natural gas, have forced operators to run pipelines under a very high pressure. If the temperature drop on in the vicinity of crack, passes the ductile to brittle temperature, the brittle fracture will be the dominant fracture mechanism. Material property varies as a function of temperature, and here the

low temperature discharge has a huge effect. Very high gas pressure, causes high hoop stress as a driving force of the crack and very low temperature due to CO_2 decompression, and consequently bringing down the pipeline material toughness would be disastrous. The concept of the crack arrest temperature can be defined as a self crack arrestor for the pipeline. At this temperature, toughness of the pipeline material is great enough to prevent any growth in the crack.

$$K_I = \frac{P}{\sqrt{h_a}} . f(m) . \left(\frac{a}{h_a} + 0.7\right) \tag{3-10}$$

Where

$$h_a = h(a) = d + ma \tag{3-11}$$

$$f(m) = 3.46 - 2.65m + 1.89m^{3/2} \quad (m < 0.5)$$

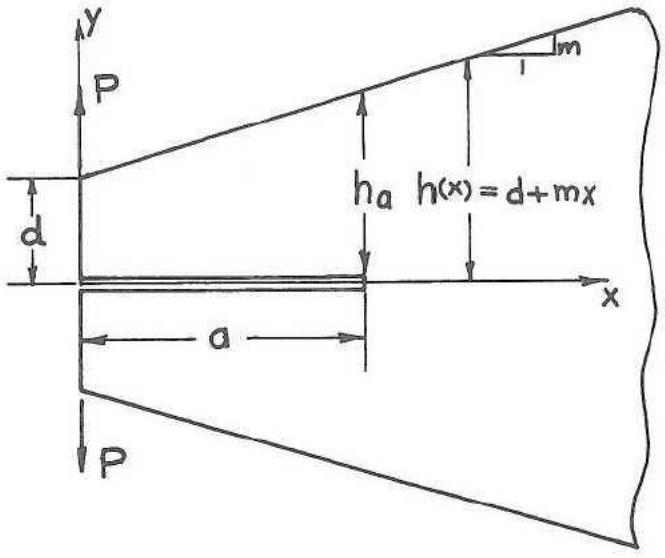

Figure 3-20 Constant K specimen
(Paris, Tada et al. 2000)

Numerical and analytical results give a very good, reliable constant K within a specified distance from the crack tip. A proper number of specimens will be manufactured for different test conditions. These tests will be conducted at room temperature and three different cold temperatures (below zero degrees C) using liquid nitrogen in a cooling chamber. The outcome of these tests will be force values over time related to measured crack growth in different temperatures. Using a cooling chamber built in thermometer and an infrared manual one, specimen temperatures can be recorded. Also crack growth will be monitored using a travelling microscopy.

At this stage, an understanding of material toughness value and yield strength is necessary. For the specimens tested at room temperature, due to constant K geometry, the values of force and displacement will be recorded. For the cold temperature environment which is a simulation of CO_2 decompression near the crack tip in the case of CO_2 pipeline with a crack, under similar test conditions, any changes in value of force and displacement will be due to temperature. From the other tests such as Charpy and DWTT, the ductile to brittle transition temperature of the specimen material will already have been obtained. For the constant K specimen test, the pure effect of temperature change on fracture toughness can be obtained.

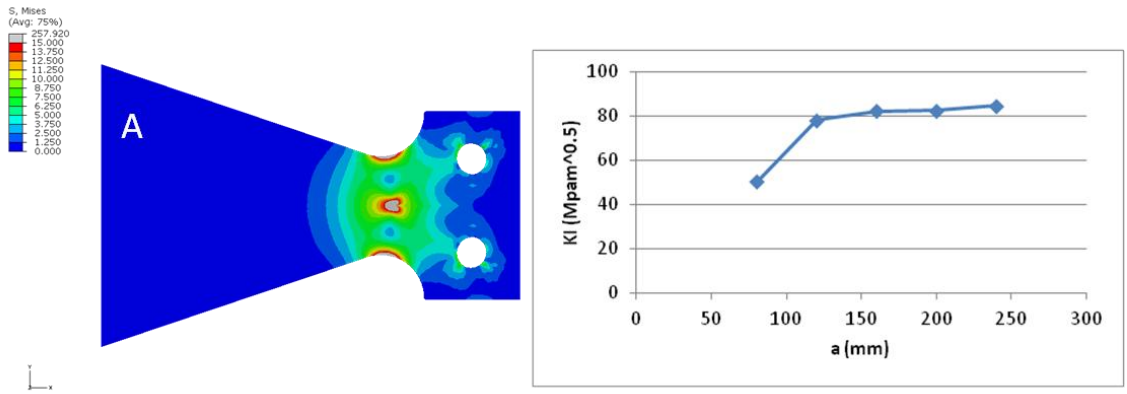

Figure 3-21 New design of constant K and its results

A series of FEA simulations have been conducted and some of the results are presented in Figure 3-22. The optimum design is illustrated in Figure 3-21.

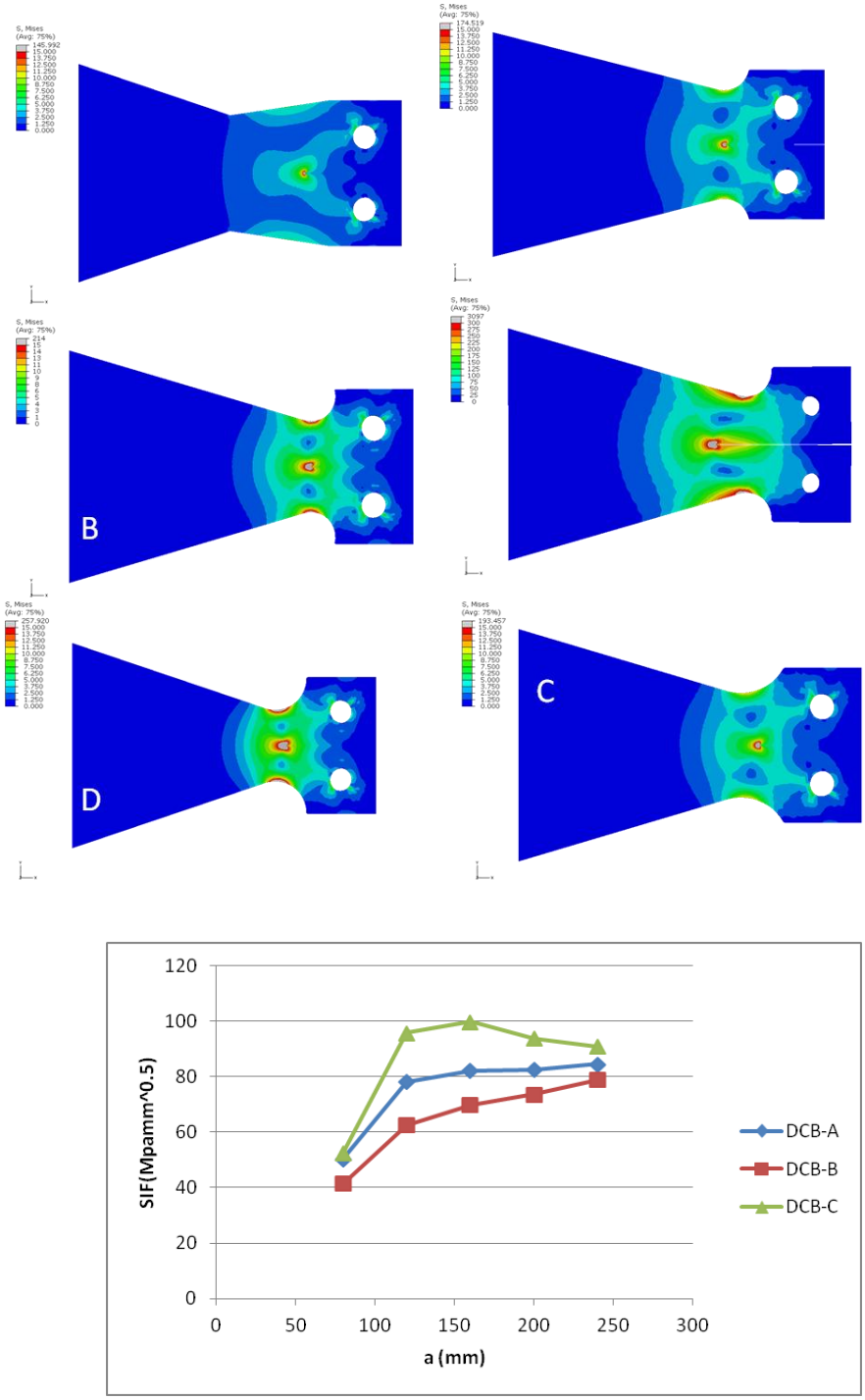

Figure 3-22 Different design dual cantilever beam SIF results

So by having constant K specimens of a material, the pure effect of low temperature on crack propagation can be observed. The constant SIF of this new specimen has been validated using FEA techniques and it is suggested to be made and validated the results as a future research.

3.6 Summary

In this chapter the finite element technique as a powerful tools to calculate SIFs for non standard geometries have been presented. Accurate modelling of the geometry and the quality of the mesh (especially around the crack tip) is important and affects the SIF results. Abaqus calculates the SIF from a J-integral and as the J-integral is path independent, the crack front contours only need to be symmetrically partitioned and defined. The FEA results for the SIF were verified using available references in the literature and the notch stress concentration effect and thickness effect in calculating SIF discussed.

For the sake of a fracture toughness test using a compact tension specimen (Chapter 4), a CT specimen with the exact geometry of an experimental test was modelled and the SIF for different loading conditions calculated. Also the SIF for different crack lengths in the CT specimen was presented. Also the effect of CT thickness on the accuracy of the SIF results was discussed.

In addition, a novel constant K design (dimensions presented in Appendix D) and the associated SIF results were presented. A series of FEAs for different constant K geometries were modelled and the SIF results discussed. Understanding the effect of low temperature on crack propagation and the SIF for pipeline material using the presented constant K specimen are noted as areas for future work.

The results of the analysis reported in this chapter will be used to perform fracture toughness tests which will be explained in Chapter 3.

Chapter 4. Fracture toughness test

In this chapter the experimental work of this research project is presented. The theoretical values and estimations of SIFs have been presented in Chapter 2 using a numerical simulation. To fully understand crack initiation and the fracture toughness of the material, it is vital to conduct experimental tests.

In fracture mechanics based design, different parameters such as CTOD, K and J are considered as part of the design parameters. Traditional engineering practice has been on conservative design with extra safety factors; also, from a materials point of view, availability, cost and adequate yield strength to overcome the calculated stresses was taken into account. In previous designs, defects and flaws were considered as failures and the structure failed in the pre-commissioning tests. Introducing material property, the so-called “fracture toughness” or material’s resistance to fracture, let fracture mechanics based design to approve the structure’s operations, despite the presence of flaws. Using enhanced non-destructive testing (NDT) techniques, flaw type, size and location are determined and put into the stress analysis calculation. The material’s fracture toughness is a very important property of the material and is an indication for designers to let them know the amount of stress required to propagate an existing crack.

4.1 Material selection, rolling direction and composition test

In general, in the design of existing gas pipelines, designers followed the American Petroleum Standard (API) 5L standards material suggestion. X60, X65, X70 and later X100 and X120 are the most popular gas transmission pipeline materials. The numbers indicate the minimum yield strength of each material in KSI.

For the assurance assessment of acquired Pipeline Materials, chemical composition tests have been conducted using Optical Emission Spectroscopy

and the results perfectly matched the related standards. Three different steel samples, X65, X70 and X100, have been sent for chemical composition tests. The aim has been to identify the material and to use the results in further corrosion based studies. The Environmental Scientifics Group (ESG) was selected to conduct these tests and the results are given in Table 4-1:

Table 4-1 Chemical composition test result (W%)

Identified		X65	X70	X100
Carbon	%	0.04	0.05	0.07
Silicon	%	0.19	0.26	0.3
Manganese	%	1.04	1.89	1.83
Sulphur	%	0.008	0.010	0.009
Phosphorus	%	0.013	0.010	0.012
Nickel	%	0.03	0.44	0.28
Chromium	%	0.03	0.41	0.17
Molybdenum	%	<0.01	0.40	0.16
Copper	%	0.02	0.45	0.15
Vanadium	%	0.04	0.07	0.01
Niobium	%	0.06	0.05	0.04
Titanium	%	0.01	0.01	0.02
Aluminium	%	0.03	0.01	0.04
Cobalt	%	<0.01	<0.01	<0.01

The original report can be found in Appendix C.

X100 has been selected as a high strength low alloy steel to be used for the purpose of this fracture toughness test. To find the fracture toughness of the selected material, a step notch compact tension (CT) has been chosen. The fracture toughness test has been accomplished based on ASTM E1290 and BS 7448 standards.

Before designing the CT specimens, it is important to know the rolling direction of the selected material plate. As the study is on longitudinal cracks along the pipe, the notch and pre-crack of the specimen should be in the direction of the plate rolling direction during its manufacturing process. After cutting pieces of material in different directions and after several surface grinding treatments, by precisely observing the surface using electron microscopes, the micro-structural analysis has been performed.

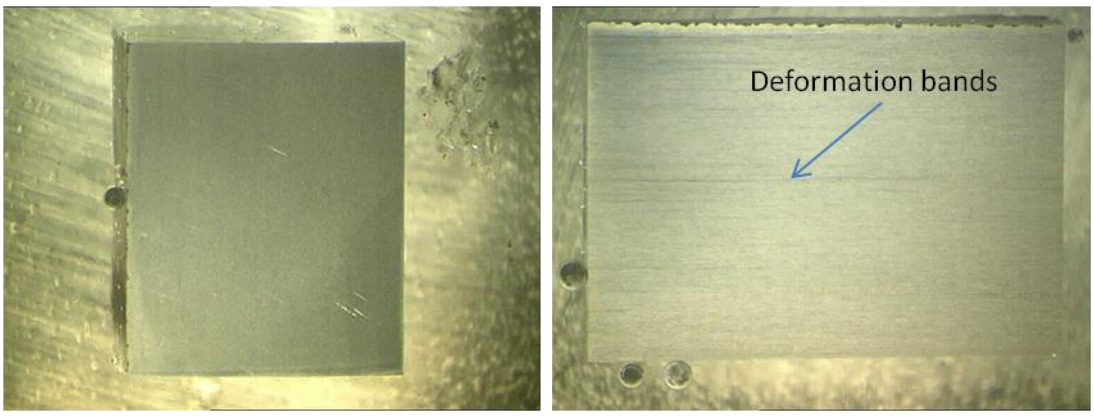

Figure 4-1 Transverse and Longitudinal Sections

The rolling direction test has been done by my colleague Mr. Wilson Vesga Rivera, in accordance with ASTM A-751 and ASTM E-3, and further details can be obtained from his thesis.

4.2 Design of specimens

After understanding the rolling direction and selecting the CT specimen type (step notch compact tension), 18 specimens were oriented on the plate for manufacturing (Figure 4-2). According to ASTM E399, the specimen orientation code is T-L (ASTME399 2009). It has been planned to perform this test at different temperatures from ambient to -70°C (the minimum that can be obtained with the existing liquid nitrogen cooling chamber). The cooling system will be explained in Appendix G.

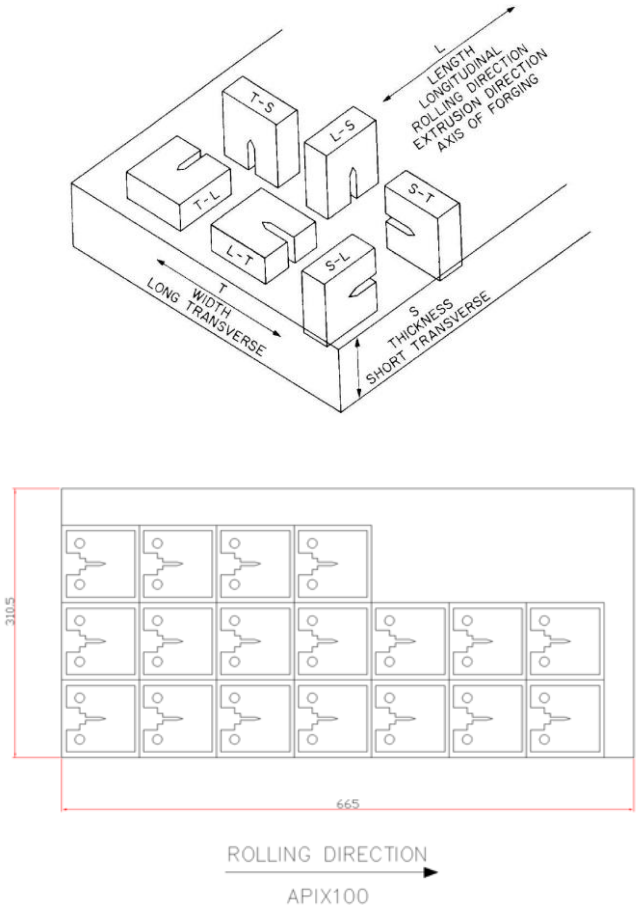

Figure 4-2 Specimens' orientation on the plate

The most important dimension of the CT specimen is the thickness. All other dimensions are related to thickness (B). To have a valid fracture toughness test and calculating a valid K_{IC} from the result of this test, the test has to be performed in a plane strain condition. The minimum thickness to fulfil this condition is dependent on the material yield strength and its fracture toughness. Based on the available materials fracture toughness database, reasonable fracture toughness should be considered and using equation (4-1) the specimen thickness can be calculated.

$$B \geq 2.5\left(\frac{K_{IC}}{\sigma_{ys}}\right)^2 \qquad (4\text{-}1)$$

Yield strength should be obtained from the same material batch (in this case, from the same plate) using the ASTM E8 standard (ASTME8 2009).

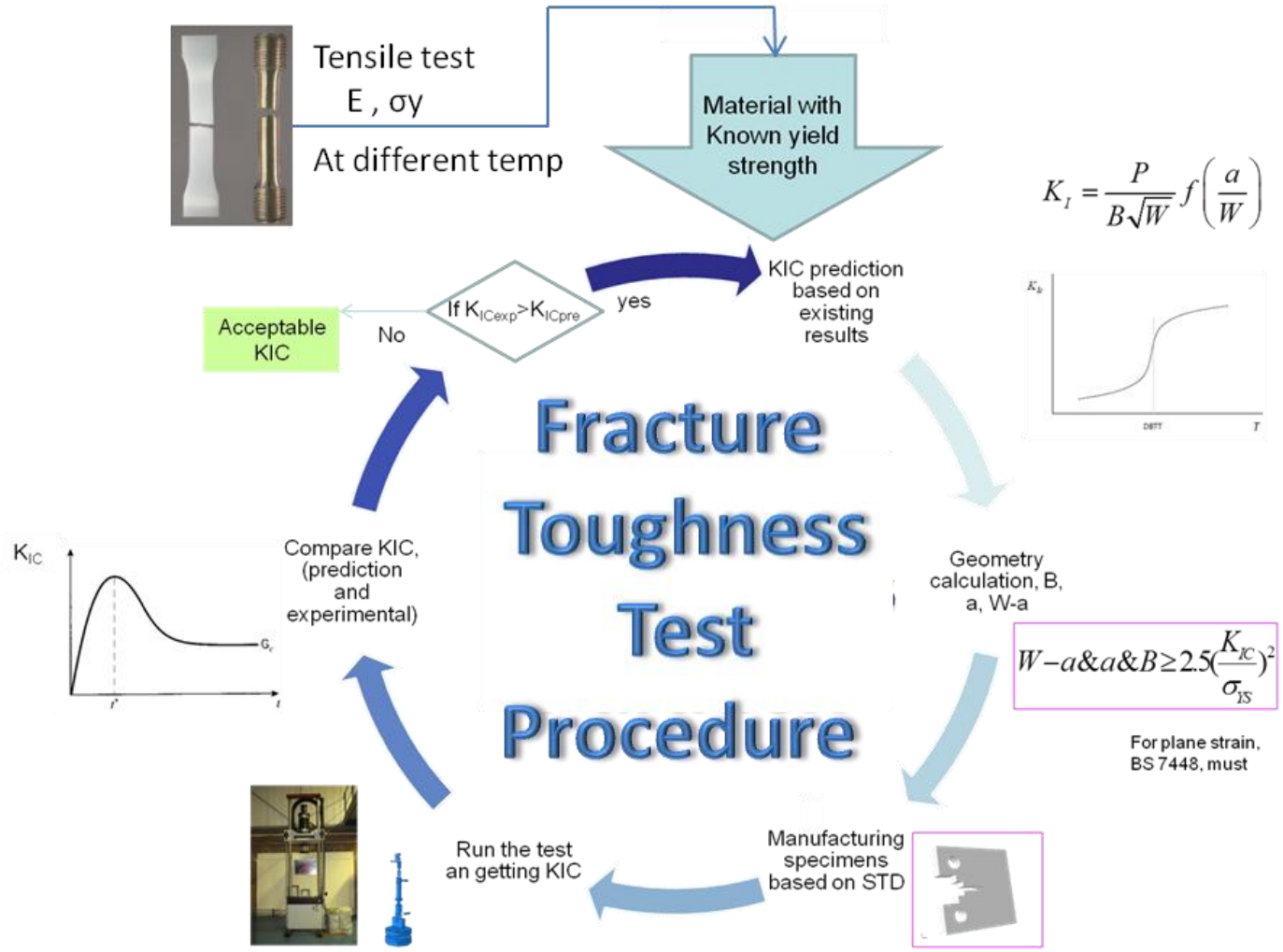

Figure 4-3 Fracture toughness test procedure

When the thickness is less than the critical value, the constraint relieving influence of the free faces extends across the thickness of the test specimen before the applied stress intensity reaches the K_{IC} (ISO12135 2002).

As illustrated in Figure 4-3, there are other conditions to be fulfilled before conducting the test. The pre-crack length plus notch (a) and remaining ligament (W-a) should also be larger than the calculated value from equation (4-1). The standard test procedure has been explained in section (2.6.3) and for a better understanding of the alphabet meaning, please refer to that section.

In pipeline manufacturing, sizing of the pipeline (especially wall thickness), depends greatly on operational pressure and pipeline material stress allowance. In this project the thickness of the pipeline is assumed to be 12mm. Based on this assumption, the specimen thickness has been selected as the same as the pipe thickness. For high alloy steels the minimum calculated thickness of the specimen in order to have a plane strain condition based on equation (4-1), is over 50mm. There are possibilities (maybe in a military application) that pipe or plate manufacturers make such a high thickness of plate. As it was almost impossible to do this test under such conditions, the test has been run with 12mm specimens.

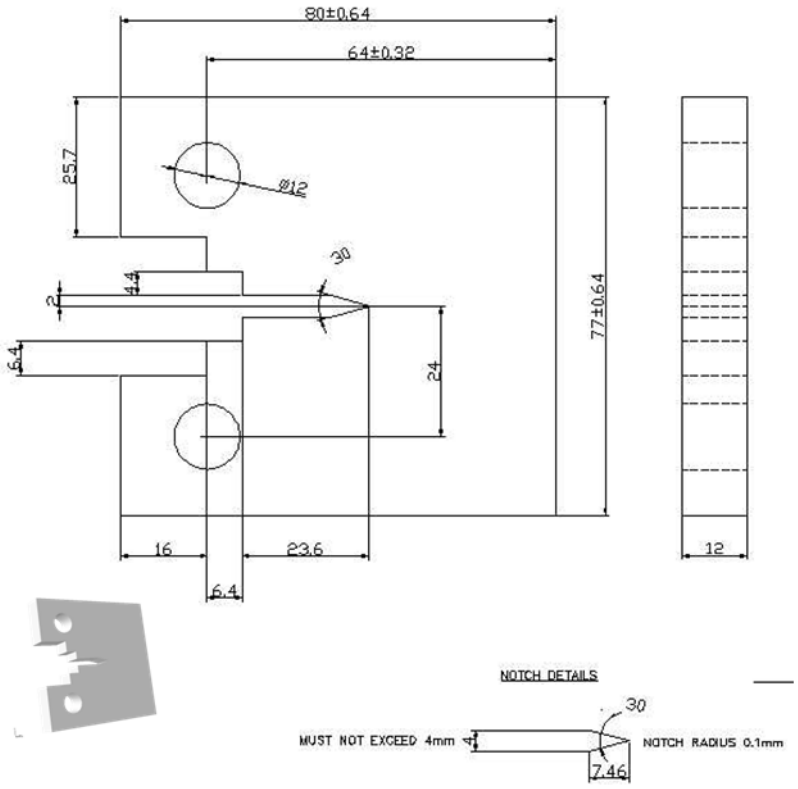

Figure 4-4 Step notch CT dimensions

A different section at the end of this chapter has been dedicated to the correlation of the results and prediction of size effects

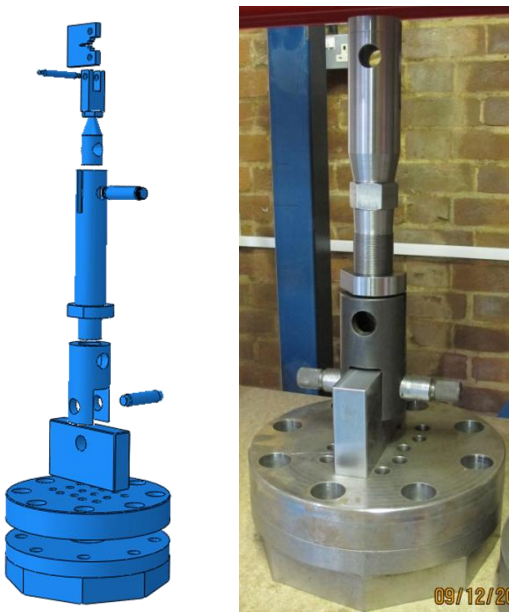

Figure 4-5 Clevis and end fittings

The design and manufacture of knife edge blades in a step notch compact tension specimen is a precise task. The knife edge holes' position and their thread, and the knife edge blades' angle and material (silver steel) should be manufactured and selected carefully. For step notch compact tension, as the load line is exactly along the knife edge blade tip, the value of the load line displacement reading from the Servo hydraulic machine should be equal to the crack opening displacement (COD) reading from the clip gauge. This will only happen in a calibrated machine with a calibrated clip gauge connected to it. So the results can be either load versus position or load versus COD. Different size end fittings have been designed and manufactured to be used for a CTOD test and tensile test (Figure 4-5).

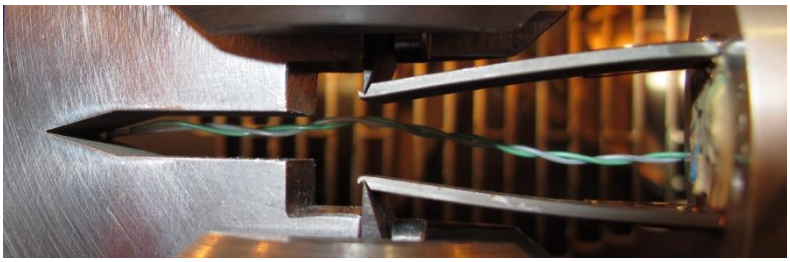

Figure 4-6 Knife edge blades

4.3 Pre-cracking

For the plane strain fracture toughness test it is necessary to develop a natural crack by fatigue loading of the specimen, whereas, in a plane stress testing condition a sharp saw cut is enough to make an acceptable pre-crack. Fatigue pre-cracking shall be done in the final material condition and at room temperature; any required heat treatment or mechanical work shall be done before pre-cracking starts. The stress distribution through the specimen thickness should be uniform and symmetrical about the crack plane. Fatigue pre-cracking can be conducted under either displacement control, force control or K control. If the displacement cycle is maintained constant, the maximum K and ΔK will decrease with crack size; if the force cycle is maintained constant, the reverse will happen. If K is maintained constant, as a function of increasing crack size, the force has to be reduced. To monitor this condition, crack growth

has been monitored on both sides in a different number of cycles, using digital and analogue microscopes (Figure 4-7). If crack initiation is not observed on both sides symmetrically, the fatigue cycling should be stopped to find a remedy for asymmetrical behaviour.

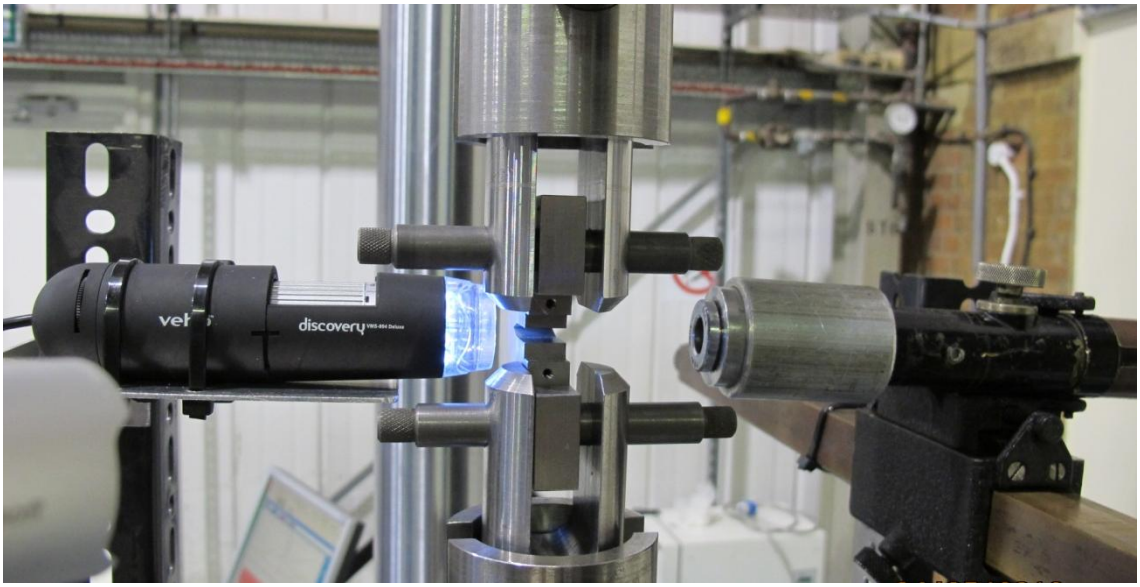

Figure 4-7 Pre-crack monitoring from both sides

The fatigue pre-cracking force should not exceed the maximum fatigue pre-cracking force (F_f) (4-2). During the pre-cracking and any other part of the test, the K applied to the specimen shall not exceed 25 MPam^0.5.

.

$$F_f = \frac{0.2B(W-a)^2(\sigma_{YSP}+\sigma_{TSP})}{(2W+a)} \qquad (4\text{-}2)$$

Where B is the thickness, W is the width, a is the initial crack length and σ_{YSP} and σ_{TSP} are 0.2% proof strength and tensile strength at the temperature of fatigue pre-cracking respectively. All the above limitations and conditions are to prevent having extensive plasticity on crack tip. Without doubt, there is a confine plasticity on crack tip during and after pre-cracking procedure but it has not a huge effect on fracture toughness test results. In case of extensive

plasticity on crack tip, it can work as a retarder on crack initiation and propagation during fracture toughness test.

To set up a test method with Servo hydraulic machine software, the load type, amplitude, and number of cycles should be defined. Considering the conditions mentioned in the previous paragraphs about the maximum fatigue pre-crack force, the pre-cracking method has been defined. To have a uniform applying load, the envelope technique has been used (Figure 4-8). The envelope defines an increscent load from zero to a certain value in a specified time. It does not let sudden plasticity or deformation happen on the specimen.

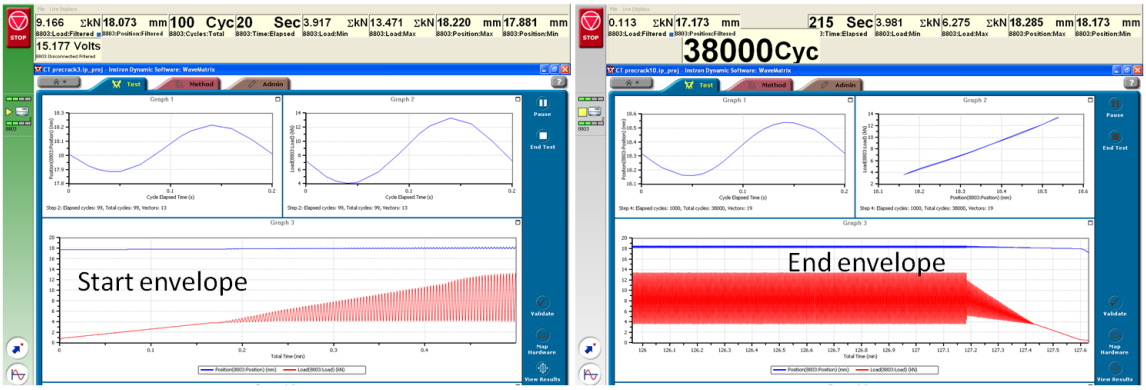

Figure 4-8 Pre-crack method developed using envelopes

The envelope duration for start and end has been set to 15 seconds. This means the Servo hydraulic machine has 15 seconds to reach its maximum amplitude.

4.3.1 Pre-cracking methodology

A method has been written for pre-cracking of CT specimens using “WaveMatrix” software. This software has been developed by Instron and came with the main Instron console software. The first important point is to select the control mode for the method. As we have calculated the maximum fatigue pre-

cracking force, F_f is the benchmark and the control mode should be set to “Load control”.

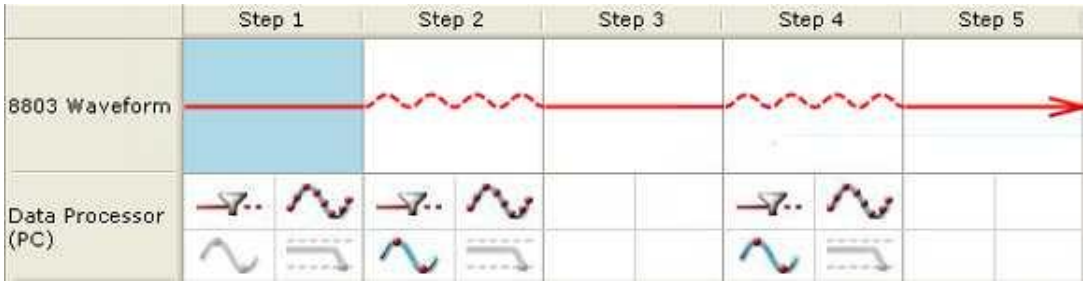

Figure 4-9 Pre-cracking method

For the purpose of pre-cracking CT specimens, five steps have been defined (Figure 4-9). Steps 3 and 4 are merely for the purpose of accurate crack length check and reducing the amplitude of the force in the last cycles.

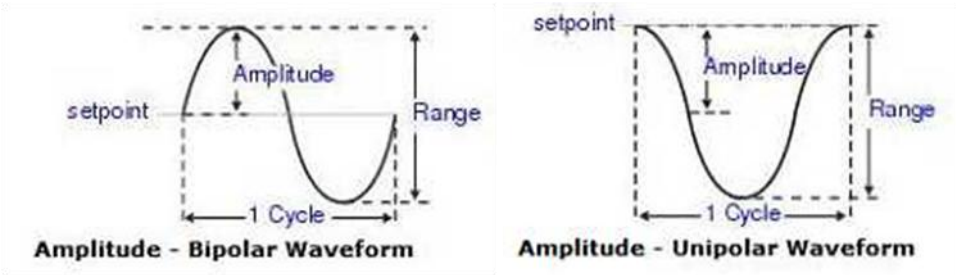

Figure 4-10 Different sine waveform definitions
(Instron 2011)

Step 1 is a ramp to preload the system. It has a 0.3 KN/s ramp rate and the end point of 3 KN. The purpose of this step is to have an aligned, steady chain of end fittings and specimens ready to pre-crack.

Step 2 is a cyclic waveform with an amplitude of 5 KN and a frequency of 5 Hz. As in pre-cracking, all the loading conditions should have positive tension; unipolar sine waveform was selected as the wave shape and the starting point was been set to 270 degrees. Selecting the starting point at 270 shifts upwards

the whole sine wave and it never goes below the starting point. The number of cycles has been set to 35,000.

Step 3 is set to be held for 5 seconds and this is enough to measure the crack growth from both sides of the specimen.

Step 4 is similar to step two with half of the previous amplitude and the same frequency. The number of cycles has been set to 5,000.

Step 5 is defined as a ramp to 0.2KN with a ramp rate of 0.3 KN/s.

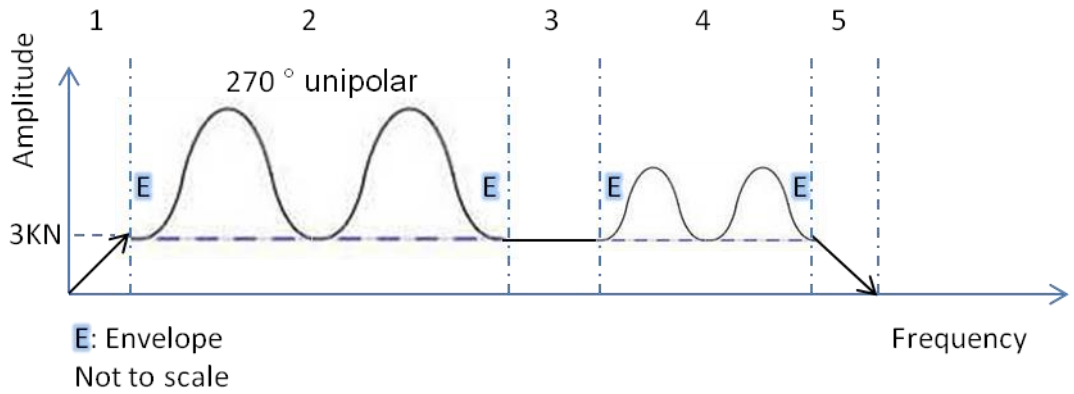

Figure 4-11 Steps of pre-cracking method

In the cyclic waveform steps, all of the load and position data have been captured. It is important to know the maximum applied force and total number of cycles. Most of the pre-cracking was planned to be conducted between 10am and 4pm, and as a result the ambient temperature was in the range of 19 to 22°C for all specimens. The ambient temperature and specimen surface temperature have been measured separately with a wall mount and infrared thermometer respectively.

Table 4-2 pre-cracking condition values

Ramp			Wave 1				Wave 2	
Rate	Start	End	Shape	Freq	Amp	Cycles	Amp	Cycles
0.3 KN/s	0	3KN	Sin	5Hz	5KN	35K	2.5KN	3-5K

Frequency of the wave form has no effect on crack growth. By increasing the frequency the duration of pre-cracking will reduce but there is possibility of introducing thermal stresses on crack tip and it is not recommended.

A target of 5mm pre-crack length has been set and marked on specimens to be easily visible with microscopes. At the end of the pre-cracking procedure all the specimens have 5±0.1mm cracks. Figure 4-12 and 3-13 depict the pre-crack length growth for a different number of cycles. The blue line is the 5mm benchmark distance from the notch end. The notch end has been manufactured with Electrical Discharge Machining (EDM) technology and should have a sharp end and be parallel on both sides.

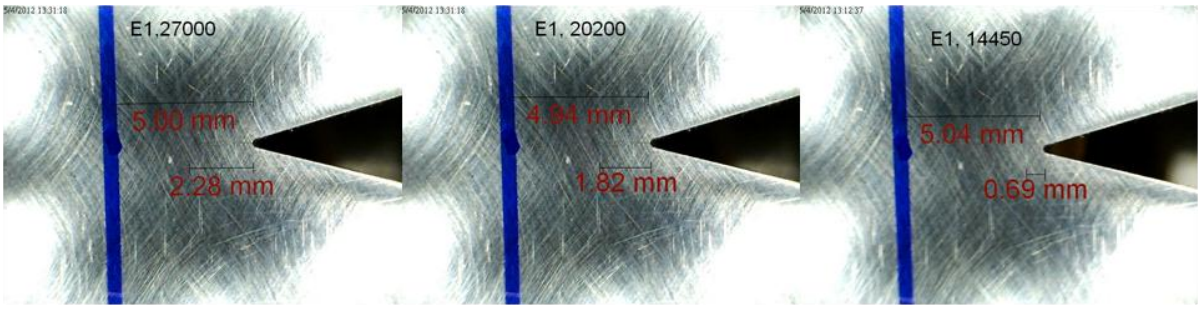

E1, xxxxx : Specimen E-Side 1- Number of cycles=xxxxx

Figure 4-12 Pre-crack length up to 27,000 cycles

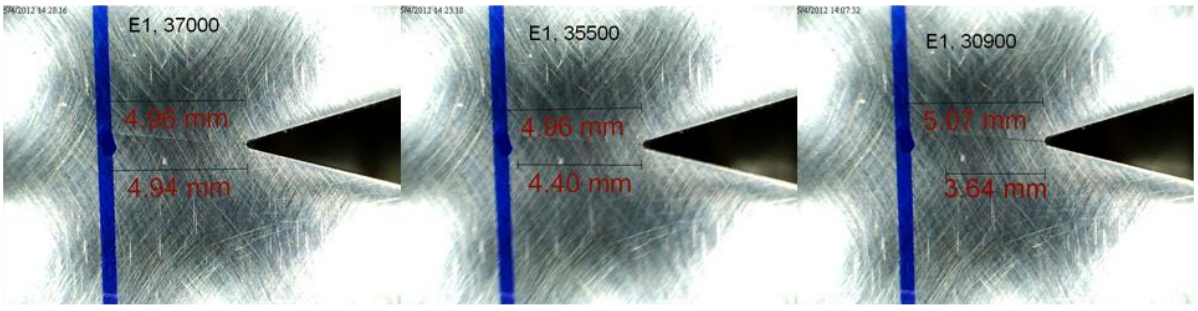

E1, xxxxx : Specimen E-Side 1- Number of cycles=xxxxx

Figure 4-13 Pre-crack length up to 37,000 cycles

In these two figures, E is the specimen identification, 1 indicates the side of the specimen and the five digit number is the number of cycles. The upper

measurement is the benchmark (blue line) distance to the notch tip and the lower dimension shows the pre-crack length in the different number of cycles.

Figure 4-14 illustrates the cross section of a broken specimen using an optical microscope. Changing the amplitude in steps 2 and 4, which are the cyclic waveform steps, caused the beach mark in the last 1.3mm of the pre-crack. This specimen has been broken in ambient temperature and, as is observable from the picture, the ductile fracture mode was dominant. The change of the thickness (so called necking in a tensile test) can be observed exactly at the start of the ductile crack propagation point.

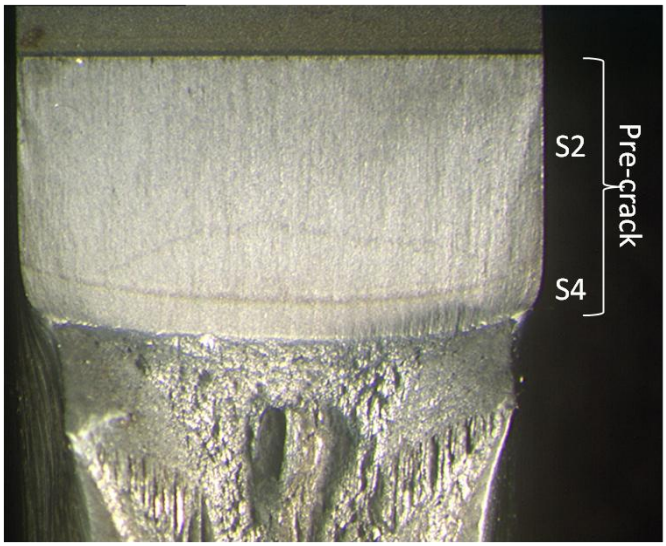

Figure 4-14 Cross section of a broken specimen step's beach mark

4.4 Fracture toughness test (CTOD) in different temperatures

Different standards are available to measure the fracture toughness of a material. Material fracture toughness can be defined as a physical property of material that is quantitatively being measured and can be used in different applications as a design variable. A proper standard test method should have an acceptable degree of precision and the results of the test should be independent of the test operator, test equipments (brands) and the laboratory performing the test. Also, it is important that the quantity measured has a physical interpretation, independent of standards used to measure it. It has been observed that fracture toughness is a function of specimen thickness and in plane stress tests it is a function of panel width.

A warm pre-stressing effect can elevate the measured fracture toughness; this effect is due to different acting temperatures of pre-cracking and actual tests. All specimens of pre-cracking are conducted at room temperature, but the CTOD test results have been attained in different, low temperatures. To minimise this effect, the maximum K that may be applied in the last steps of pre-cracking (1.3 mm) shall not exceed 15 MPam^0.5.

Basically, at higher temperatures, the fracture behaviour is more ductile and the yield strength lowered. In this condition, due to the thermally activated process (breaking of atomic bonds), there are higher dislocation motions and consequently higher plastic deformations occur. As the temperature increases, due to greater frequency and amplitude of atoms' vibration, the atoms under stress slip to new locations. This slippage of the atoms is known as plastic deformation in a ductile fracture. On the other hand, at lower temperatures and due to a less likely movement of atom dislocations, the yield strength of the material increases. From a fracture mechanics perspective, at lower temperatures the plastic zone is smaller and the fracture toughness of the material decreases (Figure 4-15). This figure showst a general example of steel behaviour.

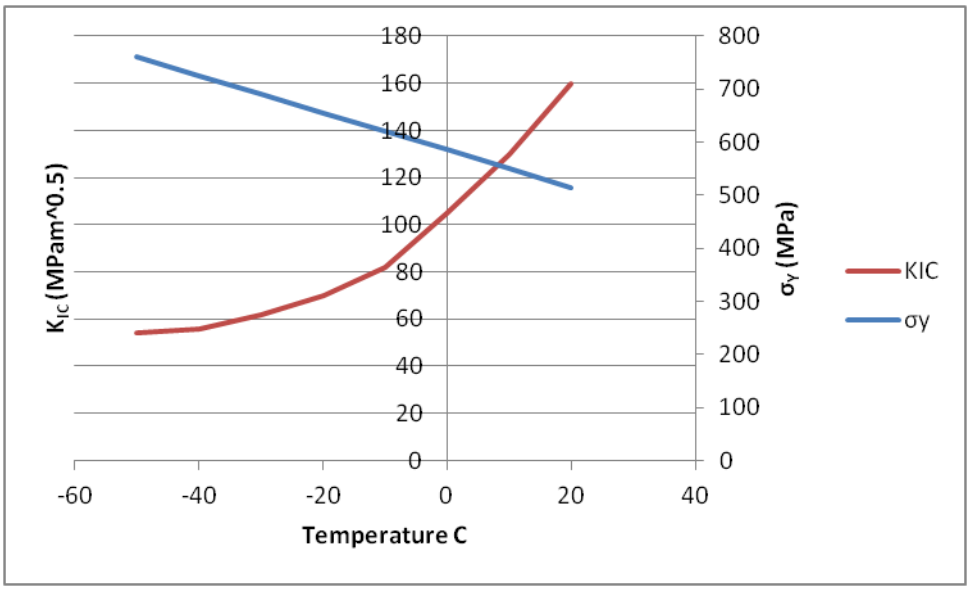

Figure 4-15 Typical steel yield strength and fracture toughness behaviour versus temperature

Each material has its own Ductile to Brittle Transition Temperature (DBTT). In general in a material under certain loading conditions, ductile failure (plastic flow) or brittle failure (crack propagation) will occur, depending on which process requires the smaller applied stress. From the micro structural perspective, atomic dislocation motion at room temperature causes plastic deformation in a metal. The stress required to move a dislocation depends on the crystal structure, atomic bonding, grain boundaries and other dislocations. Brittle fracture occurs when the stress required for moving the dislocations is too high.

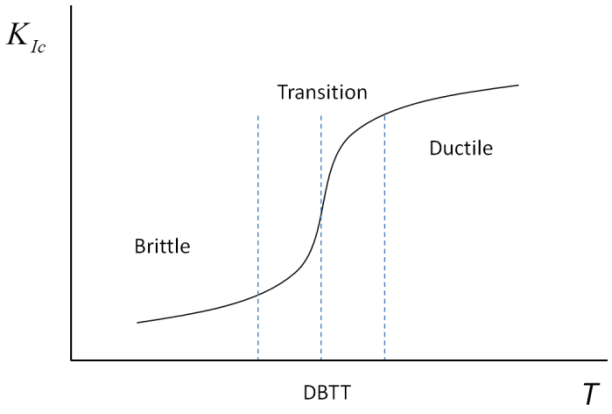

Figure 4-16 Typical fracture toughness behaviour and DBTT

4.4.1 Test setup and test results

Eighteen specimens have been manufactured to perform the test in six different temperatures. Figure 4-17 depicts the overall arrangement of CT specimens inside the cooling chamber. Magnetic surface thermometer, clip gauge, clevises and pins can be recognised from the picture. Teflon spacers have been used on both sides of a specimen to secure it from any unwanted movements. For more information about clip gauge and cooling chamber please refer to appendices F and G.

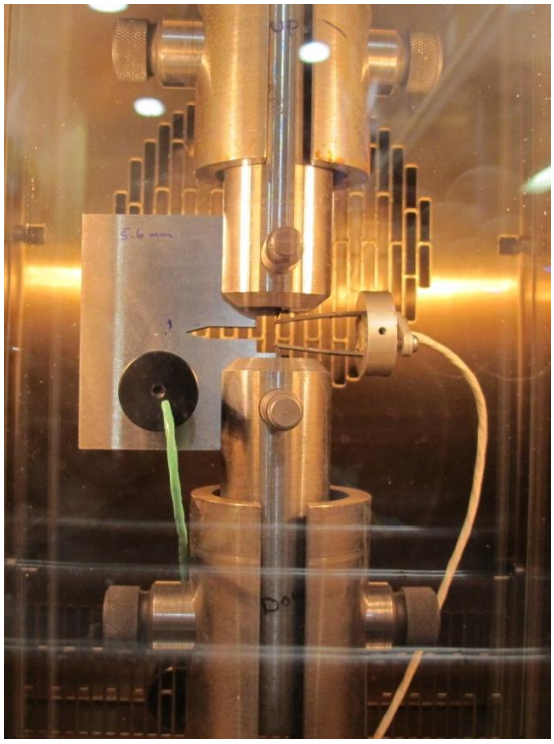

Figure 4-17 Test setup arrangement

For this test, force versus crack opening displacement (COD) is required. For the step notch CT specimens, the clip gauge reading is equal to the line load displacement reading from the Servo hydraulic machine, if everything was in ideal condition. As for this test a clip gauge has been considered, force versus COD has been recorded. For this purpose a method should be written and applied to the Servo hydraulic machine.

The method consists of three steps in position control mode. All the steps were relative ramp waveforms with different ramp rates. Only the first one, with a ramp rate of 1 mm/min, was important and the other two were just for breaking the specimen. The ramp rate should be low enough to prevent any sudden plasticity on the crack tip. For a better understanding of the crack tip deformation and crack propagation, a high speed camera has been setup to capture high quality/high speed pictures from the crack tip. Figure 4-18 is a close up picture of the apparatus at -70°C.

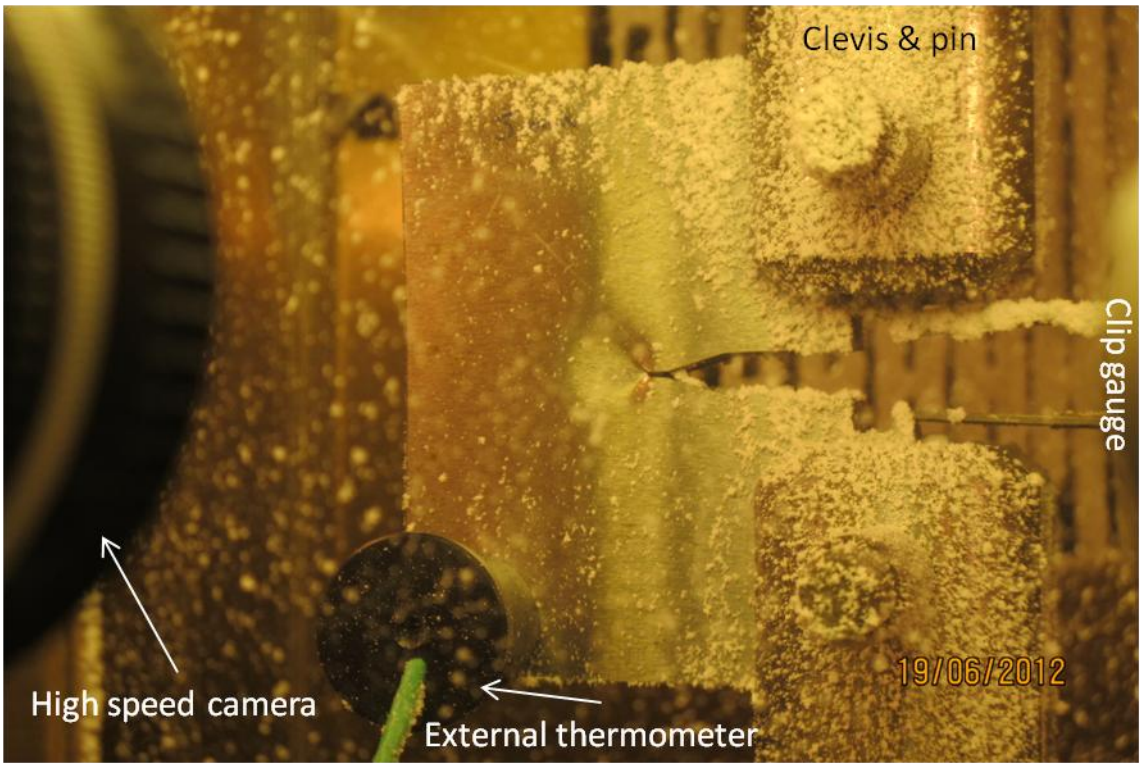

Figure 4-18 Test at -70°C, inside the cooling chamber

For the calculation of a valid fracture toughness (K_{IC}), the first condition to be met is the satisfaction of equation (4-1) . As discussed before, due to the limitations of manufacturing a very large thickness of material, a provisional fracture toughness (K_Q) has to be reported. The standard procedure for the

calculation of K_Q in all the following standards is the same (BS7448-1 1991; ASTME1290 2002; ISO12135 2002). For K_Q calculation:

$$K_Q = \frac{F_Q}{BW^{0.5}} f'(\frac{a_0}{W}) \tag{4-3}$$

Where F_Q is the provisional force (for the determination of K_Q), B is the specimen thickness, W is the specimen width and a_0 is the actual pre-crack length. The geometry function of f' can be calculated from:

$$f'(\frac{a_0}{W}) = \frac{(2+\frac{a_0}{W})(0.886+4.64(\frac{a_0}{W})-13.32(\frac{a_0}{W})^2+14.72(\frac{a_0}{W})^3-5.6(\frac{a_0}{W})^4}{(1-\frac{a_0}{W})^{1.5}} \tag{4-4}$$

In Figure 4-19, the method of calculation for the measurement of actual pre-crack length has been depicted. A minimum of nine measurements shall be made with an instrument accurate to ±0.1%. The a_0 value is obtained by first averaging the two surface measurements and then averaging these values with the sum of the seven equipage inner measurements.

$$a_0 = \frac{1}{8}[(\frac{a_1+a_9}{2})+\sum_{p=2}^{8} a_p] \tag{4-5}$$

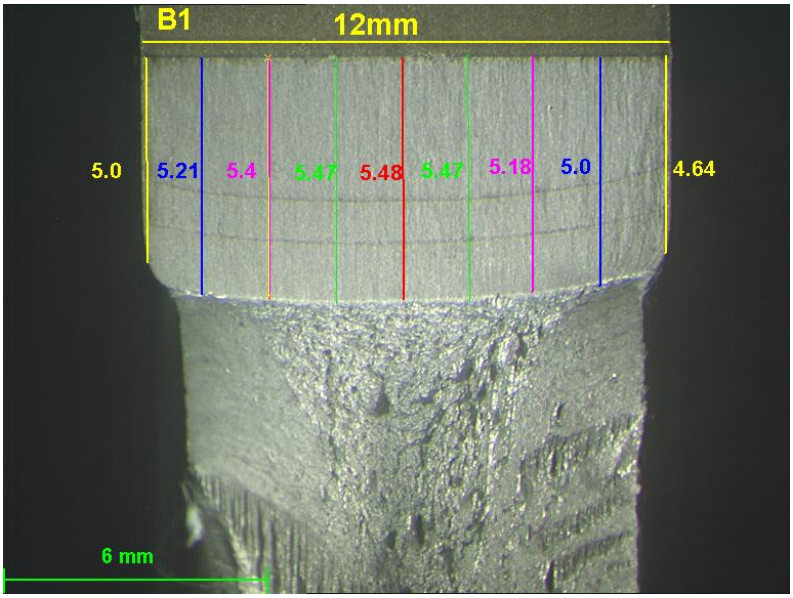

Figure 4-19 Pre-crack actual length measurement

Depends on what type of load versus displacements has been generated, Figure 4-20 gives the guideline to measure the F_Q. Line OA is the straight line in the fully elastic region of the test. Depending on the type of the graph, line OF_d/F_Q shall be drawn to satisfy the following equation:

$$\frac{\Delta F}{F} = 5\% \qquad (4\text{-}6)$$

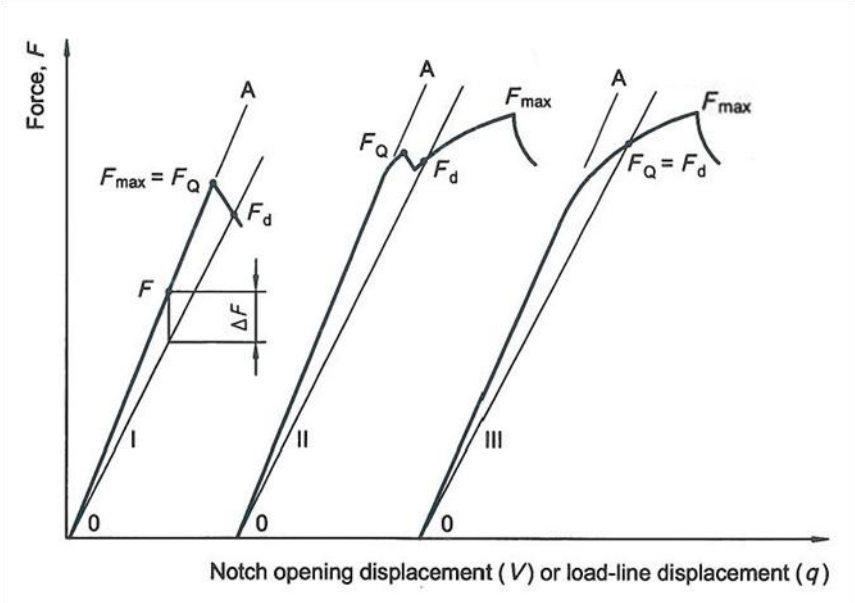

Figure 4-20 Definition of FQ for determination of KQ

Courtesy of (ASTME1290 2002; ISO12135 2002)

The following table illustrates which parameters should be reported:

Table 4-3 Interpretation of test record

Condition	To be reported
If $\frac{f_{max}}{f_Q} > 1.1$	δ or J
If $\frac{f_{max}}{f_Q} < 1.1$	K_Q

Figure 4-21 depictes the maximum force versus temperature for six different temperature categories. For lower temperatures, less force is needed to start the crack propagation and consequently less force to break the specimen. For low temperature testing, it is crucial to have a stability time for the temperature to be stabilised inside the cooling chamber.

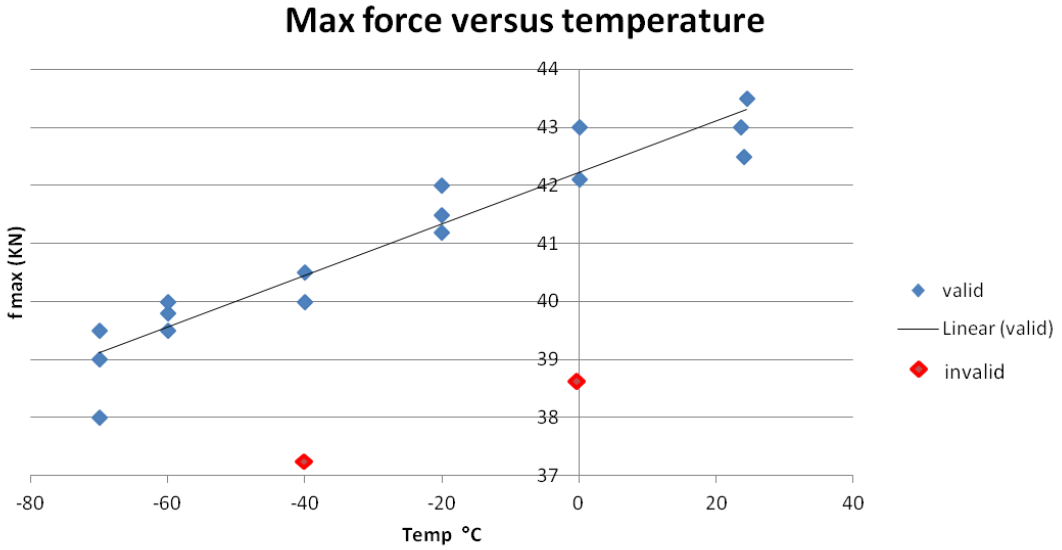

Figure 4-21 Test results of six specimen categories

The critical crack tip opening displacement can be calculated from:

$$\delta = [\frac{F}{BW^{0.5}} \times f'(\frac{a_0}{W})]^2 \frac{(1-\upsilon^2)}{2\sigma_{YS}E} + \frac{0.46(W-a_0)V_p}{0.46W+0.54a_0+z} \quad (4\text{-}7)$$

Where z is the knife edge thickness for the outward pointing knife edge and it is zero if the inward pointing attached knife edge has been used. V_p is the plastic component of notch opening displacement and is the value of COD from the test record, when a parallel line to the elastic part of the graph is drawn from the f_{max}. Analytically it is:

$$V_p = V_e - V_{total} \quad (4\text{-}8)$$

Where V_e is the theoretical elastic notch opening displacement, calculated based on elastic compliance techniques.

Figure 4-22 illustrates the test results for different temperatures. Different pop-ins and maximum forces could be observed from the graph. As the clip gauge has been calibrated only for 4mm mouth opening, the results beyond COD=4mm are not accurate. Actually, for the purpose of this test, the first 2.5mm on crack front is the most important part. As explained in the previous paragraph, depending on the graph shape (Figure 4-20) a 5% line has been drawn and F_Q calculated.

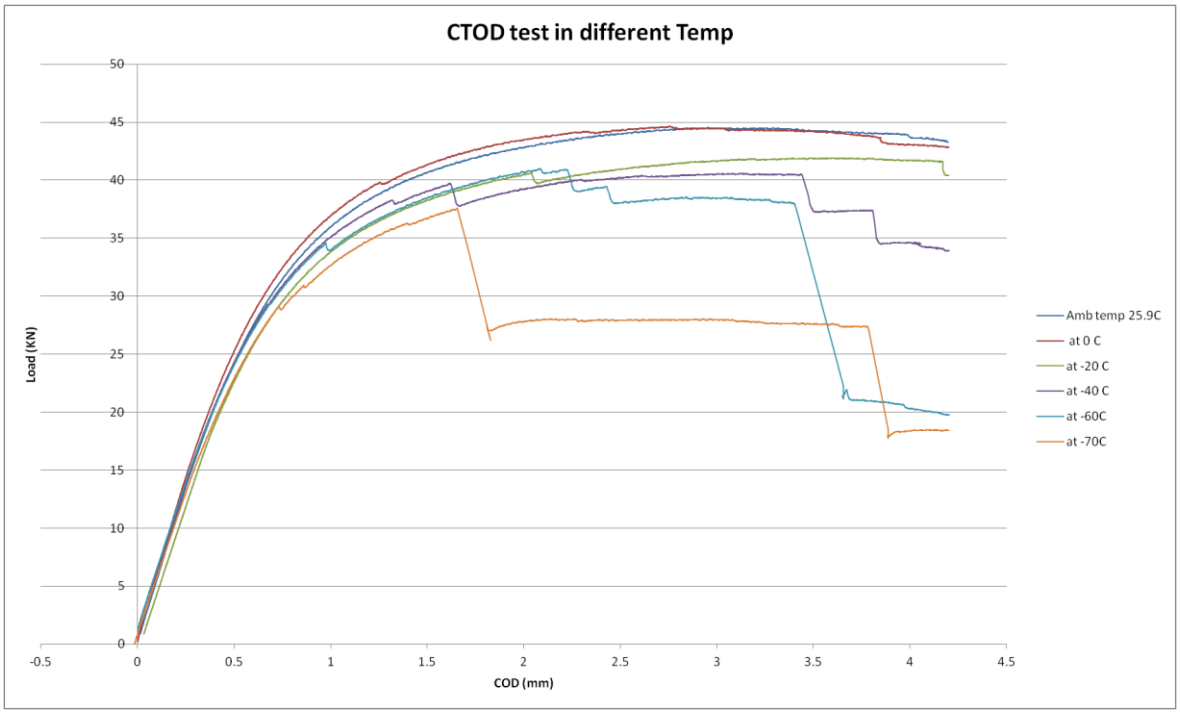

Figure 4-22 Test results for different temperature

To model specimen size effects in the transition range between upper shelf and lower shelf fracture toughness, the statistical weakest link theory has been used (ASTME1921 2012). Eq. (4-9) can be used to size adjust fracture toughness values for different temperatures.

$$K_{Jc(x)} = K_{\min} + [K_{Jc(0)} - K_{\min}](\frac{B_0}{B_x})^{1/4} \quad (4\text{-}9)$$

Where K_{min}=20MPam^0.5, B_0 is the gross thickness of test specimens, B_x is the gross thickness of prediction and K_{JC} is an elastic-plastic equivalent

stress intensity factor for specimen size B_0. Ferritic steels with yield strengths ranging from 275 to 825 MPa will have fracture toughness cumulative probability distributions of nearly the same shape, independent of specimen size and test temperature, when K_{min} is set to 20 MPam^0.5. For the above mentioned reason in Eq. (4-9), K_{min} has been set to 20MPam^0.5 (ASTME1921 2012).

Figure 4-23 shows the predicted KIC values and size effect for different temperatures. The base thickness was 12mm from the experimental results.

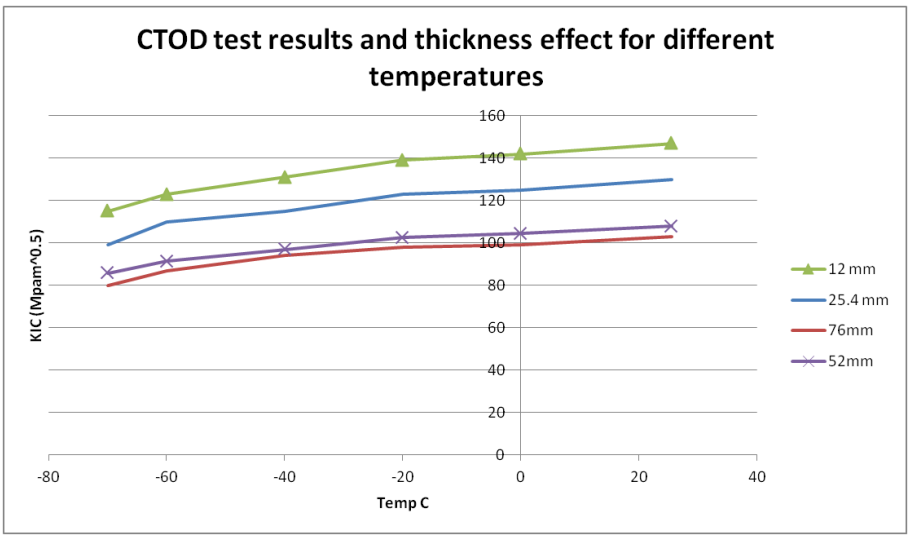

Figure 4-23 Size effect for different temperatures

4.4.2 High speed camera images, Crack Propagation

More than 100,000 photos have been captured with a high speed camera in the first two minutes of crack propagation. The aim was to precisely observe the crack propagation in very slow motion and as a future plan, compare the test results with the digital image correlation (DIC) technique.

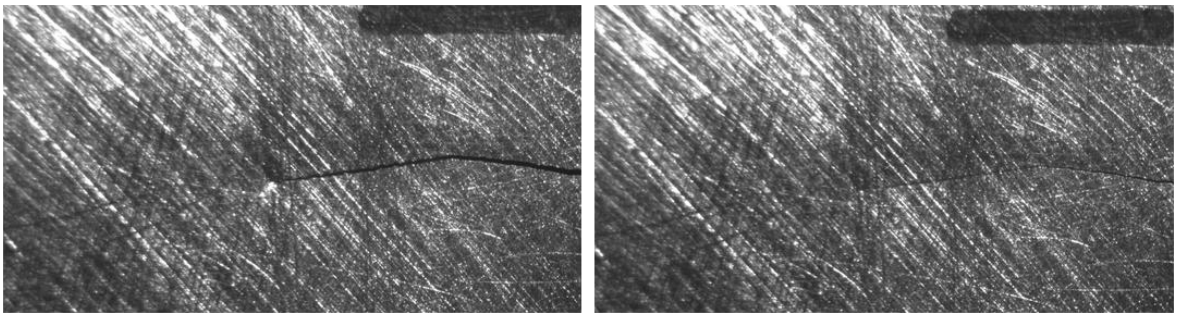

Figure 4-24 Onset of crack propagation 0-30s

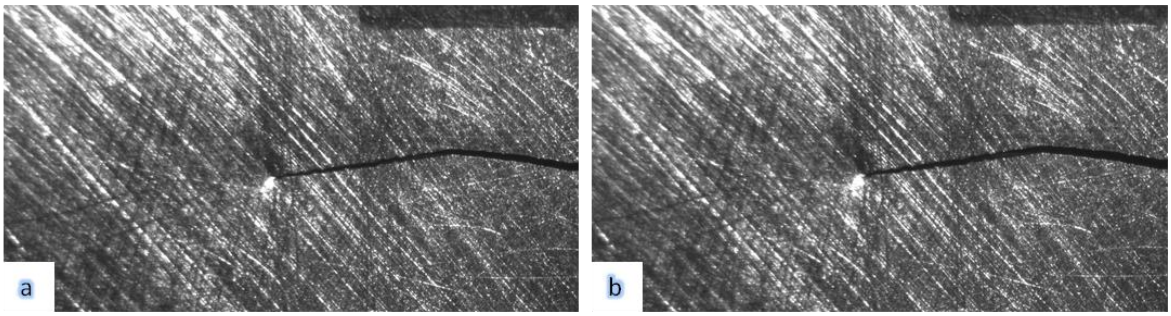

Figure 4-25 Onset of crack propagation a: 45s-b: 55s

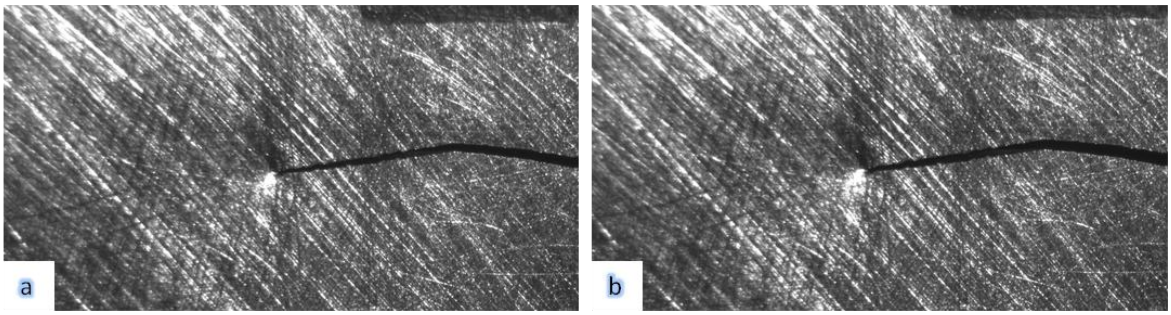

Figure 4-26 Onset of crack propagation a: 60s-b: 70s

4.5 Fractography

For several tested specimens, fractographic examinations were conducted to evaluate the micromechanisms of the fracture. Of particular interest in these examinations was ascertaining whether the fracture behaviour in low temperature was fully brittle or not. Some of Scanning Electron Microscope (SEM) fractographs are presented in this section.

In Figure 4-27, in order to have a better understanding of fracture shape in different extreme temperatures, broken sections of two specimens are presented. The left specimen has been broken in an ambient temperature of 25°C and, as can be observed, has a so-called ‘cup and cone’ shape related to ductile fracture. Plastic deformation, especially very close to both surfaces, could be noted. For fracture toughness test surface analysis of broken specimen, only surfaces very close to pre-crack is important (The area shown between two red lines). Above the upper red line is just a normal tearing to break the specimen for further analysis.

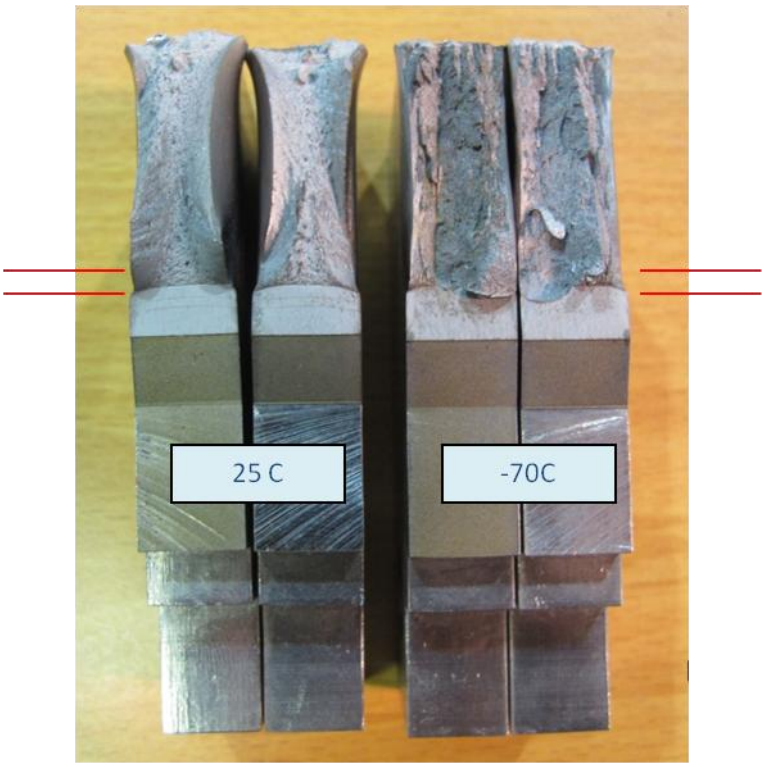

Figure 4-27 Two broken specimens for different temperatures

On the right of this figure the specimen has been broken in a cooling chamber at the minimum temperature of -70°C and semi brittle fracture behaviour could be observed. This material, based on the obtained test results, did not meet the fully brittle fracture at this temperature. Because of the limitations of the existing cooling chamber, unfortunately it was not possible to reach lower temperatures and consequently ductile to brittle temperature transition could not be obtained. It has been planned to find this information by using a Charpy test and liquid nitrogen bath.

Figure 4-28 illustrates the striations due to fatigue pre-cracking.

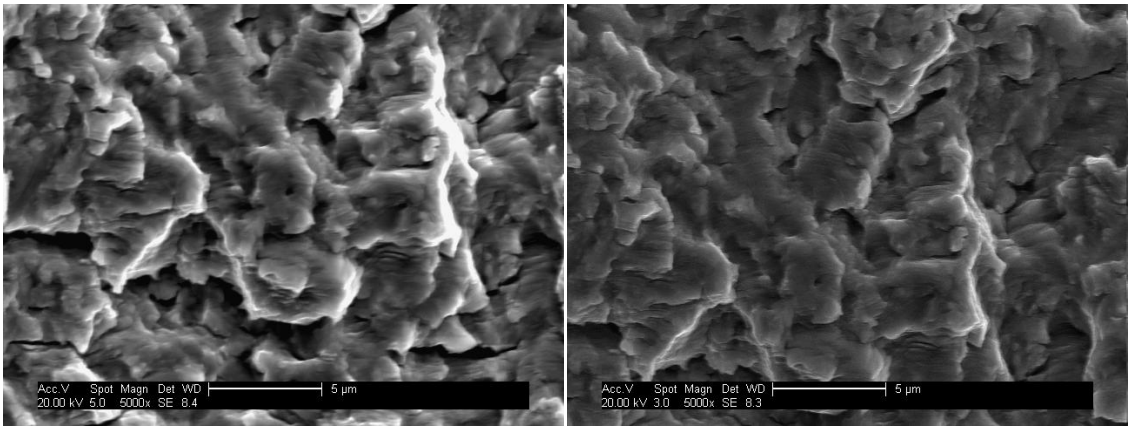

Figure 4-28 SEM fractograph showing striations due to fatigue pre-cracking

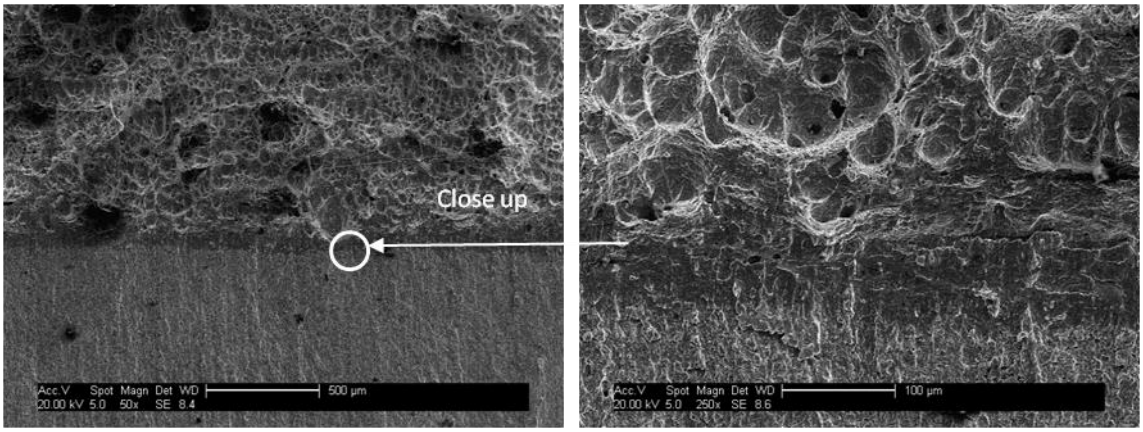

Figure 4-29 End of pre-crack and onset of fracture (at 25°C)

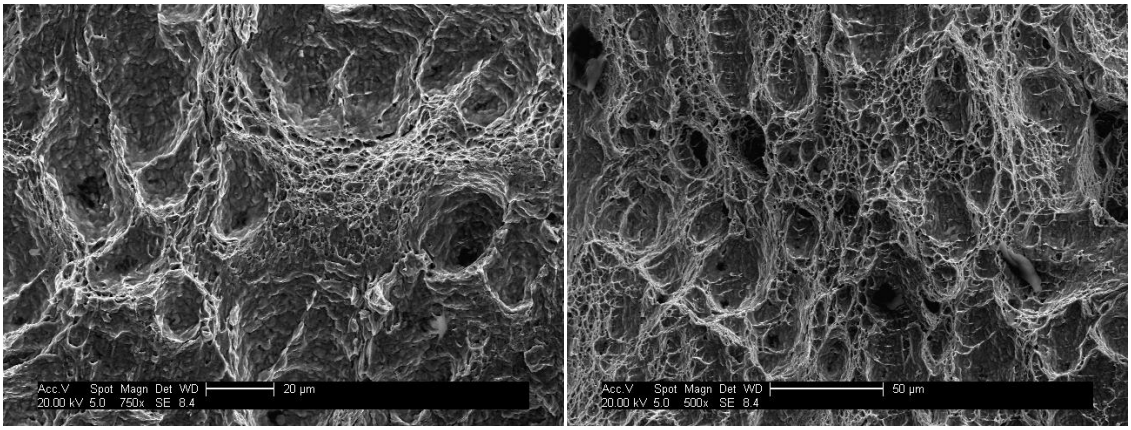

Figure 4-30 Dimples and typical spongy ductile behaviour (at 25°C)

Figure 4-29 and 3-38 are the SEM images from a broken specimen at 25°C. In Figure 4-29, the onset of fatigue pre-crack has been illustrated. The difference between electro discharge machining (EDM) that has been used to make the notch and fatigue pre-crack could be clearly observed. The order of magnification in this picture is 250. In Figure 4-30, typical spongy behaviour in the ductile fracture could be noticed.

Pictures shown in Figure 4-31, 3-40 and 3-41 are from a broken specimen at -40°C. A mixture of ductile and brittle fracture behaviour can be observed; it starts with a more ductile action and in some sections brittle jumps can be observed.

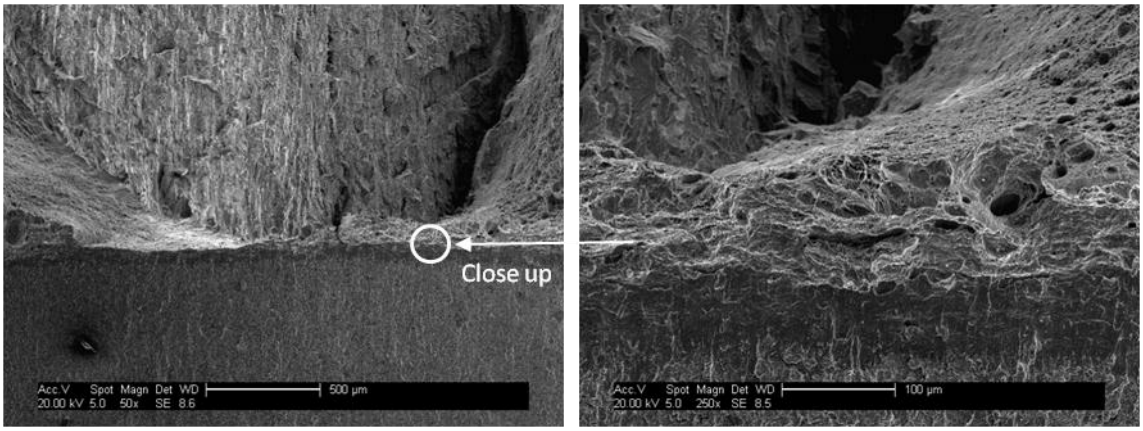

Figure 4-31 End of pre-crack and onset of fracture (at -40°C)

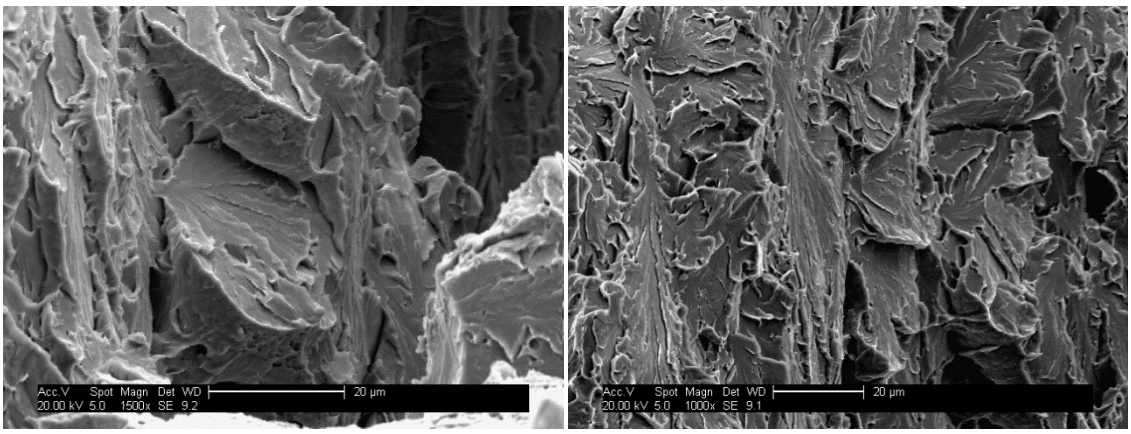

Figure 4-32 Typical cleavage behaviour (mix of ductile/brittle) (-40°C)

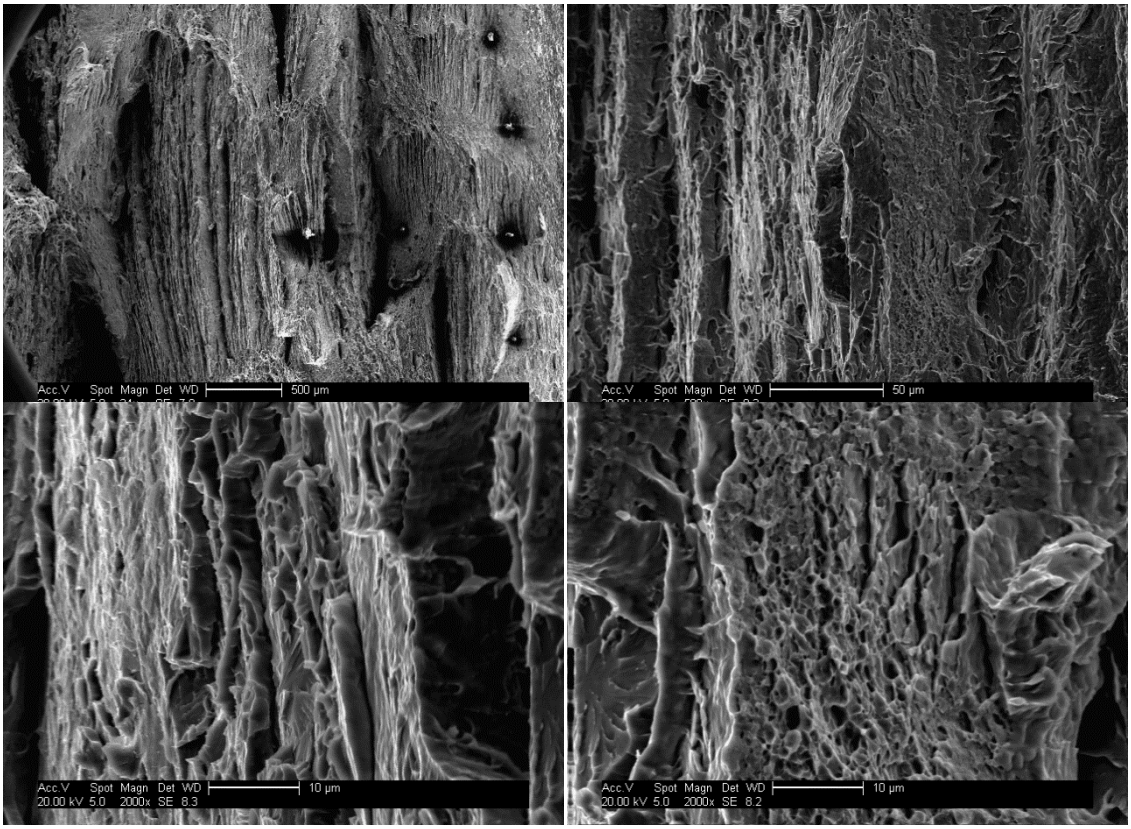

Figure 4-33 Typical cleavage behaviour (mix of ductile/brittle) (-40°C)

The pictures shown in Figure 4-34 and Figure 4-35 are from a broken specimen at -70°C. The first picture is the start point of pre-cracking at room temperature and in the magnified picture the striations can be observed. In the second picture the crack propagation in brittle behaviour is depicted. In low temperatures when the load reaches to a certain value that is larger than the fracture resistance of the material, cracks suddenly grow with a big (banging) sound. Only very high speed cameras can capture this high speed crack growth.

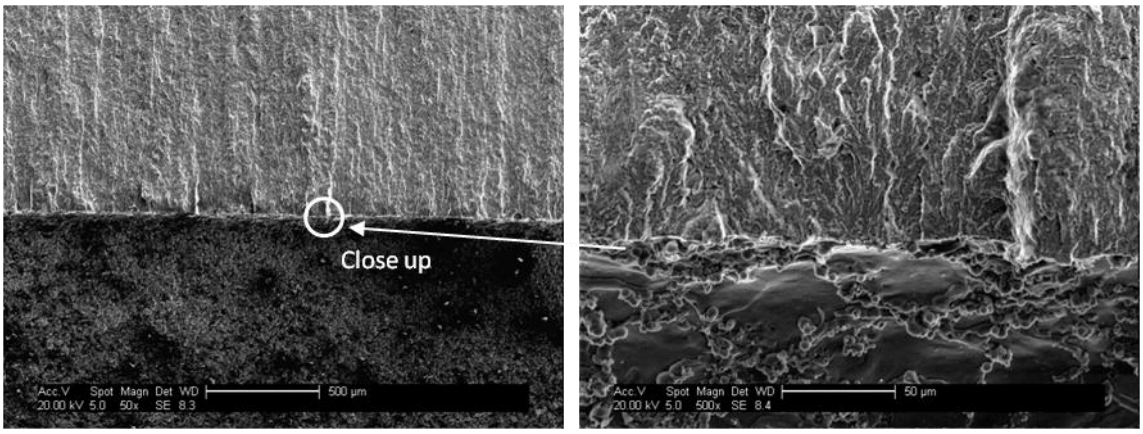

Figure 4-34 Start of pre-crack and end of EDM notch (at -70°C)

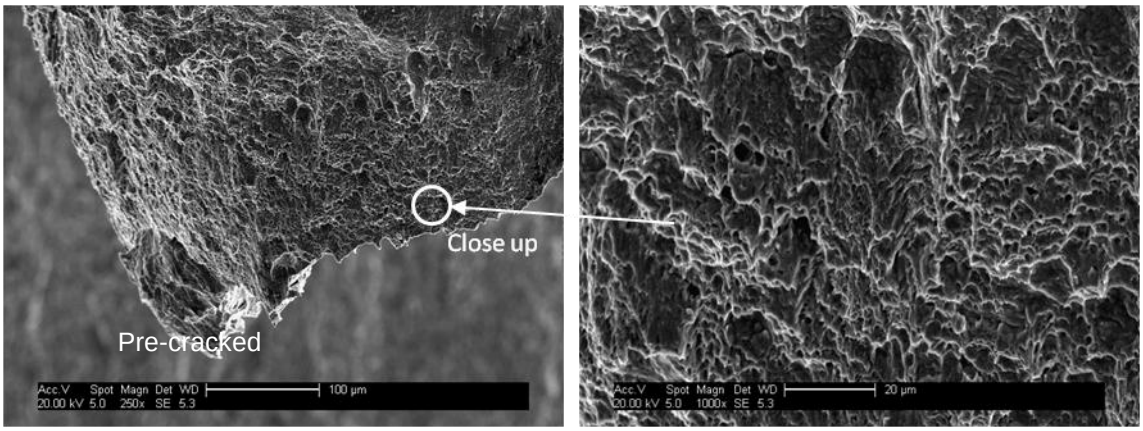

Figure 4-35 End of pre-crack and onset of fracture (at -70°C)

4.6 Back face strain compliance and state of strain in crack front

Pre-cracking CT specimens using afatigue cyclic load, have to be precise and accurate. An accurate and consistent pre-crack length for fracture toughness test specimens (more than 20 for different temperatures) is crucial. Even small differences between the crack lengths of two specimens can cause different results for K_{IC} at the end of the test. Monitoring the crack growth and measuring the crack length during the fatigue cyclic load is not an easy task. Usually pre-cracking takes hours because it should happen in a low force/displacement rate to prevent plasticity on the crack tip. A high quality camera with special lenses is one of the solutions for monitoring crack length, but it needs someone to measure the crack length during the fatigue duration.

Back face strain compliance is a reliable technique to be used in automated fatigue crack growth rate testing. For a constant load amplitude during the fatigue pre-cracking, there is a linear behaviour between crack length and back face strain (Riddell William and Piascik Robert 1998). For different CT geometries this can be changed but the relation remains linear.

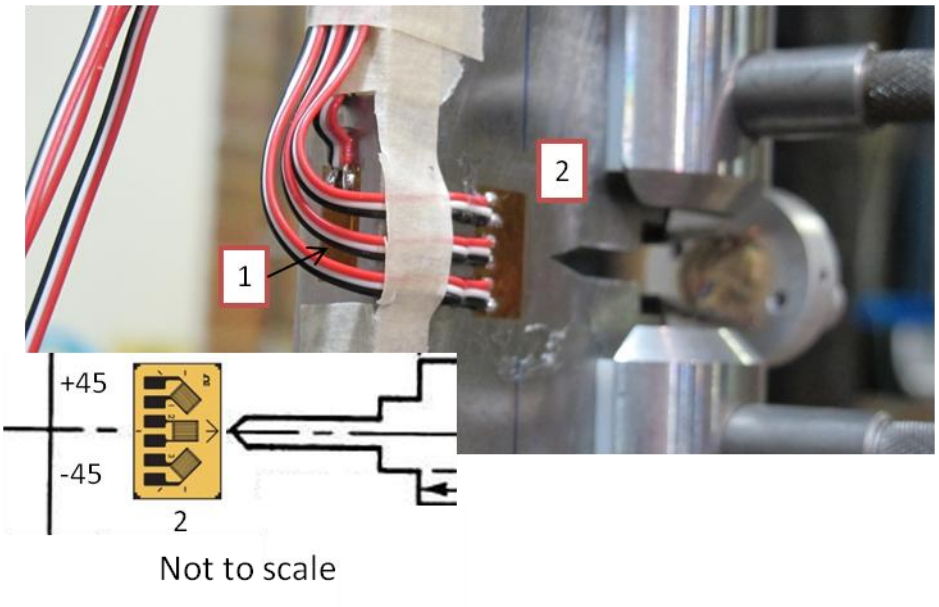

Figure 4-36 Strain gauges on CT specimen

To understand the behaviour of back face strain compliance on step notched CT specimens (this project), a linear strain gauge has been installed on the back of the CT specimen (Figure 4-36-1). The CT specimen was under a sin-wave with an amplitude of 10Kn for 35,000 cycles. The crack growth has been monitored and measured by a high quality/speed camera with a special lens. The pre-crack length was targeted to be 5mm.

The results shown in Figure 4-37 agree the linear behaviour of back face strain compliance.

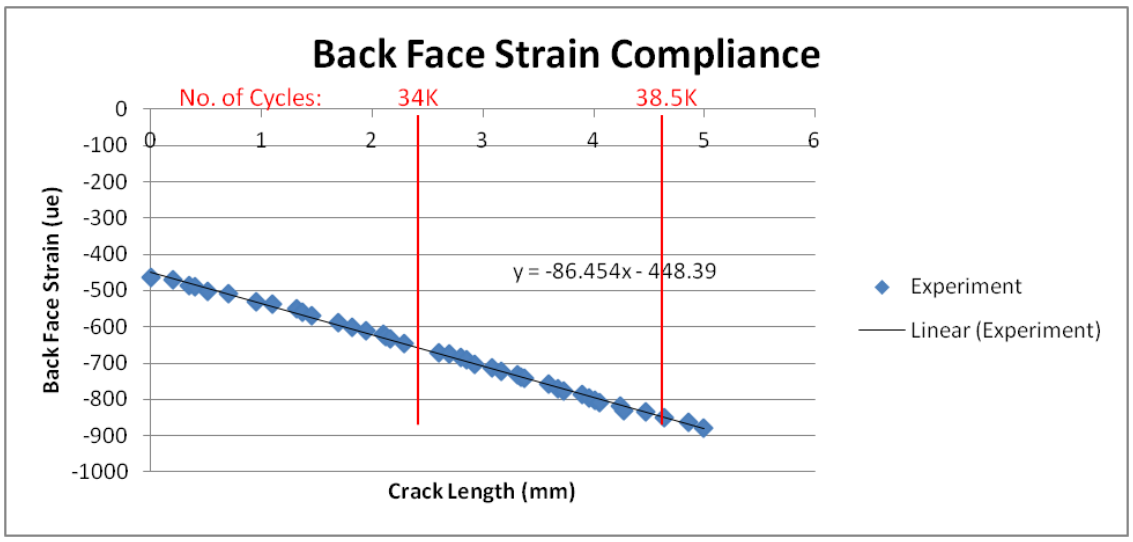

Figure 4-37 Step notched CT back face strain compliance

To automate the CT pre-cracking using back face strain compliance, for any certain crack length and geometry, a code can be written. A signal from the strain gauge reader will send the strain value to the Instron controller. A decision based on the required crack length will stop the pre-cracking procedure. Sample rating and signal synchronisation have to be considered and pre-cracking has to be ended at the minimum load.

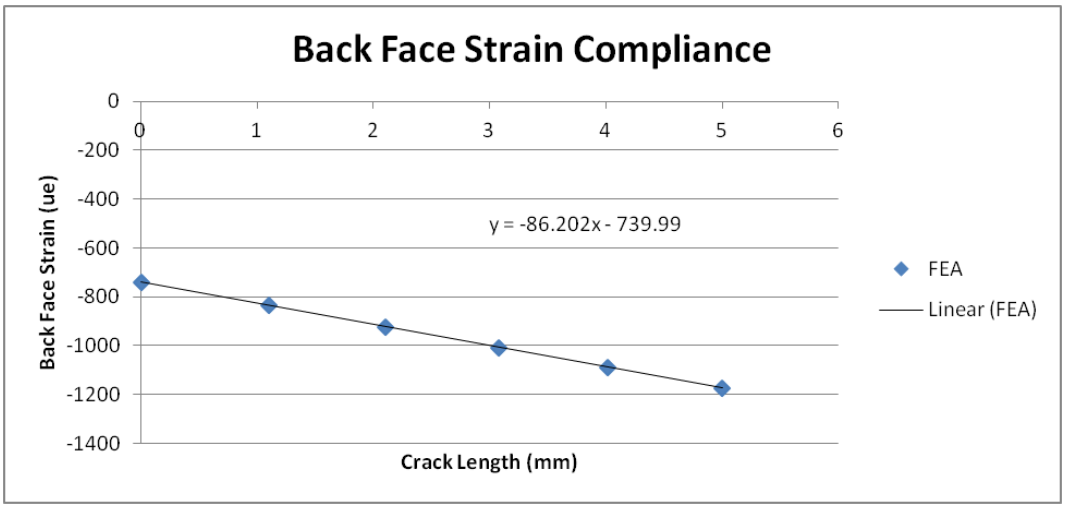

Figure 4-38 BFS results in FEA with the same slope

Figure 4-36-2 shows a rosette strain gauge that has been installed in front of the crack. To validate the FEA modelling of the CT specimen, strain values in front of the crack have been compared. Figure 4-39 shows four strain readings and applied force versus time. These data have been captured during a fracture test. All four strain readings and the force value have been synchronised with the applied load, position of the pin loads and time. The values of strain have a good agreement with the strain values for similar points under similar loading conditions from the FEA model.

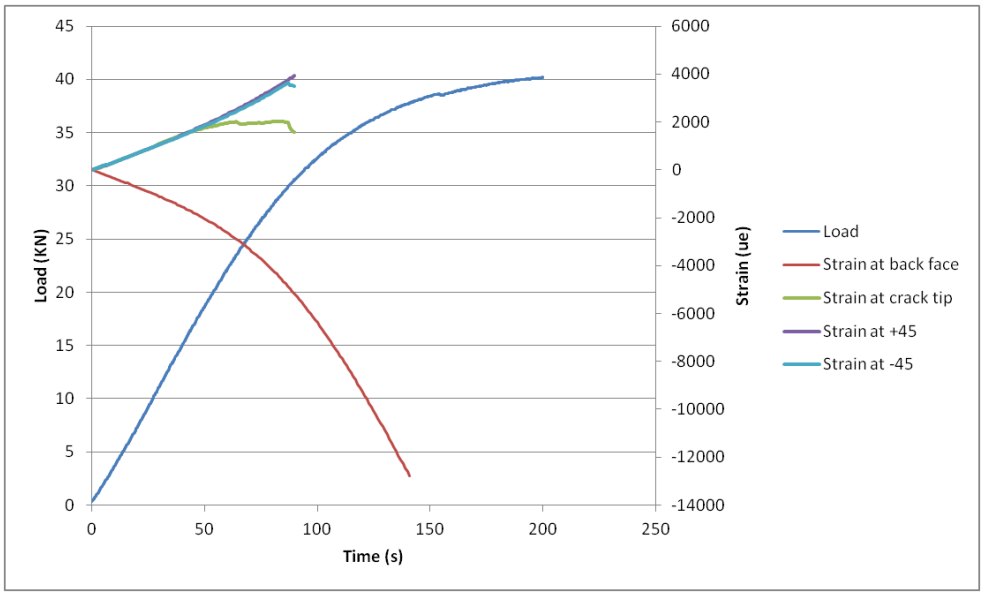

Figure 4-39 State of strain and load on crack front and side

Figure 4-40 shows the strain values along the x direction (crack front) for the CT specimen under fracture test loading conditions. The strain values from the FEA model have good agreement with the real experiment under the same boundary conditions.

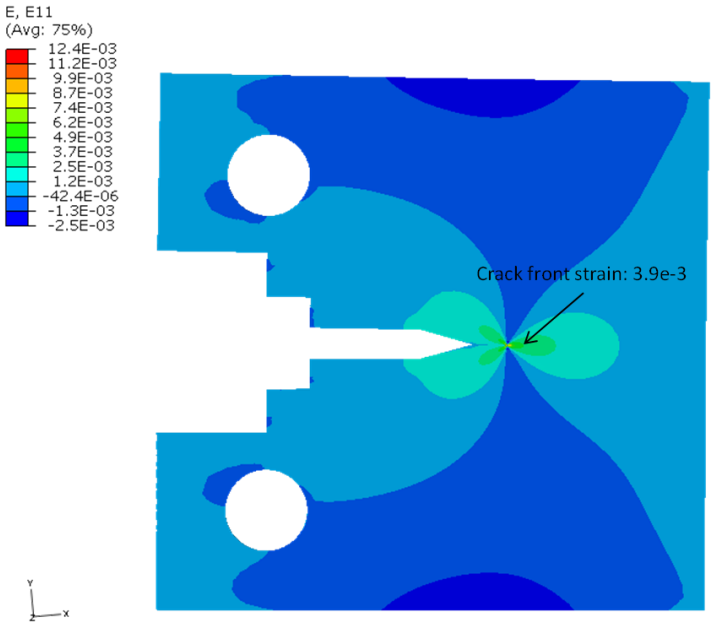

Figure 4-40 State of strain infront of the crack (→x)

4.7 Summary

In this chapter a rigorous procedure for a fracture toughness test for a pipeline material has been described. The available material was API 5L X100 and after conducting a rolling direction test, a compact tension specimen was selected for fracture toughness tests. Pre-cracking CT specimens in ambient temperatures were accomplished and fracture toughness tests for different temperatures (20 to -70°C) performed. The effects of low temperatures on fracture toughness were discussed and fracture toughness surfaces for ambient temperature and -70°C were analysed. Fractography images using a scanning electron microscope with an engineering interpretation were presented. An accurate and novel methodology for monitoring crack length during pre-cracking of step notch CT specimens has also been presented.

The following chapter will extend this approach to cracks in complex bodies.

Chapter 5. Fracture Mechanics Model Development for CO_2 Pipelines.

In Chapter one, the CCS process and its challenges for transportation have been explained. To transport a large quantity of CO_2 captured from the CCS plants, it must first be transformed into a form with a higher density, i.e. dense or supercritical phase (Aspelund, Mølnvik et al. 2006). Pipelines, as the most efficient way of transportation, have been used to transport pure CO_2 since the 1970s for enhanced oil recovery (EOR). With the development of CCS plants in different industries, such as power generation, cement plants, brick kilns, a different range of impurities has been introduced in to the CO_2 pipeline network. Additionally, differently captured CO_2 with different processing technologies has introduced a different range of impurities as well. Two of the challenges related to the transportation of CO_2 with impurities is the risk both of long running brittle fractures due to cooling effects around leaks and long running ductile fractures due to phase changes during depressurisation (Seevam, Race et al. 2010).

In this chapter, using the FEA approach and multiple reference state (MRS) weight function method, a novel solution to calculate SIF for pipelines with a longitudinal through thickness crack is presented. In this model the possibility of inducing a low temperature due to CO_2 expansion through crack has been considered. These types of defects can be developed during the pipe manufacture or during the welding of pipelines.

5.1 Materials for Next Generation CO_2 Transport Systems Project (MATTRAN)

This research is a part of larger project named MATTRAN. It is funded by EPSRC-Eon and represents the collaboration of five universities working on key challenges of next generation CO_2 transportation pipelines (MATTRAN 2011;

MATTRAN 2012)Transport is an integral and critical link in the chain between capture and storage. Carrying supercritical CO_2 under such high pressure and with impurities introduced challenges for operators and pipeline engineers to control corrosion, stress corrosion cracking and fracture propagation in pipelines and associated equipment. This research is mainly focused on fracture mechanics related issues for the MATTRAN project.

5.2 Stress intensity factor analysis of a longitudinal crack in a pipe under internal pressure

Figure 5-3 shows a through thickness crack in a pipe under internal pressure. A three dimensional model of a pipe with a crack has been modelled in Abaqus. Using FEA, the SIF for different crack lengths and pipe sizes were calculated. To have consistency between the different work packages of this project, and based on the UCL outflow model, the following specifications have been considered for this study (Mahgerefteh, Oke et al. 2006; MATTRAN 2012):

- Internal pressure =15 MPa
- Pipe Diameter = 24 inches (609.6 mm, OD)
- Pipe wall thickness = 12 mm
- Pipe material = API 5L X100, Yield stress: 690MPa
- Module of elasticity: 200 GPa, v=0.3

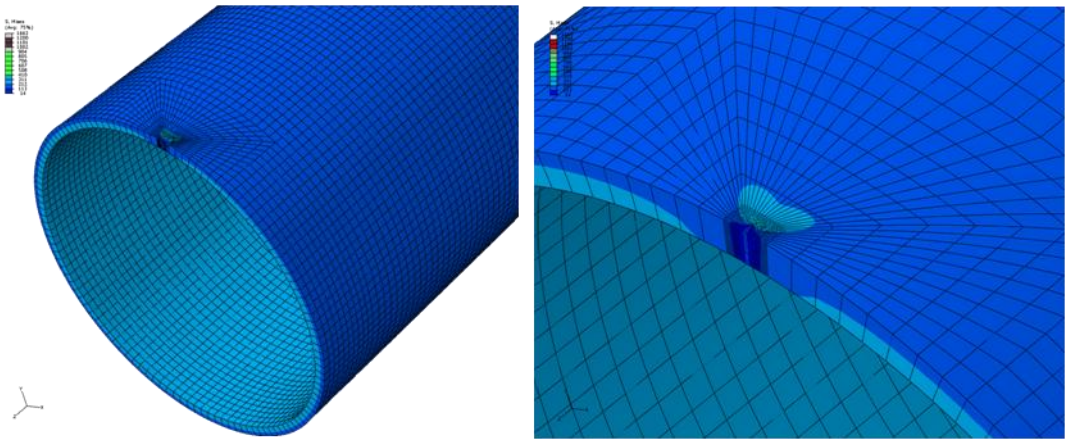

Figure 5-1 mesh size and density for a 6mm longitudinal crack

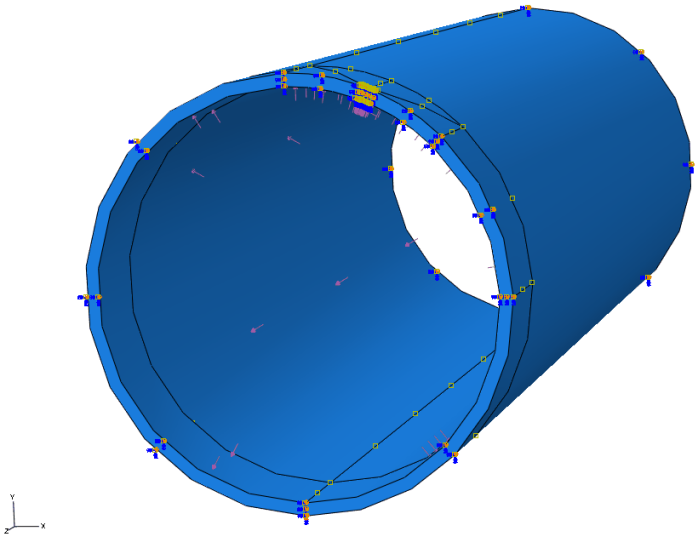

Figure 5-2 Boundary condition and internal pressure as loading

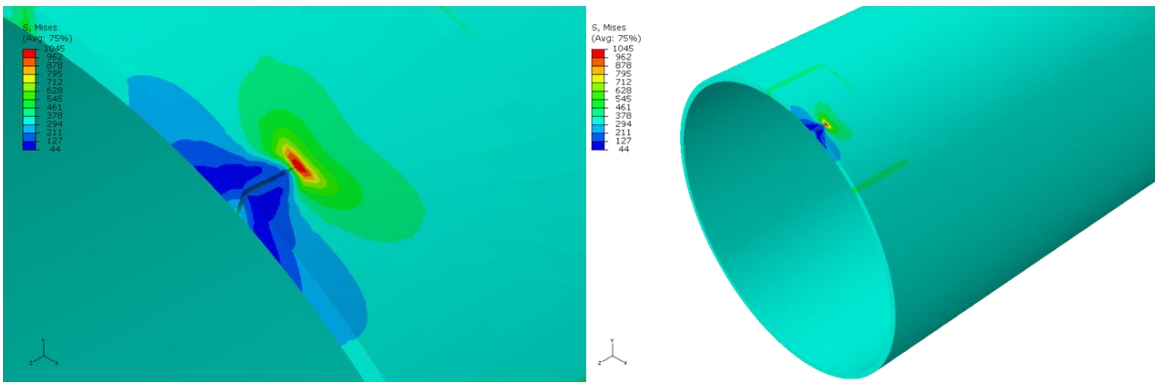

Figure 5-3 Through thickness crack in a pipe under internal pressure

For meshing the model, a C3D8R element type has been used. To obtain better results, a fine mesh around the crack and especially on the crack front is essential. Even though Abaqus calculates K from J and J is path independent, it is recommended to have closed loops in front of the crack

ending at both sides of the crack line. Figure 5-4 shows a good agreement between the FEA results and available references in the literature (Section 1-3).

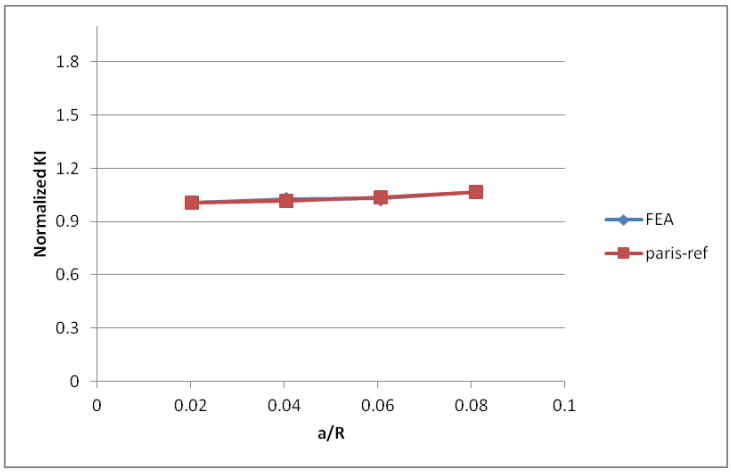

Figure 5-4 Good agreement of FEA results with reference solution (Reference solution Figure 2-11 Longitudinal crack in a pipe)

Table 5-1 presents normalised SIF values for three different pipe sizes. The SIF values are for crack lengths of 5 to 25 mm and pipe diameters of 16 to 24 inches. The internal pressure and thickness for all cases remain constant. The results are shown for a specific crack length, in a smaller pipe diameter, even though the hoop stress is lower but the SIF value is bigger. This means that for the same pipe material and the same crack length, the smaller pipe fails sooner.

Table 5-1 Normalised K values for a pipe with a longitudinal through thickness crack

a/t	Normalised K		
	R/t=16.43	R/t=20.66	R/t=24.9
0.42	1.01	1.01	1.00
0.50	1.01	1.01	1.01
0.58	1.01	1.01	1.01
0.67	1.02	1.01	1.01
0.75	1.02	1.02	1.01
0.83	1.03	1.02	1.02
0.92	1.03	1.03	1.02
1.00	1.04	1.03	1.02
1.08	1.04	1.03	1.03
1.17	1.05	1.04	1.03
1.25	1.06	1.05	1.04
1.33	1.07	1.05	1.04
1.42	1.07	1.06	1.05
1.50	1.08	1.07	1.05
1.58	1.09	1.07	1.06
1.67	1.10	1.08	1.07
1.75	1.11	1.09	1.07
1.83	1.12	1.10	1.08
1.92	1.13	1.11	1.09
2.00	1.14	1.11	1.10
2.08	1.15	1.12	1.10

5.2.1 A parametric study and sensitivity analysis of the SIF in a pipe with longitudinal crack under internal pressure to geometric characteristics

To understand the sensitivity of the model to geometry characteristics, a sensitivity analysis has been performed. A series of FEA models have been developed for different pipe diameters: 16, 20 and 24 inch pipe diameters have been selected and stress intensity factors for different longitudinal through thickness crack lengths calculated. In the previous section it has been shown that FEA simulation had a very good agreement with the available reference solution for this problem (Paris, Tada et al. 2000). The normalized stress intensity factor has been defined as:

$$Y = Y(\lambda) = \sqrt{1 + 1.25\lambda^2} \tag{5-1}$$

Where λ is a geometrical parameter defined as:

$$\lambda = \frac{a}{\sqrt{Rt}} \tag{5-2}$$

The above expression is valid for $\lambda \in (0,1]$. The numerical simulation results are expressed in terms of three other geometric parameters:

$$(\alpha = \frac{a}{R}, \beta = \frac{a}{t}, \tau = \frac{R}{t}).$$

Where “a” is the half of the crack length, “R” is the pipe radius and “t” is the pipe thickness. These parameters are related to λ as follows:

$$\lambda^2 = \alpha\beta = \alpha^2\tau = \frac{\beta^2}{\tau} \tag{5-3}$$

The normalised stress intensity factor (Y) can then be expressed in terms of these parameters as:

$$Y(\alpha, \beta) = \sqrt{1 + 1.25\alpha\beta} \tag{5-4}$$

$$Y(\alpha,\tau)=\sqrt{1+1.25\alpha^2\tau} \tag{5-5}$$

$$Y(\beta,\tau)=\sqrt{1+1.25\beta^2/\tau} \tag{5-6}$$

To analyse the sensitivity of SIF to the geometric parameters, we need to evaluate the norm of variation (here we use the absolute value) of Y to α, β and τ.

$$Y=Y(\alpha,\beta)=\sqrt{1+1.25\alpha\beta} \tag{5-7}$$

$$\frac{\partial Y}{\partial \alpha}=\frac{1.25\beta}{2Y} \qquad\qquad \frac{\partial Y}{\partial \beta}=\frac{1.25\alpha}{2Y}$$

and the ratio of the norms of the derivatives is:

$$\frac{\left\|\frac{\partial Y}{\partial \alpha}\right\|}{\left\|\frac{\partial Y}{\partial \beta}\right\|}=\frac{\beta}{\alpha}=\tau \tag{5-8}$$

It should be noted that ($\tau \gg 1$) and subsequently:

$$\left\|\frac{\partial Y}{\partial \alpha}\right\| \gg \left\|\frac{\partial Y}{\partial \beta}\right\| \tag{5-9}$$

This means that Y is much more sensitive to α than β. In other words, the SIF for a fixed crack length “2a” is much more sensitive to the pipe diameter than the pipe thickness.

With the same method we can compare the sensitivity of Y to (α,τ) and also its sensitivity to (β,τ).

$$Y=Y(\alpha,\tau)=\sqrt{1+1.25\alpha^2\tau} \tag{5-10}$$

$$\frac{\partial Y}{\partial \alpha} = \frac{1.25\alpha\tau}{Y} \qquad \frac{\partial Y}{\partial \tau} = \frac{1.25\alpha^2}{2Y}$$

and the ratio of the norms of the derivatives is:

$$\frac{\left\|\frac{\partial Y}{\partial \alpha}\right\|}{\left\|\frac{\partial Y}{\partial \tau}\right\|} = \frac{2\tau}{\alpha} \tag{5-11}$$

Thus,

$$\left\|\frac{\partial Y}{\partial \alpha}\right\| = \left\|\frac{\partial Y}{\partial \tau}\right\| \frac{2R^2}{at} \tag{5-12}$$

It is clear that ($\frac{2R^2}{at} \gg 1$) and therefore:

$$\left\|\frac{\partial Y}{\partial \alpha}\right\| \gg \left\|\frac{\partial Y}{\partial \tau}\right\| \tag{5-13}$$

Here Y again is more dependent to α. This means that for a constant pipe diameter the SIF is much more sensitive to the crack length than the pipe thickness.

For the last case we compare the sensitivity of Y to (β,τ).

$$Y = Y(\alpha, \tau) = \sqrt{1 + 1.25\beta^2/\tau} \tag{5-14}$$

$$\frac{\partial Y}{\partial \beta} = \frac{1.25\beta/\tau}{Y} \qquad \frac{\partial Y}{\partial \tau} = -\frac{1.25\beta^2/\tau^2}{2Y}$$

and the ratio of the norms of the derivatives is:

$$\frac{\left\|\frac{\partial Y}{\partial \beta}\right\|}{\left\|\frac{\partial Y}{\partial \tau}\right\|} = \frac{1}{\alpha} \tag{5-15}$$

Thus,

$$\left\|\frac{\partial Y}{\partial \tau}\right\| = \left\|\frac{\partial Y}{\partial \beta}\right\| \alpha \qquad (5\text{-}16)$$

As ($\alpha \ll 1$) therefore:

$$\left\|\frac{\partial Y}{\partial \beta}\right\| \gg \left\|\frac{\partial Y}{\partial \tau}\right\| \qquad (5\text{-}17)$$

This means that Y is much more sensitive to β than τ. For a constant pipe thickness the SIF in much more sensitive to the crack length than the pipe diameter.

Figure 5-5 shows the variation of Y versus β for different values of τ. It can be noted that the sensitivity of Y to β is much higher than its sensitivity to τ as for a relatively small variation in β, Y changes considerably.

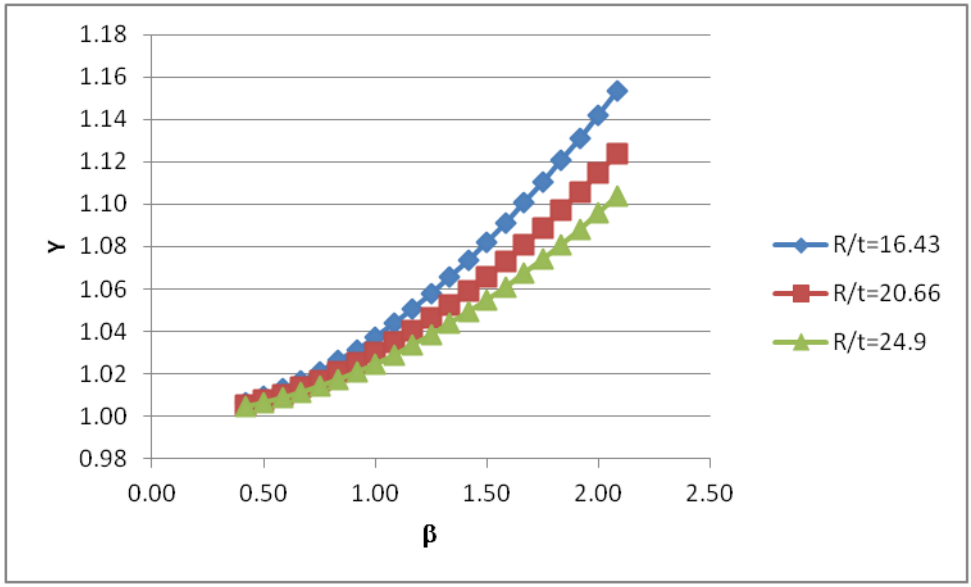

Figure 5-5 Sensitivity analysis of normalized K for different geometric characteristics

5.2.2 Localised cooling (temperature decrease)

Accurate modelling of the dense phase CO_2 during a sudden expansion situation is essential for pipeline design and operation. It forms a basis of the design to develop and justify a hazard management strategy. Analytical expressions and off-the-shelf codes can model gaseous pipelines but on the other hand modelling and understanding the behaviour of a pipeline with liquid and supercritical inventories is significantly more complex. Under such high pressure of CO_2 dense phase transportation (150 bar), the CO_2 enters the atmosphere in a two phase gas/solid state mixture. Depending on the pipeline location (exposed to atmosphere or buried) the temperature gradient in front of the crack tip in the case of a leakage scenario is totally different. The outflow model presented by the University College London (Mahgerefteh, Oke et al. 2006) shows a huge temperature drop in front of the crack. Outflow model results show the temperature in front of the crack may drop as low as -70°C.

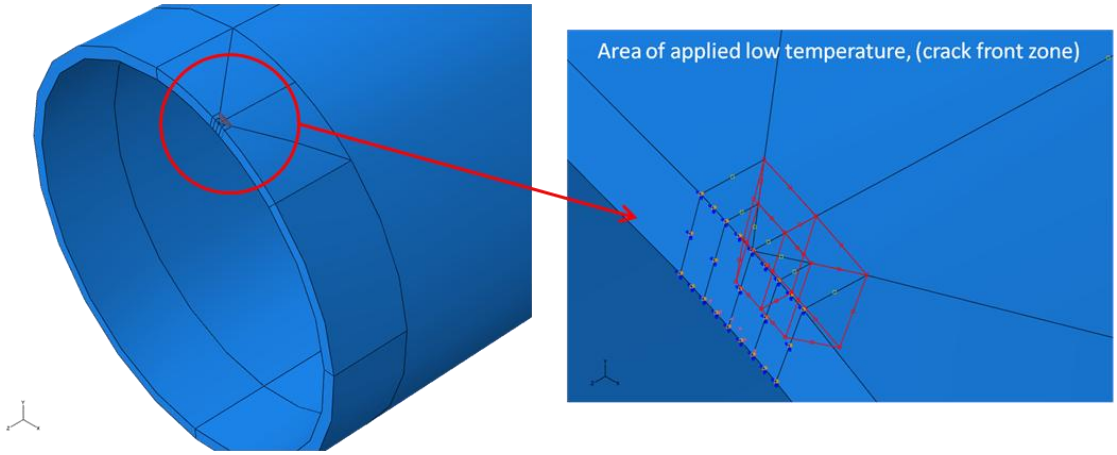

Figure 5-6 Crack front area, applied low temperature zone

Figure 5-6 shows the crack front area in a pipe with a longitudinal crack. The red zone is the area of applied low temperature. FEA modelling has been done for different crack lengths and also different applied temperatures to find the effect of cold temperatures on the SIF. In Chapter 4, the effect of low temperature on fracture toughness has been reviewed. If the very low temperature during a sudden expansion of CO_2 happens in front of the crack

(such as what has been modelled), contraction forces due to the induced low temperature affect the stresses and consequently the SIF.

Figure 5-7 illustrates two different cases for a pipe under the same internal pressure and the same crack length but different temperatures in the crack front zone.

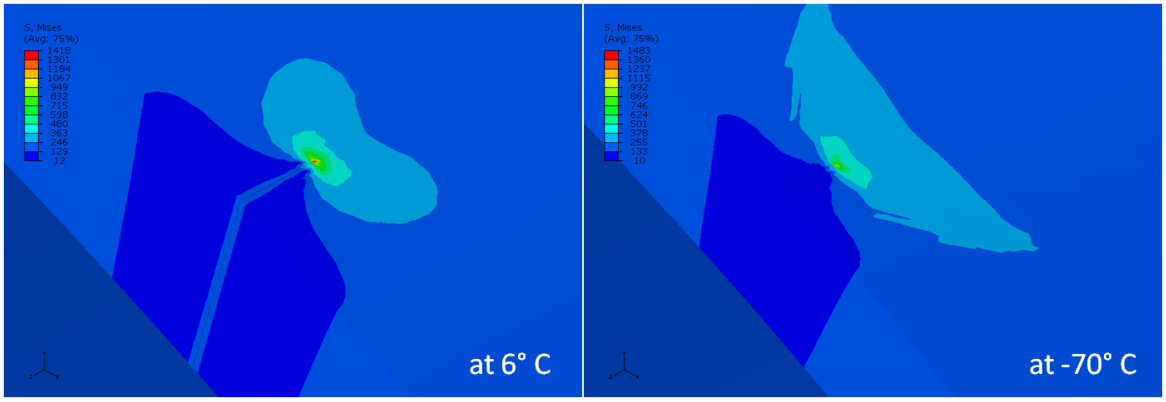

Figure 5-7 Ambient and low temperature results in front of the crack

Figure 5-8 illustrates the effect of local cooling in front of the crack on the SIF in a pipe with longitudinal through thickness crack. It can be observed that the SIF decreases due to induced low temperature. Applied low temperature in front of the crack caused contractions that are in contrast with crack propagation driving forces (internal pressure).

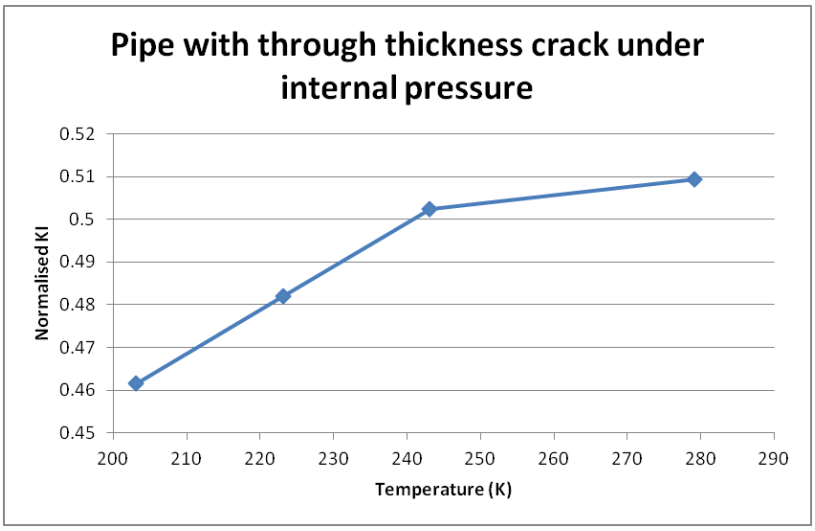

Figure 5-8 SIF behaviour due to local cooling in front of the crack in the FEA model

5.2.3 Through thickness state of stress behaviour

Figure 5-9 shows the through thickness state of stress in the pipe. The picture is of a cross section of a 12 mm thickness pipe under internal pressure of 15 MPa. For the load case of internal pressure only, a linear state of stress due to hoop stress can be observed through the thickness. It has a significant effect on the crack initiation and growth. Due to the higher stress inside the pipe cracks for similar porosity/defect inside and outside of the pipe, cracks tend to initiate and grow from inside. For thicker pipelines this makes it more complex to find cracks inside the pipelines. Some techniques such as intelligent pigging may help in such circumstances.

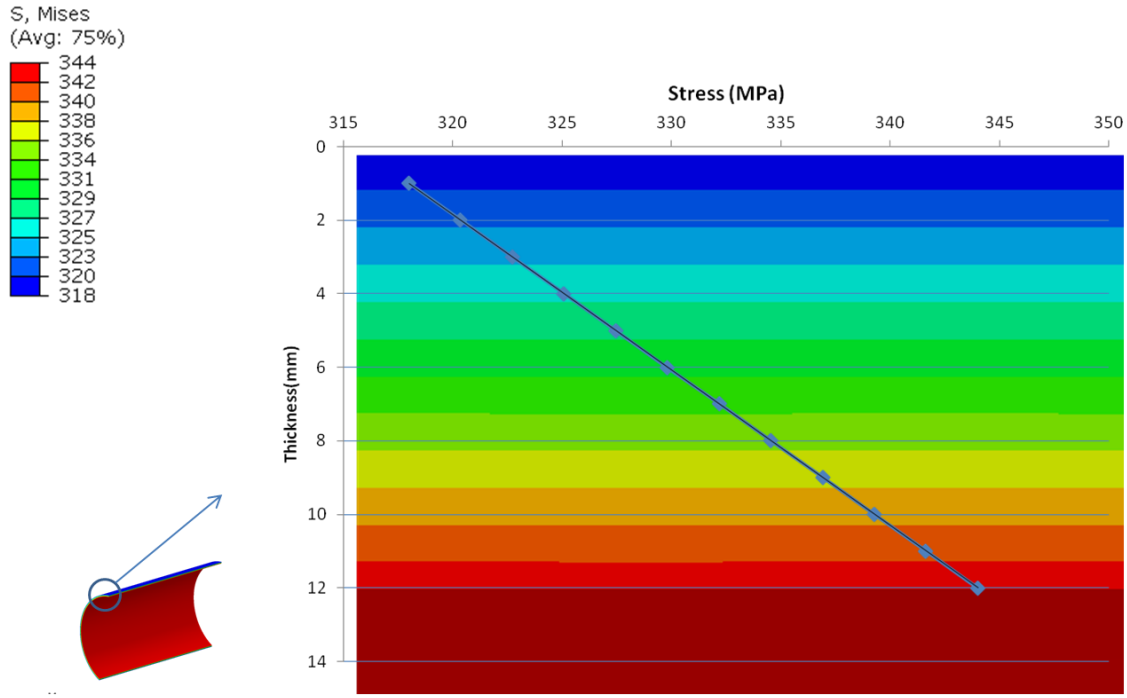

Figure 5-9 Through thickness state of stress

5.3 Evaluation of stress intensity factor for longitudinal crack in pipe, by multiple reference state weight function

5.3.1 MRS WF for a pipe with longitudinal through thickness crack

Two different references for a pipe with a longitudinal through thickness crack have been selected: the first was a pipe under internal pressure with available SIF solution (Eq. (2-6) to (2-10)) and the second was a pipe under opposing section surface load (OSSL) whose SIF has been calculated using FEA techniques (Figure 5-10 and Figure 5-11).

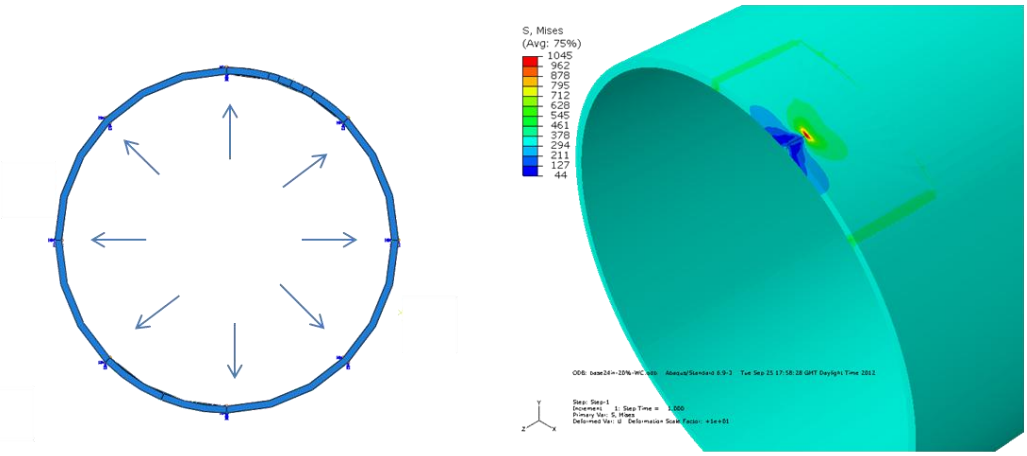

Figure 5-10 Reference 1: Internal pressure

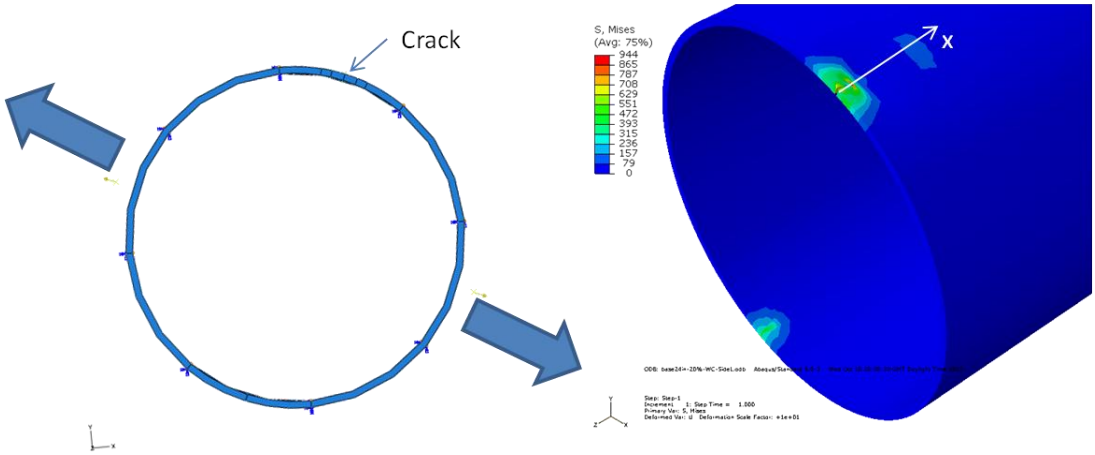

Figure 5-11 Reference 2: Opposing section surface load (OSSL)

The state of stress in Reference 1 is:

$$\sigma = P\frac{R}{t} \tag{5-18}$$

And for reference 2, the state of stress on the un-cracked body is as follows:

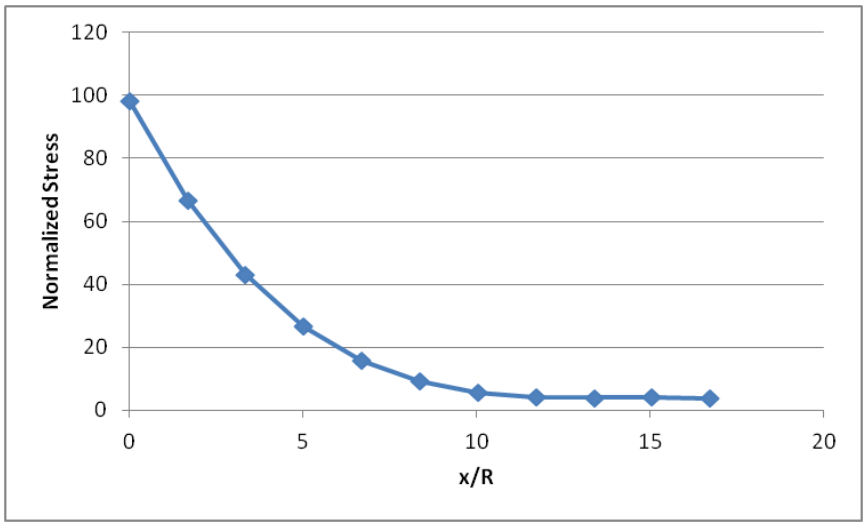

Figure 5-12 State of stress on an un-cracked pipe under OSSL

Where the x axis is positioned longitudinally along the pipe starting from its edge perpendicular to the load line (Figure 5-11). The x and y axes of the above stress function have been normalised to pipe radius and material yield stress.

Using the MRS method and the weight function equation (Equation (2-85)), for a crack to pipe radius ratio domain of 0.02 to 0.08, the references and the weight function have a very good agreement (Figure 5-13).

$$m(a,x) = 2\sqrt{2}\frac{\sigma_0}{K_1(a)}\sum_{j=0}^{n} C_j \left(1-\frac{x}{a}\right)^{\left(j-\frac{1}{2}\right)} \tag{5-19}$$

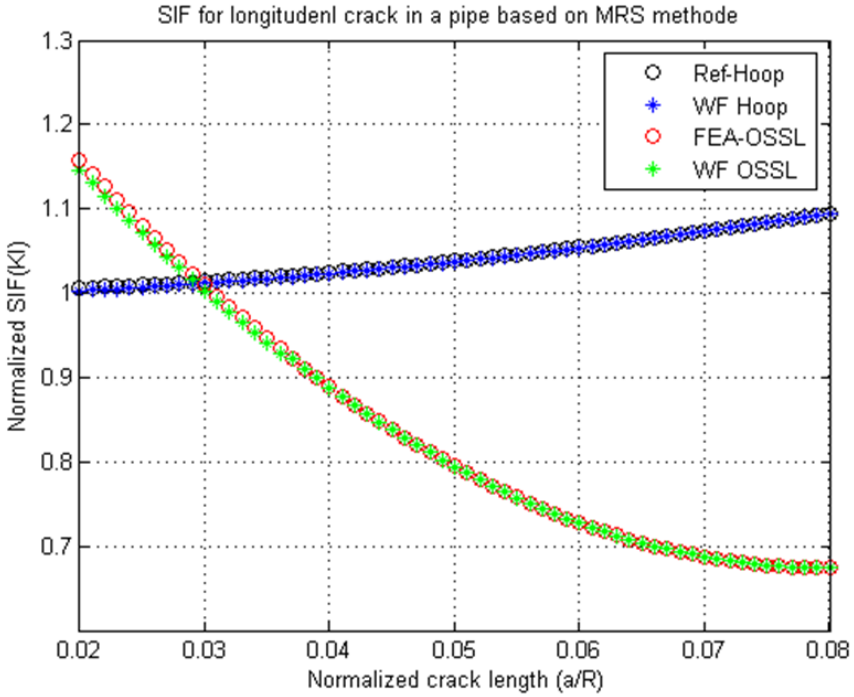

Figure 5-13 Weight function and references good agreement

5.4 Summary

In this chapter the SIF for a longitudinal crack in a pipe under internal pressure using FEA techniques has been presented, as well as the effect of induced low temperature at the front of the crack on the SIF.

A novel MRS weight function method for a pipe with longitudinal through thickness crack has been developed and discussed. The merit of having a weight function for a specific geometry is through calculating the stress intensity factor for any other loading condition. During the design stage of a project, for example a CO_2 pipeline design, if the results of CFD modelling and/or the outflow model show there is a very low induced temperature on pipe material around the crack due to gas expansion, then by knowing the state of stress due to the thermal conduction and convection, the stress intensity factor for the problem can be calculated and could be used in the pipeline design.

So, by having an MRS weight function solution, the SIF for any other loading condition for the same pipe with a through thickness crack under internal pressure can be calculated. These loading conditions include induced thermal stresses, residual stresses and soil backfill pressure.

Chapter five will now draw together this method for modelling cracks with other aspects into a comprehensive methodology for the engineering criticality assessment of defects in CO_2 pipelines.

Chapter 6. Fitness for Service and Engineering Critical Assessment

The failure assessment diagram (FAD) has been explained in Chapter 1. FAD is a powerful tool to understand the acceptability of a defect or flaw in a structure. It is usually necessary to examine critically the integrity of new or existing structures by using non destructive testing methods. Also, acceptance levels for the flaws in a structure are essential. The derivation of this acceptance is based on the concept of fitness for purpose. Several standards have dealt with this issue and a computer program has been developed, based on the R code, by British Energy (R6 2005; API579 2007; BS7910 2012). In this chapter the method of flaw assessment in a pipe with an axially through thickness crack under internal pressure (CO_2 pipeline) will be explored.

Three different levels for the assessment of fracture resistance in standards have been presented (Chapter one). The choice of level depends on the input data available, the materials involved and the conservatism required. Figure 6-1 is a detailed flow diagram for level 2, the so called normal assessment route.

At each level the limiting value of a parameter such as flaw size, applied stress or fracture toughness could be determined via iterating the calculation for the acceptability of a flaw. The material properties required for an assessment are usually related to the region in which the flaw is present, i.e. weld material, parent material of heat affected zone (HAZ).

The concept of leak-before-break assessment is a very important procedure, especially in the nuclear and pipeline industries. Before a failure happens, operators can understand the existence of a flaw in the system and take precautionary actions. Determining the limiting length of the through wall crack for the most onerous loading conditions should be done using the lower bound material properties. The aim is to have a stable leak rather than a break.

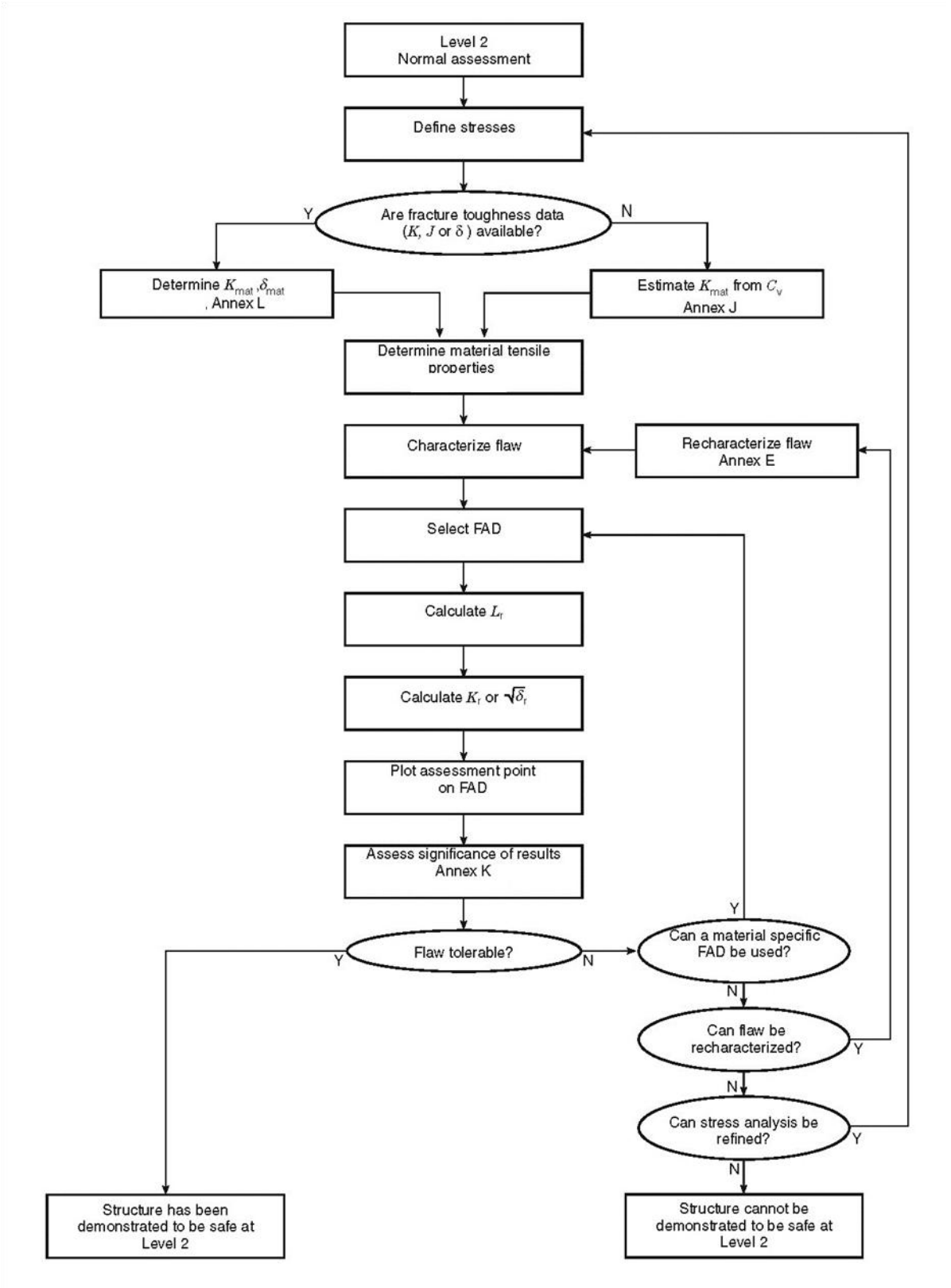

Figure 6-1 FAD Level 2 flowchart

(BS7910 2012)

6.1 Development of a Failure Assessment Diagram Based Method for Engineering Criticality Assessment of CO_2 Transportation Pipelines (published paper)

There are available methods to do a fitness for service (purpose) assessment for structures/pipelines (R6 2005; API579 2007; BS7910 2012). These standards include the most accepted methodology for crack assessment. In an elastic-plastic circumstance, failure assessment should take into account both fracture and plastic deformation. The FAD approach considers both ductile and brittle fractures as possible failure modes. In pipelines brittle fracture can happen and run with speeds of hundreds of meters per seconds and cause catastrophic results (Misawa, Imai et al. 2010). In the level 1 FAD assumption is based on an elastic-perfectly plastic stress-strain curve of material with no strain hardening and provides conservative results. As it has been briefly explained in Chapter 1, the FAD levels 2 and 3 are less conservative, more accurate and consider the actual shape of the material stress-strain curve (Figure 6-2). These three levels can cover most of the various assessment requirements.

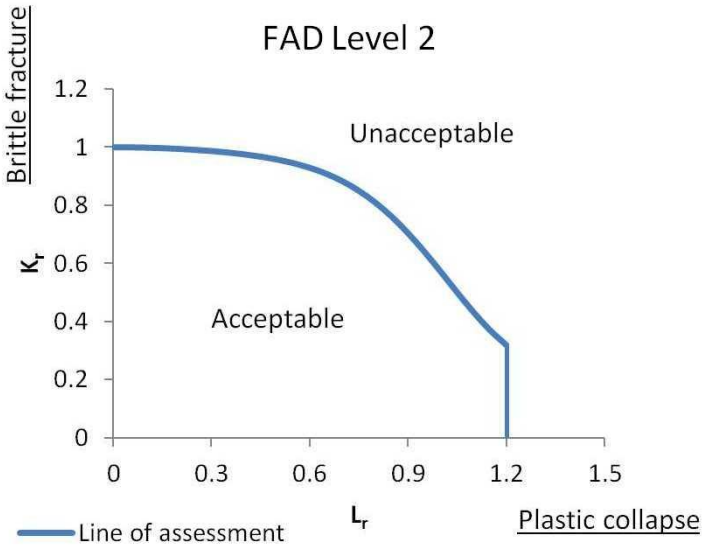

Figure 6-2 Level 2 FAD

$$K_r = \frac{K_I}{K_{IC}} \quad , \quad L_r = \frac{\sigma_{ref}}{\sigma_y} \tag{6-1}$$

The main concern is how to calculate K_I for different geometries and loading conditions. Different sources for well known geometries, crack shape and loading conditions are presented (Sih 1973; Rooke 1976; Murakami 1987; Gray 1992; Tada, Paris et al. 2000). For certain conditions in which a solution cannot be derived from handbooks, other methods such as finite element analysis, weight function and multiple reference state weight function should be used (Brennan 1994; Chahardehi and Brennan 2010). With these methods, a combination of working load, transient thermal stresses, welding heat affected zone (HAZ), and residual stresses are considered to determine K_I to be used in FAD analysis.

On the other hand, material data such as fracture toughness, yield strength and the flow strength can be obtained from different standard test methods (ASTM1290 2002; ASTME8 2009; ASTME399 2009). In the FAD, more ductility shifts the calculating point to the right and for cases of brittle behaviour it will shift it up (Figure 6-2). The cut-off point at L_{rmax} can be obtained from the following equation and in general it is 1.8 for stainless steels and 1.2 for carbon steels.

$$L_{r\max} = \frac{\sigma_y + \sigma_u}{2\sigma_y} \tag{6-2}$$

Pipeline material, chemical composition of transporting media, temperature and type of defect all have certain influences on FAD analysis. For instance, gas chemical composition changes the behaviour of CO_2 (Figure 6-3) and it has a different temperature and pressure during expansion. Decreasing temperature, affects both fracture toughness and yield strength of pipe material. Using high grade steels such as API 5L, X100, X120 with high material toughness gives better safety on K_r for different states of stress.

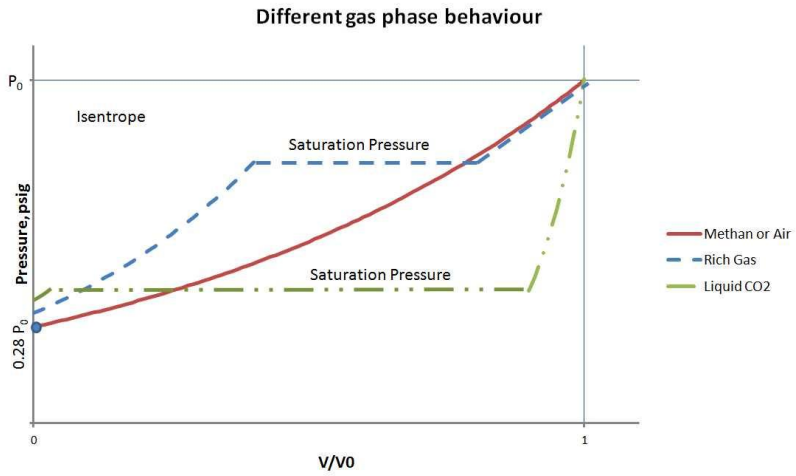

Figure 6-3 Different gas behaviour

Residual stresses due to local welding, pipe manufacturing and misalignment during installation, contribute to Kr but not to L_r. On the other hand, there are long-range residual stresses introduced by major structural components that can give rise to net sectional forces and moments. Due to the elastic follow up behaviour of these residual stresses and acting as primary stresses, they contribute to both Kr and L_r (BS7910 2012).

An understanding of maximum acceptable flaw size is one of the important criteria when making an engineering decision for pipeline fitness for service and is an input to ECA.

6.1.1 Damage mechanism

Different damage mechanisms can be dominant in captured CO_2 pipelines. The main difference between the existing CO_2 pipelines operating in North America and Canada and the new demands for transporting CCS products is in the chemical composition of the gas. Due to CO_2 phase behaviour both pipelines should operate under high pressure to remain in the dense/supercritical phase. In the first case, CO_2 is the product of coal gasification and has more than 99% CO_2, to be used in EOR. Captured CO_2 from the CCS process has different impurities that seriously affect CO_2 phase behaviour. When a defect in a pipeline reaches a certain size, leakage can

start. Expansion of high pressure gas would result in a temperature decrease in the vicinity of the defect and consequently decrease the fracture toughness of the pipe material. When the temperature drops as low as the DBTT, a catastrophic situation could arise.

The other important CO_2 behaviour, is maintaining it's pressure during depressurization (Figure 6-3). This high pressure results in having a high driving force on the crack mouth for crack propagation in a leakage scenario(Leis, Eiber et al. 1998).

At high pressure, supercritical CO_2 behaves as a liquid, and has a liquid-like density, but it yields a very large volume of gas when its pressure is lowered. Depending on its impurities the temperature can be as low as -50°C which is far below a normal pipeline operating temperature (Figure 6-4)(Mahgerefteh and Atti 2006).

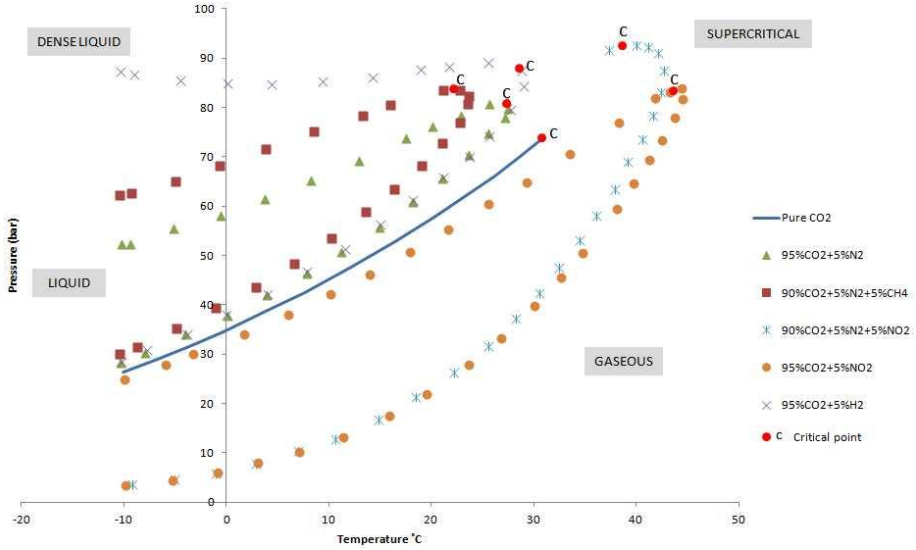

Figure 6-4 Effect of impurities on CO_2 phase behaviour

The state of stress at the defect/crack tip in this situation is a complex of Von-Mises stresses, thermally induced stresses, residual stresses and others, such as back-fill pressure. These stresses and gas decompression are the driving forces in the crack propagation scenario. In the Battelle Two Curve (BTC) method, these driving forces plus pipe material toughness and geometry

are the crack velocity curve parameters (Higuchi, Makino et al.). On the other hand, the gas decompression curve affected by the impurities is the other curve which competes with the crack velocity curve.

Corrosion due to the existence of impurities, stress corrosion cracking, ductile failure and the effects of general aging are the other possible damage mechanism (Chahardehi 2011).

6.1.2 Safe operation

Based on the latest gas pipeline incidents report, less than 15% of Europe's pipelines are designed and working over 75 bar (EGIG 2011). In the case of captured CO_2 pipelines, the optimum operating pressure is around 150 bar that changes it to a supercritical or dense phase. This shows that there are possibilities for using the existing natural gas pipelines but there is also a certain need for design of next generation of CO_2 pipelines. In the former case, the maximum allowable impurities of captured CO_2 are one of the inputs for ECA. The effect of different impurities on CO_2 phase behaviour has been studied. For example, the behaviour of pure CO_2 compared to captured CO_2 with impurities in the case of sudden expansion, is different in terms of temperature drop in the vicinity of a crack or flaw. Danger of temperature drop will be critical if it passes the ductile to brittle temperature transition (DBTT) point as it will cause catastrophic brittle fracture failure. To prevent such failure an integrated ECA at the start of the project and interval monitoring by operators should be conducted.

CO_2 is heavier than air and in some cases, depending on its concentration can cause asphyxiation. Introducing highly toxic components such as H_2S and SO_2 in the captured CO_2 increases the risk of operating such pipelines. It has been shown that pure CO_2 will be harmless after dilution by 20 times with air. However, having such toxic components in a mixture needs 500 to 1000 times more dilution to be safe (IEAGHG 2011). Due to the location of both the source

and sink of these pipelines there must be state-of-the-art technologies for leak detection.

There is the need to take appropriate actions to mitigate areas of concern regarding captured CO_2 pipelines. Introducing a code of practice by standards authorities based on different CO_2 capture technologies and related gas purification methods is a crucial need for pipeline industries. This code can ensure the operating of safe and reliable CO_2 pipelines. Understanding critical flaw size and operating safety factors from FAD analysis is a fundamental input for the proposed ECA.

6.1.3 Engineering criticality assessment

Engineering criticality assessment (ECA) is a powerful tool to determine and understand the possible failure of a system. In pipelines different criteria could cause failure and to cover most of them an integrated ECA is proposed.

Certain amounts of impurities, such as H2S, and O_2 can cause corrosion in the pipelines. Different models have been presented to predict corrosion during a pipeline's life span. For example if the partial pressure of H_2S in gas composition is more than 0.05 psi, it will be recognised as sour gas and need special consideration. For CO_2 corrosion which is well known in the oil and gas industries, with an increase of CO_2 partial pressure in the gas mixture the corrosion decreases exponentially and is not therefore crucial for captured CO_2 pipelines (Bijan Kermani, John W. Martin et al. 2006; ISO15156 2009).

Different parameters, such as pipe geometry, gas composition, loading condition and pipe material characterizations should be known as inputs to integrated ECA. An understanding of captured CO_2 phase behaviour affected by impurities is important in order to estimate gas pressure and temperature in different conditions. Also the impurities percentage helps to understand the corrosion possibilities. Following the different criteria depicted in Annex A, several damage mechanisms can be assumed. Based on their higher possibility of occurrence, they could be prioritized and weighted. In each stage,

modification on the selection of pipe material and geometry can be a correction feed-back to the whole ECA. Pipe material data and fracture resistance as a function of temperature is essential to analyse the behaviour of defects at different temperatures. As a result, an acceptable defect size in the pipeline and maximum allowable percentage of impurities in captured CO_2 can be critical outcomes of implementing integrated ECA on the pipeline (Figure 6-5).

Figure 6-5 shows a suggested ECA for CO2 pipelines. it is a novel ECA recommended to be used by CO2 pipeline designers and operators, to have most of the related concerns in one graph.

As a conclusion, engineering criticality assessment is a powerful tool for pipeline operators to use in assessing their pipelines. An integrated ECA, based on the FAD method has been developed. Different critical aspects in captured CO_2 pipelines should be considered and a fitness for purpose study should be implemented. The possibility of using existing natural gas pipelines for transporting captured CO_2 as a product of CCS process can be assessed using this integrated ECA. Also, in general, by using this method, new designs can be optimized.

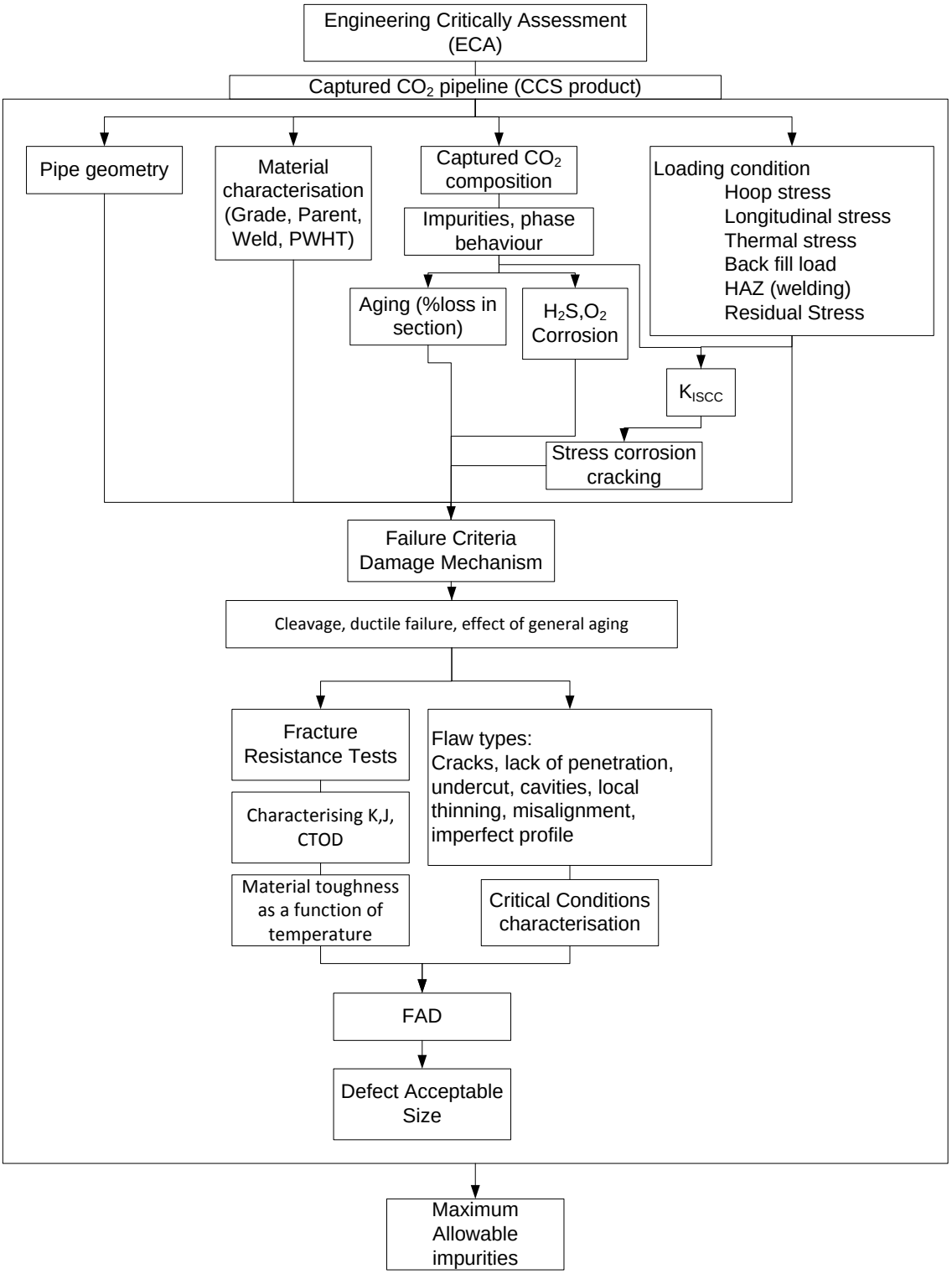

Figure 6-5 Captured CO_2 pipeline, Engineering Critically Assessment

6.2 Failure Assessment Diagram for through thickness flaws oriented axially on a pipe under internal pressure

Figure 6-6 illustrates a through thickness flaw oriented axially in a pipe under internal pressure. Determination of the critical flaw/crack length is the aim of performing this assessment.

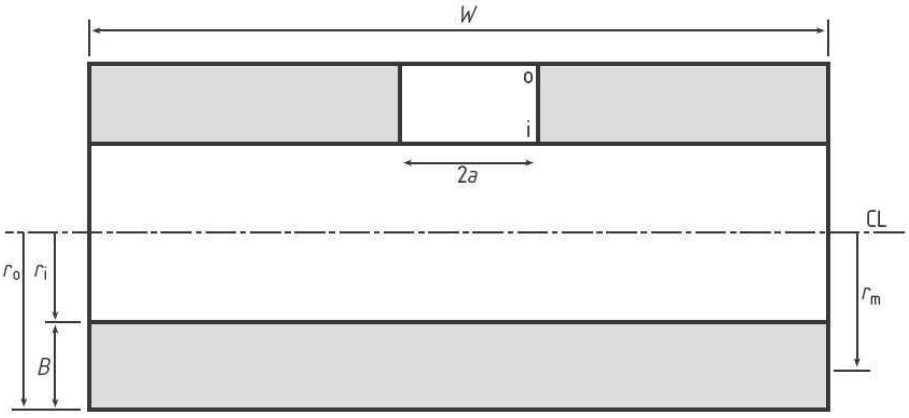

Figure 6-6 Through thickness flaw in a cylinder oriented axially (BS7910 2012)

As explained in chapter one, if it is requested to perform a level 2 assessment on the mentioned problem, the following steps should be considered:

$$K_r = \frac{K_I}{K_{mat}}, K_I = (Y\sigma)\sqrt{\pi a} \tag{6-3}$$

$$(Y\sigma) = (Y\sigma)_p + (Y\sigma)_s \tag{6-4}$$

$(Y\sigma)_p$ And $(Y\sigma)_s$ represent contributions from primary and secondary stresses, respectively. They are calculated as follows:

$$(Y\sigma)_p = Mf_W[k_{tm}M_{km}M_mP_m + k_{tb}M_{kb}M_b\{P_b + (k_m - 1)P_m\}] \tag{6-5}$$

$$(Y\sigma)_s = M_mQ_m + M_bQ_b \tag{6-6}$$

All of the parameters have to be defined for this problem and consequently Kr and Lr have to be calculated. For through thickness flaws in cylinders (pipes) oriented axially under internal pressure only:

$$K_I = K_I^{membrane} + K_I^{bending} \tag{6-7}$$

Where in this case, it can be supposed there are no bending stresses but that membrane stresses are dominant.

M=1, and any possible bulging is taken to account by parameter λ.

$$\lambda = \{12(1-\upsilon^2)\}^{0.25} \frac{a}{\sqrt{r_m B}} \tag{6-8}$$

Where v is the Poisson's ratio, "a" is half of the flaw and B is the pipe thickness.

These solutions are valid for long cylinders, or pressure vessels with closed ends, and the range of application for the above formula is:

$$0 \le \lambda \le 12.211 \tag{6-9}$$

$$5 \le \frac{r_m}{B} \le 100 \tag{6-10}$$

F_w =1 as the actual flaw area is not greater than 10% of the load bearing cross section area. M_{km} and M_{kb} apply when the flaw or crack is in a region of local stress concentration, in this problem both are equal to one (Eq. 5-5).

The stress magnification factors apply when angular or axial misalignment, or both, at a welded joint can cause an increase or decrease in stress at the joint when it is loaded. In case of misalignment, k_t , k_{tm} , k_{tb} and k_m parameters have to be calculated and consequently σ_s (the bending stress) can be determined (BS7910 2012), Annex D).

Equation (6-5) is simplified as:

$$(Y\sigma)_p = M_m P_m + M_b P_b \tag{6-11}$$

Where P_m and P_b are primary membrane stress and primary bending stress respectively.

$$\begin{aligned} M_m &= M_1 + M_2 \quad \text{at the outside surface} \\ M_m &= M_1 - M_2 \quad \text{at the inside surface} \\ M_b &= M_3 + M_4 \quad \text{at the outside surface} \\ M_b &= M_3 - M_4 \quad \text{at the inside surface} \end{aligned} \tag{6-12}$$

M_1 to M_4 are given in Table M.1(a to d), for membrane and through wall bending loading in terms of λ (BS7910 2012), Annex M). Also in Equation (6-6), Q_m and Q_b are the secondary membrane and bending stresses respectively.

Understanding the material toughness by testing the material specimens, and by calculating the different parameters discussed in this section, K_r can be determined. To calculate the other coordinate value of the assessment point in the FAD diagram, L_r should be calculated. In (BS7910 2012), Annex P) the reference stress calculated as:

$$\begin{aligned} L_r &= \frac{\sigma_{ref}}{\sigma_y} \\ \sigma_{ref} &= 1.2 M_T P_m + \frac{2P_b}{3(1-\frac{2a}{W})} \end{aligned} \tag{6-13}$$

Where

$$M_T = \{1 + 1.6(\frac{a^2}{r_i B})\}^{0.5} \tag{6-14}$$

And P_m is the hoop stress (membrane) and P_b is the bending stress transverse to the flaw (Folias 1984; Staat 2004).

R-code R6, uses the following loadings to calculate the Lr:

- The secondary stress distribution from an elastic analysis
- The secondary stress distribution from an elastic-plastic analysis
- A stress distribution obtained from the strains

Using the following formula:

$$\sigma_{yy} = \frac{E}{(1+\upsilon)(1-2\upsilon)}((1-\upsilon)e_{yy} + \upsilon(e_{xx} + e_{zz})) \quad (6\text{-}15)$$

The stress component will normally be that which acts perpendicularly to the crack plane, in this case the hoop component.

Load factor gives the overall factor on load to be applied to the variable loads. For critical load calculations this is used as a start point. This factor is particularly useful as a sensitivity variable. For critical crack analyses it is applied to all the variable loads (primary and secondary). For fatigue analyses it is applied to all the loads. In this problem it is applied to the primary load which is the hoop stress due to internal pressure (R6 2005).

6.3 Test cases

A series of assessments for the problem of this chapter has been made and the results are presented in the following tables and graphs. The problem has been defined as: a long pipe with the OD of 609.9 mm (24 inches) and length of 500m, with the thickness of 12mm, the pipe material is API 5L X100 with mechanical properties of yield stress 690MPa, Ultimate tensile stress 770MPa, 200GPa as module of elasticity and 0.3 as Poisson's ratio. The fracture toughness of the material in ambient temperature is 130MPam^0.5 and in a low temperature of -70°C is 85MPam^0.5. The pipe is under internal pressure of 15MPa and its temperature is 35°C.

Two different series of scenarios have been considered. One is based on limiting load (LL) and the second limiting crack size (LC). It has been mentioned that only primary loads contribute to the plastic collapse but all loads contribute to the stress intensity factor. More generally, primary loads include all stresses arising from internal pressure or external loads and long range thermal and residual stresses, unless there is conclusive evidence to the contrary. Secondary loads include stresses arising from thermal loading and residual stresses due to manufacturing processes, including welding.

Each case study has a dedicated number and has been defined as follows:

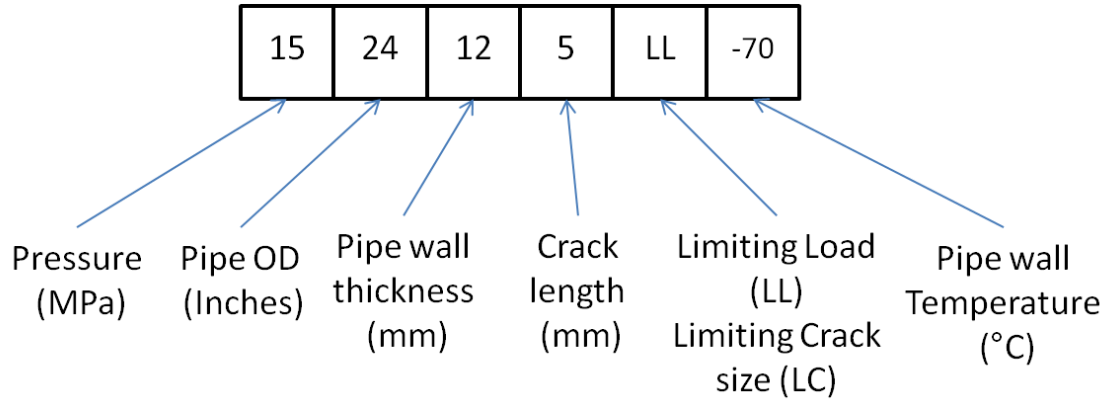

Figure 6-7 Case number definition

CO_2 expands to atmosphere with 0.1MPa pressure and temperature drops to -70°C. The load factor has been set to 1.2 to be similar to hydrostatic testing procedures.

Table 6-1 and Figure 6-8 illustrate a case where under a constant crack length (5mm) and various hoop stresses, (maximum of 1.2 σ_H that is required for hydrostatic testing before commissioning) crack initiation occurs with a load factor of 1.43. Therefore a further increase in hoop stress causes the crack to fall into the failure region of the FAD.

By increasing the crack length to 10mm, (Table 6-2 and Figure 6-9) and under similar conditions to the previous case study, crack initiation starts at 1.2 σ_H and the crack falls into the failure region.

It can be observed that by increasing the crack length to 15 and 20 mm, (Table 6-3 and Figure 6-10, Table 6-4 and Figure 6-11 respectively) by increasing the K_r/L_r ratio the crack falls into the failure region in the lower hoop stress, i.e. in the case of 20mm crack length the crack initiation starts even before the system reaches its operating pressure.

Table 6-5 and Figure 6-12 illustrate a case where the design pressure is constant and crack length increasing. The design pressure has been set to 1.2 times the operations pressure. As soon as the crack length reaches 9.9mm the crack starts initiating and falls into the failure region of the FAD.

All of the previous studies considered a low temperature of -70°C at the crack front for the wall thickness of the pipe and consequently the fracture toughness of the pipe material is in its lower value.

Table 6-6 and Figure 6-13 show a case which is under a constant design pressure and variable crack length. In this case the wall temperature of the pipe around the crack area is ambient. It can be observed that if the very low induced temperature due to CO_2 expansion takes place far from the pipe, failure happens for crack lengths longer than 20mm.

Just for comparison, the case of Table 6-7 and Figure 6-14 has been studied under similar conditions to the previous case and working under the same operating pressure. It can be observed here that the crack starts initiating for crack lengths longer than 30.8mm.

Table 6-1 CO_2 pipe-15-24-12-5-LL_-70

Crack Length (mm)	Res. Tough (MPam^0.5)	SIF (MPam^0.5)	Kr R6	Lr R6	Load Factor	Crack Status
5	85	5.564	0.065	0.092	0.143	Stable
5	85	11.13	0.131	0.185	0.285	Stable
5	85	16.69	0.196	0.277	0.428	Stable
5	85	22.26	0.262	0.37	0.571	Stable
5	85	27.82	0.327	0.462	0.713	Stable
5	85	33.39	0.393	0.554	0.856	Stable
5	85	38.95	0.458	0.647	0.999	Stable
5	85	44.52	0.524	0.739	1.14	Stable
5	85	50.08	0.589	0.832	1.28	Stable
5	85	55.64	0.655	0.924	1.43	Initiation
5	85	57.88	0.681	0.961	1.48	Failed
5	85	60.12	0.707	0.998	1.54	Failed
5	85	62.35	0.734	1.035	1.6	Failed
5	85	64.59	0.76	1.072	1.66	Failed
5	85	66.82	0.786	1.11	1.71	Failed
5	85	69.06	0.812	1.147	1.77	Failed
5	85	71.3	0.839	1.184	1.83	Failed
5	85	73.53	0.865	1.221	1.89	Failed
5	85	75.77	0.891	1.258	1.94	Failed
5	85	78	0.918	1.295	2	Failed

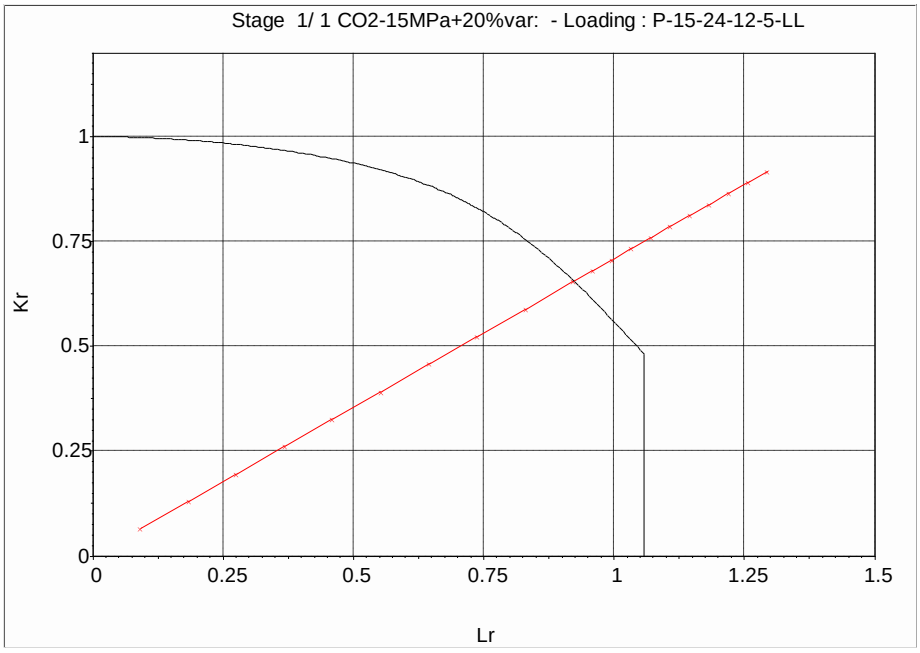

Figure 6-8 FAD, 15-24-12-5-LL_-70

Table 6-2 CO_2 pipe-15-24-12-10-LL_-70

Crack Length (mm)	Res. Tough (MPam^0.5)	SIF (MPam^0.5)	Kr R6	Lr R6	Load Factor	Crack Status
10	85	6.802	0.08	0.078	0.12	Stable
10	85	13.6	0.16	0.155	0.239	Stable
10	85	20.41	0.24	0.233	0.359	Stable
10	85	27.21	0.32	0.311	0.478	Stable
10	85	34.01	0.4	0.389	0.598	Stable
10	85	40.81	0.48	0.466	0.718	Stable
10	85	47.62	0.56	0.544	0.837	Stable
10	85	54.42	0.64	0.622	0.957	Stable
10	85	61.22	0.72	0.7	1.08	Stable
10	85	68.02	0.8	0.777	1.2	Initiation
10	85	72.59	0.854	0.83	1.28	Failed
10	85	77.16	0.908	0.882	1.36	Failed
10	85	81.74	0.962	0.934	1.44	Failed
10	85	86.31	1.015	0.986	1.52	Failed
10	85	90.88	1.069	1.039	1.6	Failed
10	85	95.45	1.123	1.091	1.68	Failed
10	85	100	1.177	1.143	1.76	Failed
10	85	104.6	1.23	1.195	1.84	Failed
10	85	109.2	1.284	1.248	1.92	Failed
10	85	113.7	1.338	1.3	2	Failed

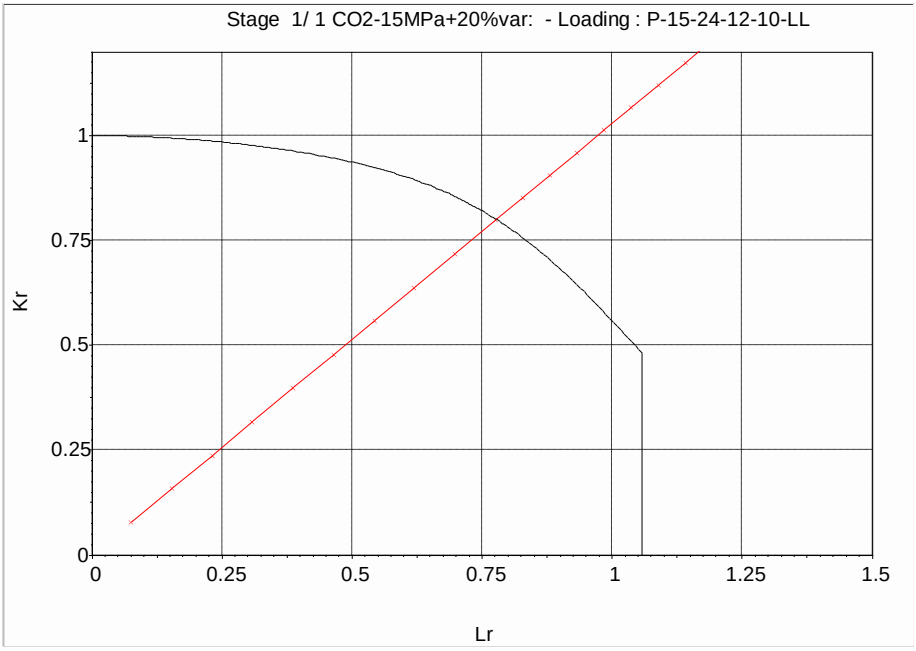

Figure 6-9 FAD, 15-24-12-10-LL_-70

Table 6-3 CO_2 pipe-15-24-12-15-LL_-70

Crack Length (mm)	Res. Tough (MPam^0.5)	SIF (MPam^0.5)	Kr R6	Lr R6	Load Factor	Crack Status
15	85	7.386	0.087	0.067	0.103	Stable
15	85	14.77	0.174	0.135	0.206	Stable
15	85	22.16	0.261	0.202	0.309	Stable
15	85	29.54	0.348	0.269	0.412	Stable
15	85	36.93	0.434	0.336	0.514	Stable
15	85	44.31	0.521	0.404	0.617	Stable
15	85	51.7	0.608	0.471	0.72	Stable
15	85	59.08	0.695	0.538	0.823	Stable
15	85	66.47	0.782	0.605	0.926	Stable
15	85	73.86	0.869	0.673	1.03	Initiation
15	85	80.83	0.951	0.736	1.13	Failed
15	85	87.8	1.033	0.8	1.22	Failed
15	85	94.76	1.115	0.863	1.32	Failed
15	85	101.7	1.197	0.927	1.42	Failed
15	85	108.7	1.279	0.99	1.51	Failed
15	85	115.7	1.361	1.053	1.61	Failed
15	85	122.6	1.443	1.117	1.71	Failed
15	85	129.6	1.525	1.18	1.81	Failed
15	85	136.6	1.607	1.244	1.9	Failed
15	85	143.6	1.689	1.307	2	Failed

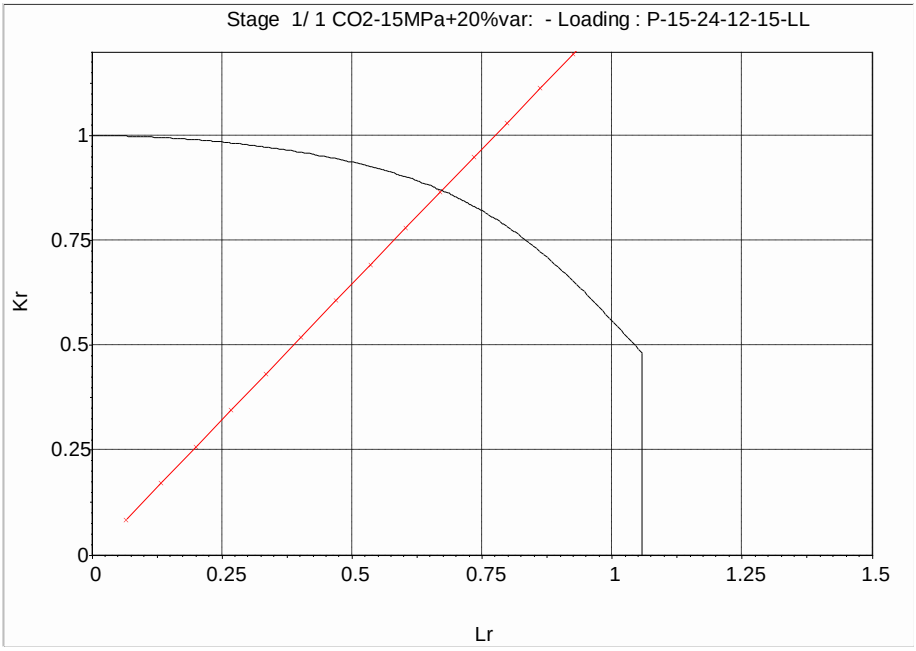

Figure 6-10 FAD, 15-24-12-15-LL_-70

Table 6-4 CO_2 pipe-15-24-12-20-LL_-70

Crack Length (mm)	Res. Tough (MPam^0.5)	SIF (MPam^0.5)	Kr R6	Lr R6	Load Factor	Crack Status
20	85	7.694	0.091	0.059	0.0901	Stable
20	85	15.39	0.181	0.119	0.18	Stable
20	85	23.08	0.272	0.178	0.27	Stable
20	85	30.78	0.362	0.238	0.361	Stable
20	85	38.47	0.453	0.297	0.451	Stable
20	85	46.17	0.543	0.356	0.541	Stable
20	85	53.86	0.634	0.416	0.631	Stable
20	85	61.56	0.724	0.475	0.721	Stable
20	85	69.25	0.815	0.535	0.811	Stable
20	85	76.94	0.905	0.594	0.901	Initiation
20	85	86.32	1.016	0.666	1.01	Failed
20	85	95.7	1.126	0.739	1.12	Failed
20	85	105.1	1.236	0.811	1.23	Failed
20	85	114.5	1.347	0.884	1.34	Failed
20	85	123.8	1.457	0.956	1.45	Failed
20	85	133.2	1.567	1.028	1.56	Failed
20	85	142.6	1.678	1.101	1.67	Failed
20	85	152	1.788	1.173	1.78	Failed
20	85	161.4	1.898	1.246	1.89	Failed
20	85	170.7	2.009	1.318	2	Failed

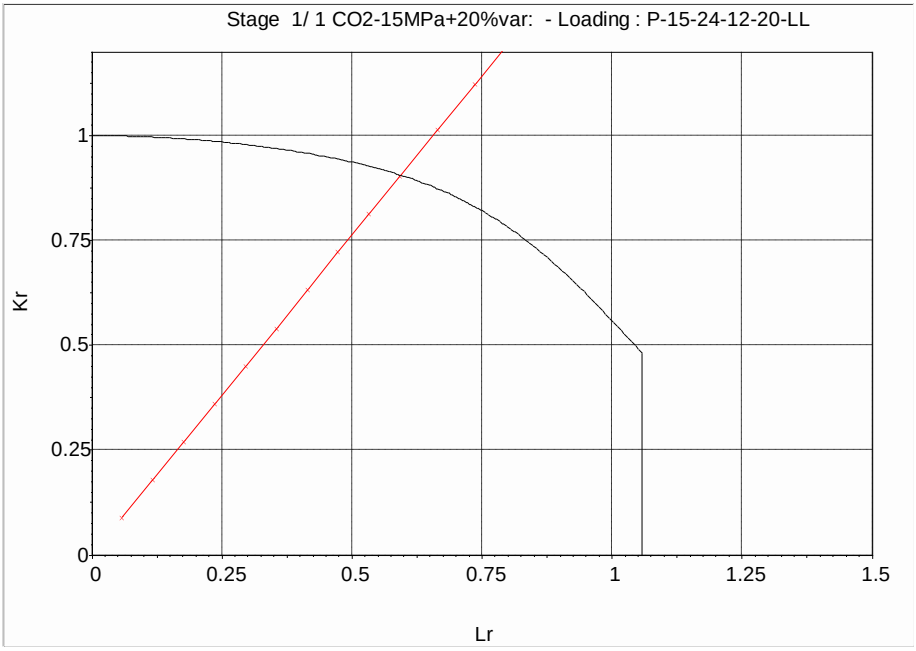

Figure 6-11 FAD, 15-24-12-20-LL_-70

Table 6-5 CO_2 pipe-15-24-12-5-LC_-70

Crack Length (mm)	Res. Tough (MPam^0.5)	SIF (MPam^0.5)	Kr R6	Lr R6	Load Factor	Crack Status
5	85	46.8	0.551	0.777	1.2	Stable
5.489	85	49.19	0.579	0.777	1.2	Stable
5.979	85	51.49	0.606	0.778	1.2	Stable
6.468	85	53.71	0.632	0.778	1.2	Stable
6.957	85	55.87	0.657	0.778	1.2	Stable
7.447	85	57.98	0.682	0.778	1.2	Stable
7.936	85	60.03	0.706	0.779	1.2	Stable
8.425	85	62.04	0.73	0.779	1.2	Stable
8.915	85	64.01	0.753	0.779	1.2	Stable
9.404	85	65.94	0.776	0.779	1.2	Stable
9.893	85	67.83	0.798	0.78	1.2	Initiation
61.598	85	225.5	2.653	0.905	1.2	Failed
113.303	85	384.8	4.527	1.155	1.2	Failed
165.008	85	556.9	6.552	1.465	1.2	Failed
216.713	85	738.3	8.686	1.804	1.2	Failed
268.418	85	926	10.894	2.158	1.2	Failed
320.123	85	1118	13.152	2.518	1.2	Failed
371.828	85	1313	15.444	2.883	1.2	Failed
423.533	85	1509	17.758	3.25	1.2	Failed
475.238	85	1707	20.086	3.618	1.2	Failed
526.943	85	1905	22.416	3.986	1.2	Failed

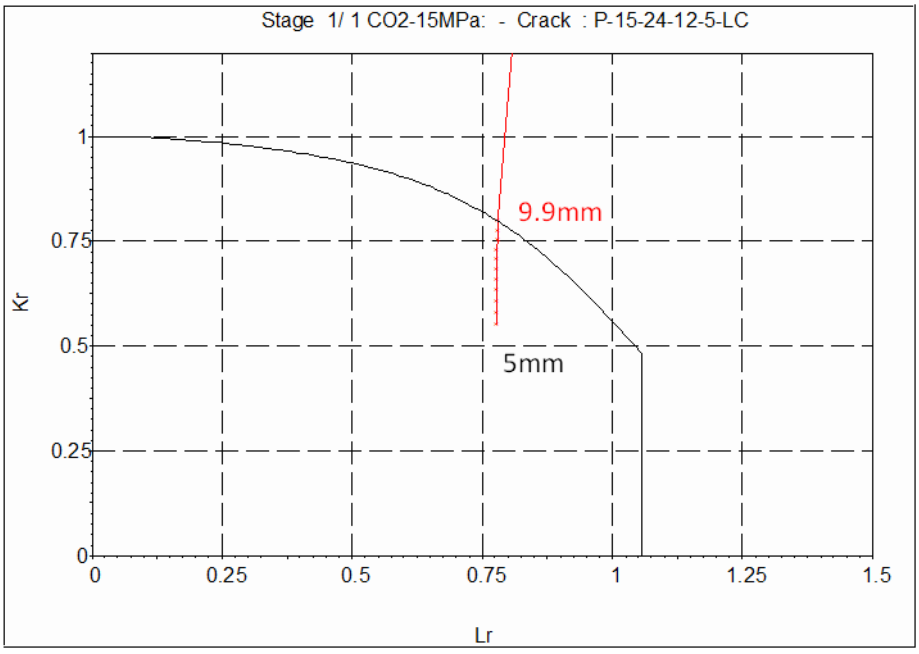

Figure 6-12 FAD, 15-24-12-5-LC_-70

Table 6-6 CO_2 pipe-15-24-12-10-LC-10

Crack Length (mm)	Res. Tough (MPam^0.5)	SIF (MPam^0.5)	Kr R6	Lr R6	Load Factor	Crack Status
10	130	68.24	0.525	0.78	1.2	Stable
11.005	130	72.02	0.554	0.781	1.2	Stable
12.009	130	75.7	0.582	0.781	1.2	Stable
13.014	130	79.28	0.61	0.782	1.2	Stable
14.018	130	82.78	0.637	0.783	1.2	Stable
15.023	130	86.21	0.663	0.784	1.2	Stable
16.028	130	89.58	0.689	0.786	1.2	Stable
17.032	130	92.9	0.715	0.787	1.2	Stable
18.037	130	96.17	0.74	0.788	1.2	Stable
19.041	130	99.4	0.765	0.789	1.2	Stable
20.046	130	102.6	0.789	0.791	1.2	Initiation
70.736	130	252.7	1.944	0.942	1.2	Failed
121.425	130	411.1	3.162	1.2	1.2	Failed
172.115	130	581.4	4.472	1.51	1.2	Failed
222.805	130	760.1	5.847	1.845	1.2	Failed
273.494	130	944.7	7.267	2.193	1.2	Failed
324.184	130	1133	8.716	2.547	1.2	Failed
374.874	130	1324	10.187	2.905	1.2	Failed
425.564	130	1517	11.671	3.265	1.2	Failed
476.253	130	1711	13.163	3.626	1.2	Failed
526.943	130	1905	14.657	3.986	1.2	Failed

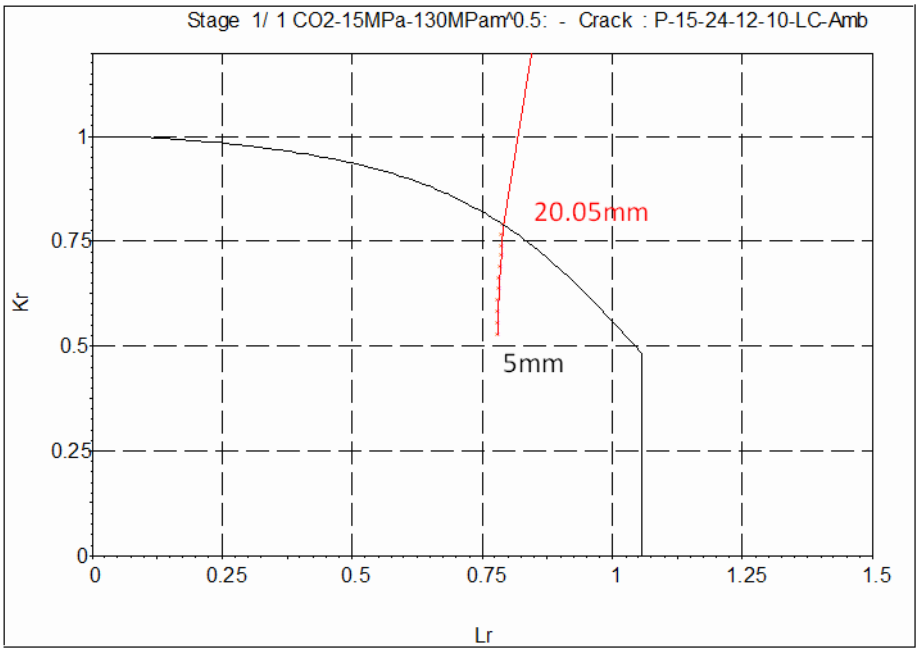

Figure 6-13 FAD, 15-24-12-10-LC-10

Table 6-7 CO_2 pipe-15-24-12-10-LC-10 (load factor=1)

Crack Length (mm)	Res. Tough (MPam^0.5)	SIF (MPam^0.5)	Kr R6	Lr R6	Load Factor	Crack Status
10	130	56.87	0.437	0.65	1	Stable
12.08	130	63.29	0.487	0.651	1	Stable
14.16	130	69.39	0.534	0.653	1	Stable
16.24	130	75.24	0.579	0.655	1	Stable
18.32	130	80.9	0.622	0.657	1	Stable
20.399	130	86.43	0.665	0.659	1	Stable
22.479	130	91.84	0.706	0.662	1	Stable
24.559	130	97.16	0.747	0.665	1	Stable
26.639	130	102.4	0.788	0.668	1	Stable
28.719	130	107.6	0.828	0.672	1	Stable
30.799	130	112.8	0.867	0.675	1	Initiation
80.413	130	234.9	1.807	0.821	1	Failed
130.028	130	366	2.816	1.042	1	Failed
179.642	130	506.2	3.894	1.299	1	Failed
229.256	130	652.8	5.021	1.574	1	Failed
278.871	130	803.7	6.183	1.858	1	Failed
328.485	130	957.7	7.367	2.148	1	Failed
378.1	130	1114	8.567	2.44	1	Failed
427.714	130	1271	9.778	2.733	1	Failed
477.328	130	1429	10.996	3.028	1	Failed
526.943	130	1588	12.214	3.322	1	Failed

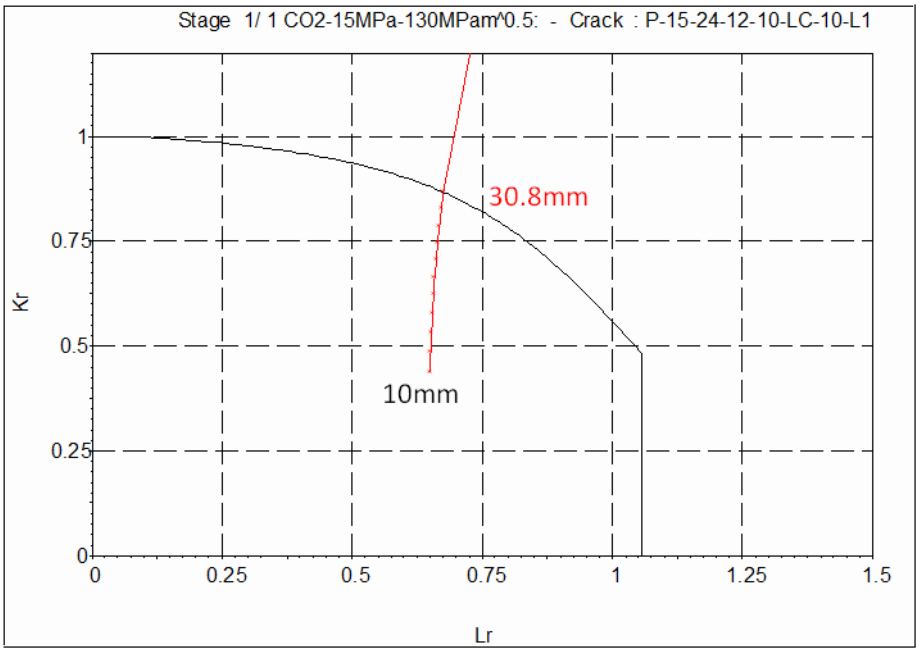

Figure 6-14 FAD, 15-24-12-10-LC-10-(load factor=1)

6.4 Summary

In this chapter the development of fitness for service and engineering criticality assessments for a CO_2 pipe using failure assessment diagrams is reported. The effect of low temperature material fracture toughness (Chapter 4) and critical crack length for different test cases have been studied. A simplified step by step approach to calculate FAD parameters for a pipe with an axial through thickness crack is presented.

It can be observed from the test case studies, that if the temperature of the pipe material around the crack decreases to a very low temperature, a 14.8 mm crack length is the critical crack length in the operating pressure condition. On the other hand, if the pipe material temperature stays at its ambient temperature the acceptable critical crack length can be extended to 30.7mm (more than double).

Additional observations, concerning the material's low temperature yield strength and implementing its effect in the calculations, were noted as areas for future work.

Chapter 7. Summary, Concluding Remarks and Recommendations for future work

7.1 Summary

This thesis presented a detailed review and fracture mechanics analysis of operational aspects of pipelines containing flue-gas CO_2. Chapter one presented CO_2 capture technology, fracture mechanics of a pipeline and failure assessment diagram methodology for pipeline assessment. Chapter 2 introduced numerical solutions using FEA to find SIF for different non-standard geometries and CT specimens, which have been used in this thesis. Chapter 3 described performing a fracture toughness test for pipeline material and concluded with the effect of low temperatures on pipe material fracture toughness. Chapter 4 presented a novel analytical model using an MRS weight function to solve SIF problems for longitudinal through thickness cracks in pipes under different loading conditions. Finally in Chapter 5, an FAD based ECA was developed for the assessment of CO_2 pipelines.

7.2 Concluding remarks

For transporting captured CO_2 from CCS plants to geological storage points, the most economical solution is the pipeline. From economic and phase behaviour points of view, CO_2 should be transported under very high pressure (150 bar) to be in a supercritical or dense phase (Figure 2-4). To select the best material for transporting high pressure CO_2, several design factors should be taken into account. Combining engineering design based with fracture design based factors establishes that the pipeline material should have high strength/high toughness properties. Having high strength in a material does not guarantee having high toughness as well. For example, during the pipe production process, accelerated cold forming could have significant increases on proof stress but not such serious effects on pipe toughness. Also, for most projects, the cost per tonne of pipeline is an important factor. So there should be an optimised solution when selecting pipeline material for transporting high

pressure CO_2 , taking into consideration the possibility of a ductile/brittle fracture and the overall cost of the pipeline.

The pipeline must have adequate resistance to propagating fractures. The fracture arrest properties of a pipeline intended for transportation of a CO_2 composition at a given pressure and temperature depend on the material properties, wall thickness of the pipe, in particular the fracture toughness, and the physical properties of the CO_2 composition in terms of saturation pressure and decompression speed. Also type and level of impurities in CO_2 play an important role in its phase behaviour and consequently the physical properties of the composition.

By increasing the number of CCS plants and in order to meet the UK targets for 2020 and 2050, CO_2 trunk line networks have to be developed. Different capture technologies and different sources of CO_2 capture, cause a mixture of different impurities in the pipeline network. It is not possible to control and operate such pipelines without having a standard or a code of practice to guide operators regarding the maximum allowable level of impurities and CO_2 operating pressure and temperature. Before compressing and injecting captured CO_2 into the pipelines, impurity levels have to be contained within acceptable standard levels determined by the operator. This is not possible without having a comprehensive engineering criticality assessment study on the whole of the network.

Figure 7-1, shows the ECA methodology presented in Chapter 5 and developed as part of this thesis. By conducting an ECA on CO_2 pipelines, the maximum allowable impurities and acceptable defect size can be obtained. Consequently by knowing the maximum acceptable defect size and corrosion level, the remaining pipe life and maintenance time can be predicted.

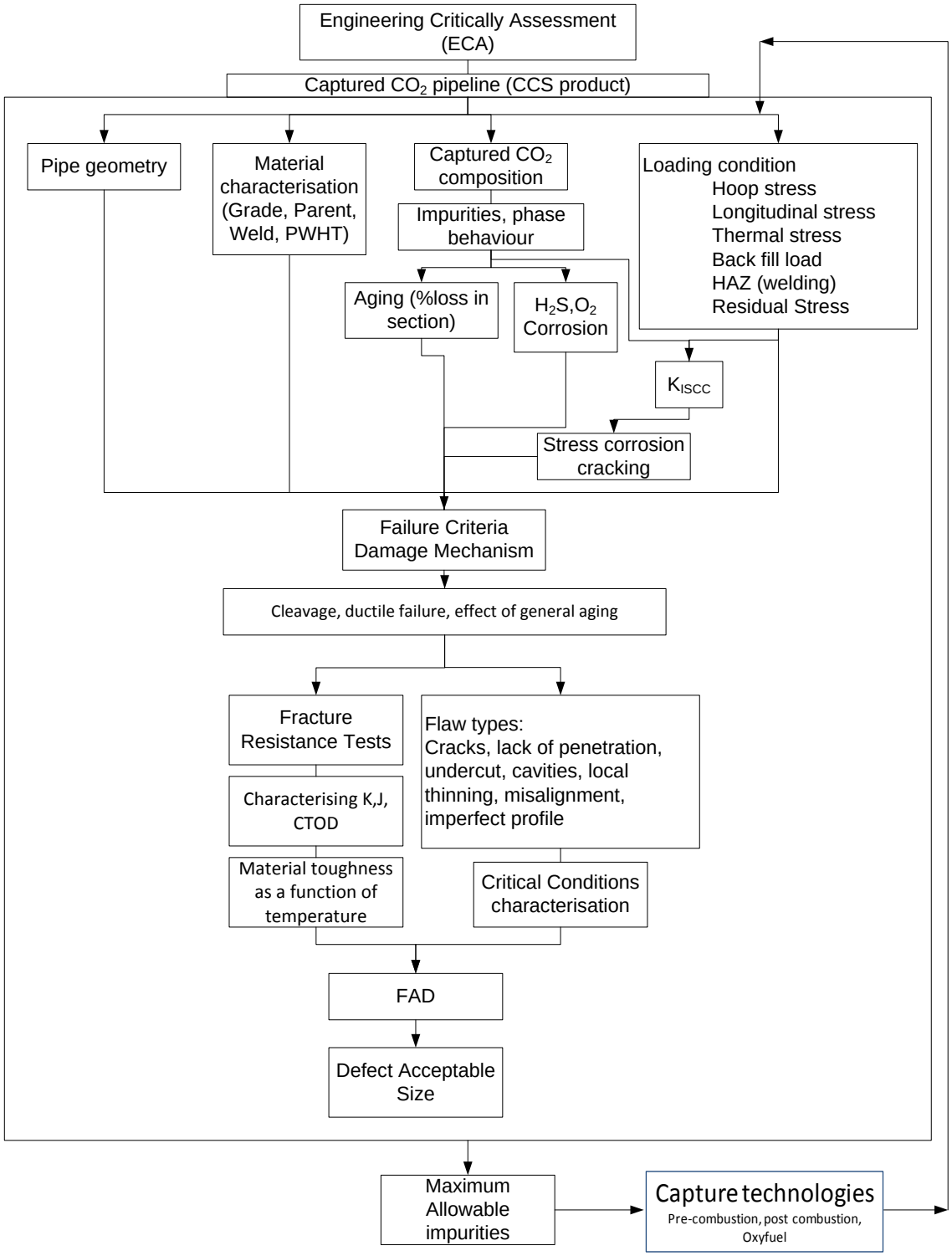

Figure 7-1 ECA for CO_2 pipeline

As shown in the above ECA, different loading conditions or combinations of them can be applied on the pipeline. In some cases, having different loading conditions and modelling them using FEA techniques to obtain the SIF, is a very

complicated task and needs a very high performance computer. By using the weight function developed and presented in Chapter 4, SIF for a longitudinal through thickness crack in a pipe under any loading condition can be calculated.

7.3 Contribution of this PhD

- A non standard step by step fracture toughness test using a modified CT specimen for steel material in very low temperature explained.
- A novel weight function to calculate stress intensity factor for longitudinal crack in a pipe has been presented.
- A novel FAD based engineering criticality assessment for CO_2 pipelines described and presented.
- Effect of induced low temperature due to gas expansion on SIF in front of longitudinal crack tip in a pipe using FEA techniques has been studied.
- Back face strain as an accurate crack length measurement during CT pre-cracking has been suggested.
- A new modified constant K specimen designed and verified using finite element techniques.

7.4 Recommendations for future works

Chapter 2 described the design of a novel constant K fracture toughness specimen (dimensions presented in Appendix D). A series of finite element analysis for different constant K geometries are modelled and the presented specimen has the most optimised dimensions to perform a constant K experiment. Also, by conducting this test the crack arrest temperature can be obtained. Understanding the effect of low temperatures on crack propagation and the SIF for pipeline material using the presented constant K specimen, are noted as areas for future work.

The weight function which has been developed in Chapter 4 can be expanded and more loading condition cases considered, such as: soil backfill compression stresses, thermal stresses due to welding and stresses due to misalignment pipe fitting.

In using FAD to assess the criticality of the pipeline, additional observations concerning the material's low temperature yield strength and implementing its effect in the calculations, were noted as areas for future work.

Stress corrosion cracking and K_{ISCC} which has been mentioned in the ECA of Chapter 5, need more research to investigate the effect of H_2S and water on the captured CO_2 composition, and on pipeline corrosion, which were not within the scope of this thesis but are noted as areas of future works.

References

(2000). Recommended Practice for Fitness-for-Service API RP 579, American Petroleum Institute.

(2005). Guide to methods for assessing the acceptability of flaws in metallic structure. BS 7910, BRITISH STANDARD.

Abaqus (2009). ABAQUS/CAE User's Manual Ver 6.9. USA, ABAQUS Inc.

Aihara, S. (2010). Question and answers. The First International Forum on Transportation of CO2 by Pipeline, Newcastle, UK.

API579 (2007). API Standard 579, Fitness For Service, American Petroleum Institute.

ASMEB31.8 (2012). GAS TRANSMISSION AND DISTRIBUTION PIPING SYSTEMS.

Aspelund, A., M. J. Mølnvik, et al. (2006). "Ship Transport of CO2: Technical Solutions and Analysis of Costs, Energy Utilization, Exergy Efficiency and CO2 Emissions." Chemical Engineering Research and Design 84(9): 847-855.

ASTM1290 (2002). Standard Test Methode for Crack-Tip Opening Displacement (CTOD) Fracture Toughness Measurement. E 1290-02.

ASTME8 (2009). Standard Test Methode for Tension Testing of Metallic Materials. E8/E8M-09.

ASTME399 (2009). Standard Test Method for Linear-Elastic Plane-Strain Fracture Toughness Ic of Metallic Materials, ASTM.

ASTME1290 (2002). Standard Test Methode for Crack-Tip Opening Displacement (CTOD) Fracture Toughness Measurement. E 1290-02.

ASTME1921 (2012). Standard Test Method for Determination of Reference Temperature, To, for Ferritic Steels in the Transition Range, ASTM.

Barnett, D. M. and R. J. Asaro (1972). "The fracture mechanics of slit-like cracks in anisotropic elastic media." Journal of the Mechanics and Physics of Solids 20(6): 353-366.

Bijan Kermani, John W. Martin, et al. (2006). Materials Design Strategy: Effects of H2S/CO2 Corrosion on Materials Selection. NACE International.

Brennan, F. P. (1994). "Evaluation of stress intensity factors by multiple reference state weight function approach." Theoretical and Applied Fracture Mechanics 20(3): 249-256.

Broek, D. (1986). Elementary Engineering Fracture Mechanics, Kluwer Academic Publishers.

Brown, W. and J. Srawley (1966). Plane Strain Crack Toughness Testing of High Strength Metallic Materials, ASTM STP 410.

Brown, W. and J. Srawley (1966). Plane strain crack toughness testing of high strength metallic materials, ASTM STP 410.

BS7448-1 (1991). Method for determination of KIC, critical CTOD and critical J values of metallic materials.

BS7910 (2012). Guide to methods for assessing the acceptability of flaws in metallic structures, British Standard.

Bueckner, H. F. (1970). "A Novel Principle for the Computation of Stress Intensity Factors." zeitschrift fur Angewandte Mathematik and mechanic 50: 529-546.

Campbell, F. C. (2012). Fatigue and Fracture, ASM international.

Caraballo, A. C., K. Patino, et al. (2011). Process and Structural Integrity Considerations During the Conversion of Pipelines to Transport “Captured” CO2. Offshore Pipeline Technology Conference. Amsterdam.

Chahardehi, A. (2011). "Structural Integrity of CO2 Transport Pipelines – A Review." Key Engineering Materials 488 - 489: 779-782.

Chahardehi, A. and F. P. Brennan (2010). "A novel weight function for RMS stress intensity factor determination in surface cracks." Engineering Fracture Mechanics 77(2): 367-373.

CO2SINK. (2008). "Taking greenhouse gases underground." from http://www.co2sink.org.

Cosham, A. and R. J. Eiber (2008). "Fracture propagation in CO2 pipelines." Journal of Pipeline Engineering 7(4): 281-292.

Demofonti, G., G. Mannucci, et al. (2007). Existing methods for the evaluation of material fracture resistance for high grade steel pipelines, EPRG.

Dowling, A. R. and C. H. A. Townley (1975). "The effect of defects on structural failure: A two-criteria approach." International Journal of Pressure Vessels and Piping 3(2): 77-107.

EGIG (2011). Gas Pipeline Incidents, 8th EGIG report, European Gas pipeline Incident data Group.

Erdogan, F. (1982). Theoritical and Experimental Study of Fracture in pipe-lines Containing Circumfrential Flaws. Washington DC.

Farris, C. B. (1983) "Unusual design factors for supercritical CO2 pipelines."

Folias, E. S. (1984). "An axial crack in a pressurized cylindrical shell." International Journal of Fracture 26(4): 251-260.

Gao, H., M. Abbudi, et al. (1992). "Interfacial crack-tip field in anisotropic elastic solids." Journal of the Mechanics and Physics of Solids 40(2): 393-416.

Gray, T. G. F. (1992). Handbook of Crack Opening Data, Abington Pub.

Gross, B. S., John E. (1964). "Stress-Intensity Factors for Single-Edge-Notch Specimens in Bending or Combined Bending and Tension by Boundary Collocation of a Stress Function." NASA CLEVELAND OH LEWIS RESEARCH CENTER.

Haigh, M. (2008) "Shell's World Energy Model."

Hara, T., Y. Shinohara, et al. (2008). DWTT properties for high strength line pipe steels.

Harris, D. O. (1967). "Stress Intensity Factors for Hollow Circumferentially Notched Round Bars." Journal of Basic Engineering 89(1): 49-54.

Harrison, R. P., K. Loosemore, et al. (1976). Assessment of the integrity of structures containing defects. Generating Board Report R/H/ R. UK, Central Electricity Generating Board.

Higuchi, R., H. Makino, et al. "New Concept and Test Method on Running Ductile Fracture Arrest for High Pressure Gas Pipeline."

Hillenbrand, H.-G., M. Gras, et al. (2001) "DEVELOPMENT AND PRODUCTION OF HIGH STRENGTH PIPELINE STEELS."

IEA (2008) "World energy outlook 2008."

IEA (2011) "World energy outlook 2011."

IEAGHG (2004) "Impact of Impurities on CO2 Capture, Transport and Storage."

IEAGHG. (2011). "IEA Greenhouse Gas R&D Programme." from http://www.ghgt.info/.

Inglis, C. E. (1913). "Stress in a plate due to the presence of cracks and sharp corners." Trans. Inst. Naval Architects 55: 219-241.

Instron (2011). Connecting Transducers (for Console V8 only). Reference Manual- Configuration. M21-14335-EN.

Instron (2011). Instron Reference Manual 8803.

Irwin, G. R. (1957). "Analysis of stresses and strains near the end of a crack traversing a plate." applied mechanics 24: 361–364.

Irwin, G. R. (1960). Plastic Zone Near A Crack and Fracture Toughness. 7th Sagamore Conf.

ISO12135 (2002). Metalic materials-Unified method of test for the determination of quasistatic fracture toughness.

ISO15156 (2009). Petroleum and natural gas industries - Materials for use in H2S-containing environments in oil and gas production, International Organization for standardization.

Kanninen, M. and C. Popelar (1985). Advanced fracture mechanics. New York, Oxford University Press.

Kyoto (1998) "KYOTO PROTOCOL TO THE UNITED NATIONS FRAMEWORK CONVENTION ON CLIMATE CHANGE."

Leis, B., R. J. Eiber, et al. (1998). Relationship between apparent (total) Charpy vee-notch toughness and the corresponding dynamic crack-propagation resistance. The 1998 International Pipeline Conference, IPC. . Calgary, Canada, ASME, FAIRFIELD, NJ, (USA). Part 2 (of 2),.

Lidbury, D. and P. Hirsch (2003). Methods for the assessment of structural integrity of components and structures, The institute of materials, minerals and mining.

Mahgerefteh, H. and O. Atti (2006). "Modeling low-temperature–induced failure of pressurized pipelines." AIChE Journal 52(3): 1248-1256.

Mahgerefteh, H., A. Oke, et al. (2006). "Modelling outflow following rupture in pipeline networks." Chemical Engineering Science 61(6): 1811-1818.

Mannucci, G., G. demofonti, et al. (2001). Fracture properties of API X100 gas pipeline steels.

MATTRAN. (2011). "Materials for Next Generation CO2 Transport Systems." from http://research.ncl.ac.uk/mattran/about.html (accessed Nov 2012).

MATTRAN. (2012). "Materials for Next Generation CO2 Transport Systems." from http://research.ncl.ac.uk/mattran/.

Maxey, W. A. and C. R. Barnes (1990). The chevron notched drop-weight-tear-test specimen: Medium: X; Size: Pages: (50 p).

Maxey, W. A., J. F. Kiefner, et al. (1976). Ductile fracture arrest in gas pipelines.

Misawa, K., Y. Imai, et al. (2010). "A New Model for Dynamic Crack Propagation and Arrest in Gas Pipelines." ASME Conference Proceedings 2010(44212): 685-694.

Mohitpour, M., H. Golshan, et al. (2007). Pipeline Design & Construction: A Practical Approach. NewYork, ASME Press.

Murakami, Y. (1987). Stress Intensity Factors Handbook, Pergamon Press.

Nippon. (2010). "Nippon Steel Corporation." from http://www.nsc.co.jp/en/index.html.

Niu, X. and G. Glinka (1989). "Stress-intensity factors for semi-elliptical surface cracks in welded joints." International Journal of Fracture 40(4): 255-270.

Niu, X. and G. Glinka (1990). Theoretical and Experimental Analyses of Surface Cracks in Weldments, In Surface Crack Growth Models. Experiments and Structures, ASTM STP1060, ASTM: 390-413.

Ojdrovic, R. P. and H. J. Petroski (1991). "Weight functions from multiple reference states and crack profile derivatives." Engineering Fracture Mechanics 39(1): 105-111.

P.N. Seevam, J. M. R., M.J.Downie (2009) "Theme A6: CO2 Transport Infrastructure Newcastle University."

Paris, P. C., H. Tada, et al. (2000). The Stress Analysis of Cracks Handbook, Professional Engineering Publication.

Petroski, H. J. and J. D. Achenbach (1978). "Computation of the weight function from a stress intensity factor." Engineering Fracture Mechanics 10(2): 257-266.

Priest, A. H. and B. Holmes (1981). "A multi-test piece approach to the fracture characterisation of linepipe steels." International Journal of Fracture 17(3): 277-299.

Priest, A. H. and B. Holmes (1988). The Characterisation of Crack Arrest Toughness in Gas Transmission Pipelines in Terms of the Shear Fracture Propagation Energy. Comm. Eur. Communities Rep., pp. 63,, British Steel.

Pussegoda, L. N. and L. Malik (1999). Interim Approach to Ductile Fracture Arrest Toughness–Progress. EPRG/PRCI 12th Joint Biennial Technical Meeting on Pipeline Research, Groningen, The Netherlands.

R6 (2005). R6 Assessment of the integrity of structures containing defects, EDF-British Energy.

Race, J. M., P. N. Seevam, et al. (2007). "Challenges for Offshore Transport of Anthropogenic Carbon Dioxide." ASME Conference Proceedings 2007(4269X): 589-602.

Rice, J. R. (1972). "Some Remarks on Elastic Crack Tip Stress Fields." International Journal of Solids and Structures 8: 751-758.

Riddell William, T. and S. Piascik Robert (1998). A Back Face Strain Compliance Expression for the Compact Tension Specimen, NASA Langley Technical Report Server.

Rooke, D. P. (1976). Compendium of stress intensity factors. Great Britain, Ministry of Defence. Procurement Executive.

Sanford, R. J. (2003). Principles of Fracture Mechanics. New Jercy, Pearson Education.

Seevam, P., J. Race, et al. (2010). Infrastructure and Pipeline Technology for Carbon Dioxide (CO2) Transport Developments and Innovation in Carbon Dioxide (CO2) Capture and Storage Technology, Woodhead Publishing Ltd. 1: 408-434.

Seevam, P., J. Race, et al. (2010). Capturing carbon dioxide: the feasibility of re-using existing pipeline infrastructure to transport CO2. Proceedings of the 8th International Pipeline Conference (IPC), American Society of Mechanical Engineers.

Seevam, P. N., J. M. Race, et al. (2009) "Theme A6: CO2 Transport Infrastructure Newcastle University." presentation.

Shih, C. F., B. Moran, et al. (1986). "Energy release rate along a three-dimensional crack front in a thermally stressed body." International Journal of Fracture 30(2): 79-102.

Sih, G. C. (1973). Handbook of stress-intensity factors, Lehigh University, Institute of Fracture and Solid Mechanics.

Staat, M. (2004). "Plastic collapse analysis of longitudinally flawed pipes and vessels."

Suo, Z. (1990). Singularities, Interfaces and Cracks in Dissimilar Anisotropic Media. Proceedings of the Royal Society of London. A. Mathematical and Physical Sciences, • London.

Tada, H., P. C. Paris, et al. (2000). The Stress Analysis of Cracks Handbook.

Teh, L. S. (2002). Library of Geometric Influences for Stress Intensity Factor Weight functions. London, University College London. PhD.

UKNG. (2010). "UK National Grid." from www.nationalgrid.com/uk/.

Vogt, G. and G. Junker (1994). Comparison of test results from Chevron and Weld Notch DWTT specimens with those from Pressed Notch specimens. 3 R INTERNATIONAL.

WBCSD. (2005). "Pathways to 2050, Energy & climate change." from http://www.wbcsd.org/web/publications/pathways.pdf (2005, accessed 08 Oct 2012).

Wilkowski, G., D. Rudland, et al. (2000). Recent Development On Determining Steady-State Dynamic Ductile Fracture Toughness From Impact Tests. Proceedings of 3rd International Pipeline Technology Conference, Brugge, Belgium.

Wilkowski, G. M. (1979). Fracture propagation toughness measurements.

Wilkowski, G. M., W. A. Maxey, et al. (1977). Use of a Brittle Notch DWTT Specimen to Predict Fracture Characteristics of Line Pipe Steels. ASME Energy Technology Conferance

Wilkowski, G. W. (1981). Studies on the precracked DWTT specimen to predict ductile fracture arrest. IV Seminar AGA-EPRG.

APPENDICES

Appendix A : 2D and 3D Crack Modelling FEA

The aim of this appendix is to describe how to analyse a crack in 2D and 3D specimens, a using finite element analysis (FEA) technique. For this purpose, ABAQUS, (an FEA commercial software) has been used. A parametric study to evaluate K at the crack tip, using different mesh configurations has been presented. This section has been written based on ABAQUS help files (Abaqus 2009).

An edge crack in a pure tension specimen in plane strain, subjected to mode I loading is considered (Figure A-1). The a/W or crack length to specimen width ratio is 0.2. The width of the specimen is 20mm and its length is 100mm. The loading is in the form of pure tension and applied to both ends of the specimen. The material is assumed to be linear elastic with Poisson's ratio of ϑ=0.3 and Young's modulus E=200 GPa.

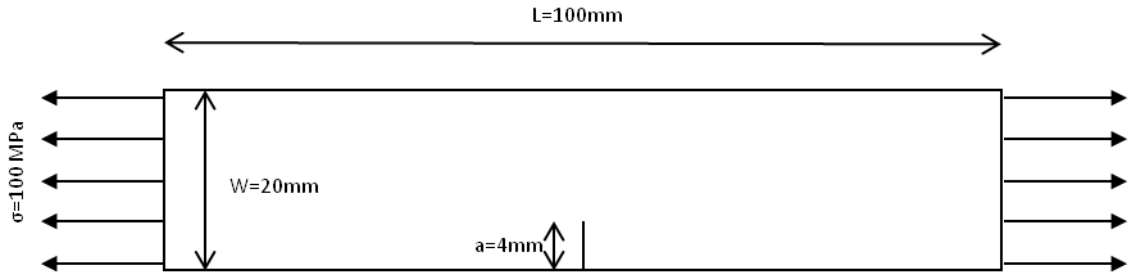

Figure A-1 Schematic of the 2D pure tension edge crack specimen

The instructions are as follows: after opening ABAQUS, create a model and double click on parts, from pop up menu (Figure A-2) select 2D planar. Next in sketch environment draw a rectangle using two points with coordinates of: (-50,0) and (50,20). Points can be created using the "Create Isolated Points" tool. Click ok and done. Now, using the "Partition Face: Sketch" tool sketch a

vertical line of length 4 mm. Use “Create lines: Connected” tool, and draw it in the centre-bottom side of the rectangle

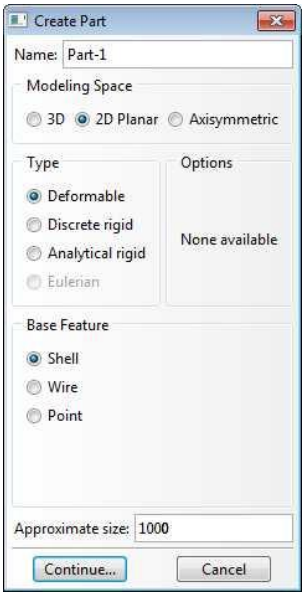

Figure A-2 Creating 2D part

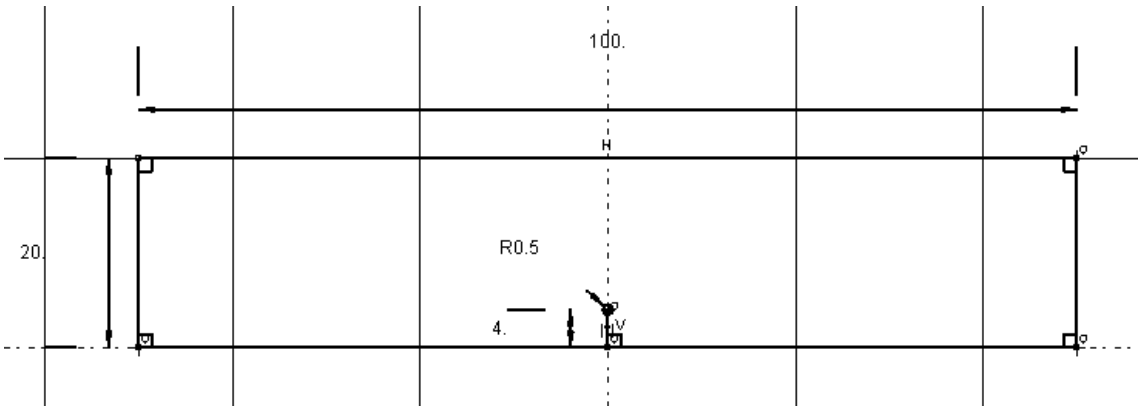

Figure A-3 Sketch of plate with edge crack

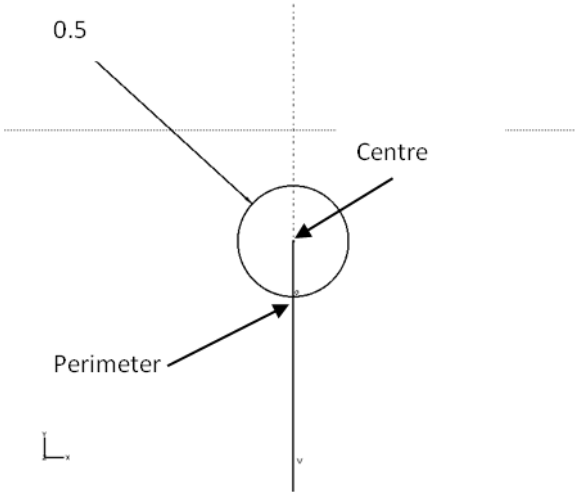

Figure A-4 Sketch of circle on crack tip

(Figure A-3). With “Edit Dimension Value” tool, the length of the line can be changed to any ideal length. Also sketch a circle of radius 0.5 mm centred at the crack tip (Figure A-4). The important point when using “Create Circle: Using centre and perimeter” tool is snapping the perimeter point to the vertical line (Crack), then it will be indicated by the small “o” at the intersection of the circle and line.

Create material by double clicking on the Materials icon and name it steel. From the menu select Mechanical>Elasticity>Elastic, and insert the assumed material properties (Figure A-5).

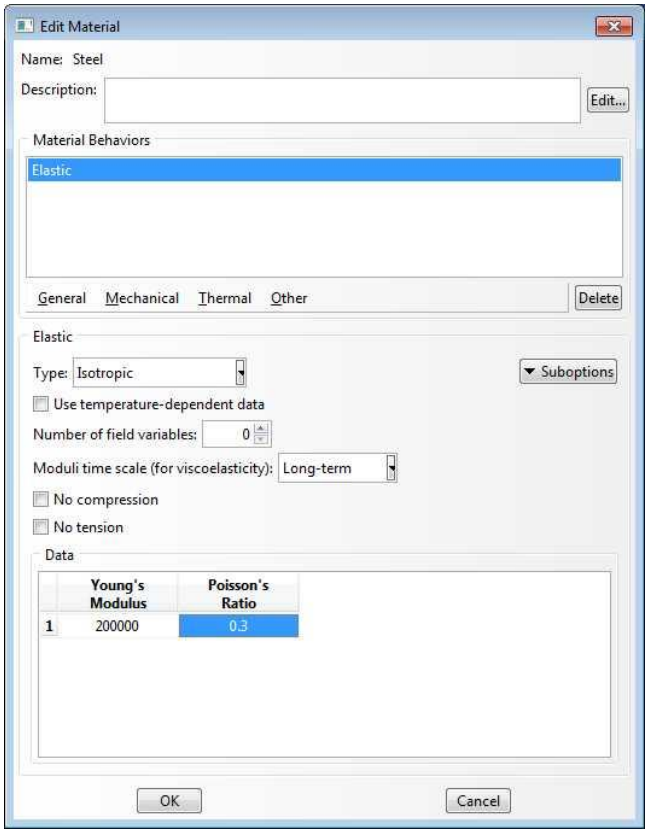

Figure A-5 Creating material and inserting material properties

Create a section>Solid>Homogeneous and assign it to steel material. As it is a two dimensional plate, it is possible to activate the “plane stress/strain thickness” option and put 1mm as thickness. Assign a section to the plate using the  “Assign section” tool. After selecting the plate and clicking ok, the colour of the plate should change to green.

Create and independent instance in the Assembly hierarchy. The crack tip singularity may only be specified for independent part instances.

To create the crack, double click cracks on the Assembly>Engineering Features container. In the “Create Crack” dialog box, select Contour integral and click continue. Select the vertex, shown in Figure A-6, as the crack front. Choose the q vectors method to define the crack extension direction.

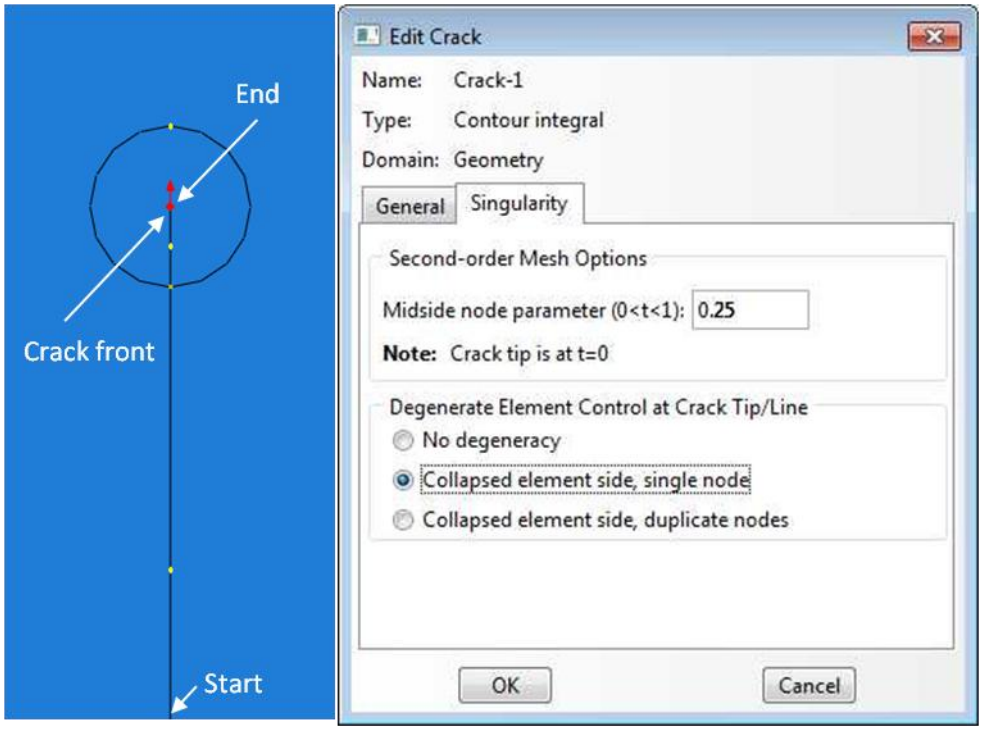

Figure A-6 Creating Crack using q vector method

As the start and end points of the vector, select the vertices highlighted in Figure A-6.

To introduce a square-root singularity at the crack tip, set the midside node parameter to 0.25 and choose Collapsed element side, single node as the element control from the Edit Crack>Singularity tab.

To define the crack seam, Special>Crack>Assign seam and select the entire length of the crack (Figure A-7).

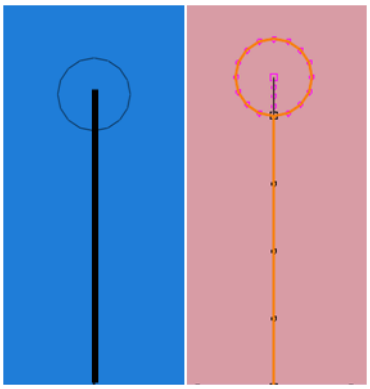

Figure A-7 Assign Seam to Crack

To mesh the model, expand Assembly>instances>plate-1>mesh and assign a global size of 1.0 to the part using (seed part instance). To assign local edge seeds to the circular region surrounding the crack tip, use (Seed edge: by number) and specify 16 elements along the circular edge. For the straight edge within the circular region, specify 4 elements (Figure A-7).

From Mesh>Controls in the menu or (Assign mesh control) tool, select swept mesh controls for the circular region through: Quad-dominated>Sweep. Assign the Quad element shape using the Medial axis algorithm to the rest of the part.

Assign mesh type using (Assign element type) to all regions as quadratic, reduced integration plane strain elements (CPE8R: An 8-node biquadratic plane strain quadrilateral, reduced integration).

Generate the mesh or Mesh>instance from the menu (Figure A-8)

Create a Step, Step>Initial>Static, General, and leave all other fields as default. To create a contour integral history output, double click on “History Output Request” in the model tree. In the dialog box, select contour integral as domain type, and choose the crack defined earlier as the domain. Set the number of contours to 5 and select Stress intensity factors as the output type. In order to do a parametric study in this step-by-step practice, repeat the above

steps and choose J-integral as the output type. To prevent confusion name the history outputs as SIF and J-Integral subsequently.

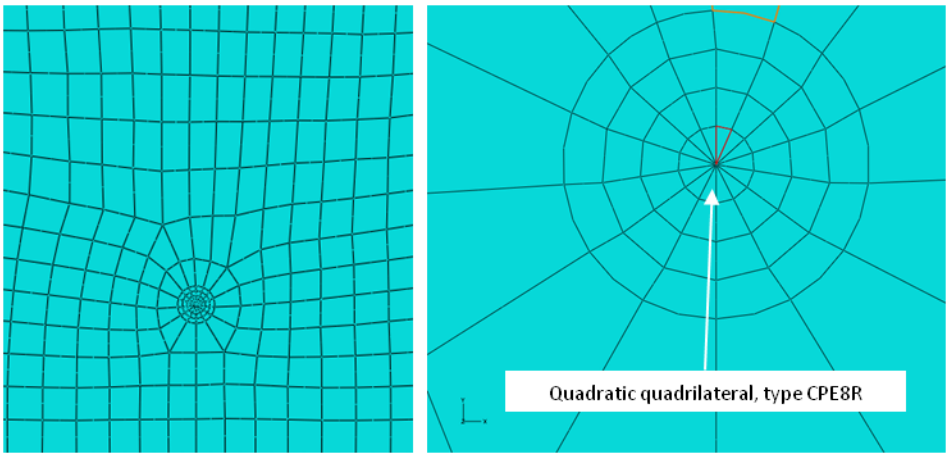

Figure A-8 Meshed plate

Create the load using: Loads>Step-1>Mechanical>Pressure and press continue. Select two edges on each side of the plate (shift + left click) and insert -100 as the magnitude of the load. The negative sign means the plate is in tension.

Create a job, name it and submit it. Right click on the job and click Results. To see the contours on the deformed shape click on:  . The results should look like Figure A-9.

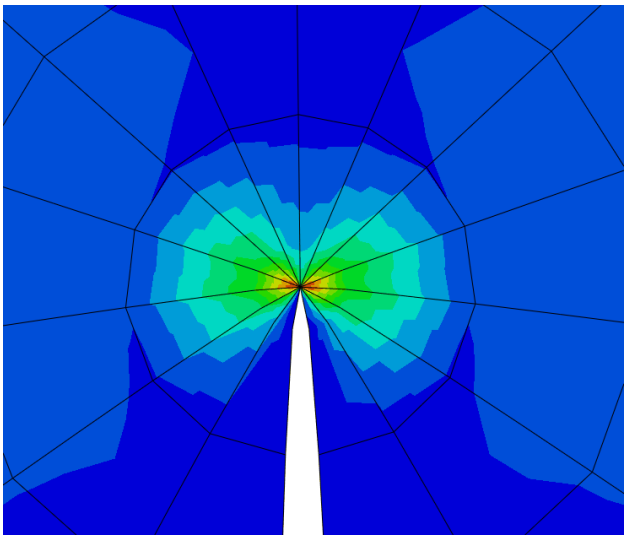

Figure A-9 Crack tip Von- Mises stress distribution

As can be seen in Figure A-9, the stress state is highly localized in the vicinity of the crack tip, and it can be predicted that the magnitude of longitudinal state of stress (along the load direction) is roughly the same as the load, except in the vicinity of the crack tip (which is maximum) and both sides of the seam (which are minimums) (Figure A-10).

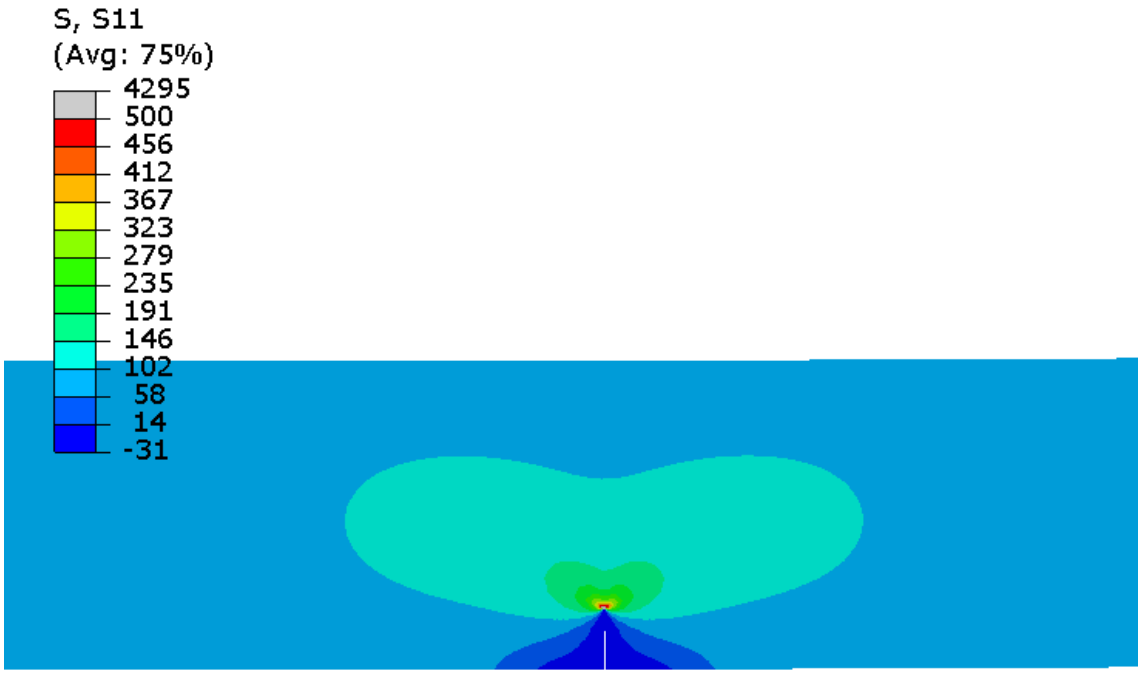

Figure A-10 Longitudinal stress distribution

On the result tab, click on each of the History outputs, then select all KI and/or J-integrals and right click>add to plot. As is seen in Figure A-11 the values of J-Integral have converged and exhibit path independence criteria. It can be observed that the values of J and K for each contour have slight discrepancies. Common practice suggests that to prevent adverse numerical effects due to singularity from influencing the interpretation of the results, the first and second contour values should be neglected. So, in this case, select values of KI for contours 3-5 and average them. To average the values, right click on selected values and select save as>average>ok.

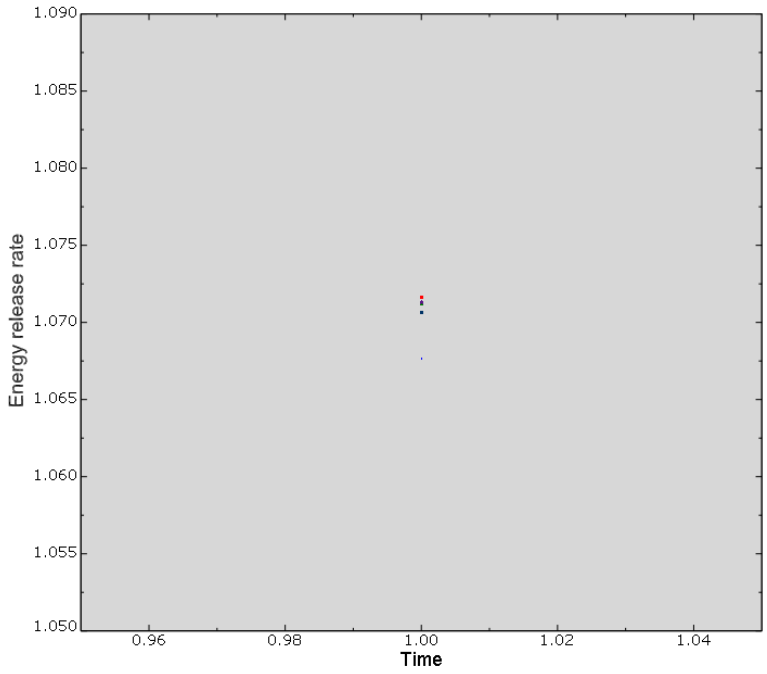

Figure A-11 J-Integral Results (path independence)

To have a parametric study, create a copy of the model and change the crack definition to “collapsed element side, duplicate nodes” by double clicking on cracks in assembly. In this case each crack tip element has the freedom to possess independent crack tip nodes. Create a new job, name it and evaluate the results and enter the average value in Table A-1.

Do this similarly for a “Midside node parameter” of 0.5 and enter the results in the Table. As has been described in this appendix, using a circle and defining the sweep mesh around the crack tip offers a fine focused mesh and shows excellent agreement with the theoretical results. When converting the KI unit to MPam^0.5, the results can be observed even closer. When the meshes are coarse (if they do not define a circle around the crack tip) and no degeneracy has been defined, the results deviate from theory due to the presence of crack tip singularity.

By including singularity in the mesh, the overall accuracy of the near tip stress and strain fields is enhanced. In addition, the singularity is necessary to achieve mesh convergence of the stress and deformation fields.

Theoretical result

From Tada, Paris and Irwin “The Stress Analysis of Cracks Handbook” the theoretical result is (Paris, Tada et al. 2000):

For

$\frac{a}{b} \leq 0.6 and\ accuracy\ of\ 5\%$ and W=b

$$K_I = \sigma\sqrt{\pi a}\, F(\frac{a}{b})$$

$$F\left(\frac{a}{b}\right) = 1.122 - 0.231\left(\frac{a}{b}\right) + 10.550(\frac{a}{b})^2 - 21.710(\frac{a}{b})^3 + 30.382(\frac{a}{b})^4$$

Based on Least squares fitting (Gross, 1964; Brown, 1966)

As can be observed, the accuracy of results are about 0.3%.

Analysis case			KI (MPamm^0.5)	KI (MPam^0.5)
Theoretical			486.61	15.39
Element Type	Midside node parameter	Crack tip: single or duplicated nodes		
CPE8R	0.25	Single node	484.93	15.33
CPE8R	0.5	Single node	484.28	15.31
CPE8R	0.25	Duplicate node	484.93	15.33
CPE8R	0.5	Duplicate node	485.43	15.35
CPS8R	0.25	Single node	484.93	15.33

Table A-1 KI values for parametric study

For 3D crack modelling, all the above-mentioned step-by-step procedures are similar. After creating a crack line and the circle, use Extrude tool  to extrude the line and circle along the thickness of the specimen. When introducing the crack front, select the extruded line as crack tip.

Appendix B : Longitudinal Crack in CO_2 Pipe Failure Assessment Diagram

Analysis of a CO_2 pipe with axial crack with R-code

```
BEBEBEBEBEBEBEBEBEBEBEBEBEBEBE757C9960BEBEBEBEBEBEBEBEBEBEBEBEBEBEBEBE
BE                                                                  BE
BE                                                                  BE
BE                                                                  BE
BE        Published in the United Kingdom by:                       BE
BE             EDF Energy Nuclear Generation Ltd.,                  BE
BE             Barnett Way, Barnwood, Gloucester GL4 3RS.           BE
BE                                                                  BE
BE        All rights reserved. No part of this publication          BE
BE        may be reproduced or transmitted in any form or by        BE
BE        any means, including photocopying and recording,          BE
BE        without the written permission of the copyright           BE
BE        holder, application for which should be addressed         BE
BE        to the publisher. Such written permission must also       BE
BE        be obtained before any part of this publication is        BE
BE        stored in a retrieval system of any nature.               BE
BE                                                                  BE
BE        Copyright EDF Energy Nuclear Generation Ltd.2010          BE
BE                                                                  BE
BE                                                                  BE
BE                                                                  BE
BEBEBEBEBEBEBEBEBEBEBEBEBEBEBE1971100000BEBEBEBEBEBEBEBEBEBEBEBEBEBEBE

             ************************************************
             *                                              *
             *             FRACTURE.THREE(LEVEL 1)          *
             *            ************************          *
             *            ************************          *
             *               R-Code Version 4.4             *
             *          Program Updated 21/04/2010          *
             *                                              *
             *            15:22:45    07/03/2013            *
             *                                              *
             ************************************************
                      ++++++++++++++++++++++
                      + Reading Input Data +
                      ++++++++++++++++++++++


     *******  Reading PREP Records

Job  15-24-12-10-LC-Amb

     *******  Reading GEOM Records

------------
 Geometry  1 - 24
------------

Geometry Code 301
Axial Through-thickness Crack In Cylinder
Subject To User-defined Loading
Section Width (mm)               1.200000E+01
Mean Radius (mm)                 2.988000E+02
```

```
Out-of-plane thickness 1.0000000E+00
At crack tip position  1 (Mid-wall):
SIF=  Property  4 - Stress intensity for geometry   1
K will be calculated using the
built-in SIF for the geometry
At crack tip position  2 (Inner surface):
SIF=  Property  5 - Stress intensity for geometry   1
K will be calculated using the
built-in SIF for the geometry
At crack tip position  3 (Outer surface):
SIF=  Property  6 - Stress intensity for geometry   1
K will be calculated using the
built-in SIF for the geometry

     *******  Reading LOAD Records

------------
 Load   1 - load-1
------------

Load type is Pressure

 by indirect value

Pressure      value is  1.500000E+01

     *******  Reading MATS Records

------------
 Material  1 - API 5L-X100
------------

The Failure Assessment Diagram is R6 Rev 4 Option 1, general
Minimum yield stress (MPa)              6.0000000E+02
Mean yield stress (MPa)                 6.9000000E+02
Mean ultimate stress (MPa)              7.7000000E+02
Young's Modulus (MPa)                   2.0000000E+05
Poisson's Ratio                         3.0000001E-01
Initiation Fracture Toughness (MPa/m)   1.3000000E+02
No J Resistance data given

No constraint effect curve data.


     *******  Reading PLAS Records

------------
 Collapse  1 - plas-1
------------

Equation Name  R6191A
Lr is based on a calculated Pressure      stress
Lr defined at position 1 by  Library Collapse solution
Lr defined at position 2 by  Library Collapse solution
Lr defined at position 3 by  Library Collapse solution

     *******  Reading ASSM Records

------------
 Assessment  1 - CO2-15MPa-130MPam^0.5
------------

Step represents a limiting crack size   analysis
analysed at at position three
by varying crack size with constant offset (if relevant)
```

```
     Load Block    1 -
     Contains the following loads:

     Variable Primary   load with factor  1.200000E+00
     Load   1 - load-1


     Stresses will not be linearised
     Rho will be evaluated using the simplified procedure of R6 Section II.6.3
     After the assessment,critical state will become the current state.
     Geometry  1 - 24
     Collapse  1 - plas-1
     Probability output is not required

          *******  Reading PROB Records

     ------------
      Problem  1 - P-15-24-12-10-LC-Amb
     ------------

     Default Material    1
     Material  1 - API 5L-X100
     Default Geometry    1
     Geometry  1 - 24
     Initial State
     State  1 Crack length 1.00E-02 Offset 0.00E+00 Load Factor 1.20E+00
     Yield stress is evaluated at crack tip
     Assessment Steps:
     Assessment  1 - CO2-15MPa-130MPam^0.5
     Repeated    1 times
     as an initiation analysis

     Crack opening/ fluid flow calculation requested
      using primary loads only
     Gas flow using CO2      temperature:
      3.5000000E+01
     Friction trough flag is    T
     Using     elastic     crack opening areas
     User gas flag is F
     Inlet pressure       =  15.000 Mpa
     Exit  pressure       =   0.100 Mpa
     Roughness            =   0.025 mm
     Crack face multiplier= 1.000
 ++++++++++++++++++++++++++++++++++++
 + Checking and Linking Input Objects +
 ++++++++++++++++++++++++++++++++++++



        ---------------------------------------
         Job is  15-24-12-10-LC-Amb
        ---------------------------------------


         Date      -     07-03-2013
         Time      -     15:22:45
         Program   -   R6-CODE Version 4.4
         System Database Version 4.4001
         Machine   -     IBMPC
-------------------------------------------------
- Input data has been checked and was acceptable. -
-------------------------------------------------

 ++++++++++++++++++++++++++++++++++++++++++++++++
 +  +==+ Problem  1 - P-15-24-12-10-LC-Amb +==+  +
```

```
++++++++++++++++++++++++++++++++++++++++++++++++++

++++++++++++++++++++++++++++++++++++++++++++++++++++++
+  +==+ Assessment  1 - CO2-15MPa-130MPam^0.5 +==+  +
++++++++++++++++++++++++++++++++++++++++++++++++++++++


    ................
      Table of Loads
    ................

    Load Block    1 -
    Contains the following loads:
    Variable Primary   load with factor  1.200000E+00
    Load   1 - load-1


       --- X (m) ---   -Stress (MPa)-
       -6.000000E-03    3.660000E+02
       -4.800000E-03    3.660000E+02
       -3.600000E-03    3.660000E+02
       -2.400000E-03    3.660000E+02
       -1.200000E-03    3.660000E+02
        0.000000E+00    3.660000E+02
        1.200000E-03    3.660000E+02
        2.400000E-03    3.660000E+02
        3.600000E-03    3.660000E+02
        4.800000E-03    3.660000E+02
        6.000000E-03    3.660000E+02



       R6 Revision 4 initiation analysis
       ---------------------------------
       The defect is analysed at external


The roughness must be < inlet width/5.
the actual values are  2.54000E+01 um 3.15786E-02 mm

The roughness must be < inlet width/5.
the actual values are  2.54000E+01 um 3.49826E-02 mm

The roughness must be < inlet width/5.
the actual values are  2.54000E+01 um 3.84290E-02 mm

The roughness must be < inlet width/5.
the actual values are  2.54000E+01 um 4.19176E-02 mm

The roughness must be < inlet width/5.
the actual values are  2.54000E+01 um 4.54485E-02 mm

The roughness must be < inlet width/5.
the actual values are  2.54000E+01 um 4.90217E-02 mm

The roughness must be < inlet width/5.
the actual values are  2.54000E+01 um 5.26372E-02 mm

The roughness must be < inlet width/5.
the actual values are  2.54000E+01 um 5.62950E-02 mm

The roughness must be < inlet width/5.
the actual values are  2.54000E+01 um 5.99950E-02 mm

The roughness must be < inlet width/5.
```

```
the actual values are  2.54000E+01 um 6.37374E-02 mm

The roughness must be < inlet width/5.
the actual values are  2.54000E+01 um 6.75220E-02 mm

The wall thickness/inlet width must be > 23.
but the values are  1.20000E+01 6.94953E-01 mm

The wall thickness/inlet width must be > 23.
but the values are  1.20000E+01 1.35812E+00 mm

The wall thickness/inlet width must be > 23.
but the values are  1.20000E+01 2.41750E+00 mm

The wall thickness/inlet width must be > 23.
but the values are  1.20000E+01 3.92923E+00 mm

The wall thickness/inlet width must be > 23.
but the values are  1.20000E+01 5.95235E+00 mm

The wall thickness/inlet width must be > 23.
but the values are  1.20000E+01 8.61976E+00 mm

The wall thickness/inlet width must be > 23.
but the values are  1.20000E+01 1.20178E+01 mm

The wall thickness/inlet width must be > 23.
but the values are  1.20000E+01 1.61531E+01 mm

The wall thickness/inlet width must be > 23.
but the values are  1.20000E+01 2.09840E+01 mm
 ++++++++++++++++++++++++++++++++++++++++++++++++++++++++++++++++++++++
 + Iteration   1 of Step   1 of problem   1 completed                +
 ++++++++++++++++++++++++++++++++++++++++++++++++++++++++++++++++++++++


  Table layout files are chosen from directories ". (current)",
       "" or  "C:\Program Files (x86)\British Energy\RCodev4.4\layouts"

 Tables were built using layout files:-

     Table A  - C:\Program Files (x86)\British
Energy\RCodev4.4\layouts\bcd6.lay
     Table B  - C:\Program Files (x86)\British
Energy\RCodev4.4\layouts\pcd6.lay
     Table C  - C:\Program Files (x86)\British
Energy\RCodev4.4\layouts\scd6.lay
     Table D  -
 C:\Program Files (x86)\British Energy\RCodev4.4\layouts\fat6b.lay
     Table E  - C:\Program Files (x86)\British
Energy\RCodev4.4\layouts\tcd6.lay
     Table F  - C:\Program Files (x86)\British
Energy\RCodev4.4\layouts\faa.lay
     Table G  -
 C:\Program Files (x86)\British Energy\RCodev4.4\layouts\r6fatr6.lay
     Table H  - C:\Program Files (x86)\British
Energy\RCodev4.4\layouts\user.lay
     Table I  -
 C:\Program Files (x86)\British Energy\RCodev4.4\layouts\r6cod1.lay
     Table M  -
 C:\Program Files (x86)\British Energy\RCodev4.4\layouts\r6cod2.lay
     Table N  -
 C:\Program Files (x86)\British Energy\RCodev4.4\layouts\r6cod3.lay
     Table O  -
 C:\Program Files (x86)\British Energy\RCodev4.4\layouts\r6cod4.lay
```

Table P -
C:\Program Files (x86)\British Energy\RCodev4.4\layouts\r6proby.lay

The default tabular preview file loaded is:-

C:\Program Files (x86)\British Energy\RCodev4.4\layouts\IGNORE

In the following tables:
Crk Tip 1 refers to midpoint
Crk Tip 2 refers to internal
Crk Tip 3 refers to external

Table A - Preliminary Data

Crk Tip	Crack Length (mm)	Res. Tough (MPa/~m)	Load Factor	Crack Status	Warn/ Err#
3	10.000	130.0	1.20	Minimum	None
3	11.005	130.0	1.20	Stable	None
3	12.009	130.0	1.20	Stable	None
3	13.014	130.0	1.20	Stable	None
3	14.018	130.0	1.20	Stable	None
3	15.023	130.0	1.20	Stable	None
3	16.028	130.0	1.20	Stable	None
3	17.032	130.0	1.20	Stable	None
3	18.037	130.0	1.20	Stable	None
3	19.041	130.0	1.20	Stable	None
3	20.046	130.0	1.20	Initiation	None
3	70.736	130.0	1.20	Failed	None
3	121.425	130.0	1.20	Failed	None
3	172.115	130.0	1.20	Failed	None
3	222.805	130.0	1.20	Failed	None
3	273.494	130.0	1.20	Failed	None
3	324.184	130.0	1.20	Failed	None
3	374.874	130.0	1.20	Failed	None
3	425.564	130.0	1.20	Failed	None
3	476.253	130.0	1.20	Failed	None
3	526.943	130.0	1.20	Maximum	None

Table B - Primary Loadings

Crk Tip	Crack Length (mm)	SIF (Var. Pri.) (MPa/~m)	Kr (Var. Pri.)	Lr (Var. Pri.)	Crack Status
3	10.000	68.24	0.525	0.780	Minimum
3	11.005	72.02	0.554	0.781	Stable
3	12.009	75.70	0.582	0.781	Stable
3	13.014	79.28	0.610	0.782	Stable
3	14.018	82.78	0.637	0.783	Stable
3	15.023	86.21	0.663	0.784	Stable
3	16.028	89.58	0.689	0.786	Stable

3	17.032	92.90	0.715	0.787	Stable
3	18.037	96.17	0.740	0.788	Stable
3	19.041	99.40	0.765	0.789	Stable
3	20.046	102.60	0.789	0.791	Initiation
3	70.736	252.68	1.944	0.942	Failed
3	121.425	411.10	3.162	1.200	Failed
3	172.115	581.35	4.472	1.510	Failed
3	222.805	760.13	5.847	1.845	Failed
3	273.494	944.66	7.267	2.193	Failed
3	324.184	1133.11	8.716	2.547	Failed
3	374.874	1324.25	10.187	2.905	Failed
3	425.564	1517.22	11.671	3.265	Failed
3	476.253	1711.24	13.163	3.626	Failed
3	526.943	1905.39	14.657	3.986	Maximum

Table E - Totals

Crk Tip	Crack Length (mm)	Res. Tough (MPa/~m)	Total SIF (MPa/~m)	Rho	Kr R6	Lr R6	Load Factor	Crack Status
3	10.000	130.0	68.24	0.000	0.525	0.780	1.20	Minimum
3	11.005	130.0	72.02	0.000	0.554	0.781	1.20	Stable
3	12.009	130.0	75.70	0.000	0.582	0.781	1.20	Stable
3	13.014	130.0	79.28	0.000	0.610	0.782	1.20	Stable
3	14.018	130.0	82.78	0.000	0.637	0.783	1.20	Stable
3	15.023	130.0	86.21	0.000	0.663	0.784	1.20	Stable
3	16.028	130.0	89.58	0.000	0.689	0.786	1.20	Stable
3	17.032	130.0	92.90	0.000	0.715	0.787	1.20	Stable
3	18.037	130.0	96.17	0.000	0.740	0.788	1.20	Stable
3	19.041	130.0	99.40	0.000	0.765	0.789	1.20	Stable
3	20.046	130.0	102.6	0.000	0.789	0.791	1.20	Initiation
3	70.736	130.0	252.7	0.000	1.944	0.942	1.20	Failed
3	121.425	130.0	411.1	0.000	3.162	1.200	1.20	Failed
3	172.115	130.0	581.4	0.000	4.472	1.510	1.20	Failed
3	222.805	130.0	760.1	0.000	5.847	1.845	1.20	Failed
3	273.494	130.0	944.7	0.000	7.267	2.193	1.20	Failed
3	324.184	130.0	1133.	0.000	8.716	2.547	1.20	Failed
3	374.874	130.0	1324.	0.000	10.187	2.905	1.20	Failed
3	425.564	130.0	1517.	0.000	11.671	3.265	1.20	Failed
3	476.253	130.0	1711.	0.000	13.163	3.626	1.20	Failed
3	526.943	130.0	1905.	0.000	14.657	3.986	1.20	Maximum

I. Crack Opening and Gas Flow Information at R6 Load

Crack Length (mm)	COD Inner Wall (mm)	COD Outer Wall (mm)	COA Inner Wall (mm^2)	COA Outer Wall (mm^2)	Mass Flow Rate (Min) (kg/sec)	Vol Flow Rate (STP Min) (m^3/s)	Warn Err

```
 10.0000 4.928E-002 5.940E-002 3.158E-001 3.461E-001 -1.000E+000 -5.091E-001
#4
 11.0046 5.427E-002 6.545E-002 3.850E-001 4.235E-001 -1.000E+000 -5.091E-001
#4
 12.0092 5.928E-002 7.152E-002 4.615E-001 5.096E-001 -1.000E+000 -5.091E-001
#4
 13.0138 6.431E-002 7.762E-002 5.455E-001 6.046E-001 -1.000E+000 -5.091E-001
#4
 14.0184 6.935E-002 8.375E-002 6.371E-001 7.087E-001 -1.000E+000 -5.091E-001
#4
 15.0230 7.441E-002 8.990E-002 7.365E-001 8.221E-001 -1.000E+000 -5.091E-001
#4
 16.0276 7.948E-002 9.608E-002 8.436E-001 9.450E-001 -1.000E+000 -5.091E-001
#4
 17.0322 8.457E-002 1.023E-001 9.588E-001 1.078E+000 -1.000E+000 -5.091E-001
#4
 18.0368 8.969E-002 1.086E-001 1.082E+000 1.220E+000 -1.000E+000 -5.091E-001
#4
 19.0415 9.483E-002 1.149E-001 1.214E+000 1.373E+000 -1.000E+000 -5.091E-001
#4

 20.0461 9.999E-002 1.212E-001 1.354E+000 1.537E+000 -1.000E+000 -5.091E-001
#4
 70.7357 4.175E-001 5.408E-001 2.209E+001 2.823E+001 5.058E-001  2.575E-001
121.4254 9.603E-001 1.333E+000 8.438E+001 1.145E+002 -1.000E+000 -5.091E-001
#3
172.1151 1.934E+000 2.717E+000 2.338E+002 3.199E+002 -1.000E+000 -5.091E-001
#3
222.8048 3.523E+000 4.877E+000 5.386E+002 7.244E+002 -1.000E+000 -5.091E-001
#3
273.4945 5.882E+000 7.966E+000 1.075E+003 1.415E+003 -1.000E+000 -5.091E-001
#3
324.1842 9.144E+000 1.211E+001 1.930E+003 2.491E+003 -1.000E+000 -5.091E-001
#3
374.8739 1.344E+001 1.743E+001 3.231E+003 4.087E+003 -1.000E+000 -5.091E-001
#3
425.5636 1.890E+001 2.404E+001 5.114E+003 6.345E+003 -1.000E+000 -5.091E-001
#3
476.2533 2.560E+001 3.203E+001 7.693E+003 9.385E+003 -1.000E+000 -5.091E-001
#3

526.9430 3.358E+001 4.142E+001 1.106E+004 1.330E+004 -1.000E+000 -5.091E-001
#3

Warnings/Errors #1 Inner COD < 6um
                #2 Inner COD > length/10
                #3 Wall thickness/inner COD < 23
                #4 Roughness > inner COD/5
                #5 Water temp outside range 0 to 100 degC

For more information and detailed values see the messages before these tables


          M. Additional Crack Opening and Gas Flow Information
          ---------------------------------------------------


 Crack     Suth.     Viscosity  Viscosity    Density   Density     Letter
Letter
 Length    Const.       (STP)    (Working)    (STP)    (Working)     Box
Box
   (mm)                (Pas.s)    (Pas.s)   (kg/m^3)   (kg/m^3)      COD
COD
```

								Inner	Outer
								(mm)	(mm)
10.0000	-1.000E+000	1.360E-005	1.493E-005	1.964E+000	1.000E+000	3.158E-002	3.461E-002		
11.0046	-1.000E+000	1.360E-005	1.493E-005	1.964E+000	1.000E+000	3.498E-002	3.849E-002		
12.0092	-1.000E+000	1.360E-005	1.493E-005	1.964E+000	1.000E+000	3.843E-002	4.244E-002		
13.0138	-1.000E+000	1.360E-005	1.493E-005	1.964E+000	1.000E+000	4.192E-002	4.646E-002		
14.0184	-1.000E+000	1.360E-005	1.493E-005	1.964E+000	1.000E+000	4.545E-002	5.055E-002		
15.0230	-1.000E+000	1.360E-005	1.493E-005	1.964E+000	1.000E+000	4.902E-002	5.472E-002		
16.0276	-1.000E+000	1.360E-005	1.493E-005	1.964E+000	1.000E+000	5.264E-002	5.896E-002		
17.0322	-1.000E+000	1.360E-005	1.493E-005	1.964E+000	1.000E+000	5.630E-002	6.328E-002		
18.0368	-1.000E+000	1.360E-005	1.493E-005	1.964E+000	1.000E+000	5.999E-002	6.766E-002		
19.0415	-1.000E+000	1.360E-005	1.493E-005	1.964E+000	1.000E+000	6.374E-002	7.212E-002		
20.0461	-1.000E+000	1.360E-005	1.493E-005	1.964E+000	1.000E+000	6.752E-002	7.665E-002		
70.7357	1.090E+002	1.360E-005	1.493E-005	1.964E+000	2.578E+002	3.123E-001	3.990E-001		
121.4254	-1.000E+000	1.360E-005	1.493E-005	1.964E+000	1.000E+000	6.950E-001	9.432E-001		
172.1151	-1.000E+000	1.360E-005	1.493E-005	1.964E+000	1.000E+000	1.358E+000	1.858E+000		
222.8048	-1.000E+000	1.360E-005	1.493E-005	1.964E+000	1.000E+000	2.418E+000	3.251E+000		
273.4945	-1.000E+000	1.360E-005	1.493E-005	1.964E+000	1.000E+000	3.929E+000	5.175E+000		
324.1842	-1.000E+000	1.360E-005	1.493E-005	1.964E+000	1.000E+000	5.952E+000	7.685E+000		
374.8739	-1.000E+000	1.360E-005	1.493E-005	1.964E+000	1.000E+000	8.620E+000	1.090E+001		
425.5636	-1.000E+000	1.360E-005	1.493E-005	1.964E+000	1.000E+000	1.202E+001	1.491E+001		
476.2533	-1.000E+000	1.360E-005	1.493E-005	1.964E+000	1.000E+000	1.615E+001	1.971E+001		
526.9430	-1.000E+000	1.360E-005	1.493E-005	1.964E+000	1.000E+000	2.098E+001	2.524E+001		

N. Minimum Gas Flow Parameters at R6 Load

Crack Length (mm)	Reyn. No. (Min)	Mach In (Min)	Mach Exit (Min)	Mass Flow Rate (Min) (kg/sec)	Vol Flow Rate (STP Min) (m^3/s)	Vol Flow Rate (Up Min) (m^3/s)	R(ough) C(hok) T(urb) S(mooth) U(nch) L(am) (Min) (Min) (Min)

```
 10.0000 -1.000E+000 -1.000E+000 -1.000E+000 -1.000E+000 -5.091E-001 -
1.000E+000 R        U      T
 11.0046 -1.000E+000 -1.000E+000 -1.000E+000 -1.000E+000 -5.091E-001 -
1.000E+000 R        U      T
 12.0092 -1.000E+000 -1.000E+000 -1.000E+000 -1.000E+000 -5.091E-001 -
1.000E+000 R        U      T
 13.0138 -1.000E+000 -1.000E+000 -1.000E+000 -1.000E+000 -5.091E-001 -
1.000E+000 R        U      T
 14.0184 -1.000E+000 -1.000E+000 -1.000E+000 -1.000E+000 -5.091E-001 -
1.000E+000 R        U      T
 15.0230 -1.000E+000 -1.000E+000 -1.000E+000 -1.000E+000 -5.091E-001 -
1.000E+000 R        U      T
 16.0276 -1.000E+000 -1.000E+000 -1.000E+000 -1.000E+000 -5.091E-001 -
1.000E+000 R        U      T
 17.0322 -1.000E+000 -1.000E+000 -1.000E+000 -1.000E+000 -5.091E-001 -
1.000E+000 R        U      T
 18.0368 -1.000E+000 -1.000E+000 -1.000E+000 -1.000E+000 -5.091E-001 -
1.000E+000 R        U      T
 19.0415 -1.000E+000 -1.000E+000 -1.000E+000 -1.000E+000 -5.091E-001 -
1.000E+000 R        U      T

 20.0461 -1.000E+000 -1.000E+000 -1.000E+000 -1.000E+000 -5.091E-001 -
1.000E+000 R        U      T
 70.7357 9.579E+005  4.160E-001  1.000E+000  5.058E-001  2.575E-001  1.962E-
003  R        C      T
121.4254 -1.000E+000 -1.000E+000 -1.000E+000 -1.000E+000 -5.091E-001 -
1.000E+000 R        U      T
172.1151 -1.000E+000 -1.000E+000 -1.000E+000 -1.000E+000 -5.091E-001 -
1.000E+000 R        U      T
222.8048 -1.000E+000 -1.000E+000 -1.000E+000 -1.000E+000 -5.091E-001 -
1.000E+000 R        U      T
273.4945 -1.000E+000 -1.000E+000 -1.000E+000 -1.000E+000 -5.091E-001 -
1.000E+000 R        U      T
324.1842 -1.000E+000 -1.000E+000 -1.000E+000 -1.000E+000 -5.091E-001 -
1.000E+000 R        U      T
374.8739 -1.000E+000 -1.000E+000 -1.000E+000 -1.000E+000 -5.091E-001 -
1.000E+000 R        U      T
425.5636 -1.000E+000 -1.000E+000 -1.000E+000 -1.000E+000 -5.091E-001 -
1.000E+000 R        U      T
476.2533 -1.000E+000 -1.000E+000 -1.000E+000 -1.000E+000 -5.091E-001 -
1.000E+000 R        U      T

526.9430 -1.000E+000 -1.000E+000 -1.000E+000 -1.000E+000 -5.091E-001 -
1.000E+000 R        U      T
```

O. Maximum Gas Flow Parameters at R6 Load

```
 Crack      Reyn.         Mach         Mach       Mass Flow    Vol Flow     Vol Flow
R(ough)  C(hok) T(urb)
 Length       No.           In          Exit         Rate         Rate         Rate
S(mooth) U(nch) L(am)
   (mm)       (Max)        (Max)        (Max)        (Max)      (STP Max)     (Up Max)
(Max)     (Max)   (Max)
                                                    (kg/sec)      (m^3/s)      (m^3/s)

 10.0000 -1.000E+000 -1.000E+000 -1.000E+000 -1.000E+000 -5.091E-001 -
1.000E+000 R        U      T
 11.0046 -1.000E+000 -1.000E+000 -1.000E+000 -1.000E+000 -5.091E-001 -
1.000E+000 R        U      T
```

```
 12.0092 -1.000E+000 -1.000E+000 -1.000E+000 -1.000E+000 -5.091E-001 -
1.000E+000 R        U      T
 13.0138 -1.000E+000 -1.000E+000 -1.000E+000 -1.000E+000 -5.091E-001 -
1.000E+000 R        U      T
 14.0184 -1.000E+000 -1.000E+000 -1.000E+000 -1.000E+000 -5.091E-001 -
1.000E+000 R        U      T
 15.0230 -1.000E+000 -1.000E+000 -1.000E+000 -1.000E+000 -5.091E-001 -
1.000E+000 R        U      T
 16.0276 -1.000E+000 -1.000E+000 -1.000E+000 -1.000E+000 -5.091E-001 -
1.000E+000 R        U      T
 17.0322 -1.000E+000 -1.000E+000 -1.000E+000 -1.000E+000 -5.091E-001 -
1.000E+000 R        U      T
 18.0368 -1.000E+000 -1.000E+000 -1.000E+000 -1.000E+000 -5.091E-001 -
1.000E+000 R        U      T
 19.0415 -1.000E+000 -1.000E+000 -1.000E+000 -1.000E+000 -5.091E-001 -
1.000E+000 R        U      T

 20.0461 -1.000E+000 -1.000E+000 -1.000E+000 -1.000E+000 -5.091E-001 -
1.000E+000 R        U      T
 70.7357 1.041E+006  4.648E-001  1.000E+000  5.495E-001  2.797E-001  2.132E-
003  R        C      T
121.4254 -1.000E+000 -1.000E+000 -1.000E+000 -1.000E+000 -5.091E-001 -
1.000E+000 R        U      T
172.1151 -1.000E+000 -1.000E+000 -1.000E+000 -1.000E+000 -5.091E-001 -
1.000E+000 R        U      T
222.8048 -1.000E+000 -1.000E+000 -1.000E+000 -1.000E+000 -5.091E-001 -
1.000E+000 R        U      T
273.4945 -1.000E+000 -1.000E+000 -1.000E+000 -1.000E+000 -5.091E-001 -
1.000E+000 R        U      T
324.1842 -1.000E+000 -1.000E+000 -1.000E+000 -1.000E+000 -5.091E-001 -
1.000E+000 R        U      T
374.8739 -1.000E+000 -1.000E+000 -1.000E+000 -1.000E+000 -5.091E-001 -
1.000E+000 R        U      T
425.5636 -1.000E+000 -1.000E+000 -1.000E+000 -1.000E+000 -5.091E-001 -
1.000E+000 R        U      T
476.2533 -1.000E+000 -1.000E+000 -1.000E+000 -1.000E+000 -5.091E-001 -
1.000E+000 R        U      T

526.9430 -1.000E+000 -1.000E+000 -1.000E+000 -1.000E+000 -5.091E-001 -
1.000E+000 R        U      T

 ++++++++++++++++++++++++
 +  Problem  1 complete +
 ++++++++++++++++++++++++
```

Appendix C : Chemical composition test result

Environmental Scientifics Group Ltd
Acrewood Way, St Albans
Hertfordshire, AL4 0JY

Telephone: + 44 (0) 1727 840580
Fax: + 44 (0) 1727 816700

ESG Environmental Scientifics Group

UKAS TESTING 0001

TEST REPORT

Cranfield University
Whittle Building – Bldg 52
School of Engineering
Cranfield
Bedfordshire MK43 0AL
For the attention of Mr Graham Lee

Your Ref O/No. 613446
Our Ref 000000969
Date 23/08/2011

STEEL SAMPLES FOR CHEMICAL ANALYSIS

Certificate Number **M9527**

Date of Receipt 11/08/2011 Date of Test 22/08/2011

Description Steel samples

		Weight		
Identified		x 60	x 70	x 100
Carbon	%	0.04	0.05	0.07
Silicon	%	0.19	0.26	0.30
Manganese	%	1.04	1.89	1.83
Sulphur	%	0.008	0.010	0.009
Phosphorus	%	0.013	0.010	0.012
Nickel	%	0.03	0.44	0.28
Chromium	%	0.03	0.41	0.17
Molybdenum	%	<0.01	0.40	0.16
Copper	%	0.02	0.45	0.15
Vanadium	%	0.04	0.07	0.01
Niobium	%	0.06	0.05	0.04
Titanium	%	0.01	0.01	0.02
Aluminium	%	0.03	0.01	0.04
Cobalt	%	<0.01	<0.01	<0.01

Analytical Technique – Optical Emission

David Poole

D Poole
Metallurgical Analyst

End of Report

Appendix D : A New Constant K Specimen Design

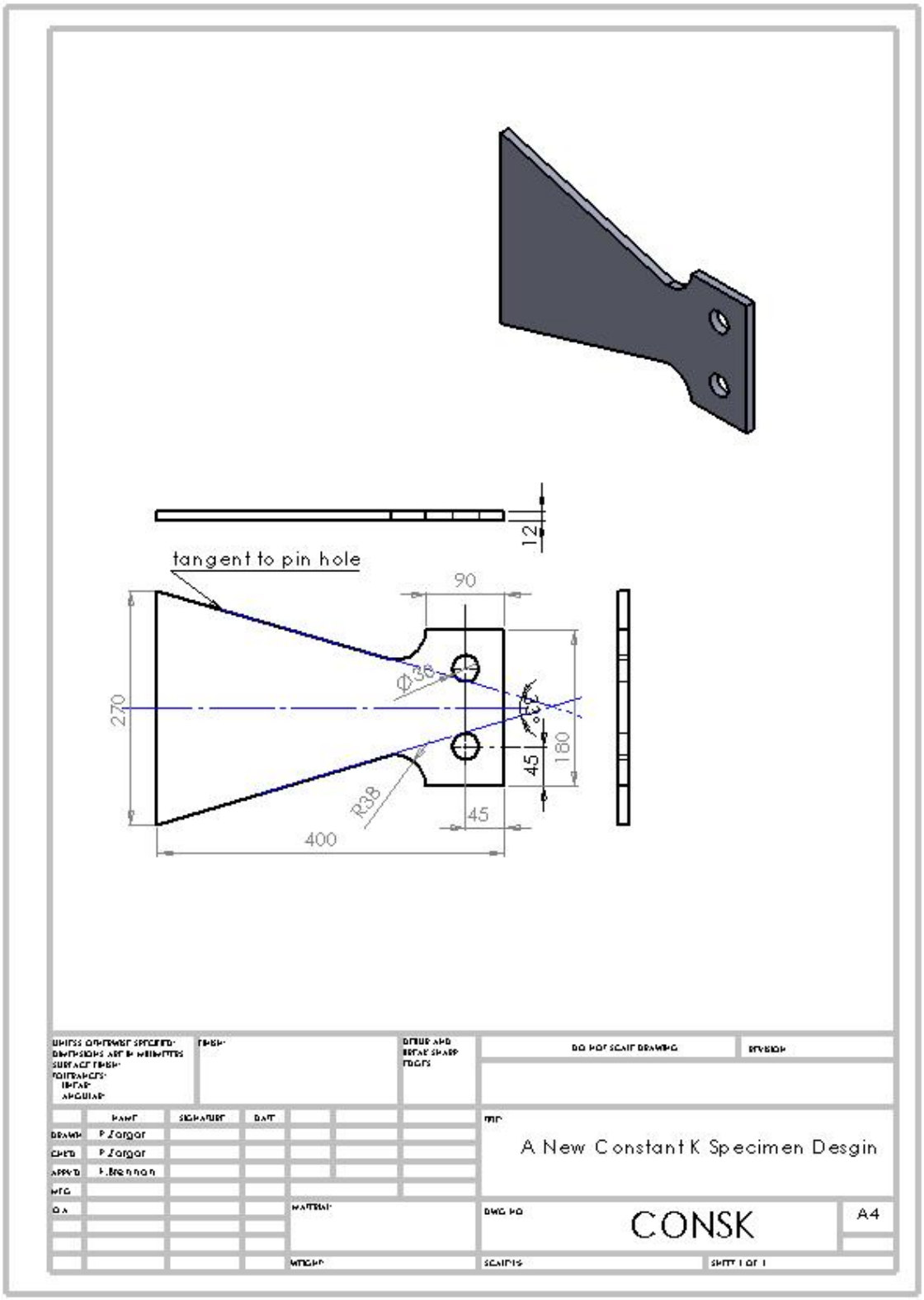

Appendix E : CT shop drawing

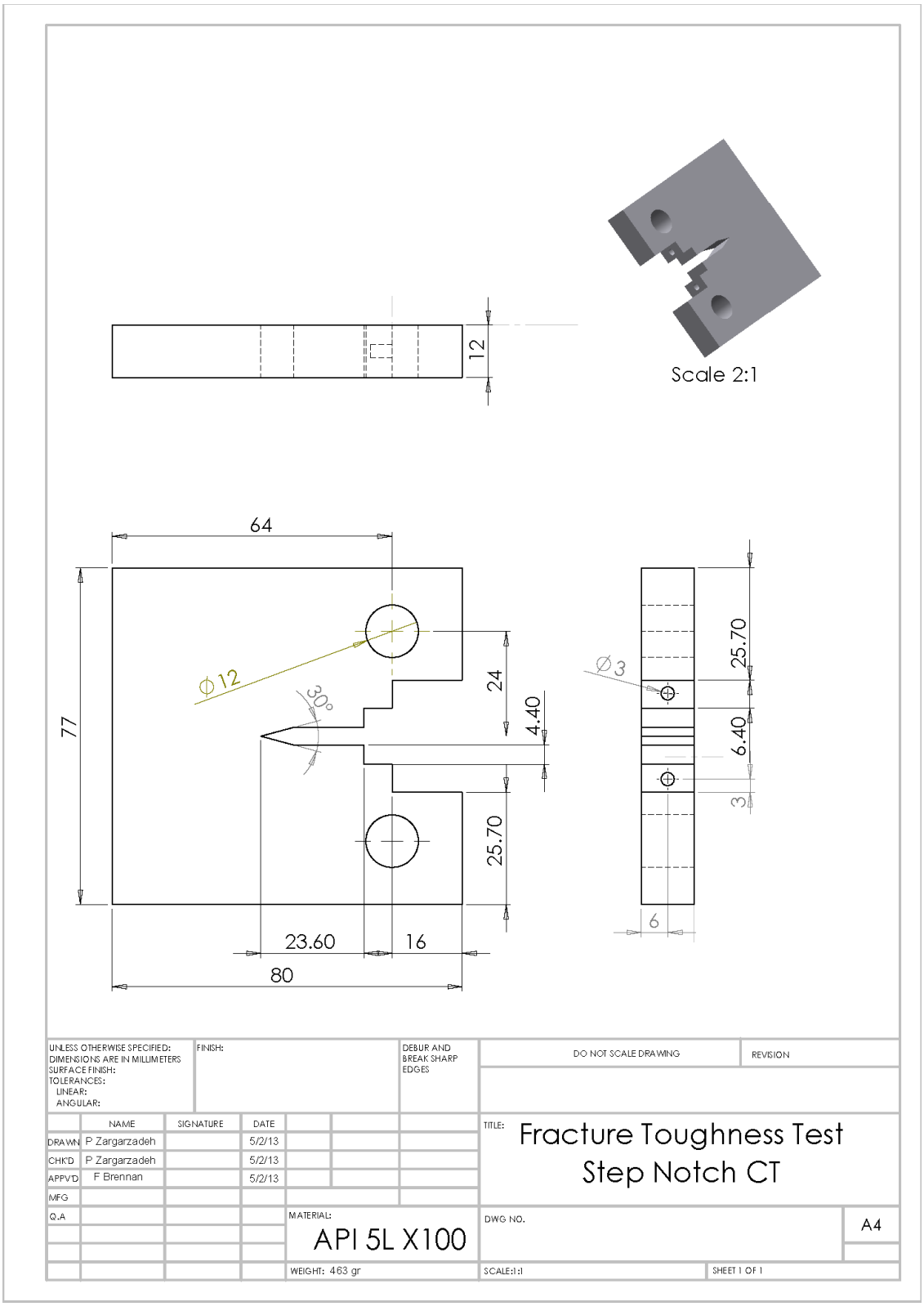

Appendix F : Clip gauge

To measure a small displacement (in this test a crack opening) with great accuracy and reliability, a clip gauge needs to be used. A non standard clip gauge transducer was used for the CTOD test (Figure F-1). The Servo hydraulic tensile machine (Instron) did not recognise this type of clip gauge. It should, therefore, be calibrated and modified to be used by the Servo hydraulic machine. The clip gauge transducer was the twin cantilever gauge type which consists of four, linear pattern, strain gauges oriented as a full bridge connection.

Figure F-1 A customised clip gauge

As the clip gauge was a non standard one that was not defined for a Servo hydraulic machine, it should be modified to be recognised by the machine. In Figure F-1, the cable connections diagram and short bridge on pins 4 and 5 are depicted. All of this modification should be done on the 25 pin D-type connector, connected to the clip gauge. Also, to prevent any noise disturbance, all cables should be shielded and the shield should be connected to pin number 3. The same as for the other clip gauges and extensometers, it consists of four linear patterned strain gauges that are connected to each other

as a full bridge. They are connected as a Wheatstone bridge circuit, as illustrated in Figure F-1.

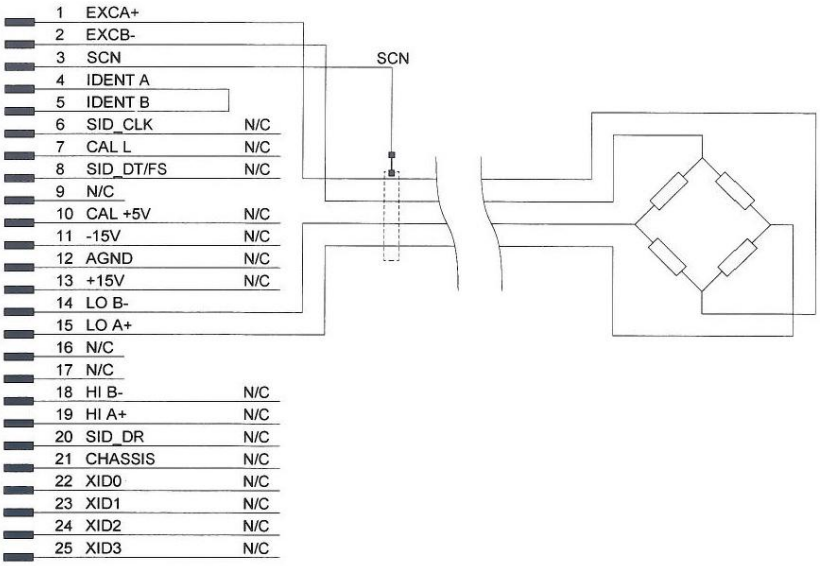

Figure F-2 Full bridge user defined transducer
(Instron 2011)

To calibrate the clip gauge, a precise length measurement device is needed. The Instron micro measurement instrument has been used to calibrate the clip gauge (Figure F-2).

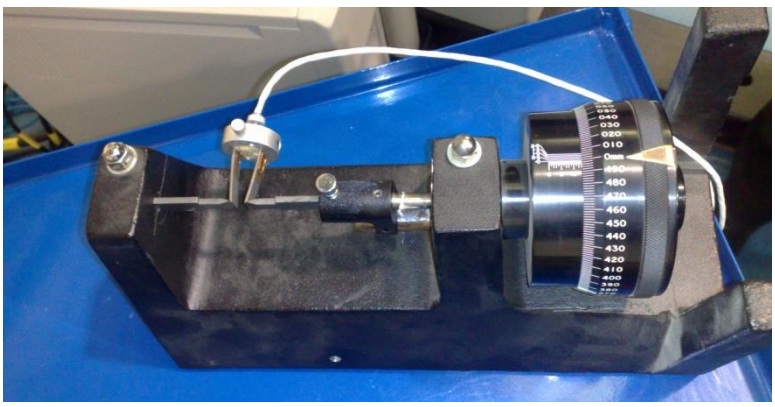

Figure F-3 Precise Instron micrometer

To read the related micro strain corresponding to the measured length by micrometer, a Vishay P3 strain reader was used (Figure F-3). The principal formulae of a full bridge clip gauge are as follows:

For the two gauges that are in tension, gauge resistance (R_G) will change to (R_G+Δ R_G) due to the strain of $\frac{\Delta l}{l}$ and for the two gauges that are in compression R_G → R_G-Δ R_G ,.at positive output, the voltage is:

$$V_{OP+} = \frac{(V_{EXC+} - V_{EXC-})(\mathrm{R_G} + \Delta\,\mathrm{R_G})}{2\mathrm{R_G}} \qquad \text{(F-1)}$$

And in the negative output the voltage is:

$$V_{OP-} = \frac{(V_{EXC+} - V_{EXC-})(\mathrm{R_G} - \Delta\,\mathrm{R_G})}{2\mathrm{R_G}} \qquad \text{(F-2)}$$

The differential output voltage is:

$$V_{OUT} = (V_{OP+} - V_{OP-}) = \frac{(V_{EXC+} - V_{EXC-})\Delta\,\mathrm{R_G}}{\mathrm{R_G}} \qquad \text{(F-3)}$$

Senility is:

$$\frac{V_{OUT}}{V_{EXC}} = \frac{(V_{OP+} - V_{OP-})}{(V_{EXC+} - V_{EXC-})} = \frac{\Delta\,\mathrm{R_G}}{\mathrm{R_G}} \qquad \text{(F-4)}$$

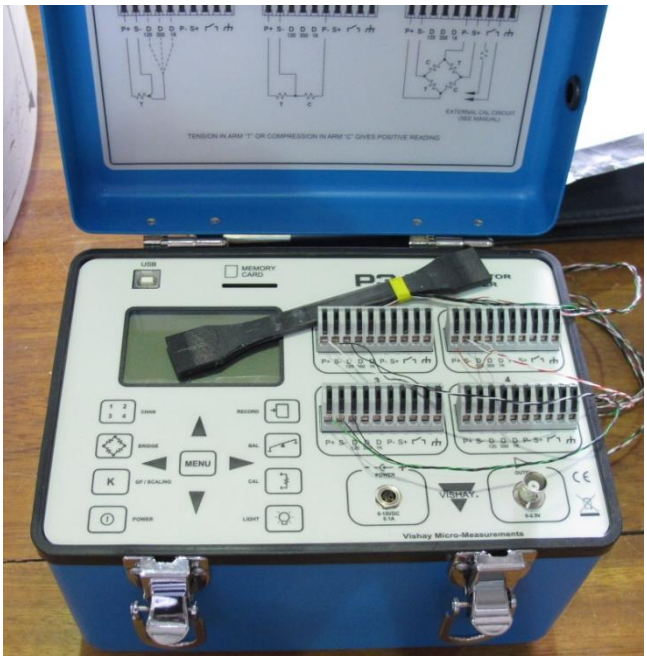

Figure F-4 Vishay P3 strain reader

The test has been accomplished under laboratory conditions of 26°C temperature and 29% humidity and an opening length of 0 to 4mm and back to 0. It showed a good trend upward (from 0 to 4mm) and downward (from 4mm to 0) (see Figure F-5).

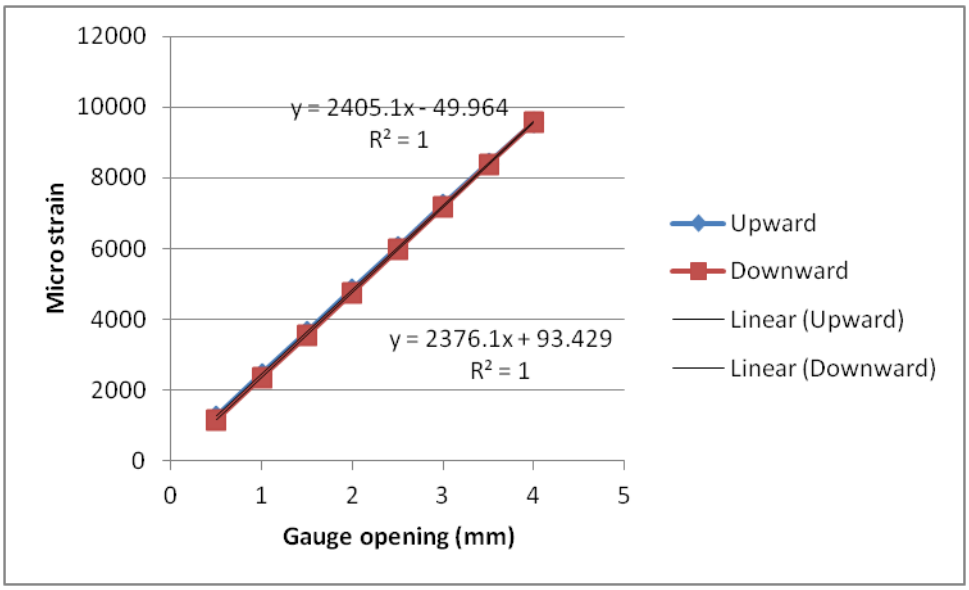

Figure F-5 Clip gauge calibration hysteresis

After finishing calibration with the strain reader, and modifing the connection port of the clip gauge, the port of the clip gauge should be connected to the Servo hydraulic machine and recalibrated. In Table F-1 the result of the clip gauge opening and COD reading of the Servo hydraulic machine has been illustrated. Any transducer made by Instron automatically calibrates itself using the calibration button after connection to the machine. As in this test a user defined clip gauge has been used before each use and after connection, it should be calibrated manually. A calibration text file based on what has been explained in this section has been generated and should be recalled during the calibration procedure.

Table F-7-1 Proof of calibration with the Servo hydraulic machine

Clip gauge opening (mm)	Instron COD reading (mm)
0.5	0.513
1	1.021
1.5	1.525
2	2.026
2.5	2.521
3	3.012
3.5	3.504
4	3.99

Appendix G : Cooling chamber and liquid nitrogen Dewar

The environmental chamber is manufactured by Instron with internal dimensions of Height: 560mm x Width: 240mm x Depth: 230mm, and operating temperatures of: -70 to 350°C. It has a digital temperature controller that accurately maintains the set temperature. The end fittings have been designed in such a way as to perform both CT and Tensile tests in low temperatures using a cooling chamber. A series of CT tests in low temperatures of 0, -20, -40, -60 and -70°C were conducted. The results presented in 3.4.1.

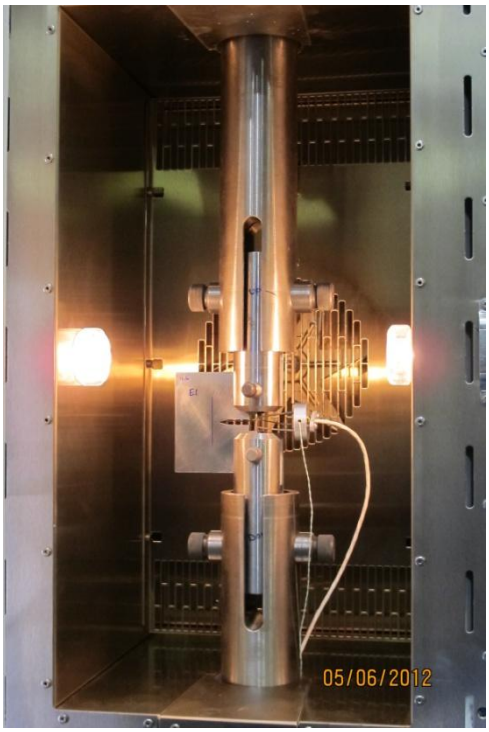

Figure G-1 Cooling chamber

The self-pressurising cryogenic vessel for liquid nitrogen (briefly Dewar) has a 120 litre capacity and maximum operating pressure of 4 bar. It has been connected directly to the cooling chamber with an insulated pipe (Figures G-1 and G-2). There are some safety issues associated with using liquid nitrogen and all personnel working in that area should be aware of the potential hazards and the actions necessary to be taken in an emergency.

Figure G-2 120 litre liquid nitrogen Dewar

To double check and understand the temperature difference between the cooling chamber environment and the specimen, a calibrated external thermometer has been used (Figure G-3). Two different probes (thermocouples), magnetic and bare, have been utilised and the readings conform perfectly to each other. For testing in low temperatures, at least 35 minutes should be given for the system to be stabilised at the set temperature. It is very important point to have meaningful results and, depending on the thickness of the specimen, this time may vary.

Figure G-3 Internal and external thermometers